frontiers | Research Topics

Chemometric approach to distribution, source apportionment, ecological and health risk of trace pollutants

Edited by
Antonije Onjia, Johnbosco C. Egbueri, Juan Manuel Trujillo-González and Xin Huang

Published in
Frontiers in Environmental Science
Frontiers in Analytical Science

ISSN 1664-8714
ISBN 978-2-83251-133-6
DOI 10.3389/978-2-83251-133-6

About Frontiers

Frontiers is more than just an open access publisher of scholarly articles: it is a pioneering approach to the world of academia, radically improving the way scholarly research is managed. The grand vision of Frontiers is a world where all people have an equal opportunity to seek, share and generate knowledge. Frontiers provides immediate and permanent online open access to all its publications, but this alone is not enough to realize our grand goals.

Frontiers journal series

The Frontiers journal series is a multi-tier and interdisciplinary set of open-access, online journals, promising a paradigm shift from the current review, selection and dissemination processes in academic publishing. All Frontiers journals are driven by researchers for researchers; therefore, they constitute a service to the scholarly community. At the same time, the *Frontiers journal series* operates on a revolutionary invention, the tiered publishing system, initially addressing specific communities of scholars, and gradually climbing up to broader public understanding, thus serving the interests of the lay society, too.

Dedication to quality

Each Frontiers article is a landmark of the highest quality, thanks to genuinely collaborative interactions between authors and review editors, who include some of the world's best academicians. Research must be certified by peers before entering a stream of knowledge that may eventually reach the public - and shape society; therefore, Frontiers only applies the most rigorous and unbiased reviews. Frontiers revolutionizes research publishing by freely delivering the most outstanding research, evaluated with no bias from both the academic and social point of view. By applying the most advanced information technologies, Frontiers is catapulting scholarly publishing into a new generation.

What are Frontiers Research Topics?

Frontiers Research Topics are very popular trademarks of the *Frontiers journals series*: they are collections of at least ten articles, all centered on a particular subject. With their unique mix of varied contributions from Original Research to Review Articles, Frontiers Research Topics unify the most influential researchers, the latest key findings and historical advances in a hot research area.

Find out more on how to host your own Frontiers Research Topic or contribute to one as an author by contacting the Frontiers editorial office: frontiersin.org/about/contact

Chemometric approach to distribution, source apportionment, ecological and health risk of trace pollutants

Topic editors

Antonije Onjia — University of Belgrade, Serbia
Johnbosco C. Egbueri — Chukwuemeka Odumegwu Ojukwu University, Nigeria
Juan Manuel Trujillo-González — University of the Llanos, Colombia
Xin Huang — Nanjing University, China

Citation

Onjia, A., Egbueri, J. C., Trujillo-González, J. M., Huang, X., eds. (2023). *Chemometric approach to distribution, source apportionment, ecological and health risk of trace pollutants*. Lausanne: Frontiers Media SA.
doi: 10.3389/978-2-83251-133-6

Table of contents

frontiers | Frontiers in Environmental Science

TYPE Editorial
PUBLISHED 09 December 2022
DOI 10.3389/fenvs.2022.1107465

OPEN ACCESS

EDITED AND REVIEWED BY
Oladele Ogunseitan,
University of California, Irvine,
United States

*CORRESPONDENCE
Antonije Onjia,
onjia@tmf.bg.ac.rs

SPECIALTY SECTION
This article was submitted to Toxicology, Pollution and the Environment, a section of the journal Frontiers in Environmental Science

RECEIVED 24 November 2022
ACCEPTED 05 December 2022
PUBLISHED 09 December 2022

CITATION
Onjia A, Huang X, Trujillo González JM and Egbueri JC (2022), Editorial: Chemometric approach to distribution, source apportionment, ecological and health risk of trace pollutants. *Front. Environ. Sci.* 10:1107465. doi: 10.3389/fenvs.2022.1107465

Editorial: Chemometric approach to distribution, source apportionment, ecological and health risk of trace pollutants

Antonije Onjia[1]*, Xin Huang[2], Juan Manuel Trujillo González[3] and Johnbosco C. Egbueri[4]

[1]Faculty of Technology and Metallurgy, University of Belgrade, Belgrade, Serbia, [2]School of Atmospheric Sciences, Nanjing University, Nanjing, China, [3]Institute of Environmental Sciences of la Orinoquia, University of the Llanos, Villavicencio, Colombia, [4]Department of Geology, Chukwuemeka Odumegwu Ojukwu University, Uli, Nigeria

KEYWORDS

geostatistics, positive matrix factorization, Monte Carlo simulation, hazard index, carcinogenic, potentially toxic elements, UV filters, PFAS

Editorial on the Research Topic
Chemometric approach to distribution, source apportionment, ecological and health risk of trace pollutants

Intensive technological development has led to tremendous pressure on the quality of the environment, which is reflected in its pollution by toxic trace pollutants. The modern approach to studying risks from these pollutants includes the integration of analytical chemistry, environmental science, mathematics, statistics, and toxicology. A dramatic increase in data generated by modern analytical instruments in studies on trace pollutants in the environment imposes a quite complex task to extract meaningful information from these data. Thus, the use of chemometrics became irreplaceable.

Principal component analysis (PCA) (Radomirović et al., 2020; Trujillo-González et al., 2022a), hierarchical cluster analysis (HCA) (Lučić et al., 2022), positive matrix factorization (PMF) (Radomirović et al., 2021), geostatistical analysis (GIS) (Trujillo-González et al., 2022b); (Miletić et al., 2022), Monte Carlo simulation (MCS) (Seyednejad and Ghiasi, 2022), numerical modeling (Wang et al., 2019), machine learning and artificial intelligence modeling (ANN) (Egbueri, 2021; Agbasi and Egbueri, 2022) have been frequently used chemometric methods for trace pollutants data evaluation. Since there is great competitivity or complementarity between these methods, it is common to use several methods together in a single study. Therefore, a comprehensive approach is needed in this area where different research can be incorporated, covering a range of chemometric methods and their combinations for various pollutants in the environment.

This Research Topic addressed recent advances in the application of chemometrics in studies on the occurrence, distribution, and fate of trace pollutants in different media (soil,

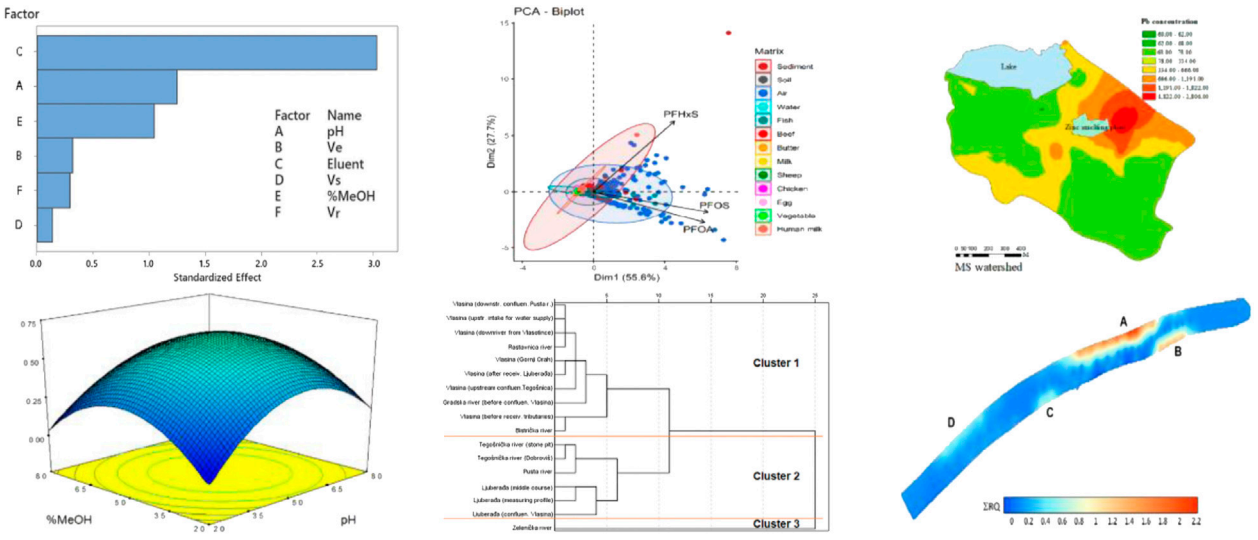

FIGURE 1
Some of the figures from the research topics. **(A)** Pareto chart from the screening Plackett-Burman experimental design. **(B)** Response surface optimization graph. **(C)** PCA-Biplot. **(D)** Dendrogram from HCA. **(E)** GIS map of soil. **(F)** GIS map of water.

air, water, plants, and food). It was focused not only on pattern recognition, classification, and pollution source identification but also on ecological and health risk assessment.

Nine articles after peer review were published in this Research Topic. These articles highlighted a diversity of chemometric methods for the fate of toxic pollutants and their influence on the environment and human health. Figure 1 illustrates how some of the mentioned methods present the data in these articles.

The contamination by toxic trace elements was investigated in several articles. Heavy metals in urban dust and possible ecological and human health risk in six Mexican cities were studied by Aguilera et al. It was found that all studied cities were contaminated, while the highest metal contribution to the potential ecological risk in all the cities was from Pb. Therefore, the importance of identifying the main sources of Pb in cities and seeking mitigation strategies to reduce its possible adverse effects was highlighted.

Yu et al. investigated the superposition effects of atmospheric deposition from zinc smelting on soil heavy metal pollution under geochemical anomaly. The results showed much higher concentrations of heavy metals in the atmospheric deposition area where a zinc smelting plant was situated than those in the control area with the local background values. PCA reflected more diversified pollution sources, while the GIS distribution of soil heavy metals indicated that the content of heavy metals in soil was highly dependent on the location of zinc smelting.

A case study in Peninsular Malaysia on the health and ecological risk of Sb and As in the vegetable *Centella asiatica*, topsoils, and mangrove sediments was conducted by Yap et al. The findings indicated that 56% of the topsoils with As hazard index (HI) values for children exceeded one. The ingestion pathway contributed almost all the As total HI values. Furthermore, a high ecological risk of As and carcinogenic health risk of As in the topsoils and mangrove sediments were evident, with the HI values in children being higher than those in adults. Anthropogenic sources of Sb and As originated from land-based activities before reaching the mangrove near the coast were apportioned.

An integrated approach in the assessment of the Vlasina river system pollution by toxic elements was used by Sakan et al. The water and sediments of rivers in the Vlasina region (Serbia) were analyzed to assess the current state of pollution with toxic elements. No significant spatial variability of potentially toxic elements in water and sediments was observed. The positive correlations between most of the examined elements in sediments indicated their dominant geochemical origin. It was found no notable pollution in the water and sediments in the Vlasina region.

Zhang et al. investigated bioaccumulation and assessed the risk of potentially toxic elements (PTEs) in the soil-rice system in a karst area (Southwest China). The results revealed that weathering of parent rocks and alluvial deposits was the major source of heavy metals in soils, while fossil fuel combustion and agricultural activities also contribute to the accumulation of soil PTE. The high excessive rate of Cd and Pb could be attributed to their high bioaccumulation factor and high content in the soil. At the same time, residents may be exposed to As and Cd through rice consumption. The average targeted hazard quotient values (THQ) of PTE for the rice samples decreased in the order of

As > Cd > Cr > Cu > Zn > Pb > Hg, and the degree of a health risk it posed to the population was Children > Female > Male. Therefore, health risks caused by excessive consumption of wild heavy metal-enriched rice should be avoided.

A consumption risk from trace metal residues in swimming warrior crab (*Callinectes bellicosus*) has been studied by Castro-Elenes et al. They found a high contamination level of trace metals in the edible tissue of crabs, resulting from a constant discharge of these pollutants to the lagoon from the agricultural and aquaculture activities after irrigation or wastewater drainage. These trace metal residues are being bioaccumulated in the edible tissues of the crab due to its feeding habits, resulting in carcinogenic and non-carcinogenic health risks if its consumption is high.

Bacterial Cd immobilization activity (CIA) in cacao-growing soils from Colombia has been studied by Bravo. He measured CIA by Cd-tolerant bacteria (CdtB) using isothermal microcalorimetry (IMC). A Pearson correlation analysis was made between kinetical growth parameters and thermodynamic data, while PCA of CdtB cadA gene copies, soil pH, and soil organic matter indicated the effect of CdtB in Cd translocation. The research importance of his work was the use of combined tools for quantitative IMC measurements to identify and assess Cd metabolic capacities of CdtB populations in soil, *in situ*.

In the study of Fiedler et al., a multivariate evaluation of perfluoroalkyl substances (PFAS) in environmental samples, including air, water, sediment, soil, food samples comprising fish, meat (beef, sheep, chicken), egg, butter, and milk as well as human milk samples have been done. This assessment of PFAS in abiotic and biota samples showed that perfluorooctane sulfonic acid (PFOS) and perfluorooctanoic acid (PFOA) dominated the scale and the pattern in all matrices.

Chemometric optimization of the solid-phase extraction (SPE) procedure used in the extraction of eleven ultraviolet filters (UVFs) from urban lake water was reported by Lukić et al. They applied the Plackett-Burman design, the Box-Behnken design, and Derrindzer desirability function to screen and optimize six SPE variables. The optimized SPE was then implemented to prepare the water samples prior to liquid chromatography-tandem mass spectrometry (LC-MS/MS) measurements. Finally, the Monte Carlo simulation of environmental risks and sensitivity analysis were performed, revealing a safety concern due to UVFs in the long term. Geostatistical mapping of the risk quotient in a lake showed that its was highly dependent on recreational activities.

In conclusion, combining chemometric techniques and risk indices is helpful in assessing environmental pollution status. Potentially toxic elements are still the most studied pollutants. Among the organic trace pollutants, emerging organic contaminants are of particular safety concern. Future works are expected to address new contaminants, lower concentrations, larger datasets, and new approaches to health risk assessment.

Author contributions

All authors listed have made a substantial, direct, and intellectual contribution to the work and approved it for publication.

Funding

This study was supported by the Ministry of Education, Science and Technological Development of Serbia (No. 451-03-68/2022-14/200135) and the University of the Llanos, Colombia (RR No. 033/18-01-2022).

Acknowledgments

We deeply thank all the authors and reviewers who have participated in this Research Topic.

Conflict of interest

The authors declare that the research was conducted in the absence of any commercial or financial relationships that could be construed as a potential conflict of interest.

Publisher's note

References

Agbasi, J., and Egbueri, J. (2022). Assessment of PTEs in water resources by integrating HHRISK code, water quality indices, multivariate statistics, and ANNs. *Geocarto Int.* 1–27. doi:10.1080/10106049.2022.2034990

Egbueri, J. C. (2021). Prediction modeling of potentially toxic elements' hydrogeopollution using an integrated Q-mode HCs and ANNs machine learning approach in SE Nigeria. *Environ. Sci. Pollut. Res.* 28, 40938–40956. doi:10.1007/s11356-021-13678-z

Lučić, M., Miletić, A., Savić, A., Lević, S., Sredović Ignjatović, I., and Onjia, A. (2022). Dietary intake and health risk assessment of essential and toxic elements in pepper (Capsicum annuum). *J. Food Compos. Analysis* 111. doi:10.1016/j.jfca.2022.104598

Miletić, A., Radomirović, M., Đorđević, A., Bogosavljević, J., Lučić, M., and Onjia, A. (2022). Geospatial mapping of ecological risk from potentially toxic elements in soil in the Pannonian-Carpathian border area south of the Danube. *Carpathian J. Earth Environ. Sci.* 17 (2), 251–263. doi:10.26471/cjees/2022/017/227

Radomirović, M., Ćirović, Ž., Maksin, D., Bakić, T., Lukić, J., Stanković, S., et al. (2020). Ecological risk assessment of heavy metals in the soil at a former painting industry facility. *Front. Environ. Sci.* 8, 1–15. doi:10.3389/fenvs.2020.560415

Radomirović, M., Stanković, S., Jović, M., Janković-Mandić, L., Dragović, S., Onjia, A., et al. (2021). Spatial distribution, radiological risk assessment and positive matrix factorization of gamma-emitting radionuclides in the sediment of the Boka Kotorska Bay. *Mar. Pollut. Bull.* 169, 112491. doi:10.1016/j.marpolbul.2021.112491

Seyednejad, F., and Ghiasi, H. (2022). Monte Carlo code calculation for the characterization of 10nm nano-layers coated 50nm 90 Y radionuclide nanospheres radiation in the liver radionuclide therapy. *fbt.* 9 (2), 102–109. doi:10.18502/fbt.v9i2.8849

Trujillo-González, J. M., Torres-Mora, M. A., Serrano-Gómez, M., Castillo-Monroy, E. F., Ballesta, R. J., and Rodrigo-Comino, J. (2022a). Mapping potential toxic elements in agricultural and natural soils of the piedemonte llanero in Colombia. *Water Air Soil Pollut.* 233 (4), 102–112. doi:10.1007/s11270-022-05550-8

Trujillo-González, J. M., Torres-Mora, M. A., Serrano-Gomez, M., Castillo-Monroy, E. F., and Jímenez Ballesta, R. (2022b). Baseline values and environmental assessment for metal(loid)s in soils under a tropical rainy climate in a Colombian region. *Environ. Monit. Assess.* 194 (7), 494–515. doi:10.1007/s10661-022-10036-5

Wang, Z., Huang, X., and Ding, A. (2019). Optimization of vertical grid setting for air quality modelling in China considering the effect of aerosol-boundary layer interaction. *Atmos. Environ.* 210, 1–13. doi:10.1016/j.atmosenv.2019.04.042

frontiers in Environmental Science

ORIGINAL RESEARCH
published: 01 December 2021
doi: 10.3389/fenvs.2021.772221

Trace Metal Residues in Swimming Warrior Crab *Callinectes bellicosus*: A Consumption Risk

*Marisol Castro-Elenes, G. Durga Rodríguez-Meza†, Ernestina Pérez-González and Héctor A. González-Ocampo *†*

Instituto Politécnico Nacional - CIIDIR Unidad Sinaloa, Guasave, Mexico

OPEN ACCESS

Edited by:
Johnbosco C. Egbueri, Chukwuemeka Odumegwu Ojukwu University, Nigeria

Reviewed by:
Orish Ebere Orisakwe, University of Port Harcourt, Nigeria
Michael Omeka, University of Calabar, Nigeria

****Correspondence:***
Héctor A. González-Ocampo
hgocampo@yahoo.com

†These authors have contributed equally to this work and share first authorship

Specialty section:
This article was submitted to Toxicology, Pollution and the Environment, a section of the journal Frontiers in Environmental Science

Received: *07 September 2021*
Accepted: *25 October 2021*
Published: *01 December 2021*

Citation:
Castro-Elenes M, Rodríguez-Meza GD, Pérez-González E and González-Ocampo HA (2021) Trace Metal Residues in Swimming Warrior Crab Callinectes bellicosus*: A Consumption Risk. Front. Environ. Sci. 9:772221. doi: 10.3389/fenvs.2021.772221*

This study was carried out in the Navachiste coastal lagoon, Mexico, surrounded by intensive agricultural and aquaculture activities that cause environmental pollution by the deposition of trace metal residues in the sediments of this coastal lagoon. The trace metals are bioaccumulated by benthic organisms such as the blue swimming warrior crab, *Callinectes bellicosus*, which inhabits this lagoon and is consumed by humans. Ninety-five *C. bellicosus* edible tissue samples were collected (April 2014–January 2015). The extraction procedure of the trace metals in edible tissue samples was carried out by acid digestion with nitric acid. Based on the Environmental Protection Agency (EPA) of the United States, two indices were used to measure health risk: the estimated daily intake (EDI) and the target hazard quotient (THQ). The hazard index (HI) was used to calculate the probability of adverse carcinogenic risk and the target hazard quotient per sample (MHI) to calculate the probability of developing a carcinogenic or non-carcinogenic risk. The analysis of variance (ANOVA) showed significant differences among trace metal concentrations ($p < 0.01$), but all trace metal concentrations in the edible tissues of *C. bellicosus* were higher than the maximum residual limits (MRLs). The highest EDI was for Zn, Fe, and Cu, showing that the consumption of these crabs might represent health risks. The THQ >1 was for Ni, Zn, Cd, and Cu, and the HI = 16 revealed the risk of *C. bellicosus* for high-level consumers. The MHI showed that 98% of samples presented a THQ >1, implying a high rate of bioaccumulation of trace metals by the crabs independent of the sampling site in the NAV. The presence of trace metals in the edible tissue of crabs reflects contamination by trace metals, and the indices results mean that the NAV lagoon is constantly polluted with trace metal residues by neighboring agriculture and aquaculture activities. These trace metal residues are being bioaccumulated in the edible tissues of *C. bellicosus* due to its feeding habits, resulting in a health risk if its consumption is high, including carcinogenic and non-carcinogenic risks.

Keywords: seafood, heavy metal, trace elements, Navachiste, environmental pollution

Abbreviations: NBay, Navachiste Bay, Sinaloa, Mexico; NAV, Navachiste coastal lagoon system; PCA, principal components analysis.

INTRODUCTION

The risk of exposure by humans to trace metals has increased significantly in industrial and agricultural regions. Coastal lagoons are some of the areas most impacted by the discharges of these pollutant residues (Pan and Wang, 2012; Meena et al., 2017; Yang et al., 2018). One of these impacted regions is the coastal lagoon system of Navachiste (NAV) located in the southeastern part of the Gulf of California. It is a semiclosed coastal lagoon in a semiarid and subtropical area with sand barrier islands and significant extensions of mangrove areas, columnar cacti, dry deciduous forests, wetlands, and shrublands. NAV is surrounded by the largest agricultural region in Mexico and more than 9,000 ha of shrimp aquaculture farms (Carrasquilla-Henao et al., 2013) that are constantly discharging pollutant residues, such as trace metals, which enter the coastal lagoons (Pan and Wang, 2012; Meena et al., 2017; Yang et al., 2018). Metal residues are found naturally in soils and sediments, but enrichment has been related to agricultural and aquaculture practices (Jalali and Hemati, 2013). NAV is being impacted by the residues drained from the agricultural Guasave Valley (Martínez-Valenzuela et al., 2009) and by the large quantities of fish excrement, uneaten feed, antibiotics, fungicides, and antifouling agents released by the aquaculture activities (Mateo-Sagasta et al., 2018).

Previous studies carried out in NAV have described how trace metal concentrations in its sediments have become bioavailable to marine species (Páez-Osuna and Osuna-Martínez, 2015), including those of commercial interest (Páez-Osuna and Osuna-Martínez, 2015; Góngora-Gómez et al., 2018; Delgado-Alvarez et al., 2019). In the NAV, one of the most important artisanal fisheries is the blue swimming warrior crab (*Callinectes bellicosus*) which is exported to international markets at up to 13,000 tons year^{-1} (Ortega-Lizárraga et al., 2020).

Due to the commercial importance of *C. bellicosus*, the increased bioavailability of trace metals in sediments of NAV, and the ability of this crab to induce bioturbation of sediments because of its omnivorous feeding habit that resuspends the metal residues, which, in turn, become bioaccumulated in its tissues, *C. bellicosus* represents a human health risk to consumers. In this sense, monitoring these metal traces in the edible tissue of *C. bellicosus* is a significant concern for health risks. Thus, the main objective of this study was to determine the trace metal residue content in the edible tissue of the *C. bellicosus* crab to evaluate the carcinogenic and non-carcinogenic risks posed by the consumption of this species.

MATERIAL AND METHODS

The NAV encloses three lagoons (San Ignacio, Macapule, and Navachiste) located in the southeastern Gulf of California (25° 27′59″N and 108° 50′24″W). Samples were collected during spring, summer, autumn, and winter, with crab traps from April 2014 to January 2015 (**Figure 1**). The sampling sites were selected based on two characteristics: their proximity to discharge drainages from agricultural, urban, and shrimp farming areas and locations not influenced by any drainage effluents. Water parameters (pH, temperature, salinity, and dissolved oxygen) were recorded with a HANNA® HI-9828 multiparameter (HANNA Instruments, Italy). The samples were packed in polyethylene bags to avoid contamination with trace metal residues of other packing materials, like aluminum foils, and cold stored in a 40-L cooler to delay the oxidation of organic matter in sediments until freezing in the Environmental Contamination Laboratory of the CIIDIR-IPN, Sinaloa Unit.

Ninety-five samples of edible tissues of the crab species *C. bellicosus* were processed. The trace metals were extracted by acid digestion with nitric acid based on the Breder method for the extraction of metal residues in sediments by atomic absorption spectrometric methods and for silicate sediments (Breder, 1982). The muscle tissues of each sample were dehydrated; subsequently, 0.5 g per sample was supplemented with 5 ml of HNO_3 (65%) and placed for 4 h in an aluminum heating block with precise temperature control to dissolve the organic matter strongly adhered to sediments. A similar procedure was performed with 0.5 g of the sediment that was tested with 5 ml of a 1:3 HCl–HNO_3 mix. This mixture does not decompose the sediment, and high recovery of the metallic elements is achieved, and the extractions are precise in determining metals such as As, Cu, Cr, Hg, Mn, Ni, Pb, V, and Zn. After digestion, the samples were cooled to room temperature, gauged to 50 ml with deionized water, and transferred to a graduated polypropylene Falcon® tube. A GBC AVANTA®, USA, atomic absorption spectrometer, with a programmable air-acetylene flame and hollow cathode lamps, was used to detect and determine trace metals. The precision of the instruments and techniques was adjusted using the TORT-2 lobster hepatopancrea reference material, NRC-CNRC®, which was treated like the samples. Six calibration curves (0.125, 0.25, 0.5, 1, 2, and 4 mg L^{-1}) were prepared using the standard certified PerkinElmer® solution (1000 mg L-1). The limit of detection (LOD) for each metal was calculated using the following equation (INMETRO 2016) (**Eq. 1**):

$$\mathrm{LOD} = 10 \times S_{bl} \tag{1}$$

where S_{bl} is the standard deviation of 10 control blanks analyzed, in the present report, and the LOD was 0.0158 mg $CaCO_3$ L^{-1}.

As recommended by the U.S. Environmental Protection Agency of the (USEPA), three indices were used to measure health risks: estimated daily intake (EDI), target hazard quotient (THQ), and hazard index (HI). In this study, we propose the use of the total metal THQ per sample (MTHQ) index. The estimated daily intake (EDI) (μg kg^{-1} day^{-1}) is the exposure to a chemical residue or consumption of a nutrient and was calculated considering the resulting metal concentration, crab consumption, and mean body weight chart for U.S. adults, following the next equation (**Eq. 2**) (U.S. Environmental Protection Agency, 2013):

$$EDI = \frac{C_m \times F_{IR}}{BW} \tag{2}$$

Here, Cm = metal concentration of the sample (mg kg^{-1} ww); FIR = seafood ingestion rate in the United States (0.227 g pers^{-1} day^{-1})

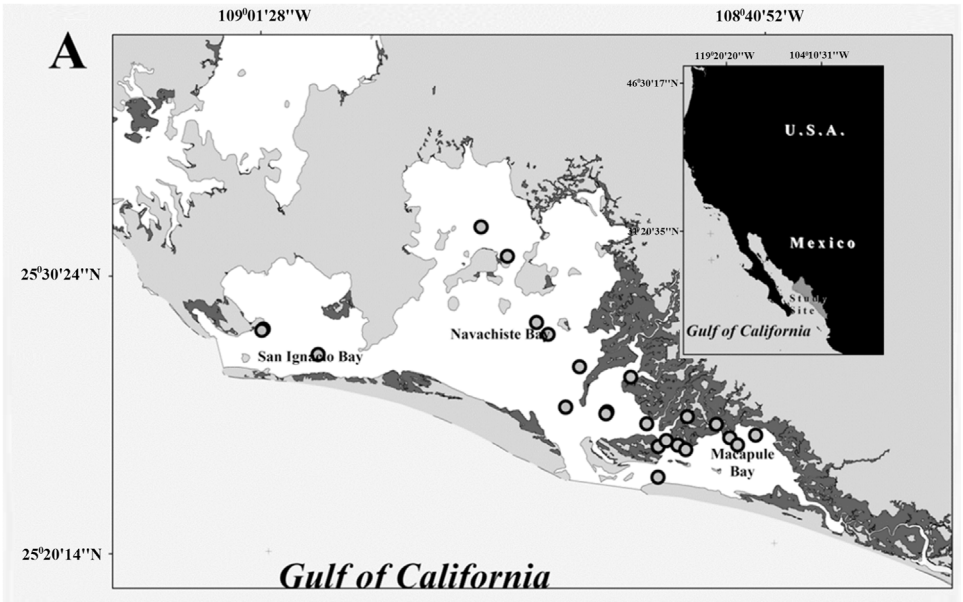

FIGURE 1 | NAV lagoon complex location and *C. bellicosus* sampling points.

(USEPA, 2000); and BW is the average body weight of adults, which was determined at 70 kg.

The target hazard quotient (THQ) (U.S. Environmental Protection Agency, 2005) is the health risk posed by the swimming warrior blue crab and was calculated based on the following equation (U.S. Environmental Protection Agency, 2018) (**Eq. 3**):

$$THQ = \frac{EF \times ED \times CS \times MC}{BW \times AT \times R_{FD}} \times 10^{-3} \quad (3)$$

where EF = exposure frequency (350 days year^{-1}), ED = human exposure duration—70 years (average lifetime), CS = seafood meal size in the United States for average crab consumers (0.227 g pers^{-1} day^{-1}), MC = metal concentration in one crab edible portion (mg kg^{-1} ww), BW = adult body weight (70 kg), AT = average time ($ED \times 365$ days/year), and R_{FD} = oral reference dose (mg kg^{-1} of body weight per day) (USEPA, 1989; 2000). R_{FD} is an estimate of daily oral exposure to a toxic substance during a lifetime for a human population (Bress, 2009). R_{FD} reported for Cd and Pb were 0.0003 and 0.00005 mg kg^{-1} day^{-1}, respectively (Hassett-Sipple et al., 1997); for Cu, Fe, Mn, Ni, and Zn, they were 0.04, 0.7, 0.024, 0.00026, and 0.3 mg kg^{-1} day^{-1}, respectively (U.S. Environmental Protection Agency, 2018).

The hazard index (HI) is the probability of developing a carcinogenic or non-carcinogenic risk and was calculated to evaluate the risk of all trace metals. It corresponds to the total of calculated THQ trace metal concentrations in all samples and indicates the ratio between exposure and the reference dose as follows (Jović and Stanković, 2014) (**Eq. 4**):

$$HI = \sum_{i=1}^{n} THQ_i \quad (4)$$

where THQ_i = target hazard quotient of individual trace metals and n = number of examined trace metals (in the present study, n = 7). HI, ≤1 means a non-probability of adverse carcinogenic risk; HI >1 indicates a probability of adverse effects, and HI ≥10 suggests the presence of a high likelihood of chronic risk (Lei et al., 2015).

In the present study, we calculated the target hazard quotient per sample (MHI) to determine the carcinogenic and non-carcinogenic risk per sample as follows (**Eq. 5**):

$$MHI = \left(\sum_{i=1}^{n} M_i THQ_i \right) \quad (5)$$

where MiTHQi = is the sum of the target hazard quotient of each trace metal per sample n (in the present study, n = 95). As in the THQ index, values of MHI ≤1 mean a non-probability of adverse carcinogenic risk, MHI >1 indicates a probability of adverse effects. MHI ≥10 suggests the presence of a high likelihood of chronic risk.

The data were statistically analyzed with SAS® (v. 9) and Statistica® (ver. 7) and $\log_{10}$ transformed for a Kolmogorov–Smirnov ($p > 0.05$, $\alpha = 0.05$) test and ANOVA ($p < 0.05$, $\alpha = 0.05$); when significant differences were detected a post hoc Tukey HSD (Vasavada, 2014) test was applied. Pearson's correlation test ($p < 0.05$) was used for trace metal concentration and weight, size, and physicochemical seawater parameters. A Spearman's correlation, followed by principal components analysis (PCA) ($p < 0.05$), was performed among seasons and physicochemical seawater parameters and trace metal concentrations.

RESULTS AND DISCUSSION

The weight of crabs ranged from 102 to 386 g ww (238.2 ± 76.7 g ww), the width and length of shell oscillated from 10.5 to 16.5 cm,

and 5.5–9 cm, respectively. The trace metal average concentrations (mg kg^{-1}) detected in the 95 edible samples of *C. bellicosus* were 1.77 ± 2.98 (Cd), 64.23 ± 30.94 (Cu), 65.18 ± 35.35 (Fe), 6.0 ± 4.04 (Mn), 6.34 ± 3.38 (Ni), 5.27 ± 2.97 (Pb), and 184.37 ± 76.21 (Zn). The ranges of trace metal concentrations were for Cd 0.073–11.034, Ni 0.18–12.63, Pb 0.88–13.63, Cu 18.15–190.77, Fe 24.57–257.64, Mn 0.024–14.82, and Zn 77.29–571.20. The concentration sequence of trace metals was Zn > Fe > Cu > Mn ≈ Ni > Pb > Cd. Higher concentrations of Zn, Fe, and Cu could be attributed to agricultural residues. This activity uses formulants that contain glyphosate-based herbicides and other pesticides usually rich in one or more of these metals (Defarge et al., 2018). This suggests that discharges from the surrounding agricultural or aquaculture activities are currently present at the NAV (Martínez-López et al., 2017) increasing after irrigation activities (Páez-Osuna and Osuna-Martínez, 2015). Discharged trace metal residues have been trapped in the NAV sediments, as previously reported (Montes et al., 2012) and bioaccumulated by *Callinectes* species. As previously reported, the presence of traces of metals in the edible tissue of crabs reflects contamination by metal residues in estuarine ecosystems (Anandkumar et al., 2019; Truchet et al., 2020), as occurring in NAV. Metals (Hg, Zn, Cd, Cu, and others), metalloids (As), and radioisotope residues are degraded very slowly due to their long geochemical cycle and the increase in disturbances and acceleration of metal residues produced by anthropogenic activities that may be accumulated in the sediments, where they can stay for years (Wuana and Okieimen, 2011), leading to the persistence of toxicants in the environment (Peng et al., 2009). After that, they become bioavailable and are absorbed by marine biota after the irrigation season that begins in October (presowing) and ends in January (Sifuentes et al., 2016). However, more studies must be done to correlate the bioavailability of trace metal concentrations with sedimentation rates, pollutants, and organic matter concentrations in the effluents.

In the NAV system, anthropic source metals are added and dispersed in the lagoon. These anthropic compounds contain Cd and Pb impurities, which increase their content in the soil after fertilization application (Wuana and Okieimen, 2011). Local reports indicate that in phosphate fertilizers, the average content of Pb and Cd is 10.9 and 10.4 mg kg^{-1}, respectively; for nitrogen fertilizers, Pb and Cd contents are 4.7 mg and 2.03 mg kg^{-1}, respectively (Romano Casas et al., 2019). The primary source of phosphorus fertilizers is phosphorite rocks, mainly consisting of apatite naturally enriched by lanthanides such as Cu, Ni, and Zn (Boumaza et al., 2021). These fertilizers, widely used in Sinaloa, are an essential source of diverse elements in soils. In the region, Cd concentrations are low during the spring, with a slight increase in late summer (Romano Casas et al., 2019). These concentrations could be associated with the indiscriminate use/application of fertilizers that, consequently, drain their residues into the NAV and with primary productivity in the water column, the content of organic matter, clay minerals, and hydrothermal events during its formation.

In the present study, the highest concentrations of metals in sediments and tissues of *C. bellicosus* were found in April, 2 months after the irrigation season, and in sites nearby or in front of the effluents of wastewater from agriculture or aquaculture activities (sites 2, 3, 4, and 5; **Figure 2**). It has been observed that an increase in trace metal concentrations begins in the spring (dry) and decreases during the summer (wet) and winter (dry), 2–3 months after agricultural or aquaculture wastewater discharges. During the sedimentation process that can take months, trace metal residues are precipitated to the sediments (Saleh, 2021), and their composition varies by resuspension, biogeochemical interactions with sourcing areas, sediment resuspension transport, depositional rates, and diagenesis processes (Spagnoli and Bergamini, 1997; Spagnoli et al., 2021). Griboff et al. (2020) found correlations between some trace metals and the dry seasons, resembling the results found in this work. The accumulation of metal residues in sediments of an aquatic system contributes to their dispersion and bioavailability to marine biota. These dispersions and bioavailability in the NAV increase with the presowing irrigation from October to January in the Guasave valley (Sifuentes et al., 2016).

The presence of trace metals in the edible tissue of biota, and sediments from the NAV have been previously reported (Orduna-Rojas and Longoria-Espinoza, 2006; Reyes-Montiel, 2013; Aguilar-Gonzalez et al., 2014; Granados-Galván et al., 2015; Páez-Osuna and Osuna-Martínez, 2015). Trace metals have an affinity with organic matter, which is incorporated into the marine sediments of coastal lagoons, such as NAV. In the sediments, these trace metals become bioavailable, and bioaccumulation of metals in *C. bellicosus* could be related to the feeding habits of the species, the rates of absorption and depuration, the environmental conditions, the bioavailability of the metals, the fine texture of the sediments, $CaCO_3$ content, and organic matter content (Jerome and Chukwuka, 2016; Álvaro et al., 2016; Chuan et al., 2017; Genç and Yilmaz, 2017; Çoğun et al., 2017; Annabi et al., 2018; Baki et al., 2018; Durmus et al., 2018; Saber et al., 2018; Hao et al., 2019; Cruz et al., 2021). *C. bellicosus* is an omnivorous species that induces bioturbation of sediments by mixing and resuspending the organic matter associated with the sediment, improving the bioavailability of trace metals (Andrade et al., 2020; Truchet et al., 2020), which are ingested and bioaccumulated in different tissues of this crab.

In invertebrates, the molting stage occurs as a growth process. It is a critical moment in the detoxification of bioaccumulated metals (Anandkumar et al., 2019) that depends mainly on the presence of metallothioneins. Metallothioneins play a role in detoxifying trace metals in estuarine crabs that can translocate and bioaccumulate in the tissues (Truchet et al., 2020). However, the concentrations of these proteins are related to changes in natural factors, such as salinity, weight, or sex (Legras et al., 2000). Indeed, for *C. bellicosus*, it is recommended to carry out studies regarding the concentration of these molecules and perform a correlation with the physiochemical seawater parameters to elucidate whether trace metal concentrations in *C. bellicosus* tissues are

TABLE 1 | Average metal content (mg^{-1} kg^{-1}) in muscle tissue of different crab species.

Element	*C. bellicosus* (this study)	*P. marmoratus*[a]	*P. segnis*[b]	*C. sapidus*	*C. amnicola*[f]	*P. sanguinolentus*	*T. crenata*	*M. victor*	*E. verrucosa*	*Scylla* spp.
Cu	64.23 ± 30.94	172.91 ± 7.88	206.45 ± 71.88	**9.26 ± 0.53**[c] **18.214 ± 2.60**[d] **2.8 ± 0.21**[e]	**9.48–12.76**	**17.205 ± 0.53**[g]	**30.735 ± 0.36**[g]	**11.4 ± 0.44**[g]	**42.2± 4.8**[h]	65.8[i]
Cd	1.77 ± 2.98	**1.22 ± 1.13**	**0.21 ± 0.03**	**1.23 ± 0.19**[c] **0.161 ± 0.24**[d] **0.313 ± 0.048 SE**[e]	**0.16–0.46**	19.48 ± 0.06[g]	12.1 ± 0.29[g]	8.03 ± 0.29[g]		**0.17**[i]
Fe	65.18 ± 35.35	658.33 ± 0.1	85.05 ± 18.58	120.64 ± 0.81[e]		**29.56 ± 1.71**[g]	168.62 ± 1.68[g]	69.9 ± 2.5[g]	81.68 ± 5.32[h]	
Ni	6.34 ± 3.38	**5.56 ± 0.80**		12.02 ±					**2.13 ± 0.19**[h]	
Mn	6.00 ± 4.04	36.42 ± 11.05	**0.41 ± 0.08**	0.29[e]		89.706 ± 1.26[g]	10.147 ± 0.2[g]	6.5 ± 3.48[g]	39 ± 2.9[h]	
Pb	5.27 ± 2.97	**0.38**	**0.4 ± 0.17**	**2.66 ± 0.23**[c] **1.208 ± 0.13**[d]	**1.48 ± 3.17**	< **0.06**[g]	< **0.06**[g]	< **0.06**[g]		**0.20**[i]
Zn	184.37 ± 76.21	**146.19 ± 6.1**	590.04 ± 196.9	**28.71 ± 2.23**[c] **43.98 ± 3.44**[d] **11.197 ± 0.77**[e]	**2.21—3.65**[f] **16.71 ± 0.77**	**47.37 ± 0.37**[g]	**61.921 ± 0.43**[g]	**22.6 ± 0.2**[g]	284.85 ± 12.9[h]	**175**[i]

Bold data indicate lower trace metal concentrations than those detected in the present study.
[a]*Álvaro et al. (2016).*
[b]*Annabi et al. (2018).*
[c]*Çoğun et al. (2017).*
[d]*Gençand Yilmaz (2017).*
[e]*Saber et al. (2018).*
[f]*Jerome and Chukwuka (2016).*
[g]*Baki et al. (2018).*
[h]*Durmus et al. (2018).*
[i]*Chuan et al. (2017).*

affected. The crab *C. bellicosus* showed higher Cu, Pb, and Zn traces than other estuarine crabs (**Table 1**). Higher trace metal concentrations in tissues indicate a more significant human disturbance of aquatic systems (Chuan et al., 2017; Genç and Yilmaz, 2017; Baki et al., 2018; Saber et al., 2018). In this sense, the agriculture and aquaculture activities and the increased number of sailing vessels and artisanal outboard fishing in the NAV (Carrasquilla-Henao et al., 2013; Aguilar-Gonzalez et al., 2014) are increasing the bioavailability of trace metals. This correlation of bioavailability and human pollution sources has been previously described. Hamed and Emara (2006) reported high Cu, Zn, Pb, Cd, Cr, Ni, Fe, and Mn in *Patella caerulea* tissue in the Suez Canal. Bazzi (2014) determined that in sediments and marine organisms of the Gulf of Chabahar, the highest values of Zn, Pb, and Cu. In both studies, as in the present, a correlation was found between trace metal concentrations in organisms and human activities, such as shipping, marine transportation, fisheries, and drainage. This higher concentration of Pb in *C. bellicosus* could be explained by the potential use of glyphosate-based pesticides in the region (Balderrama-Carmona et al., 2020), which includes Pb in their formulation (Defarge et al., 2018), and its bioavailability could be increased by the constant wastewater discharges from urban and agricultural areas into the NAV (Álvaro et al., 2016). Zn has been reported to have a high affinity for organic carbon in sediments (Cyriac et al., 2021) and is an essential component of the reproductive coenzymes in the genus *Callinectes* (Çoğun et al., 2017). In this report, the concentration of Zn and the higher concentrations of Cu confirm the relevance of these elements in the metabolism of estuarine crabs (Anandkumar et al., 2019) like *C. bellicosus*. In addition, the high concentration of Zn and Cu (and the other trace metals) could also be attributed to the high phosphorus, urea, and TSS concentrations that have been reported in the area from April to November drained by agriculture and shrimp aquaculture (Martínez-López et al., 2017; Góngora-Gómez et al., 2018).

Among seasons, Spearman's correlation revealed no significant differences ($p < 0.05$) between trace metals and pH in the spring, salinity, and temperature in the winter (**Table 2**).

TABLE 2 | Pearson's correlation results of the trace metal concentration in the edible tissue of *C. bellicosus* and the seawater physicochemical parameters of salinity (‰), pH, conductivity (σ), and temperature (T°C).

Trace metal	‰	pH	σ	T°C
Cu	–0.1	–0.2	–0.3	0.2
Fe	0.1	–0.1	0.1	–0.1
Mn	0.5	0.1	0.4	–0.2
Zn	0.1	0.0	0.0	–0.1
Cd	0.2	–0.1	–0.9	–0.1
Ni	0.4	–0.2	0.3	–0.1
Pb	–0.1	0.1	0.1	0.3

Principal components analysis showed that Mn concentration, conductivity (σ), and salinity (S‰) were negatively correlated. Summer Pb concentrations showed a negative correlation with temperature (**Figure 3**). Associations of Mn and Ni were revealed with conductivity, pH, and salinity in the spring and late autumn and between Pb and temperature in the summer. About weight and trace metal concentrations, a significantly low mean negative correlation ($p < 0.01$) was determined between Zn and weight ($r = -0.4$). The rest of the trace metals showed a non-significant correlation with weight. After the PCA per season ($p < 0.05$), the spring Ni concentrations were high and low negative with *s* and pH, respectively. The first two principal components of the multivariate analysis explained 95% of the variance (**Figure 2**).

Metal concentrations in the edible tissue of *C. bellicosus* from the NAV revealed the presence of trace metals that could pose a risk if higher concentrations and portions are consumed. ANOVA showed significant differences among trace metal concentrations ($p < 0.01$). At a consumption rate of $0.227\ g^{-1}\ day^{-1}$, the average of all trace metal concentrations in the present study was higher than the

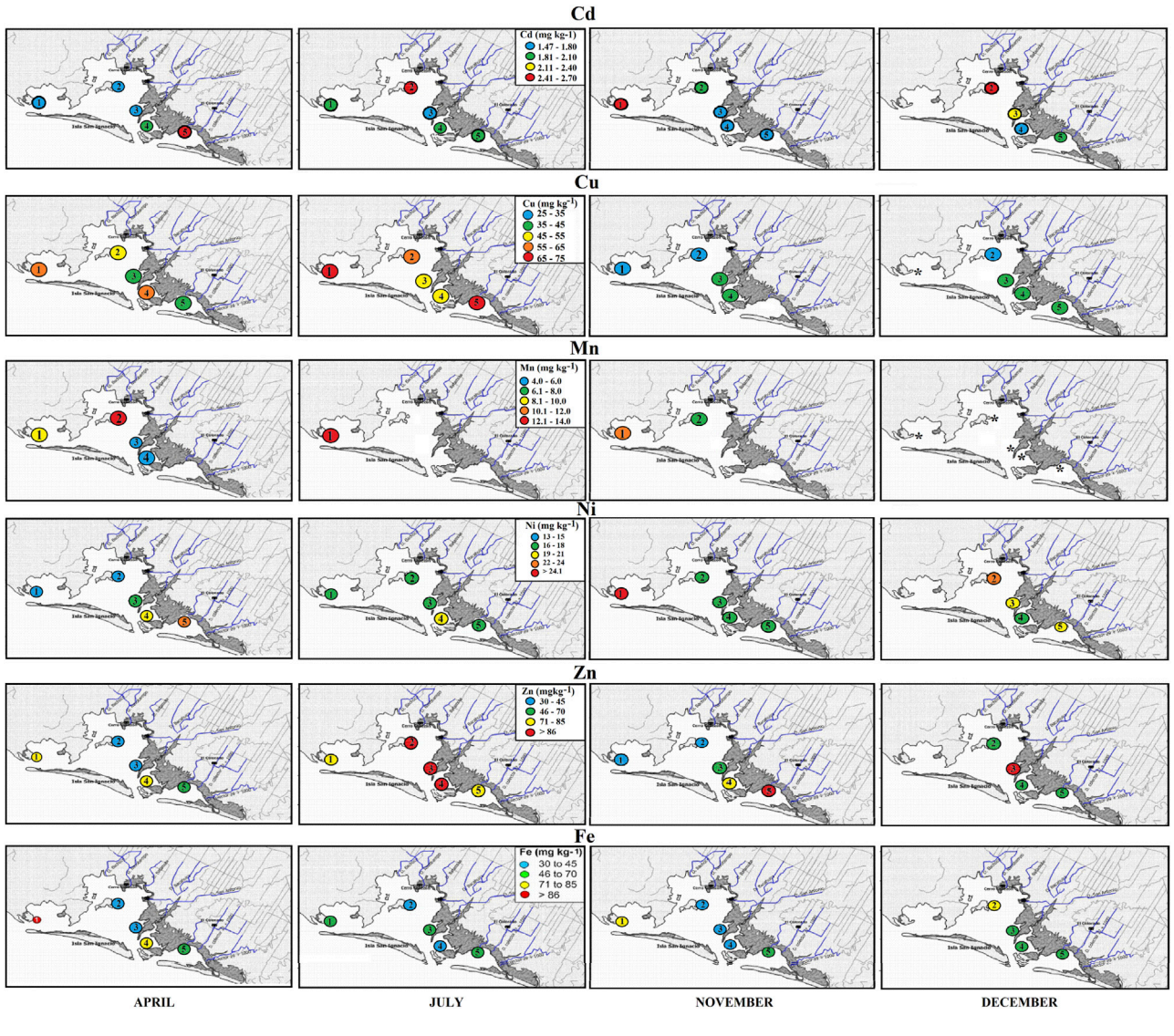

FIGURE 2 | Average trace metal concentration in the edible tissue of *C. bellicosus* from the collecting sites in the NAV complex, Mexico.

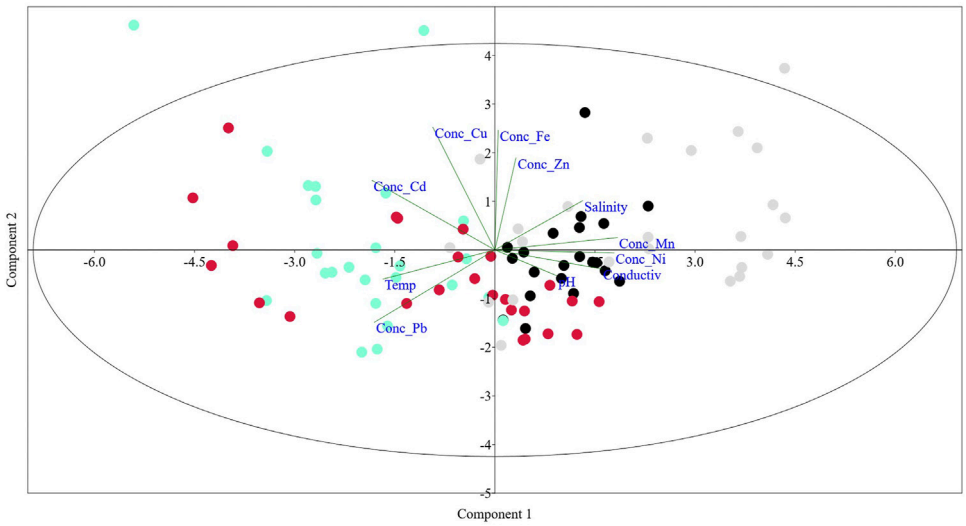

FIGURE 3 | PCA correlation between water physicochemical parameters and trace metals in the edible tissue of *C. bellicosus* from the NAV complex, Mexico.

maximum residual limits (MRLs) delineated by the European Union (EC, 2008), and the United States Food and Drug Administration (National Shellfish Sanitation Program, 2007). The MRLs (in mg kg^{-1} dw) in edible tissues of crustaceans for the EU and the United States are, respectively, for Cd of 0.5 and 3.0; for Ni of 2.8 and 70; and for Pb of 0.5 and 1.5; whereas for Cu, Fe, Mn, and Zn, no records of allowable limits were found. For sediment reference, the Canadian Sediment Quality Guidelines for the Protection of Aquatic Life reference (Canadian Council of Ministers of the Environment, 1999) were used. Fe, Mn, and Zn were abundant elements and presented the following order of concentration: Fe > Mn > Zn > Pb > N > Cu. The primary source of the first element's contribution is weathering of the rocks in the drainage basin. A local report by the Consejo de Recursos Minerales (1991) indicates mineral deposits of Au, Ag, Zn, Pb, Cu, and some of Fe, Ni, Co, Bi, and ferriferous deposits constituted by Fe_3O_4 (72% of Fe). Iron is present in sediments as iron oxyhydroxides that influence the release of other elements in response to pH changes, affecting the adsorption or desorption of other metals (Queiroz et al., 2021). Correlation coefficients (r^2) indicated positive values mainly between Fe and Zn (0.8), Fe and Mn (0.6), Mn and Ni (0.70), and Mn and Cu (0.8), indicating the influence of Fe and Mn oxides on the release of elements. Fe and Mn oxides exert control on the adsorption or coprecipitation of elements in sediments (Turner, 2000) in the lagoon system. These properties during seasonal rains, irrigation in agricultural fields, water exchange in aquaculture farms, and others probably contribute to the flow of these inorganic and organic components in the system, thus modifying the natural conditions and bioaccumulation in organisms.

The enrichment factor (EF) and the geoaccumulation index (Igeo) data of ISQG, the continental crust content (Taylor, 1964), preindustrial levels, and Fe as a normalizing element (Salomons and Förstner, 2012) were used as references (Appendix 1). The geochemical index indicated Pb as uncontaminating to moderately contaminating in January (2017) and Cd as moderately contaminating in April (2016). On the other hand, the enrichment factor presented a similar condition to that of Cd, revealing a severe enrichment of sediments, and Pb as moderately severe to moderately enriched (**Table 3**). The normalized data of the other elements indicated a lower enrichment and related them with natural sources in the system.

Regarding the risk assessment, the mean EDI values (μg kg^{-1} bw d^{-1}) of the selected metals ranged from 0.005 to 0.537 in the following sequence: Zn > Fe > Cu > Ni > Mn > Pb > Cd. The highest EDI was for Zn, Fe, and Cu (0.54, 0.19, and 0.19 μg kg^{-1} day^{-1}, respectively); Zn, Cu, and Cd were above the acceptable daily intake consumption. In contrast, Ni and Mn were similar to reference values (FAO and WHO, 2013), at a rate of 0.227 g^{-1} day^{-1}, and represent a low concentration for the portion established for consumption of trace metals in the *C. bellicosus* edible tissue (EDI < 1). The average THQ ranged between 0.03 and 6.32. Zn, Cu, and Cd were the trace metals with a THQ > 1 (7.68, 4.74, and 1.76, respectively), turning these ratios into an exposure risk to trace metals in the edible tissue of the blue swimming warrior crab. The values of HI > 1 represent a potential exposure to trace metals and adverse effects (Jerome and Chukwuka, 2016; Genç and Yilmaz, 2017; Baki et al., 2018). In the present study, the HI = 16.11 showed a potential exposure to trace metals in the edible tissue of *C. bellicosus* (**Table 4**). The MHI for each sample showed that 93 samples (98%) exhibited an MHI > 1, indicating a potential carcinogenic or non-carcinogenic health risk of *C. bellicosus* edible tissue consumption (**Figure 4**).

TABLE 3 | Enrichment factor and the geoaccumulation index of trace metals in sediment samples of the Navachiste coastal lagoon system, Mexico.

	Cu	Fe (%)	Mn	Zn	Cd	Ni	Pb
April-16	7.0 ± 2.3	1.6 ± 0.2%	228.2 ± 73.6	50.2 ± 54.4	0.97 ± 0.49	10.0 ± 3.7	9.0 ± 4.2
Jan-17	2.33 ± 1.6	1.8 ± 0.3%	286.1 ± 47.0	50.9 ± 9.3	—	12.5 ± 1.6	24.6 ± 8.4
April-17	6.2 ± 2.7	1.94 ± 0.25%	295.5 ± 55.6	48.35 ± 7.6	—	6.6 ± 2.6	9.9
Bazzi (2014) Inv	21.85–46.8	14.2–53.5	43.2–84.4	16.2–43.1	0.4–0.8	11.7–26.4	13.9–28.2
Bazzi (2014) Ver	10.97–54.76	12.8–52.1	46.9–89.1	18.8–40.1	0.2–0.5	8.3–28.7	10.7–25.6
Laguna Unare, Venezuela (Marquez)	41.1	1.56%	516.4	127.5	1.51	52.4	29
ISQG[a]	18.7	—	—	124	0.7	—	30.2
SQS2	390	—	—	410	5.1	—	450
TEL2	18.7	—	—	124	0.6	15.9	30.2
PEL[a]	108	—	—	271	4.2	42.8	112
ERL2	34	—	—	150	1.2	20.9	46.7
ERM2	270	—	—	410	9.6	51.6	218
Continental crust (Taylor, 1964)	55	5.6%	950	70	0.2	75	12.5
Sadiq (1992)[b] Ref	<10	—	—	<110	<1	<10	<5
Salomons and Forstner (1984)[c]	45	47000	600	95	0.2	68	20

[a]*Interim marine sediments quality guidelines (Canadian sediment quality guidelines for the protection of aquatic life) (ISQG, Interim sediment quality guideline; PEL, Probable effect level).*
[b]*Non-contaminated sediments Marquez et al. (2008) TEL.*
TEL2, threshold effect levels. Concentrations below TEL are not associated with any adverse biological effect. Between TEL and PEL, an adverse biological effect can occur occasionally and frequently above PEL. SQS, quality standards of marine sediments. The quality criterion corresponding to sediments neither related with adverse effects on biological resources, including acute and chronic, nor significant risks for human health (WAC, 1995; cited in Fuentes-Hernandez et al., 2019). ERL, low effects interval; ERM, moderate effect interval.
[c]*Preindustrial data, from Salomons & Forstner (2012).*

TABLE 4 | Average concentration of trace metals, reference dose (RfD), non-carcinogenic health risk (THQ), and hazard risk (HI) in the edible tissue of *C. bellicosus* from the Navachiste coastal lagoon system in Mexico.

Trace metal	Concentration (mg kg^{-1}) *M* ± *SD*	RfD (mg kg^{-1} day^{-1})	(THQ)	EDI
Cu	64.23 ± 30.94	0.04[a]	5.29	0.18723
Cd	1.77 ± 2.98	0.001[b]	5.13	0.00535
Fe	65.18 ± 35.35	0.7[a]	0.30	0.18999
Mn	6.00 ± 4.04	0.024[a]	0.75	0.01790
Ni	6.34 ± 3.38	0.02[a]	1.01	0.01847
Pb	5.27 ± 2.97	0.5[c]	0.03	0.01502
Zn	184.37 ± 76.21	0.3[a]	2.15	0.53741
Hazard Index (HI)	14.74	∑ THQ	10.72	

[a]*Hassett-Sipple et al. (1997).*
[b]*U.S. Environmental Protection Agency (2018).*
[c]*Limit of lead content in white edible tissues of crustaceans (European Commission, 2014).*

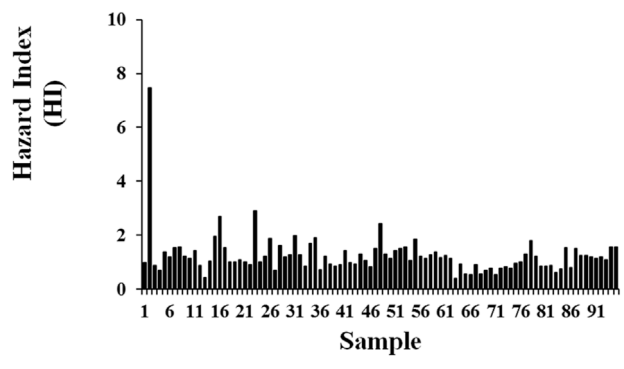

FIGURE 4 | HI per sample of metal residues in the edible tissue of *C. bellicosus* from the NAV complex, Mexico.

CONCLUSION

The metal residue concentrations in the edible tissue of *C. bellicosus* from the NAV complex were above the maximum allowed metal concentrations in crabs for consumption. Consumption of the edible tissue of *C. bellicosus* from the NAV reveals a risk hazard, including carcinogenic or non-carcinogenic risks. The constant drains from the agricultural Guasave Valley and aquaculture activities after irrigation or wastewater drainage maintain trace metal bioavailability and uptake by the lagoon biota, including the *C. bellicosus* crab species. Pollution from human activities has been reported for a long time. Findings from the present study confirm the lack of strategies to reduce or avoid the discharge of these pollutants into the lagoon or the use of banned pesticides and fertilizers, whose residues are being discharged into the NAV lagoon complex.

According to the estimated daily intake (EDI), target hazard quotient (THQ), hazard index (HI), and THQ per sample (MHI), the consumption of *C. bellicosus* edible tissue represents a health risk at a rate of 0.227 g^{-1} day^{-1} consumption. This risk would be intensified if the consumption rate increases above 1.2 g^{-1} day^{-1} $pers^{-1}$.

DATA AVAILABILITY STATEMENT

The raw data supporting the conclusion of this article will be made available by the authors, without undue reservation.

AUTHOR CONTRIBUTIONS

All authors listed have made a substantial, direct, and intellectual contribution to the work and approved it for publication.

FUNDING

This work was supported by the Instituto Politécnico Nacional (Grants: SIP-2012-0079, SIP-2013-0398, SIP-2014-0036, SIP-2015-0346, Multidisciplinary SIP-2016-1452) and the FOMIX CONACYT-CAMPECHE (grant number 144280, 2014).

REFERENCES

Aguilar-gonzález, M. E., Luna-gonzález, A., Aguirre, A., Zavala-Norzagaray, A. A., Mundo-Ocampo, M., and González-ocampo, H. A. (2014). Perceptions of fishers to Sea Turtle Bycatch, Illegal Capture and Consumption in the San Ignacio-Navachiste-Macapule Lagoon Complex, Gulf of California, Mexico. *Integr. Zoolog.* 9, 70–84. doi:10.1111/1749-4877.12024

Álvaro, N. V., Neto, A. I., Couto, R. P., Azevedo, J. M. N., and Rodrigues, A. S. (2016). Crabs Tell the Difference - Relating Trace Metal Content with Land Use and Landscape Attributes. *Chemosphere* 144, 1377–1383. doi:10.1016/j.chemosphere.2015.10.022

Anandkumar, A., Nagarajan, R., Prabakaran, K., Bing, C. H., Rajaram, R., Li, J., et al. (2019). Bioaccumulation of Trace Metals in the Coastal Borneo (Malaysia) and Health Risk Assessment. *Mar. Pollut. Bull.* 145, 56–66. doi:10.1016/j.marpolbul.2019.05.002

Andrade, V. S., Wiegand, C., Pannard, A., Gagneten, A. M., Pédrot, M., Bouhnik-Le Coz, M., et al. (2020). How Can Interspecific Interactions in Freshwater Benthic Macroinvertebrates Modify Trace Element Availability from Sediment? *Chemosphere* 245, 125594. doi:10.1016/j.chemosphere.2019.125594

Annabi, A., Bardelli, R., Vizzini, S., and Mancinelli, G. (2018). Baseline Assessment of Heavy Metals Content and Trophic Position of the Invasive Blue Swimming Crab Portunus Segnis (Forskål, 1775) in the Gulf of Gabès (Tunisia). *Mar. Pollut. Bull.* 136, 454–463. doi:10.1016/j.marpolbul.2018.09.037

Baki, M. A., Hossain, M. M., Akter, J., Quraishi, S. B., Haque Shojib, M. F., Atique Ullah, A. K. M., et al. (2018). Concentration of Heavy Metals in Seafood (Fishes, Shrimp, Lobster and Crabs) and Human Health Assessment in Saint Martin Island, Bangladesh. *Ecotoxicology Environ. Saf.* 159, 153–163. doi:10.1016/j.ecoenv.2018.04.035

Balderrama-Carmona, A. P., Valenzuela-Rincón, M., Zamora-Álvarez, L. A., Adan-Bante, N. P., Leyva-Soto, L. A., Silva-Beltrán, N. P., et al. (2020). Herbicide biomonitoring in agricultural workers in Valle del Mayo, Sonora Mexico. *Environ. Sci. Pollut. Res.* 27, 28480–28489. doi:10.1007/s11356-019-07087-6

Bazzi, A. O. (2014). Heavy Metals in Seawater, Sediments and marine Organisms in the Gulf of Chabahar, Oman Sea. *J. Oceanogr. Mar. Sci.* 5, 20–29. doi:10.5897/joms2014.0110

Boumaza, B., Kechiched, R., and Chekushina, T. V. (2021). Trace Metal Elements in Phosphate Rock Wastes from the Djebel Onk Mining Area (Tébessa, Eastern Algeria): A Geochemical Study and Environmental Implications. *Appl. Geochem.* 127, 104910. doi:10.1016/j.apgeochem.2021.104910

Breder, R. (1982). Optimization Studies for Reliable Trace Metal Analysis in Sediments by Atomic Absorption Spectrometric Methods. *Z. Anal. Chem.* 313, 395–402. doi:10.1007/bf00495841

Bress, B. (2009). "Risk Assessment," in *Chapter 14 - Risk AssessmentPharmacology*. Editors M. Hacker, W. Messer, and K. Bachmann (San Diego: Academic Press), 353–369. doi:10.1016/b978-0-12-369521-5.00014-2

Carrasquilla-Henao, M., González Ocampo, H. A., Luna González, A., and Rodríguez Quiroz, G. (2013). Mangrove forest and Artisanal Fishery in the Southern Part of the Gulf of California, Mexico. *Ocean Coastal Manag.* 83, 75–80. doi:10.1016/j.ocecoaman.2013.02.019

Canadian Council of Ministers of the Environment (1999). in *Canadian Sediment Quality Guidelines for the protection of Aquatic Life*. Editor C. C. O. M. O. T. Environment (Winnipeg, CA).

Chuan, O. M., Ali, N. a. M., Shazili, N. a. M., and Bidai, J. (2017). Selected Heavy Metals Concentration in Edible Tissue of the Mud Crab, Genus *Scylla* from Setiu Wetlands, Terengganu. *J. Sustainability Sci. Manag.* 12, 112–118.

Çoğun, H. Y., Firat, Ö., Aytekin, T., Firidin, G., Firat, Ö., Varkal, H., et al. (2017). Heavy Metals in the Blue Crab (*Callinectes sapidus*) in Mersin Bay, Turkey. *Bull. Environ. Contam. Toxicol.* 98, 824–829. doi:10.1007/s00128-017-2086-6

Cruz, A. C. F., Pauly, G. F. E., Araujo, G. S., Gusso-Choueri, P., Fonseca, T. G., Campos, B. G., et al. (2021). Metal Bioaccumulation by the Neotropical Clam *Anomalocardia Flexuosa* to Estimate the Quality of Estuarine Sediments. *Bull. Environ. Contam. Toxicol.* 107 (1), 106–113. doi:10.1007/s00128-020-03062-x

Cyriac, M., Gireeshkumar, T. R., Furtado, C. M., Fathin, K. P. F., Shameem, K., Shaik, A., et al. (2021). Distribution, Contamination Status and Bioavailability of Trace Metals in Surface Sediments along the Southwest Coast of India. *Mar. Pollut. Bull.* 164, 112042. doi:10.1016/j.marpolbul.2021.112042

Defarge, N., Spiroux de Vendômois, J., and Séralini, G. E. (2018). Toxicity of Formulants and Heavy Metals in Glyphosate-Based Herbicides and Other Pesticides. *Toxicol. Rep.* 5, 156–163. doi:10.1016/j.toxrep.2017.12.025

Delgado-Alvarez, C., Ruelas-Inzunza, J., Escobar-Sánchez, O., Covantes-Rosales, R., Pineda-Pérez, I. B., Osuna-Martínez, C. C., et al. (2019). Metal Concentrations in Age-Groups of the Clam, *Megapitaria Squalida*, from a Coastal Lagoon in Mexico: A Human Health Risk Assessment. *Bull. Environ. Contam. Toxicol.* 103, 822–827. doi:10.1007/s00128-019-02723-w

Durmus, M., Ayas, D., Aydin, M., Kosker, A. R., Ucar, Y., and Ozogul, Y. (2018). The Effects of Sex and Seasonality on the Metal Levels of Warty Crab (*Eriphia Verrucosa*) in the Black Sea. *J. Aquat. Food Product. Tech.* 27, 749–758. doi:10.1080/10498850.2018.1485196

Ec (2008). *Commission Regulation (EC) No 629/2008 of 2 July 2008 Amending Regulation (EC) No 1881/2006 Setting Maximum Levels for Certain Contaminants in Foodstuffs*. Luxemburgo: Official Journal of the European Union.

Fao, and Who (2013). *Pesticide Residues In Food And Feed* [Online]. Food and Agriculture Organization Af the United Nations - World Health Organization. Available: http://www.codexalimentarius.net/pestres/data/pesticides/index.html?lang=en (Accessed Aug 10th, 2013).

Genç, T. O., and Yilmaz, F. (2017). Metal Accumulations in Water, Sediment, Crab (*Callinectes sapidus*) and Two Fish Species (*Mugil cephalus* and *Anguilla anguilla*) from the Köyceğiz Lagoon System-Turkey: An Index Analysis Approach. *Bull. Environ. Contam. Toxicol.* 99, 173–181. doi:10.1007/s00128-017-2121-7

Góngora-Gómez, A. M., Domínguez-Orozco, A. L., Domínguez-Orozco, A. L., Villanueva-Fonseca, B. P., Muñoz-Sevilla, N. P., and García-Ulloa, M. (2018). Seasonal Levels of Heavy Metals in Soft Tissue and Muscle of the Pen Shell *Atrina Maura* (Sowerby, 1835) (Bivalvia: Pinnidae) from a Farm in the southeastern Coast of the Gulf of California, Mexico. *Rev. Int. Contam. Ambie.* 34, 57–68. doi:10.20937/rica.2018.34.01.05

Granados-Galván, I. A., Rodríguez-Meza, D. G., Luna-González, A., and González-Ocampo, H. A. (2015). Human Health Risk Assessment of Pesticide Residues in

Snappers (Lutjanus) Fish from the Navachiste Lagoon Complex, Mexico. *Mar. Pollut. Bull.* 97, 178–187. doi:10.1016/j.marpolbul.2015.06.018

Griboff, J., Wunderlin, D. A., Horacek, M., and Monferrán, M. V. (2020). Seasonal Variations on Trace Element Bioaccumulation and Trophic Transfer along a Freshwater Food Chain in Argentina. *Environ. Sci. Pollut. Res.* 27, 40664–40678. doi:10.1007/s11356-020-10068-9

Hamed, M. A., and Emara, A. M. (2006). Marine Molluscs as Biomonitors for Heavy Metal Levels in the Gulf of Suez, Red Sea. *J. Mar. Syst.* 60, 220–234. doi:10.1016/j.jmarsys.2005.09.007

Hao, Z., Chen, L., Wang, C., Zou, X., Zheng, F., Feng, W., et al. (2019). Heavy Metal Distribution and Bioaccumulation Ability in marine Organisms from Coastal Regions of Hainan and Zhoushan, China. *Chemosphere* 226, 340–350. doi:10.1016/j.chemosphere.2019.03.132

Hassett-Sipple, B., Swartout, J., and Schoeny, R. (1997). "Mercury Study Report to Congress," in *Volume 5. Health Effects of Mercury and Mercury Compounds* (Research Triangle Park, NC (United State): Environmental Protection Agency).

Jalali, M., and Hemati, N. (2013). Chemical Fractionation of Seven Heavy Metals (Cd, Cu, Fe, Mn, Ni, Pb, and Zn) in Selected Paddy Soils of Iran. *Paddy Water Environ.* 11, 299–309. doi:10.1007/s10333-012-0320-8

Jerome, F. C., and Chukwuka, A. V. (2016). Metal Residues in Flesh of Edible Blue Crab,Callinectes Amnicola, from a Tropical Coastal Lagoon: Health Implications. *Hum. Ecol. Risk Assess. Int. J.* 22, 1708–1725. doi:10.1080/10807039.2016.1219220

Jović, M., and Stanković, S. (2014). Human Exposure to Trace Metals and Possible Public Health Risks via Consumption of Mussels *Mytilus galloprovincialis* from the Adriatic Coastal Area. *Food Chem. Toxicol.* 70, 241–251. doi:10.1016/j.fct.2014.05.012

Legras, S., Mouneyrac, C., Amiard, J. C., Amiard-Triquet, C., and Rainbow, P. S. (2000). Changes in Metallothionein Concentrations in Response to Variation in Natural Factors (Salinity, Sex, Weight) and Metal Contamination in Crabs from a Metal-Rich Estuary. *J. Exp. Mar. Biol. Ecol.* 246, 259–279. doi:10.1016/s0022-0981(99)00187-2

Lei, M., Tie, B.-Q., Song, Z.-G., Liao, B.-H., Lepo, J. E., and Huang, Y.-Z. (2015). Heavy Metal Pollution and Potential Health Risk Assessment of white rice Around Mine Areas in Hunan Province, China. *Food Sec.* 7, 45–54. doi:10.1007/s12571-014-0414-9

Martínez-López, A., Hakspiel-Segura, C., Escobedo-Urías, D. C., and González-Acosta, B. (2017). Influence of Agriculture and Aquaculture Activities on the Response of Autotrophic Picoplankton in Laguna Macapule, Gulf of California (Mexico). *Ecol. Process.* 6, 6. doi:10.1186/s13717-017-0074-8

Martínez-Valenzuela, C., Gomez-Arroyo, S., Villalobos-Pietrini, R., Waliszewski, S., Calderon-Segura, M. E., Felix-Gastelum, R., et al. (2009). Genotoxic Biomonitoring of Agricultural Workers Exposed to Pesticides in the North of Sinaloa State, Mexico. *Environ. Int.* 35 (8), 1155–1159. doi:10.1016/j.envint.2009.07.010

Mateo-Sagasta, J., Zadeh, S. M., and Turral, H. (2018). *More People, More Food, Worse Water?: A Global Review of Water Pollution from Agriculture*. Italy: Rome.

Meena, R. a. A., Sathishkumar, P., Ameen, F., Yusoff, A. R. M., and Gu, F. L. (2017). Heavy Metal Pollution in Immobile and mobile Components of Lentic Ecosystems—A Review. *Environ. Sci. Pollut. Res.* 25, 1–15. doi:10.1007/s11356-017-0966-2

Montes, A. M., González-Farias, F. A., and Botello, A. V. (2012). Pollution by Organochlorine Pesticides in Navachiste-Macapule, Sinaloa, Mexico. *Environ. Monit. Assess.* 184, 1359–1369. doi:10.1007/s10661-011-2046-2

National Shellfish Sanitation Program (2007). "Guide for the Control of Molluscan Shellfish: 2007 Revision," in *Section IV. Guidance Documents. Chapter II. Growing Areas*. Editor N. S. S. Program (Food and Drug Administration: National Shellfish Sanitation Program).

Orduña-Rojas, J., and Longoria-Espinoza, R. M. (2006). Metal Content in *Ulva Lactuca* (Linnaeus) from Navachiste Bay (Southeast Gulf of California) Sinaloa, Mexico. *Bull. Environ. Contam. Toxicol.* 77, 574–580. doi:10.1007/s00128-006-1102-z

Ortega-Lizárraga, G. G., Rodríguez-Domínguez, G., Pérez-González, R., Aragón-Noriega, E. A., and Mendivil-Mendoza, J. E. (2020). Análisis de la pesquería de jaiba en la región sureste del golfo de California, México. *Rbmo* 55, 59–67. doi:10.22370/rbmo.2020.55.1.2393

Páez-Osuna, F., and Osuna-Martínez, C. C. (2015). Bioavailability of Cadmium, Copper, Mercury, lead, and Zinc in Subtropical Coastal Lagoons from the Southeast Gulf of California Using Mangrove Oysters (*Crassostrea Corteziensis* and *Crassostrea Palmula*). *Arch. Environ. Contam. Toxicol.* 68, 305–316. doi:10.1007/s00244-014-0118-3

Pan, K., and Wang, W.-X. (2012). Trace Metal Contamination in Estuarine and Coastal Environments in China. *Sci. Total Environ.* 421-422, 3–16. doi:10.1016/j.scitotenv.2011.03.013

Peng, Y., Li, X., Wu, K., Peng, Y., and Chen, G. (2009). Effect of an Integrated Mangrove-Aquaculture System on Aquacultural Health. *Front. Biol. China* 4, 579–584. doi:10.1007/s11515-009-0056-z

Queiroz, H. M., Ying, S. C., Bernardino, A. F., Barcellos, D., Nóbrega, G. N., Otero, X. L., et al. (2021). Role of Fe Dynamic in Release of Metals at Rio Doce Estuary: Unfolding of a Mining Disaster. *Mar. Pollut. Bull.* 166, 112267. doi:10.1016/j.marpolbul.2021.112267

Reyes-Montiel, N. J., Santamaría-Miranda, A., Rodríguez-Meza, G. D., Galindo-Reyes, J. G., and González-Ocampo, H. A. (2013). Concentrations of Organochlorine Pesticides in Fish (*Mugil cephalus*) From a Coastal Ecosystem in the Southwestern Gulf of California. *Biol. Environ.* 113B (3), 1–11. doi:10.3318/BIOE.2013.25

Romano Casas, G., Martínez Valenzuela, C., Cuadras Berrelleza, A. A., and Ortega Martínez, L. D. (2019). Pesticides, health and environment impact in Sinaloa (México): implications and challenges in environmental governance [Plaguicidas, impacto en salud y medio ambiente en sinaloa (México): implicaciones y retos en gobernanza ambiental]. *Trayectorias Humanas Trascontinentales* (4), 103–122. doi:10.25965/trahs.1615

Saber, T. M., Khedr, M. H., and Darwish, W. S. (2018). Residual Levels of Organochlorine Pesticides and Heavy Metals in Shellfish from Egypt with Assessment of Health Risks. *Slovenian Vet. Res.* 55, 101–113. doi:10.26873/svr-453-2017

Saleh, Y. S. (2021). Evaluation of Sediment Contamination in the Red Sea Coastal Area Combining Multiple Pollution Indices and Multivariate Statistical Techniques. *Int. J. Sediment Res.* 36, 243–254. doi:10.1016/j.ijsrc.2020.07.011

Salomons, W., and Förstner, U. (2012). *Metals in the Hydrocycle*. Springer Berlin Heidelberg.

Sifuentes, E., Macías, J., Ojeda, W., González, V. M., Salinas, D. A., and Quintana, J. G. (2016). Irrigation Management for Potato Crops Based on Climate Variability: Application in Irrigation District 075, Fuerte River, Sinaloa, Mexico [Gestión del riego enfocada a variabilidad climática en el cultivo de papa: aplicación al Distrito de Riego 075, Río Fuerte, Sinaloa, México]. *Tecnología y Ciencias Del. Agua* 7, 149–168.

Spagnoli, F., and Bergamini, M. C. (1997). Water-sediment Exchange of Nutrients during Early Diagenesis and Resuspension of Anoxic Sediments from the Northern Adriatic Sea Shelf. *Water Air Soil Pollut.* 99, 541–556. doi:10.1007/bf02406894

Spagnoli, F., De Marco, R., Dinelli, E., Frapiccini, E., Frontalini, F., and Giordano, P. (2021). Sources and Metal Pollution of Sediments from a Coastal Area of the Central Western Adriatic Sea (Southern Marche Region, Italy). *Appl. Sci.* 11, 1118. doi:10.3390/app11031118

Taylor, S. R. (1964). Abundance of Chemical Elements in the continental Crust: a New Table. *Geochimica et Cosmochimica Acta* 28, 1273–1285. doi:10.1016/0016-7037(64)90129-2

Truchet, D. M., Buzzi, N. S., Simonetti, P., and Marcovecchio, J. E. (2020). Uptake and Detoxification of Trace Metals in Estuarine Crabs: Insights into the Role of Metallothioneins. *Environ. Sci. Pollut. Res.* 27, 31905–31917. doi:10.1007/s11356-020-09335-6

Turner, A. (2000). Trace Metal Contamination in Sediments from U.K. Estuaries: An Empirical Evaluation of the Role of Hydrous Iron and Manganese Oxides. *Estuarine, Coastal Shelf Sci.* 50, 355–371. doi:10.1006/ecss.1999.0573

Usepa (2000). *Guidance for Assessing Chemical Contaminant Data for Use in Fish Advisories: Risk Assessment and Fish Consumption Limit*. Third ed. Washington, DC: Unites States Environmental Agency.

U.S. Environmental Protection Agency (2005). *Human Health Risk Assessment Protocol for Hazardous Waste Combustion Facilities*. Office of Solid Waste and Emergency Response, US Environmental Protection Agency.

U.S. Environmental Protection Agency (2013). "Integrated Risk Information System (IRIS)," in *Full List of IRIS Chemicals* (U.S.A. Environnmental Protection Agency).

U.S. Environmental Protection Agency (2018). *Regional Screening Levels (RSLs)–Generic Tables*. USA Environmental Protection Agency.

Usepa (1989). "Risk Assessment Guidance for Superfund," in *Vol. I: Human Health Evaluation Manual (Part A)* (Washington, DC: EPA).

Vasavada, N. (2014). *One-way ANOVA (Analysis of Variance) with post-hoc Tukey HSD (Honestly Significant Difference). Test Calculator for comparing multiple treatments* [Online]. Available: http://astatsa.com/OneWay_Anova_with_TukeyHSD/ (Accessed APR 04, 2016).

Wuana, R. A., and Okieimen, F. E. (2011). Heavy Metals in Contaminated Soils: a Review of Sources, Chemistry, Risks and Best Available Strategies for Remediation. *Int. Scholarly Res. Notices* 2011, 1–20. doi:10.5402/2011/402647

Yang, Q., Li, Z., Lu, X., Duan, Q., Huang, L., and Bi, J. (2018). A Review of Soil Heavy Metal Pollution from Industrial and Agricultural Regions in China: Pollution and Risk Assessment. *Sci. Total Environ.* 642, 690–700. doi:10.1016/j.scitotenv.2018.06.068

Conflict of Interest: The authors declare that the research was conducted in the absence of any commercial or financial relationships that could be construed as a potential conflict of interest.

frontiers in Environmental Science

ORIGINAL RESEARCH
published: 25 February 2022
doi: 10.3389/fenvs.2022.777894

Superposition Effects of Zinc Smelting Atmospheric Deposition on Soil Heavy Metal Pollution Under Geochemical Anomaly

Enjiang Yu[1], Hongyan Liu[2,3], Yu Tu[2], Xiaofeng Gu[2], Xiaozhui Ran[2], Zhi Yu[1,4] and Pan Wu[1,3]*

[1]College of Resources and Environmental Engineering, Guizhou University, Guiyang, China, [2]College of Agriculture, Guizhou University, Guiyang, China, [3]Key Laboratory of Karst Georesources and Environment of Ministry of Education, Guizhou University, Guiyang, China, [4]Research and Design Institute of Environmental Science of Guizhou Province, Guiyang, China

Guizhou Province is covered by a large area of carbonate rocks where, with a higher background of heavy metals under the geochemical anomaly, more than 3.6×10^5 ha of heavy metal–contaminated soil in the northwest area is related to historical indigenous zinc smelting. To explore the superposition effect of industrial source atmospheric deposition on soil, two watersheds were selected for study: 1) Maoshui reservoir watershed (MS), where there is a zinc smelting plant, and 2) Haishe lake watershed (HS), which was the control. We collected atmospheric depositions and soil for 3 years and analyzed Cadmium (Cd), lead (Pb), chromium (Cr), copper (Cu), nickel (Ni), and zinc (Zn) content. The results show that the heavy metals in the atmospheric deposition of the pollution watershed in MS were much higher than those in the control site, HS. The deposition fluxes of Cd, Pb, Cr, Ni, and Zn in MS were 27.8, 602, 145, 43.9, and 2,225 $mg{\cdot}m^{-2}{\cdot}a^{-1}$, respectively, and were 1.37–2.01 times higher than in HS. Soil heavy metals in MS were 1.01–5.69 times higher than in HS. The elevated concentrations were found focused from northeast to southwest around the plant but was distributed uniformly in HS. The average concentration of Cd, Pb, and Zn in the soil was 6.54, 67.4, and 264 $mg{\cdot}kg^{-1}$, respectively, in HS, which represents a high geochemical background even without pollution. After 13 years of deposition by prediction, the contribution of the atmospheric deposition on the soil in the zinc-smelting area was lowest, at 5.10%, for Ni, and highest, at 17.9%, for Cd. Principal component analysis of atmospheric deposition and soil heavy metals reflected that the pollution sources in MS were more diversification than those in HS. Zinc smelting atmospheric deposition showed superposition effects on the accumulation of heavy metals in soil under the geochemical anomaly in this region.

Keywords: atmospheric deposition, zinc smelting, heavy metals, soil, geochemical anomaly

OPEN ACCESS

Edited by:
Xin Huang,
Nanjing University, China

Reviewed by:
Michael Edward Deary,
Northumbria University,
United Kingdom
Katarzyna Nowińska,
Silesian University of Technology,
Poland

****Correspondence:***
Hongyan Liu
hyliu@gzu.edu.cn

Specialty section:
This article was submitted to Toxicology, Pollution and the Environment, a section of the journal Frontiers in Environmental Science

Received: *16 September 2021*
Accepted: *03 February 2022*
Published: *25 February 2022*

Citation:
Yu E, Liu H, Tu Y, Gu X, Ran X, Yu Z and Wu P (2022) Superposition Effects of Zinc Smelting Atmospheric Deposition on Soil Heavy Metal Pollution Under Geochemical Anomaly. Front. Environ. Sci. 10:777894. doi: 10.3389/fenvs.2022.777894

1 INTRODUCTION

The term "geochemical anomaly" refers to the deviation of chemical element content distribution or other chemical indexes from the normal geochemical model in a given space or area (Luo et al., 2019; Zhang and Song, 2018). Guizhou Province is covered by a large area of carbonate rocks and, with its much higher background of heavy metals than other provinces, represents a geochemical anomaly.

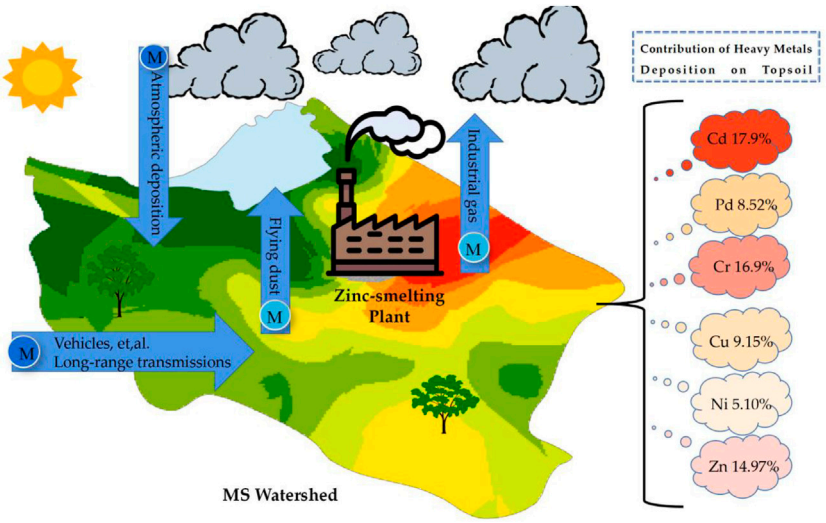

GRAPHICAL ABSTRACT | Superposition effects of zinc smelting atmospheric deposition on soil heavy metal pollution.

The background values of the heavy metals Cd, Pb, Cr, Cu, Ni, and Zn are 0.4668, 33.40, 139.6, 66.58, 56.89, and 111.4 mg kg^{-1} (He and Chen, 2002), respectively, and are much higher than the national background value (Luo and Liu, 2020). In the face of such a geochemical anomaly, the geological source becomes an important source of heavy metals in atmospheric deposition (Wang et al., 2015).

Atmospheric deposition is an important means by which heavy metals can enter the soil, such as through irrigation water, sewage sludge use, and so on (Cao et al., 2020; Yu and Liu, 2021). Air pollutants enter the water and soil environment in the form of depositions (Yu et al., 2019), causing environmental problems such as water eutrophication, soil acidification, and heavy metal pollution in water and soil (Xia et al., 2014). Sedimentation flux and sedimentation rate are the main research indexes of atmospheric deposition. Some studies have investigated the deposition rate of heavy metals in the atmosphere on a local scale (Kara et al., 2014; Pan and Wang, 2015; Shamsaddin et al., 2020), but reported few results of a closed region.

Due to the limited critical radius of atmospheric transport and the reduction of emissions caused by human activities, it is expected that the number of heavy metals deposited in the atmosphere in industrial areas will be higher than compared to those in natural ecosystems (Al-Khashman et al., 2013; Kiyoshi et al., 2019). Many studies have shown that atmospheric deposition can transport industrial compounds over long distances, causing pollution to the atmosphere and soil around factories (Hermanson et al., 2020; Xing et al., 2020a). The accumulation of heavy metals in atmospheric deposition in the ecosystem can more effectively be accurately reflected in closed regions (Kara et al., 2014; Pan et al., 2021). The atmospheric deposition of heavy metals in farmland soils in Hunan Province accounted for 51.24~94.74% of the total input (Hunan, 2016) (Yi et al., 2018). The atmospheric deposition of the heavy metal Cd in nine counties in central and eastern Guangxi accounted for 90.65% of the total input (Guangxi, 2014~2015) (Chen et al., 2019). The importation of heavy metals into surrounding soil by atmospheric deposition in industrial areas has also been reported (Sonia et al., 2013; Wang et al., 2018; Hernández-Pellón and Fernández-Olmo, 2019). Therefore, it is necessary to study the sources and impacts of soil heavy metal pollution around industrial areas.

There is more than 3.6×10^5 ha of heavy metal contaminated soil in northwest Guizhou Province, according to a national investigation of farmland soil pollution conducted in 2018. Guizhou Province has the maximum range of heavy metal pollution soil in China (more than 3.6×10^5 h), and studies have indicated that this is rooted in zinc smelting that occurred 30 years ago in this region. Artisanal zinc smelting began 600 years ago in the region, and large-scale artisanal zinc smelting was conducted for about 20 years, from the 1980s to 2004. In the absence of pollution treatment of waste gas, water, and mineral waste residue, the amount of waste residue reached 24 million tons and is still present in the environment today, causing serious heavy metal pollution (Luo et al., 2018; Zhou et al., 2020), which has resulted in severe ecological, environmental, and health risks (Peng et al., 2018). The artisanal zinc smelting process used indigenous methods: two major Zn ores, a sulfide ore in the form of sphalerite (ZnS), and a carbonate Zn ore in the form of smithsonite ($ZnCO_3$). These were mixed with coal as a reducing agent, placed in ceramic jars, and roasted for a few hours at a high temperature (800°C), using coal as fuel to generate heat in a furnace to produce liquid metallic Zn (**Figure 1**). Therefore, in this study, we trace the soil pollution caused by the historical artisanal zinc smelting through one zinc oxide powder plant that carried out production in this region.

We selected two watersheds as closed regions to study the superposition effect of heavy metals in the atmospheric deposition on soil: 1) Maoshui reservoir watershed (MS),

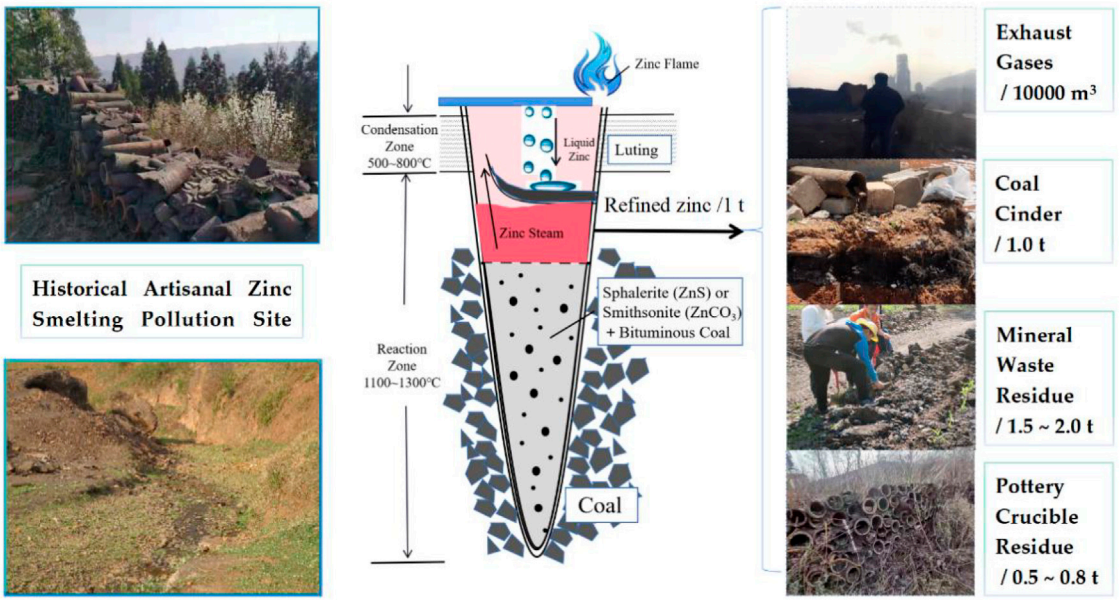

FIGURE 1 | Schematic diagram of historical artisanal zinc smelting.

which has a zinc smelting plant, and 2) Haishe lake watershed (HS), which was the control. The main objectives of this study were to: 1) test the Cd, Pb, Cr, Cu, Ni, and Zn concentrations in wet and dry atmospheric deposition in different seasons; 2) determine the association between soil heavy metal content and atmospheric deposition; 3) predict the incremental content of heavy metals in topsoil from atmospheric deposition; and 4) trace the influence of historical artisanal zinc smelting on soil heavy metal pollution in the context of a geochemical anomaly.

2 MATERIALS AND METHODS

2.1 Study Area

The study area was Weining County, an administrative area of Bijie City located in Guizhou Province in southwestern China. The area has been affected by lead and zinc smelting and contains a geological anomaly (**Figure 2**). In the fourth quarter of the test area, spring levels of precipitation reached 163 mm, while summer, autumn, and winter levels were 476.8, 182.9, and 180 mm, respectively. Weining County has a subtropical monsoon climate. The average annual temperature is 11.2°C, with a 3.9°C average in January, and 17.0°C in July. In Weining, southerly winds prevail from January to September, switching to northerlies from October to December, and the average wind speed is 3.5 m/s (Guizhou Meteorological Bureau). Weining county is one of the most important artificial Zn mining regions in China. Zn smelting activities began in the last century but ceased in 2004 due to grave issues with environmental pollution (Luo et al., 2018).

The two watersheds studied, MS and HS, are located in the Karst landscape of Weining County, northwest Guizhou Province, China (**Figure 2**). The two sites are part of the Permian Xuanwei Formation and contain yellow acid topsoil. The MS is located northwest of Jinzhong Town, Weining County ($26°47'10''N$,$104°23'8''E$) at an altitude of about 2,122 m and covers an area of about 1.5 km^2, a county-level highway serving as the boundary of the MS watershed northeast. The zinc smelting plant uses rotary kiln technology and was established in August 2006, the raw ore mean heavy metal content are 57.73 mg/kg for Cd, 29,850 mg/kg for Pb, 94.27 mg/kg for Cr, 144.6 mg/kg for Cu, 32.75 mg/kg for Ni, and 44,090 mg/kg for Zn. HS is located north of Lushan Town, Weining County, at $26°48'14''N$, $104°23'42''E$ and served as the control area. This key watershed is unpolluted by industry and is protected by the county government because it supplies the lake at the center of the mountainous region. Its natural water is historically unused for irrigation or drinking. HS has an altitude of 2,110 m and an area of about 1.8 km^2. The distance between MS and HS is approximately 6.8 km (**Figure 2**).

2.2 Sample Collection and Determination

2.2.1 Atmospheric Deposition

Samples of atmospheric deposition were collected each quarter (spring, summer, autumn, and winter) from May 2017 to May 2020. Wet and dry atmospheric depositions were collected at five sampling points in each experimental area, with three replicates for each sampling point (**Figure 2**). Polyethylene cylinders (15 cm in diameter and 30 cm in height) were used to collect atmospheric depositions. The cylinders were mounted on 1.5 m tall frames on the flat roofs of local buildings at each sampling site, approximately 4–6 m above the ground. The height difference

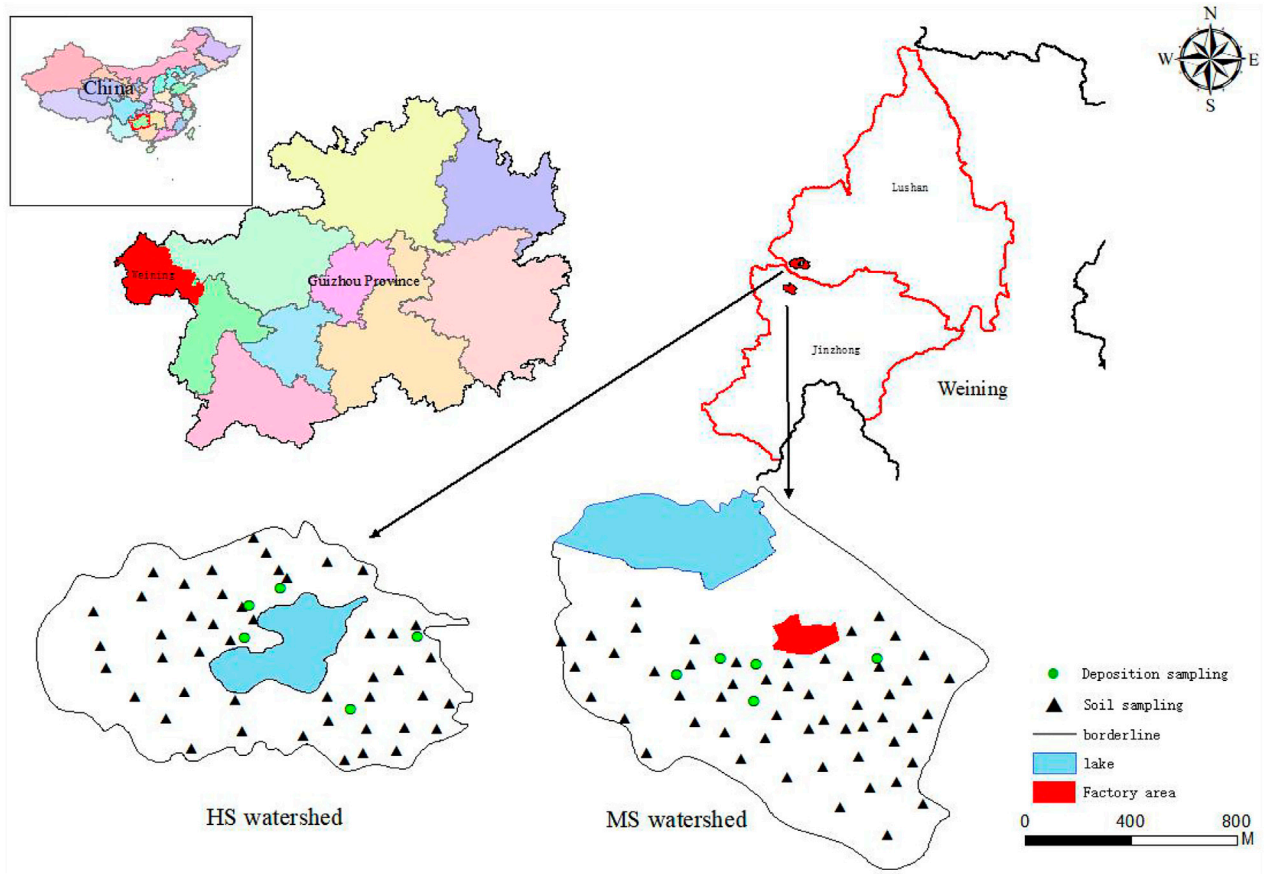

FIGURE 2 | Location of sampling sites in Weining County, Guizhou Province, China.

between roof, ground, and cylinder was set to minimize the contamination of the samples by re-suspended dust or soil from the ground or roof. Before installation, the cylinders were washed and soaked in a 5% nitric acid (HNO_3) bath for more than 2 h to remove potential contaminants. Three cylinders were installed at each site at the beginning of each quarter, and 100 ml 1% HNO_3 was added to each cylinder to prevent the growth of microorganisms.

The upper liquid was collected in polyethylene bottles when the precipitation had reached halfway up the cylinders, and its total volume and weight were measured. After determining the pH value of the bottles, we reduced the pH value to below 2 by adding 1% HNO_3, preventing changes in the chemical species of the elements. We then refrigerated the bottles at 4°C for analysis. The remaining precipitate was filtered with 0.45 μm polyester fiber filters, and the volume of filtrate was recorded, then discarded. The filter cake was air-dried or dried at temperatures lower than 65°C, and its weight was then recorded. At this point, the dried precipitates were ready for analysis. Samples from each cylinder for each quarter were combined into one sample and tested. The annual precipitation was collected, and the precipitation time and amount were recorded. This method duplicated that of Yi et al. (2018).

2.2.2 Surface Soil

The samples were taken between May 2017 and May 2020. To ensure an even distribution of the sites selected, systematic sampling using a regular grid was used (State Environmental Protection Administration of China, 2004). Soil samples were collected in December of each year, with 58 samples taken from MS and 46 from HS. Each sample was taken from the top 20 cm of soil at a density of 1 sample/40,000 m^2. The samples were air-dried, ground, and passed through a 20-mesh (<0.84 mm) nylon sieve. Four surface soil sub-samples were combined to make a representative soil sample. These sampling methods complied with relevant specifications (State Environmental Protection Administration of China, 2004).

2.3 Sample Analysis

2.3.1 Atmospheric Deposition (Precipitation)

The heavy metal (Cd, Pb, Cr, Cu, Ni, and Zn) content of precipitation was analyzed according to the microwave digestion method set out in National Environmental Standard HJ678-2013 (Ministry of Environmental Protection, 2014). After filtering the precipitation samples, samples of 25 ml were transferred to the microwave digestion tank, where 1 ml of H_2O_2 (30%) and 5 ml of HNO_3 were added to each sample.

These were placed in a ventilation cabinet, and placed in the microwave digestion instrument. The temperature of the microwave digestion instrument temperature was set at 180°C. This temperature was reached in 10 min and was sustained for 15 min. The digestion tank was then removed and cooled to room temperature, whereupon the solution was transferred to a 50 ml volumetric flask. The tank was then rinsed twice with deionized water and transferred to another 50 ml volumetric flask, where it was topped up with deionized water, as required. The heavy metal content was determined by inductively coupled plasma mass spectrometer (ICP-MS; Thermo Fisher Scientific X2).

2.3.2 Surface Soil

Soil samples of 0.1 g were weighed and placed into the polytetrafluoroethylene inner tanks of the digestion kettle through a 100-mesh sieve. 3 ml HNO_3 (guarantee reagent) and 3 ml HF (guarantee reagent) were added and the sample was left for 8 h. Then, 2 ml of $HClO_4$ (guarantee reagent) was added and placed in the metal outer tank of the digestion kettle to dissolve in the oven at 180°C for 12 h. When the digestion was complete, the inner polytetrafluoroethylene tanks on the electric hotplate were heated to completely dry the acid and remove any HF residue. 1 ml of HNO_3 (guarantee reagent) was added to dissolve and the volume of 3% diluted HNO_3 (guarantee reagent) was fixed to 50 ml before the heavy metal (Cd, Pb, Cr, Cu, Ni, and Zn) concentrations were determined by inductively coupled plasma mass spectrometer (ICP-MS; Thermo Fisher Scientific X2).

2.3.3 Atmospheric Deposition (Dry Precipitation)

The levels of dried precipitate heavy metal were determined in the same way as for the surface soil.

2.3.4 Predicted Concentrations of Heavy Metals in Deposited Atmospheric Emissions

A survey of the job site revealed that the zinc smelting plant used a desulfurization tower and a chimney of 30 m, which emitted smoke outlet with a temperature of 240°C, the annual output of zinc oxide was 3,000 t and the dust output was 4,000 t. The impact range of emissions was 1.5 km, according to the Gaussian model of elevated continuous point sources developed by Hao et al. (2010).

The ground-level deposition of dust from industrial atmospheric emissions was predicted using Hao et al.'s model (2010). The origin is the zinc smelting plant, the x-axis displays the wind direction with the average positive wind direction on the left side of the axis. The y-axis is perpendicular to the x-axis, the z-axis is perpendicular to the horizontal plane, and the upward direction is the positive direction; namely, the right-hand coordinate system. The formula for establishing ground concentrations is

$$\rho(x, y, 0) = \frac{Q}{\pi \bar{\mu} \sigma_y \sigma_z} \exp\left(-\frac{y^2}{2\sigma_y^2} \right) \exp\left(-\frac{H^2}{2\sigma_z^2} \right)$$

where σ_y is the standard deviation of pollutant distribution in the y direction of a smoke stream at x distance from origin, m; σ_z- is the standard deviation of pollutant distribution in the y direction of a smoke stream at distance z from origin, m; ρ- is the concentration of pollutants at any point, $g{\cdot}m^{-3}$; $\bar{\mu}$- is the mean wind speed, $m{\cdot}s^{-1}$; and Q is the source strength, $g{\cdot}s^{-1}$; H is source valid high (the sum of the chimney height and the raised height of the soot), m.

The coefficients of σ_y, σ_z,Q, and H refers to the methodological guidelines of technical guidelines on environmental impact assessment for the atmospheric environment, HJ/T 2.1~2.3-93 (State Bureau of Environmental Protection, 1994).

2.3.5 The Contribution of Depositions to Soil

The values of the Cd, Pb, Cr, Cu, Ni, and Zn concentrations in the digests were converted into deposition fluxes ($mg{\cdot}m^{-2}{\cdot}a$) based on the duration of sampling and the aperture size of each cylinder. To further investigate the potential implications of elevated depositions of atmospheric heavy metals, attempts were made to estimate surface soil contamination in the region using the calculated annual flux of atmospheric deposition. The contribution of deposition to soil was calculated as the ratio of deposition flux to the average concentration of surface soil heavy metal in the test areas, assuming a soil bulk density of 1,300 kg m^{-3} (Cao et al., 2020). The worst-case scenario was calculated using the same assumption that atmospheric deposition was the sole source of heavy metal in the soil and was retained in the top 20 cm of arable soils (Cao et al., 2020).

2.3.6 Quality Control and Quality Analyse

All glassware was soaked in a 5% nitric acid solution for more than 2 h before use and then triple-rinsed with DI water. Along with the triplicate samples, analytical blanks and a standard reference soil (Gss-5) were included in the digestion of each sample batch. The recovery rates of heavy metals in the reference soil were 86.7–113.3% (Mean = 93.2%) for Cd, 94.8–105.3% (Mean = 98.6%) for Pb, 94.3–105.9% (Mean = 101.3%) for Cr, 95.8–104.2% (Mean = 101.2%) for Cu, 90.0–110.0% (Mean = 102.6%) for Ni, and 94.9–105.1% (Mean = 98.8%) for Zn.

The multi-element standard solution used by ICP-MS to determine the samples complied with national standard GSB 04-1767-2004. Standard reference materials (GSB 04-1767-2004) were used to validate the accuracy and precision of the analytic methods. The analytical quality control was precise, with the relative standard deviation being <8.50%. The limits of detection (LODs) of the ICP-MS for Cd, Pb, Cr, Cu, Ni and Zn were 0.03, 2, 5, 2.4, 4, and 44 mg/kg, respectively.

2.4 Statistical Analysis

The experimental area was obtained from a satellite map, measured on site via GPS (Trimble GEO 7X, Shanghai Navearth, Shanghai). Descriptive statistical analyses and plotting of figures were carried out using Origin 9.0 (Origin Lab Corporation, Northampton, MA) and Excel 2013 (Microsoft Corp., Waltham, MA, United States); Kriging interpolation was conducted using ArcGIS 10.6. Summary statistics were used to calculate the average values, standard deviations and analysis of variance by using SPSS version 22.0. One-way analysis of variance

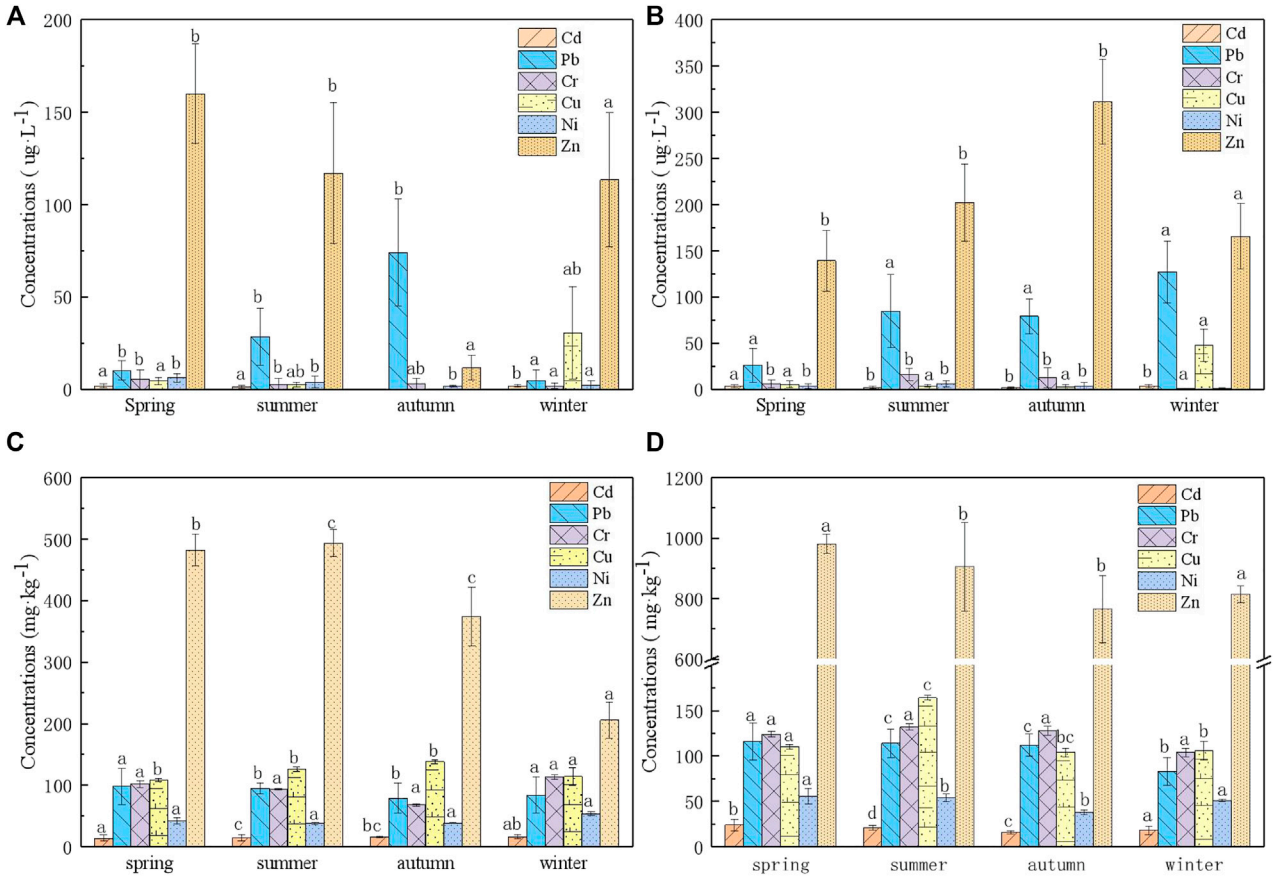

FIGURE 3 | Heavy metal concentration of atmospheric deposition: **(A)** HS wet deposition; **(B)** MS wet deposition; **(C)** HS dry deposition; **(D)** MS dry deposition. ANOVA was performed on the same elements in different seasons of samples from the same site.

(ANOVA) was conducted with the post hoc Tukey test method using a significance level of 0.05 to determine differences. Principal component analyses were conducted to compare different elements of samples from the same site. The rainfall data came from the official website of the Weining County Meteorological Bureau.

3 RESULTS AND DISCUSSION

3.1 Heavy Metal Concentrations in Atmospheric Depositions

3.1.1 Heavy Metal Concentrations in Wet Depositions

Heavy metal concentrations in wet depositions at the control site (HS) were higher in spring and winter than those in summer and autumn (**Figure 3A**). This trend contrasted with local levels of precipitation, which were higher in the latter two seasons. Precipitation was a critical factor determining the flux of heavy metals in wet atmospheric deposition; the concentration of heavy metals in precipitation is affected by many factors, including the timeliness of the precipitation season and the interval of precipitation time (Li and Jia, 2018). Zn reached the highest concentrations among the six heavy metals, with 159.81 ± 56.81 μg L^{-1} in spring, 116.77 ± 68.15 μg L^{-1} in summer, 11.44 ± 6.73 μg L^{-1} in autumn, and 113.28 ± 86.32 μg L^{-1} in winter. In contrast, there were no obvious regularities in heavy metal concentrations in wet depositions at the pollution site (MS; **Figure 3B**). This phenomenon resulted from the local zinc oxide smelting facilities, whose operations contributed to the accumulation of heavy metals via atmospheric deposition all year round (Xing et al., 2020a).

Thus, heavy metal concentrations of wet deposition were much higher in MS than HS but the seasonal distribution was quite different. Moreover, the concentrations of all heavy metals in atmospheric depositions in the zinc smelting region were much higher than those in the nonindustrial region. This conclusion is consistent with the results of other studies (Cui et al., 2012; Cereceda-Balic et al., 2020). The concentration of these metals was higher at the MS site, in agreement with the proximity of this location to the zinc smelting plant (Hernández-Pellón and Fernández-Olmo, 2019).

3.1.2 Heavy Metal Concentrations in dry Depositions

Figure 3C shows that the concentrations of dry depositions of heavy metals at the control site (HS) were uniform across the four seasons, except for Zn, which varied, reaching 493 ±

TABLE 1 | Deposition flux of heavy metals from atmospheric deposition in MS watershed/(mg·m^{-2}·a^{-1}).

Watershed	Atmospheric deposition	Cd	Pb	Cr	Cu	Ni	Zn
HS	Wet deposition	11.1	424	30.7	81.9	21.0	1,170
	Dry deposition	2.76	16.7	18.8	21.0	8.49	122
	Total	13.8	440	49.5	102	29.5	1,292
MS	Wet deposition	20.3	564	101	34.9	24.8	1897
	Dry deposition	7.54	38.3	44.0	41.1	19.1	328
	Total	27.8	602	145	76.0	43.9	2,225
	deposition flux $_{MS}$/deposition flux $_{HS}$	2.01	1.37	2.93	0.75	1.49	1.72

22.07 mg kg^{-1} in spring, 482 ± 25.57 mg kg^{-1} in summer, 374 ± 47.60 mg kg^{-1} in autumn, and 206 ± 29.49 mg kg^{-1} in winter.

In MS, the most concentrated heavy metal in the dry depositions was Zinc (**Figure 3D**), with Cd recording the lowest concentrations across all seasons although these were far in excess of the background value of 0.4668 mg kg^{-1} (He and Chen, 2002) in northwestern Guizhou Province. Concentrations of all six elements from these two sites followed the order MS > HS, industrial site > non-industrial control site. Compared with the control, the concentration of Zn in dry depositions from the zinc smelting plant area was four times higher in MS than HS, with levels of Pb, Cr, and Cu also significantly greater. The test region was located southwest of the zinc smelter, in the main wind direction of northwestern Guizhou (Guizhou Meteorological Bureau). Differences in the distribution of the heavy metal concentrations between this region and the control demonstrated that the main source of heavy metals in MS region was zinc smelting. These results corroborate previous research which found much higher concentrations of heavy metals in the test area than the control region (Xing et al., 2020b); studies have also shown that industrial emissions from the industrial belt exerted a notable influence on atmospheric deposition (Sonia et al., 2013; Wang et al., 2018; Hernández-Pellón and Fernández-Olmo, 2019).

3.1.3 Deposition Fluxes of Heavy Metals

In HS, the Zn deposition flux of 1,292 mg m^{-2}·a^{-1} was the largest among the six heavy metals, followed by Pb, at 440 mg m^{-2}·a^{-1}, with the lowest flux recorded for Cd, at 13.8 mg m^{-2}·a^{-1} (see **Table 1**). The overall order of deposition flux for all elements was as follows: Zn > Pb > Cu > Cr > Ni > Cd. The pattern of deposition flux for MS was similar, with Zn recording the largest value, at 2,225 mg m^{-2}·a^{-1}, followed by Pb at 602 mg m^{-2}·a^{-1}, with Cd the lowest, at 27.8 mg m^{-2}·a^{-1}. The overall order was Zn > Pb > Cr > Cu > Ni > Cd. Other studies (Pereira et al., 2007; Pan and Wang, 2015; Chen et al., 2018; Cao et al., 2020) have recorded the same findings.

In this study, the deposition fluxes of Zn, Pb, and Cd were significantly higher than non-industrial zone study of Liang et al. (2014), who detected Zn levels of 205 mg m^{-2}·a^{-1}, with Pb levels of 122 mg m^{-2}·a^{-1}, and those of Cd, 3.06 mg m^{-2}·a^{-1}. Furthermore, the deposition fluxes far exceeded those of China's Chang-Zhu-Tan industrial zone in our study (Cao et al., 2020). The main reasons for these difference that the type of industry was different (Cao et al., 2020) and, likewise, the geological background was not the same (Liang et al., 2014). The analysis of samples collected over 3 years demonstrated that the dry atmospheric deposition input flux in HS was 190 g m^{-2}·a^{-1} and 378 g m^{-2}·a^{-1} in MS. Similarly, the wet deposition input flux in HS was 1,739 g m^{-2}·a^{-1}, rising to 2,642 g m^{-2}·a^{-1} in MS. This confirms the deposition flux of heavy metals is higher in industrial than nonindustrial areas. To understand the accumulation of atmospheric settlement in the MS basin relative to the control HS more intuitively, we calculated the ratio of settlement flux between the two (Qiu et al., 2016). **Table 1** shows that all five heavy metals (except for Cu) had accumulated more in MS than HS, strengthening the conclusion that zinc oxide smelters are the main source of heavy metals in soils in the MS basin.

3.2 Distribution of Heavy Metals in Soil

3.2.1 Concentrations in Surface Soil

As **Table 2** shows, the average heavy metal soil concentrations in HS were 6.54 mg kg^{-1} (Cd), 67.4 mg kg^{-1} (Pb), 30.8 mg kg^{-1} (Cr), 44.6 mg kg^{-1} (Cu), 47.6 mg kg^{-1}(Ni), and 264 mg kg^{-1} (Zn). These were 0.22–14.2 times the background values (He and Chen, 2002). The soil levels of Cd, Pb, and Zn soil were 14.2, 2.02 and 2.40 times than the background value, while those of Cr, Cu, and Ni were lower than the background value. These findings reflect the location of the study in a karst landscape, a geological anomaly that impacts soil levels of Cd, Pb, and Zn (He and Chen, 2002). In HS soil samples, a small–moderate coefficient of variation (CV) in heavy metal concentrations was detected (20.5–38.2%), indicating that the soil was less affected by human activities at this site (see also Adimalla, 2020; Chai et al., 2021).

In MS, the average concentrations of Cd, Pb, Cr, Cu, Ni, and Zn in the soil were 8.43 mg kg^{-1}, 383 mg kg^{-1}, 46.5 mg kg^{-1}, 45.0 mg kg^{-1}, 46.6 mg kg^{-1}, and 805 mg kg^{-1}, respectively. The heavy metal soil concentrations were 0.33 (Ni) to 18.3 (Cd) times the background value of the northwestern area of Guizhou Province (He and Chen, 2002). In total, the concentrations of heavy metals in soil were much higher in MS than HS, which were as much 5.68 and 3.05 times higher than in control HS, except for Ni. The coefficients of variation for Cd, Cr, Cu, and Ni in the soil ranged between 30.1 and 33.6%, all medium levels, while those for Pb and Zn were 115 and 102%, respectively. It could therefore be inferred that the concentration of heavy metals in the soil was not only affected by the local geology background but also by the surrounding small zinc smelters and other human activities (Adimalla, 2020; Chai et al., 2021).

TABLE 2 | Concentration of heavy metals in soil/(mg·kg^{-1}).

Index	Watershed	Min	Max	Mean ± SD	CV(%)	Background value
Cd	HS	1.44	12.9	6.54 ± 2.50^{a}	38.2	0.4668
	MS	1.26	13.9	8.43 ± 2.83^{a}	33.6	
Pb	HS	33.9	91.8	67.4 ± 13.8^{a}	20.5	33.40
	MS	65.0	2,968	383 ± 442^{b}	115	
Cr	HS	9.39	42.9	30.8 ± 8.11^{a}	26.3	139.6
	MS	26.0	108	46.5 ± 14.0^{b}	30.1	
Cu	HS	15.1	70.4	44.6 ± 10.5^{a}	23.5	66.58
	MS	15.3	229	45.0 ± 28.9^{b}	64.2	
Ni	HS	13.2	79.7	47.6 ± 14.8^{a}	31.1	56.89
	MS	12.2	70.4	46.6 ± 14.1^{b}	30.3	
Zn	HS	90.8	369	264 ± 68.9^{a}	26.1	111.4
	MS	156	5,279	805 ± 825^{a}	102	

Different letters within the same column indicate significant differences at $p < .05$ *as determined by the Tukey's honestly significant difference pairwise comparisons test.*

3.2.2 Spatial Distribution of Heavy Metals

The spatial distribution of the six heavy metals was calculated via Kriging interpolation through the semi-variance model (**Figure 4**). In general, all six heavy metals were uniformly distributed over the surface soil in HS, meaning that soil concentrations of heavy metal were influenced by the terrain and patterns of land use, rather than a source of pollution. In contrast, the soil in MS was characterized by obvious patterns in heavy metal distribution (**Figure 4**). High concentrations of Cd, Pb, Cr, Cu, and Zn were distributed from northeast to southwest around the zinc smelting plant, in distinction to the control site (although Ni was concentrated in the soil from southeast to northwest at levels only slightly higher than those recorded for HS). **Figure 4** shows clearly that the differences between these distributions of heavy metals (except Ni) are caused by the exhaust from the zinc smelting. From **Table 2** as well as the spatial interpolation (**Figure 4**), it can be seen that the mean concentration of Ni is lower than the northwest Guizhou background value (He and Chen, 2002) in both basins. The input of Ni is predominantly governed by the natural composition of the soil of the study region. The Ni CV was very low, signifying that natural and anthropogenic factors governed its spatial distribution (Adimalla, 2020).

This research found significantly higher soil concentrations of heavy metals than prior studies (Cai et al., 2019). While the main source of these was the local geochemistry, which was more influential than previously indicated (He and Chen, 2002). A national investigation of farmland soil pollution in 2018 showed that Cd exceeded the national standard the most, followed by Pb and Zn. This soil heavy metal pollution issue was well-supported by our experimental data. The effects of zinc smelting and historical artisanal zinc smelting in the area were also considerable. Atmospheric deposition and mineral waste residues are known to be the principal causes of soil contamination (Luo et al., 2018; Zhou et al., 2020). ArcGIS Kriging was used to capture the spatial variations of heavy metal distributions in the soil. Our comparison of the pollution caused by different forms of zinc smelting indicated that historical artisanal zinc smelting caused the highest levels of pollution, corroborating the findings of research carried out on other locations (Li et al., 2013). Compounds in the waste produced by this form of smelting continue to decompose and contaminate local soil (Peng et al., 2018). Even long after smelting operations had ended, exceptionally high levels of Pb, Zn, Cd, and As arising from atmospheric deposition were still detected in the local surface soil of northwestern Guizhou Province (Zhou et al., 2020). These originate from a history of artisanal zinc smelting in the region lasting over 600 years.

3.3 Principal Component Analysis of the Atmospheric Deposition and Soil Content of Heavy Metals

3.3.1 Principal Component Analysis of the Atmospheric Deposition of Heavy Metals

To perform the matrix analysis of rotated components (**Table 3**), components with eigenvalues of >1 were extracted. Two main components explained 92.5% of the variance in the source of the atmospheric deposition of heavy metals in HS. Component 1 (PC1) accounted for 70.5% of the total variance, while Cd, Pb, Cu, and Zn had the largest loads, indicating a significant homology among these four elements. Given the high background levels of cadmium, lead, and zinc in northwestern Guizhou (Luo and Liu, 2020), the main source of atmospheric deposition may be the soil minerals caused by this geochemical anomaly. Clay and organic colloids can easily absorb heavy metals and fine particles of this soil are the primary source of atmospheric depositions with much higher heavy metal content in the area (Cereceda-Balic et al., 2020). Component 2 (PC2) accounted for 22.0% of the total difference, with Cr and Ni contributing the highest loads. Cr is a by-product of metal smelting, while Ni is typically produced by petroleum combustion, steel smelting, motor vehicle exhaust emissions and geological sources (Li and Jia, 2018; Yasser et al., 2019; Wang et al., 2020; Pan et al., 2021).

The PCA of the atmospheric deposition of the heavy metals identified three main components explaining a total of 92.5% of the variance in the pollution recorded in MS. PC1 accounted for 52.3% of the total variance, with Pb and Zn the most important factors. PC2 accounted for 26.4% of the difference and Cu and Cd were the main eigenvalue factors. PC3 accounted for 13.9% of the total variance, with Cr and Ni showing the strongest associations. Zinc smelting is the main source of Pb and Zn in atmospheric deposition (Gu et al., 2021), demonstrating the importance of zinc oxide smelting and production to PC1. Atmospheric

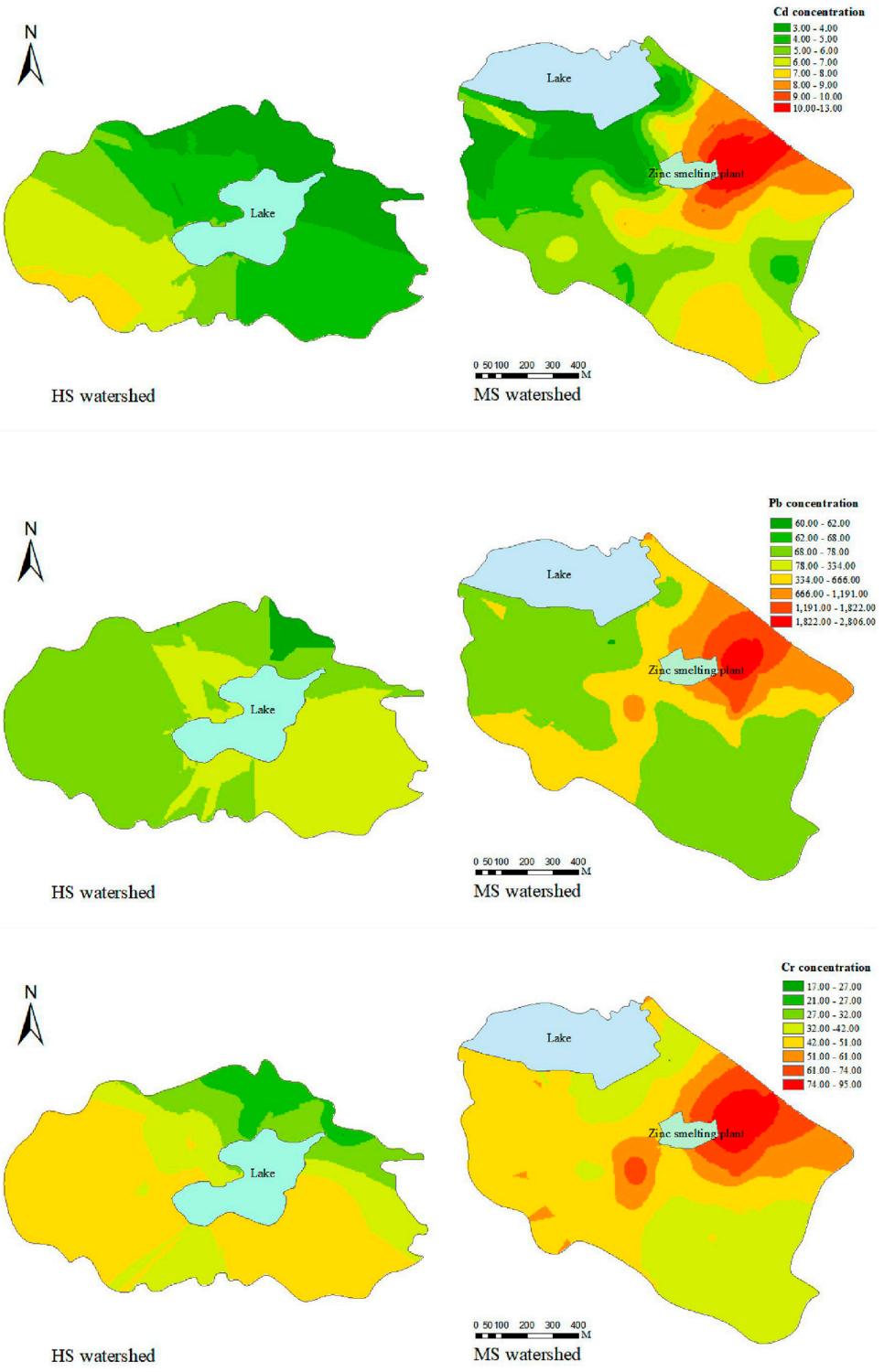

FIGURE 4 | Soil heavy metals distribution in 2 watersheds.

deposition varies according to the production methods of different industries (Garg et al., 2000; Li, 2020). Cadmium is produced by the smelting of non-ferrous metals (Liu et al., 2018), linking the high loadings of Cu and Cd in PC2 to zinc smelting, which PC2 was zinc smelting compound soil minerals. Chromium and nickel indicated sources such as traffic and

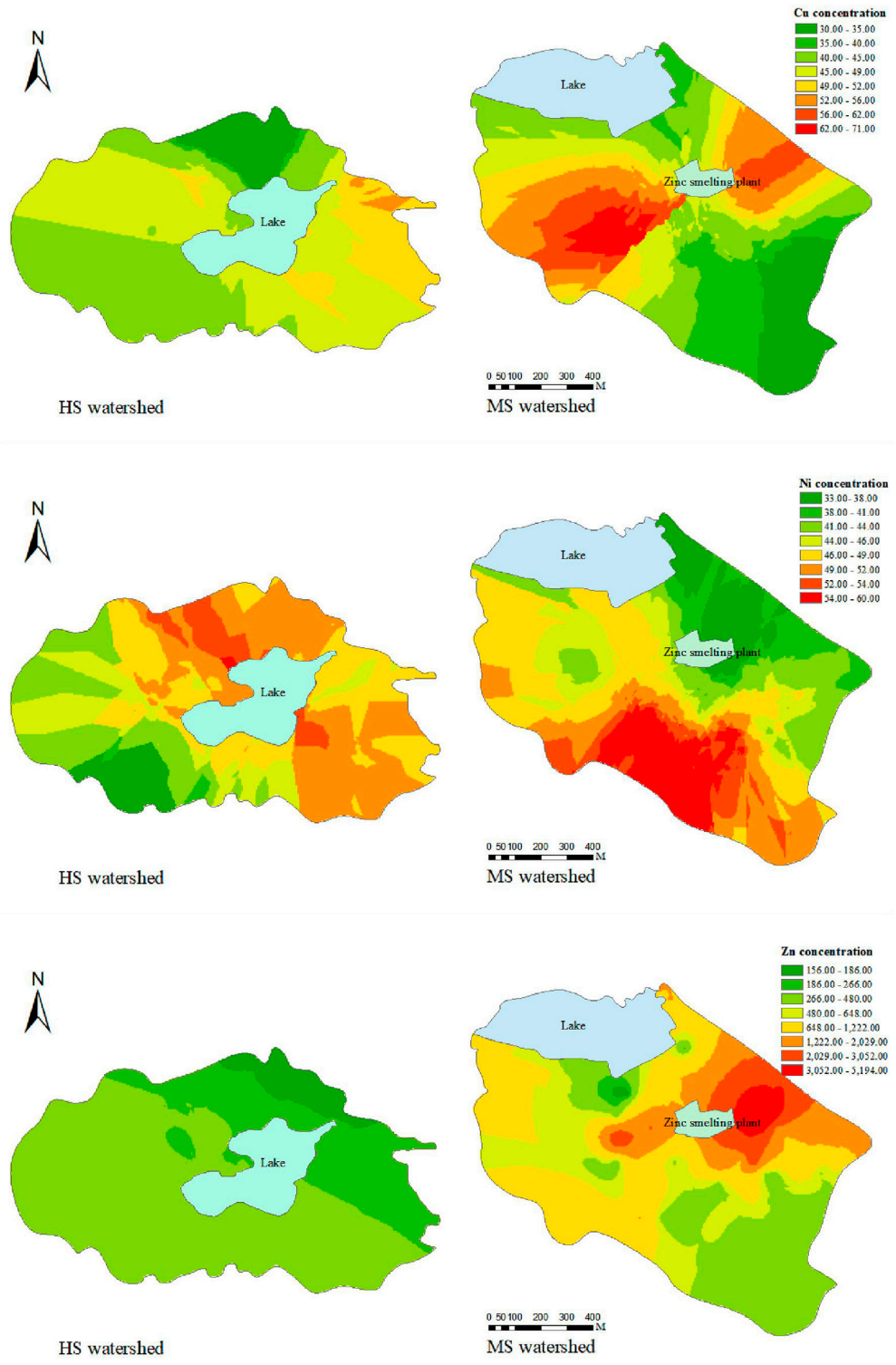

FIGURE 4 | (Continued)

metal smelting (Li and Jia, 2018; Yasser et al., 2019; Wang et al., 2020; Pan et al., 2021). The plate analysis of soil concentrations demonstrated the importance of geological sources in determining Ni levels and the re-suspended soil particles were also a potential source of atmospheric deposition (Xing et al., 2020b). Therefore, we contend that PC3 indicates the

TABLE 3 | Principal component analysis of heavy metals in atmospheric deposition and soil.

Watershed	Atmospheric deposition					Soil				
	HS		MS			HS		MS		
Component	1	2	1	2	3	1	2	1	2	3
Cd	0.469	−0.192	0.357	0.570	−0.033	0.431	0.057	0.415	0.042	0.482
Pb	0.438	−0.354	0.538	−0.217	0.019	0.441	−0.352	0.488	0.077	0.215
Cr	0.237	0.743	0.342	0.274	−0.751	0.286	0.691	−0.279	0.166	0.813
Cu	0.453	−0.137	−0.186	0.699	0.234	0.425	−0.278	0.475	0.054	−0.180
Ni	0.388	0.496	0.420	0.139	0.609	0.374	0.487	−0.017	0.980	−0.165
Zn	0.420	−0.146	0.505	−0.214	0.091	0.465	−0.282	0.532	−0.034	0.008
Total	4.23	1.32	3.14	1.58	0.832	3.97	1.01	3.20	1.01	0.90
% of Variance	70.5	22.0	52.3	26.4	13.9	66.2	16.77	53.4	16.9	15.0
Cumulative %	70.5	92.5	52.3	78.6	92.5	66.2	83.0	53.4	70.3	85.3

contribution of traffic and geological sources to the concentrations of heavy metals in depositions.

Compared to HS, the major source of heavy metal accumulation in atmospheric deposition in MS was the exhaust emitted from the local zinc oxide smelters. In both HS and MS, the atmospheric deposition of heavy metals originated in their geology.

3.3.2 Principal Component Analysis of Heavy Metals in Soil

Findings from the PCA of heavy metals in soil samples taken from the two watersheds revealed similar to those of atmospheric deposition.

The PCA extracted two major components which explained 83.0% of the total variance of heavy metals in the control site, HS. PC1 accounted for 66.2% of the total variance. The loading values of Zn (0.465), Pb (0.441), Cu (0.425), and Cd (0.431) were similar and derived from the geochemical makeup of the substrate. Our knowledge of the test region and prior research (Wang et al., 2015; Luo and Liu, 2020) indicated that PC1 was likely to be rooted in local geology. PC2 accounted for 16.7% of the total difference. The eigenvalues for Cr and Ni pointed to traffic, metal smelting, or other anthropocentric sources (Pan et al., 2021), and geological sources (Li and Jia, 2018; Yasser et al., 2019; Wang et al., 2020; Pan et al., 2021). However, the concentrations of Cr and Ni were below the background value, meaning that such sources were absent from the control site (He and Chen, 2002). Thus, the PCA indicated that the control watershed was mainly affected by geological sources.

A total of three components were able to explain 85.3% of the total variance of heavy metals in the polluted soil of MS, similar to the PCA of atmospheric depositions in this study area. PC1 accounted for 53.4% of the total variance. Zn, Pb, and Cd in the soil came from the residue of waste from the zinc oxide smelter, together with the input of atmospheric deposition and the residues of historical indigenous zinc smelting (Gu et al., 2021). Cupric elements have multiple sources, such as mining production and steel smelting (Zhang et al., 2016). PC1 therefore represented the emission of industrial waste residue, the waste residue from historical indigenous zinc smelting, and exhaust emissions. PC2 accounted for 16.9% of the variance, with the factor loading of Ni in this component reaching 0.98. Nonetheless, **Table 2** shows that the concentration of Ni in the soil did not exceed the background value of this heavy metal, which points to the sources of geology and the re-suspended soil particles (Xing et al., 2020b). PC3 contributed 15.0% of the variance, with the Cr loading much higher, at 0.81. Coal burning and chemical production are known to emit Cr, and industrial atmospheric deposition was thus the most probable source of this pollution (Sternbeck et al., 2002; Vallius et al., 2003; Pan et al., 2021).

PCA with Varimax rotation was applied to heavy metal elemental of atmospheric depositions and soil to assess the possible emission sources (Cereceda-Balic et al., 2020). We identified two major emission sources of heavy metal content in atmospheric depositions and soil in HS, and three major emission sources in MS. Combined with the specific environmental situation of the MS, the findings pointed to more diverse sources of the heavy metals in MS soil, and one of the major means by which heavy metals can contaminate areas was found to be atmospheric deposition, as reported in other studies (Zheng et al., 2016).

3.4 The Impact of Heavy Metals From Atmospheric Deposition on Soil

As shown in **Table 4**, the zinc smelting plant was established in 2006, after 13 years of heavy metal deposition accumulated in the soil surface. Heavy metals from atmospheric deposition on soil after 13 years deposition were Zn > Pb > Cr > Cu > Ni > Cd, which were 120 mg kg^{-1} ~ 1.51 mg kg^{-1}, respectively. The contribution rate of the atmospheric deposition on soil was 15.0% (Zn)~17.9% (Cd) (**Table 4**).

We predicted increments of heavy metal content from the atmospheric deposition based on the Gaussian model of elevated continuous point source (Hao et al., 2010), and the predicted heavy metal concentration is according to the proportion of dust in the bag dust collector in the zinc oxide smelter [Cd (311 mg kg^{-1}), Pb (10,570 mg kg^{-1}), Cr (1780 mg kg^{-1}), Cu (735 mg kg^{-1}), Ni (351 mg kg^{-1}), and Zn (26,700 mg kg^{-1})]. After 13 years deposition, the order of heavy metals follow Zn > Pb > Cr > Cu > Ni > Cd, that was the similarity as the monitoring values in this study, and the input contents were

TABLE 4 | The impact of heavy metals from atmospheric deposition on soil.

Watershed	Index	Cd	Pb	Cr	Cu	Ni	Zn
HS	Deposition flux of heavy metals/(mg m^{-2}·a^{-1})	13.8	440	49.5	102	29.5	1,292
MS	Deposition flux of heavy metals/(mg m^{-2}·a^{-1})	27.8	602	145	76.0	43.9	2,225
	Increment contents in topsoil after 13 years deposition/(mg·kg^{-1})	1.51	32.6	7.91	4.10	2.40	120
	Contribution of deposition on soil/(%)	17.9	8.52	16.9	9.15	5.10	15.0
MS Predictive value	Deposition flux of prediction of emission/(mg m^{-2}·a^{-1})	17.5	381	100	41.3	19.7	1,500
	Increment contents in topsoil after 13 years deposition/(mg·kg^{-1})	0.95	20.6	5.44	2.23	1.07	81.2
	Contribution of deposition on soil/(%)	11.3	5.38	11.7	4.96	2.30	10.1
Northwest of Guizhou province	Atmospheric deposition from historical artisanal zinc smelting/(t)× 10^4	0.56 ~ 2.08	1.02 ~ 5.20	2.00 ~ 4.71	1.00 ~2.46	0.89 ~ 3.32	25.2 ~ 72.0

81.25 mg kg^{-1}~0.95 mg kg^{-1}. The contribution rates of the atmospheric deposition of the soil were 10.1~11.3%. This result was generally smaller compared to the monitoring value. One reason for this was that the heavy metal content of zinc ore and coal was not fixed, and we only used one parameter in the Gaussian model (Hao et al., 2010). Another reason was that the monitoring atmospheric deposition was included in the soil mineral source, traffic source, and other sources of pollution.

The total concentration of cadmium in the soil comprises the contribution from the geological parent material together with inputs from extraneous sources, which, for the most part, were anthropogenic in origin. Compared to other studies, our results were significantly higher; for example, Cd content was 1.51 mg kg^{-1} here, but it was just 23.5 μg kg^{-1} in the industrial area and 3.46 μg kg^{-1} in the nonindustrial area (Cao et al., 2020). As Xie et al. (2019) reported, the contribution of atmospheric deposition to soil Cd, Pb, and Zn input in nonindustrial areas was 50.3, 70.3, and 36.5%, respectively, while the atmospheric heavy metal input flux was lower than in our context. This was because the soil heavy metal concentration was generally lower in such studies. We can conclude that the increments of heavy metal content from the atmospheric deposition on soil grow quickly within the zinc smelting plant pollution area.

We estimated the superposition of the atmospheric deposition of heavy metals in soil based on the 24 million tons of waste residue from historical indigenous zinc smelting from 30 years ago. We estimated that heavy metals deposited in the soil reached 0.56 ~ 2.08 × 10^4 t (Cd), 1.02 ~ 5.20 × 10^4 t (Pd), 2.00 ~ 4.71 × 10^4 t (Cr), 1.00 ~2.46 × 10^4 t (Cu), 0.89~3.32 × 10^4 t (Ni), and 25.2~ 72.0 × 10^4 t (Zn), respectively (Table 5) (Xia and Huang, 2011; Shang, 2012). In the absence of pollution treatment of waste gas, water, and residue, large-scale historical indigenous zinc smelting in northwest Guizhou Province could have more serious superposition effects on soil heavy metal pollution than we expected.

4 CONCLUSION

Soil heavy metals Cd, Pb, and Zn were much higher than local background values in the context of geochemical anomaly in northwest Guizhou Province. Heavy metals from atmospheric deposition were higher in the zinc smelting plant watershed than in the control watershed, and after 13 years of deposition the contribution rate of atmospheric deposition on topsoil was lowest for Ni, at 5.10%, and highest for Cd, at 17.9%. The spatial distribution of soil heavy metal indicates that the content of heavy metals in soil was highly coupled with the location of zinc smelting in MS watershed. Combined with the principal component analysis of atmospheric deposition and soil heavy metal, it can be concluded that zinc smelting atmospheric deposition showed superposition effects on the accumulation of heavy metals in topsoil under the geochemical anomaly in this area.

DATA AVAILABILITY STATEMENT

The original contributions presented in the study are included in the article/Supplementary Material, further inquiries can be directed to the corresponding author.

AUTHOR CONTRIBUTIONS

EY: Formal analysis, Data curation, Writing—Original Draft, Writing—Review and Editing, Visualization; HL: Conceptualization, Validation, Resources, Funding acquisition; YT, XG, XR: Methodolog, Investigation, Project administration; PW, ZY: Supervision.

FUNDING

This project was supported by the China National Natural Science Foundation (42067028); the National Natural Science Foundation of China and Guizhou Province (U1612442); the National Key Research and Development Plan Project (2018YFC1802602); and the Guizhou Province Science and Technology Planning Project (Qiankehehoubuzu (2020) 3001).

REFERENCES

Adimalla, N. (2020). Heavy Metals Contamination in Urban Surface Soils of Medak Province, India, and its Risk Assessment and Spatial Distribution. *Environ. Geochem. Health* 42 (1), 59–75. doi:10.1007/s10653-019-00270-1

Al-Khashman, O. A., Jaradat, A. Q., and Salameh, E. (2013). Five-year Monitoring Study of Chemical Characteristics of Wet Atmospheric Precipitation in the Southern Region of Jordan. *Environ. Monit. Assess.* 185, 5715–5727. doi:10.1007/s10661-012-2978-1

Cai, K., Li, C., and Na, S. (2019). Spatial Distribution, Pollution Source, and Health Risk Assessment of Heavy Metals in Atmospheric Depositions: a Case Study from the Sustainable City of Shijiazhuang, China. *Atmosphere* 10 (4), 222. doi:10.3390/atmos10040222

Cao, X., Tan, C., Wu, L., Luo, Y., He, Q., Liang, Y., et al. (2020). Atmospheric Deposition of Cadmium in an Urbanized Region and the Effect of Simulated Wet Precipitation on the Uptake Performance of rice. *Sci. Total Environ.* 700, 134513. doi:10.1016/j.scitotenv.2019.134513

Cereceda-Balic, F., Gala-Morales, M. d. l., Palomo-Marín, R., Fadic, X., Vidal, V., Funes, M., et al. (2020). Spatial Distribution, Sources, and Risk Assessment of Major Ions Ad Trace Elements in Rainwater at Puchuncaví Valley, Chile: The Impact of Industrial Activities. *Atmos. Pollut. Res.* 11 (6), 99–109. doi:10.1016/j.apr.2020.03.003

Chai, L., Wang, Y. H., and Wang, X. (2021). Pollution Characteristics, Spatial Distributions, and Source Apportionment of Heavy Metals in Cultivated Soil in Lanzhou, China. *Ecol. Indicators* 125, 107507. doi:10.1016/J.ECOLIND.2021.107507

Chen, L., Zhou, S., Wu, S., Wang, C., Li, B., Li, Y., et al. (2018). Combining Emission Inventory and Isotope Ratio Analyses for Quantitative Source Apportionment of Heavy Metals in Agricultural Soil. *Chemosphere* 204, 140–147. doi:10.1016/j.chemosphere.2018.04.002

Chen, X., Yang, Z. F., and Chen, Y. (2019). Cadmium Input Flux in farmland Soil of Nine Counties in Middle and East Guangxi. *Geophys. Geochemical Exploration* 43 (02), 415–427. doi:10.11720/wtyht.2019.139

Cui, X. T., Luan, W., and Li, S. (2012). An Analysis of the Sources of Heavy Metals in Atmospheric Dust Fall of Shijiazhuang City. *Geology. China* 39 (4), 1108–1114. doi:10.14050/j.cnki.1672-9250.2012.03.004

de P. Pereira, P. A., Lopes, W. A., Carvalho, L. S., da Rocha, G. O., de Carvalho Bahia, N., Loyola, J., et al. (2007). Atmospheric Concentrations and Dry Deposition Fluxes of Particulate Trace Metals in Salvador, Bahia, Brazil. *Atmos. Environ.*, 41, 7837–7850. doi:10.1016/j.atmosenv.2007.06.013

Garg, B. D., Cadle, S. H., Mulawa, P. A., Groblicki, P. J., Laroo, C., and Parr, G. A. (2000). Brake Wear Particulate Matter Emissions. *Environ. Sci. Technol.* 34, 4463–4469. doi:10.1021/es001108h

Gu, H., Zhao, T., and Sun, R. G. (2021). Pollution Characteristics and Source Analysis of Heavy Metals in Soils of a Typical Lead-zinc Mining Area in Guizhou Province. *Earth and Environment* 1–10. doi:10.14050/j.cnki.1672-9250.2022.50.003

Hao, J. M., Ma, G. D., and Wang, S. X. (2010). *Air Pollution Control Engineering*. Third Edition. Beijing: Higher Education Press5

He, S. L., and Chen, Z. (2002). The Zoning of Surface Tectonic Geochemistry in Guizhou and its Significance. *Guizhou Geology.* 03, 148–155.

Hermanson, M. H., Isaksson, E., Hann, R., Teixeira, C., and Muir, D. C. G. (2020). Atmospheric Deposition of Organochlorine Pesticides and Industrial Compounds to Seasonal Surface Snow at Four Glacier Sites on Svalbard, 2013-2014. *Environ. Sci. Technol.* 54 (15), 9265–9273. doi:10.1021/acs.est.0c01537

Hernández-Pellón, A., and Fernández-Olmo, I. (2019). Airborne Concentration and Deposition of Trace Metals and Metalloids in an Urban Area Downwind of a Manganese alloy Plant. *Atmos. Pollut. Res.* 10 (3), 712–721. doi:10.1016/j.apr.2018.11.009

Kara, M., Dumanoglu, Y., Altiok, H., Elbir, T., Odabasi, M., and Bayram, A. (2014). Seasonal and Spatial Variations of Atmospheric Trace Elemental Deposition in the Aliaga Industrial Region, Turkey. *Atmos. Res.* 149, 204–216. doi:10.1016/j.atmosres.2014.06.009

Kiyoshi, M., Keisuke, S., and Yuuya, W. (2019). Water-soluble and Water-Insoluble Organic Nitrogen in the Dry and Wet Deposition. *Atmos. Environ.* 218, 117022. doi:10.1016/j.atmosenv.2019.117022

Li, S., and Jia, Z. (2018). Heavy Metals in Soils from a Representative Rapidly Developing Megacity (SW China): Levels, Source Identification and Apportionment. *Catena* 163, 414–423. doi:10.1016/j.catena.2017.12.035

Li, X. H. (2020). *Effects of Environmental Factors on Heavy Metal Release and Biological Effects in Lead-Zinc Smelting Slag. [Master's Thesis]*. Gui Yang, China: Guizhou University.

Li, Z. G., Feng, X. B., Bi, X. Y., Sun, G. Y., Zhu, J. M., Qin, H. B., et al. (2013). Heavy Metals in the Ground Surface Dust and Agricultural Soil in Artisanal and Medium-Scale Zinc Smelting Area in Northwest Guizhou Province, China. *E3S Web of Conferences* 1, 19004. doi:10.1051/e3sconf/20130119004

Liang, J. N., Liu, J., Chen, J., et al. (2014). Characteristics of Heavy Metals in Atmospheric Deposition in Heating Periods of an Industrial Park in Western Shanxi Province, China. *Acta Scientiea Circumstantiae* 34 (2), 318–324. doi:10.13671/j.hjkxxb.2014.02.015

Liu, F. Z., Hu, J. L., and Liu, J. S. (2018). Spatial Distribution and Risk Assessment of Heavy Metals in Soil in the Metal Mining Area of Paojinshan, Hunan, China. *J. Agro-Environment Sci.* 37 (1), 86–95.

Luo, K., Liu, H., Liu, Q., Tu, Y., Yu, E., and Xing, D. (2020). Cadmium Accumulation and Migration of 3 Peppers Varieties in Yellow and limestone Soils under Geochemical Anomaly. *Environ. Technol.* 29, 1–11. doi:10.1080/09593330.2020.1772375

Luo, K., Liu, H., Zhao, Z., Long, J., Li, J., Jiang, C., et al. (2019). Spatial Distribution and Migration of Cadmium in Contaminated Soils Associated with a Geochemical Anomaly: A Case Study in Southwestern China. *Pol. J. Environ. Stud.* 28 (5), 3799–3807. doi:10.15244/pjoes/94847

Luo, Y., Wu, Y., Wang, H., Xing, R., Zheng, Z., Qiu, J., et al. (2018). Bacterial Community Structure and Diversity Responses to the Direct Revegetation of an Artisanal Zinc Smelting Slag after 5 Years. *Environ. Sci. Pollut. Res.* 25, 14773–14788. doi:10.1007/s11356-018-1573-6

Ministry of Environmental Protection (2014). *Water Quality - Digestion of Total Metals - Microwave Assisted Acid Digestion Method(HJ 678-2013)*.

Pan, Y., Liu, J., Zhang, L., Cao, J., Hu, J., Tian, S., et al. (2021). Bulk Deposition and Source Apportionment of Atmospheric Heavy Metals and Metalloids in Agricultural Areas of Rural Beijing during 2016-2020. *Atmosphere* 12 (2), 283. doi:10.3390/ATMOS12020283

Pan, Y. P., and Wang, Y. S. (2015). Atmospheric Wet and Dry Deposition of Trace Elements at 10 Sites in Northern China. *Atmos. Chem. Phys.* 15, 951–972. doi:10.5194/acp-15-951-2015

Peng, Y., Chen, J., Wei, H., Li, S., Jin, T., and Yang, R. (2018). Distribution and Transfer of Potentially Toxic Metal(loid)s in Juncus Effusus from the Indigenous Zinc Smelting Area, Northwest Region of Guizhou Province, China. *Ecotoxicology Environ. Saf.* 152, 24–32. doi:10.1016/j.ecoenv.2018.01.026

Qiu, K., Xing, W., Scheckel, K. G., Cheng, Y., Zhao, Z., Ruan, X., et al. (2016). Temporal and Seasonal Variations of as, Cd and Pb Atmospheric Deposition Flux in the Vicinity of lead Smelters in Jiyuan, China. *Atmos. Pollut. Res.* 7 (1), 170–179. doi:10.1016/j.apr.2015.09.003

Shamsaddin, H., Jafari, A., Jalali, V., and Schulin, R. (2020). Spatial Distribution of Copper and Other Elements in the Soils Around the Sarcheshmeh Copper Smelter in southeastern Iran. *Atmos. Pollut. Res.* 11 (10), 1681–1691. doi:10.1016/j.apr.2020.07.002

Shang, X. H. (2012). Environmental Impact of Old-Styled Zinc Smelting and its Solution in Mile County. *Environ. Sci. Surv.* 31 (4), 76–78. doi:10.13623/j.cnki.hkdk.2012.04.027

Sonia, C., Jesús, D., and Ana, M. (2013). Heavy Metal Deposition Fluxes Affecting an Atlantic Coastal Area in the Southwest of Spain. Atmos. *Environ* 77, 509–517. doi:10.1016/j.atmosenv.2013.05.046

State Bureau of Environmental Protection. (1994). *Technical Guidelines for Environmental Impact Assessment-Atmospheric Environment(HJ/T 2.1~2.3-93)*. Bei Jing, China: China Environmental Science Press

State Environmental Protection Administration of China. (2004). *The Technical Specification for Environmental monitoring(HJ/T 166 -2004)*. Bei Jing, China: China Environmental Science Press

Sternbeck, J., Sjödin, A., and Andréasson, K. (2002). Metal Emissions from Road Traffic and the Influence of Resuspension-Results from Two Tunnel Studies. *Atmos. Environ.* 36, 4735–4744. doi:10.1016/S1352-2310(02)00561-7

Vallius, M., Lanki, T., Tiittanen, P., Koistinen, K., Ruuskanen, J., and Pekkanen, J. (2003). Source Apportionment of Urban Ambient PM2.5 in Two Successive

Measurement Campaigns in Helsinki, Finland. *Atmos. Environ.* 37, 615–623. doi:10.1016/S1352-2310(02)00925-1

Wang, J., Huang, Y., Li, T., He, M., Cheng, X., Su, T., et al. (2020). Contamination, Morphological Status and Sources of Atmospheric Dust in Different Land-Using Areas of a Steel-Industry City, China. *Atmos. Pollut. Res.* 11 (2), 283–289. doi:10.1016/j.apr.2019.10.014

Wang, J., Zhang, X., Yang, Q., Zhang, K., Zheng, Y., and Zhou, G. (2018). Pollution Characteristics of Atmospheric Dustfall and Heavy Metals in a Typical Inland Heavy Industry City in China. *J. Environ. Sci.* 71 (9), 283–291. doi:10.1016/j.jes.2018.05.031

Wang, Q., Xie, Z., and Li, F. (2015). Using Ensemble Models to Identify and Apportion Heavy Metal Pollution Sources in Agricultural Soils on a Local Scale. *Environ. Pollut.* 206, 227–235. doi:10.1016/j.envpol.2015.06.040

Xia, X., Yang, Z., Cui, Y., Li, Y., Hou, Q., and Yu, T. (2014). Soil Heavy Metal Concentrations and Their Typical Input and Output Fluxes on the Southern Song-Nen Plain, Heilongjiang Province, China. *J. Geochemical Exploration* 139, 85–96. doi:10.1016/j.gexplo.2013.06.008

Xia, Y., and Huang, M. J. (2011). Risk Assessment on Abandoned Traditional Smelting Zinc Sites in Bijie Prefecture. *Guizhou Agric. Sci.* 39 (8), 218–222. doi:10.1016/j.enpol.2011.03.051

Xie, G. X., Ying, J. Y., and Zhang, M. K. (2019). Mass Balance of Heavy Metals in Typical Pear Orchard Ecological System Affected by Fertilization and Atmospheric Deposition. *Chin. Agric. Bull.* 35 (16), 88–94.

Xing, W., Yang, H., Ippolito, J. A., Zhang, Y., Scheckel, K. G., and Li, L. (2020b). Lead Source and Bioaccessibility in Windowsill Dusts within a Pb Smelting-Affected Area. *Environ. Pollut.* 266, 115110. doi:10.1016/j.envpol.2020.115110

Xing, W., Yang, H., Ippolito, J. A., Zhao, Q., Zhang, Y., Scheckel, K. G., et al. (2020a). Atmospheric Deposition of Arsenic, Cadmium, Copper, lead, and Zinc Near an Operating and an Abandoned lead Smelter. *J. Environ. Qual.* 49 (6), 1667–1678. doi:10.1002/jeq2.20151

Yasser, M. G., Jesús, M. S., and David, E. (2019). Determination and Source Apportionment of Major and Trace Elements in Atmospheric Bulk Deposition in a Caribbean Rural Area. *Atmos. Environ.* 202, 93–204. doi:10.1016/j.atmosenv.2019.01.019

Yi, K., Fan, W., Chen, J., Jiang, S., Huang, S., Peng, L., et al. (2018). Annual Input and Output Fluxes of Heavy Metals to Paddy fields in Four Types of Contaminated Areas in Hunan Province, China. *Sci. Total Environ.* 634, 67–76. doi:10.1016/j.scitotenv.2018.03.294

Yu, E. J., and Liu, H. Y. (2021). Effect of Atmospheric Deposition on Cadmium Accumulation in Soils: a Review. *Environ. Anal. Eco. Stud.* 8 (1), 432–846. doi:10.31031/EAES.2021.08.000676

Yu, Z., Chen, F., and Zhang, J. J. (2019). Contamination and Risk of Heavy Metals in Soils and Vegetables from Zinc Smelting Area. *China Environ. Sci.* 39 (5), 2086–2094. doi:10.19674/j.cnki.issn1000-6923.2019.0250

Zhang, S., and Song, J. (2018). Geochemical Cadmium Anomaly and Bioaccumulation of Cadmium and lead by Rapeseed (Brassica Napus L.) from Noncalcareous Soils in the Guizhou Plateau. *Sci. Total Environ.* 644, 624–634. doi:10.1016/j.scitotenv.2018.06.230

Zhang, W., Long, J., Wei, Z., and Alakangas, L. (2016). Vertical Distribution and Historical Loss Estimation of Heavy Metals in an Abandoned Tailings Pond at HTM Copper Mine, Northeastern China. *Environ. Earth Sci.* 75 (22), 1462. doi:10.1007/s12665-016-6271-4

Zheng, X., Guo, X., Zhao, W., Shu, T., Xin, Y., Yan, X., et al. (2016). Spatial Variation and Provenance of Atmospheric Trace Elemental Deposition in Beijing. *Atmos. Pollut. Res.* 7 (2), 260–267. doi:10.1016/j.apr.2015.10.006

Zhou, Y., Wang, L., Xiao, T., Chen, Y., Beiyuan, J., She, J., et al. (2020). Legacy of Multiple Heavy Metal(loid)s Contamination and Ecological Risks in farmland Soils from a Historical Artisanal Zinc Smelting Area. *Sci. Total Environ.* 720, 137541. doi:10.1016/j.scitotenv.2020.137541

Conflict of Interest: The authors declare that the research was conducted in the absence of any commercial or financial relationships that could be construed as a potential conflict of interest.

Publisher's Note: All claims expressed in this article are solely those of the authors and do not necessarily represent those of their affiliated organizations, or those of the publisher, the editors and the reviewers. Any product that may be evaluated in this article, or claim that may be made by its manufacturer, is not guaranteed or endorsed by the publisher.

frontiers in Environmental Science

ORIGINAL RESEARCH
published: 14 March 2022
doi: 10.3389/fenvs.2022.854460

Heavy Metal Contamination (Cu, Pb, Zn, Fe, and Mn) in Urban Dust and its Possible Ecological and Human Health Risk in Mexican Cities

*Anahi Aguilera[1,2], José Luis Cortés[1], Carmen Delgado[3], Yameli Aguilar[4], Daniel Aguilar[5], Ruben Cejudo[3], Patricia Quintana[5], Avto Goguitchaichvili[3] and Francisco Bautista[1]**

[1]Laboratorio Universitario de Geofísica Ambiental, Centro de Investigaciones en Geografía Ambiental, Universidad Nacional Autónoma de México, Michoacán, México, [2]Posgrado en Ciencias Biológicas, Universidad Nacional Autónoma de México, Michoacan, Mexico, [3]Laboratorio Universitario de Geofísica Ambiental, Instituto de Geofísica Unidad Michoacán, Universidad Nacional Autónoma de México, Michoacán, México, [4]Instituto Nacional de Investigaciones Forestales, Agrícolas y Pecuarias, Merida, Mexico, [5]Applied Physics Dept Centro de Investigación y de Estudios Avanzados Unidad, Merida, Mexico

OPEN ACCESS

Edited by:
Juan Manuel Trujillo-González, University of the Llanos, Colombia

Reviewed by:
Raimundo Jimenez Ballesta, Autonomous University of Madrid, Spain
Rogelio Flores Ramírez, Universidad Autónoma de San Luis Potosí, Mexico

***Correspondence:**
Francisco Bautista
leptosol@ciga.unam.mx

Specialty section:
This article was submitted to Toxicology, Pollution and the Environment, a section of the journal Frontiers in Environmental Science

Received: *14 January 2022*
Accepted: *16 February 2022*
Published: *14 March 2022*

Citation:
Aguilera A, Cortés JL, Delgado C, Aguilar Y, Aguilar D, Cejudo R, Quintana P, Goguitchaichvili A and Bautista F (2022) Heavy Metal Contamination (Cu, Pb, Zn, Fe, and Mn) in Urban Dust and its Possible Ecological and Human Health Risk in Mexican Cities. Front. Environ. Sci. 10:854460. doi: 10.3389/fenvs.2022.854460

Cities occupy a relatively small percentage of the Earth's surface. However, they influence the entire biosphere, affect biodiversity and environmental conditions, which end up affecting human health and well-being. Therefore, it is necessary to evaluate the level of contamination by heavy metals in urban environments, as well as the possible ecological and human health risks. In this study, the urban dust of six Mexican cities was analyzed and it was found that all studied cities were contaminated, except for Mérida, when soil world background value was used as reference. In contrast, Mérida and Morelia were the most contaminated when a local background was used (decile 1). The concentrations in the cities for the metals Cu, Pb and Zn, decreased in the order CDMX > San Luis Potosí > Toluca > Morelia-Ensenada > Mérida. In the particular case of Cu and Pb, SLP accompanied CDMX as the most polluted city. For Mn and Fe concentrations, the order was CDMX > Toluca > Ensenada > SLP > Morelia-Mérida. No potential ecological risk was found due to contamination by Cu, Pb, and Zn, in the urban dust of the studied cities. However, the higher metal contribution to the potential ecological risk in all the cities was from Pb; and it represented a moderate ecological risk of more than 25% on CDMX, SLP, and Toluca sites. Pb can also be a potential risk for children's health. In addition, chronic exposure to Fe and Mn could trigger many ailments. In the future, it is important to identify the main sources of Pb in cities and seek mitigation strategies to reduce the possible adverse effects that this metal may be causing.

Keywords: street dust, pollution load index, risk assessment, lead, Mexico

1 INTRODUCTION

Cities occupy a small percentage of the global land surface (~5%) but can influence the entire biosphere (Angeoletto et al., 2015). Between the multiple challenges of cities, the constant impact of human activities can have unintended repercussions on biodiversity, the functioning of ecosystems, and environmental quality, causing, in turn, a negative impact on human health and well-being (Lawrence 2003).

Urban dust is made up of solid particles deposited on impermeable materials that originate from the interaction of solids, liquids, and gases in the environment (Keshavarzi et al., 2018). Urban dust is a receptor for solid particles from different sources, therefore it becomes a sink for atmospheric particles. At the same time, urban dust can also be considered as a pollutant source into the atmosphere and soils, through the re-suspension of this material. It can also be a source of contaminants for water (Keshavarzi et al., 2018; Safiur Rahman et al., 2019), through rain runoff (Jayarathne et al., 2018).

Among the pollutants present in urban dust, heavy metals can be toxic or harmful to the environment and living beings, even at low concentrations. They are generally associated with relatively high densities (>5 g/cm^3) since their density is assumed to be related to toxicity. Additionally, heavy metals are persistent in the environment and bioaccumulate, thus gaining public attention (Lin et al., 2017). The mechanism of toxicity of heavy metals can be explained by their ability to interact with nuclear proteins and DNA, causing deterioration of biological macromolecules (Helaluddin et al., 2016).

Ensenada, San Luis Potosí, Mexico City, Toluca, Morelia, and Mérida are Mexican cities located at different latitudes and with different geological environments. These urban areas are within the 20 Metropolitan Zones with the highest total gross production and number of inhabitants (CONAPO and SEDESOL 2012) and they could highlight the current situation in terms of contamination by heavy metals and let us explore the influence of the city size (number of inhabitants) and geological environment (physiographic province) on the pollution.

Diagnoses of contamination by heavy metals in urban dust have been carried out in some of these cities of Mexico. In Mérida and Ensenada the color of urban dust has proved to be an indicator of heavy metal pollution, dark colors are more polluted than light ones (Cortés et al., 2015; Aguilar et al., 2021). In San Luis Potosí, the highest concentrations of heavy metals in urban dust have been related to the metallurgical complex and the industrial park (Aguilera et al., 2019); and heavy metals in soils could also be an important pathway of exposure (Perez-Vazquez et al., 2015; Pérez-Vázquez et al., 2015), indeed metal concentrations have been identified in children (Flores-Ramírez et al., 2018). Mexico City has been identified as polluted by heavy metals in urban dust (Delgado et al., 2019), and heavy metal concentrations have been measured in mothers and children (Lewis et al., 2018). However, the effects of urbanization on environmental quality vary between regions with different degrees of development, topography, natural resources, and public policies (Liang, Wang, and Li 2019).

In this study, we wonder whether there is heavy metal contamination in the urban dust of six Mexican cities and if this contamination may represent a potential ecological and human health risk. It is expected that the largest and most industrialized cities will have the highest concentrations of heavy metals, however, we do not know if this happens proportionally with size and if this is the case for all metals. We also explore the differences in the pollution between located in the same and different physiographic provinces.

2 METHODS

2.1 Data Collection

In previous studies, urban dust samples were collected during the dried season in Mexico City in 2011 (CDMX, n = 89), Ensenada in 2012 (ESE, n = 86), San Luis Potosí in 2017 (SLP, n = 100), Morelia in 2014 (MLM, n = 100), Mérida in 2016 (MID, n = 101) and Toluca in 2013 (TLC, n = 89). For all the cities, a standard sampling procedure was followed which consisted of sweeping 1 m^2 of street surface, following a systematic, homogeneously distributed sampling design. The samples were packed in plastic bags and georeferenced (**Supplementary Figure S1**). Description of the study sites can be seen in the Supplementary material. They were dried in the shade and at room temperature for 2 weeks to avoid any kind of oxidation. Subsequently, they were passed through a number 10 sieve with a 2 mm opening, to remove the coarse fragments.

Chemical analysis of heavy metals in cities was done by X-ray fluorescence energy dispersive (XRF-ED). Only in the case of Morelia inductively coupled plasma optical emission spectroscopy (ICP-OES) was used. The details of the methodology can be consulted in previous studies: CDMX (Delgado et al., 2019), Ensenada (Cortés et al., 2015), SLP (Aguilera et al., 2019), Mérida (Aguilar et al., 2021). We selected the heavy metals that were measured for all the cities, those metals were copper (Cu), lead (Pb), zinc (Zn), manganese (Mn), and iron (Fe).

2.2 Identification of the Most Polluted Cities

To evaluate the level of contamination of each heavy metal, the contamination factor (CF) was used, which is a technique used to find the state of contamination of each element, as well as the pollutant load index (PLI), which is the geometric average of the five metals studied (Tomlinson et al., 1980):

$$CF = C_n / F_n \tag{1}$$

$$PLI = \sqrt[n]{CF1 * CF2 * \ldots * CFn} \tag{2}$$

C_n represents the concentration of a heavy metal n and F_n is the background value of the same heavy metal. Generally, the background values found in soils with little anthropization or a general reference value such as the world background values for soils are used (Kabata-Pendias 2011). This study used both the background values reported for soils worldwide (Kabata-Pendias 2011), as well as the first decile of the distribution of frequencies of the heavy metals in each city, to compare what happens when considering the particularities of each site against a general reference value.

A CF less than 1 indicates insignificant contamination, between 1–3 a moderate contamination, between 3–6 considerable and greater than 6 a high contamination level (Ihl et al., 2015). A PLI close to one indicates that the heavy metal load is close to the background level, while a PLI > 1 indicates contamination (Mehr et al., 2017).

Subsequently, Kruskal-Wallis analyzes were carried out to identify if there were statistically significant differences in the concentrations of heavy metals between cities. To perform the

statistical analysis (descriptive statistics, Pearson correlation, and Kruskal-Wallis test) and the figures, the R Project software, version 4.0.4 (2021-02-15) "Lost Library Book" was used.

2.2.1 Ecological Risk Assessment

The ecological risk factor (E_i) for each heavy metal (Cu, Pb y Zn) was calculated with the **Eq. 3** (Hakanson 1980):

$$E_i = \left(T_f\right)_n x\ (CF)_n \tag{3}$$

where T_f is the toxic response factor of each metal, Cu = Pb = 5, Zn = 1, Mn = 1; and CF is the corresponding pollution factor, in this study we used the soil worldwide background (Kabata-Pendias 2011). E_i is classified as low potential ecological risk ($E_i < 40$), moderate potential ecological risk ($40 \leq E_i < 80$), considerable potential ecological risk ($80 \leq E_i < 160$), high potential ecological risk ($160 \leq E_i < 320$) and a very high potential ecological risk ($E_i \geq 320$) (Hakanson 1980; Hua et al., 2018; Jahandari 2020).

Toxic response factors (T_f) They are based on the principle of abundance, which indicates that the potential toxicological effect of an element is proportional to its abundance, or rarity, in nature. In addition, T_f considers the tendencies of each metal to be deposited in the lake sediments and a dimension correction (order of magnitude) was also made so that they could be compared with the CF (Hakanson 1980).

To obtain the potential ecological risk of several metals (PER) we used the following equation:

$$PER = \sum_{n=1}^{n} (E_i)_n \tag{4}$$

Where E_i is the potential ecological risk index for each metal, and n is the number of heavy metals analyzed. PER is divided into four classes: low potential ecological risk ($PER \leq 150$), moderate potential ecological risk ($150 < PER \leq 300$), considerable potential ecological risk ($300 < PER \leq 600$), high potential ecological risk ($PER > 600$) (Yesilkanat et al., 2021).

2.2.2 Human Health Risk Assessment

To estimate the risk of heavy metals, present in urban dust on the health of the population, the USEPA methodology will be used. First, the estimated daily intakes were calculated per ingestion (EDI_{ing}), inhalation (EDI_{inh}) and dermal contact (EDI_{dermal}) (**Eqs 5–7**); as well as the average daily dose for life (LADD) to estimate the carcinogenic risk (CR) (**Eq. 8**).

$$EDI_{ing} = \frac{C{*}IngR{*}EF{*}ED{*}CF}{BW{*}AT} \tag{5}$$

$$EDI_{inh} = \frac{C{*}InhR{*}EF{*}ED}{PEF{*}BW{*}AT} \tag{6}$$

$$EDI_{dermal} = \frac{C{*}SA{*}AF{*}ABS{*}EF{*}ED{*}CF}{BW{*}AT} \tag{7}$$

$$LADD = \frac{C}{PEFxAT_{can}} x\left(\frac{CR_{child}xEF_{child}xED_{child}}{BW_{niño}} + \frac{CR_{adulto}xEF_{adulto}xED_{adulto}}{BW_{adulto}}\right) \tag{8}$$

CR is the contact or absorption rate. CR = IngR for ingestion, CR = InhR for inhalation, and CR = SA * AF * ABS for dermal contact. We calculated the *EDIs* for each of the sampling points.

The use of local parameters improves the reliability of the model; however, exposure factors have not been estimated for any Mexican city, therefore those of reference populations were used in this study (**Supplementary Table S1**).

Hazard ratios for ingestion, inhalation, and dermal contact ($HQ_{ing/inh/derm}$) were obtained by dividing the EDI between the reference dose (RfD) as shown in **Eq. 9**. RfD are presented in **Supplementary Table S2**.

$$HQ_{ing/inh/derm} = \frac{EDI_{ing/inh/derm}}{RfD} \tag{9}$$

The non-carcinogenic risk index (HI) represents the sum of the HQ for all three routes of exposure. If HI is greater than 1, there could be non-carcinogenic effects on the health of the population, if it is less than 1 the opposite would be expected (USEPA 2001).

For carcinogenic elements, the risk of developing cancer during life ($ILCR$) is commonly calculated by the following equation:

$$ILCR = LADD * CSF \tag{10}$$

The accepted or tolerable risk is in the range of 1E-06 to 1E-04 (USEPA 2001). These values indicate that an additional case in a population of 1,000,000 and 10,000 people is acceptable (Lu et al., 2014).

3 RESULTS AND DISCUSSION

Considering all the cities, Mn and Fe had a strong positive correlation (r = 0.9), and a strong negative correlation with Cu, Pb, and Zn (r < −0.7). Cu and Zn were also strongly correlated (r = 0.82), and they had a weaker correlation with Pb (Pb-Cu, r = 0.5; Pb-Zn, r = 0.35). This seems to indicate that Fe and Mn are elements that can share similar sources; in fact, they have been reported as elements of natural or mixed origin (Dehghani et al., 2016), in studies of heavy metals. On the other hand, Zn and Cu may also be sharing similar sources, some of which may be the same as those for Pb, while the latter metal could have other sources, in addition to those shared with Zn and Cu.

In general, the distribution of frequencies of the metals in the different studied cities was asymmetric to the right, this can be seen due to the differences between the median and the mean (**Supplementary Table S3**). The city with the greatest differences between the median and the mean of Cu and Pb was Morelia, in the case of Mn and Zn it was SLP, and for Fe it was Mérida. Within each city, when comparing the mean and the median among the different metals, Pb had the greatest differences. Such differences have been considered as a qualitative indicator of an anthropic enrichment of metal in the urban environment (Aguilera et al., 2019).

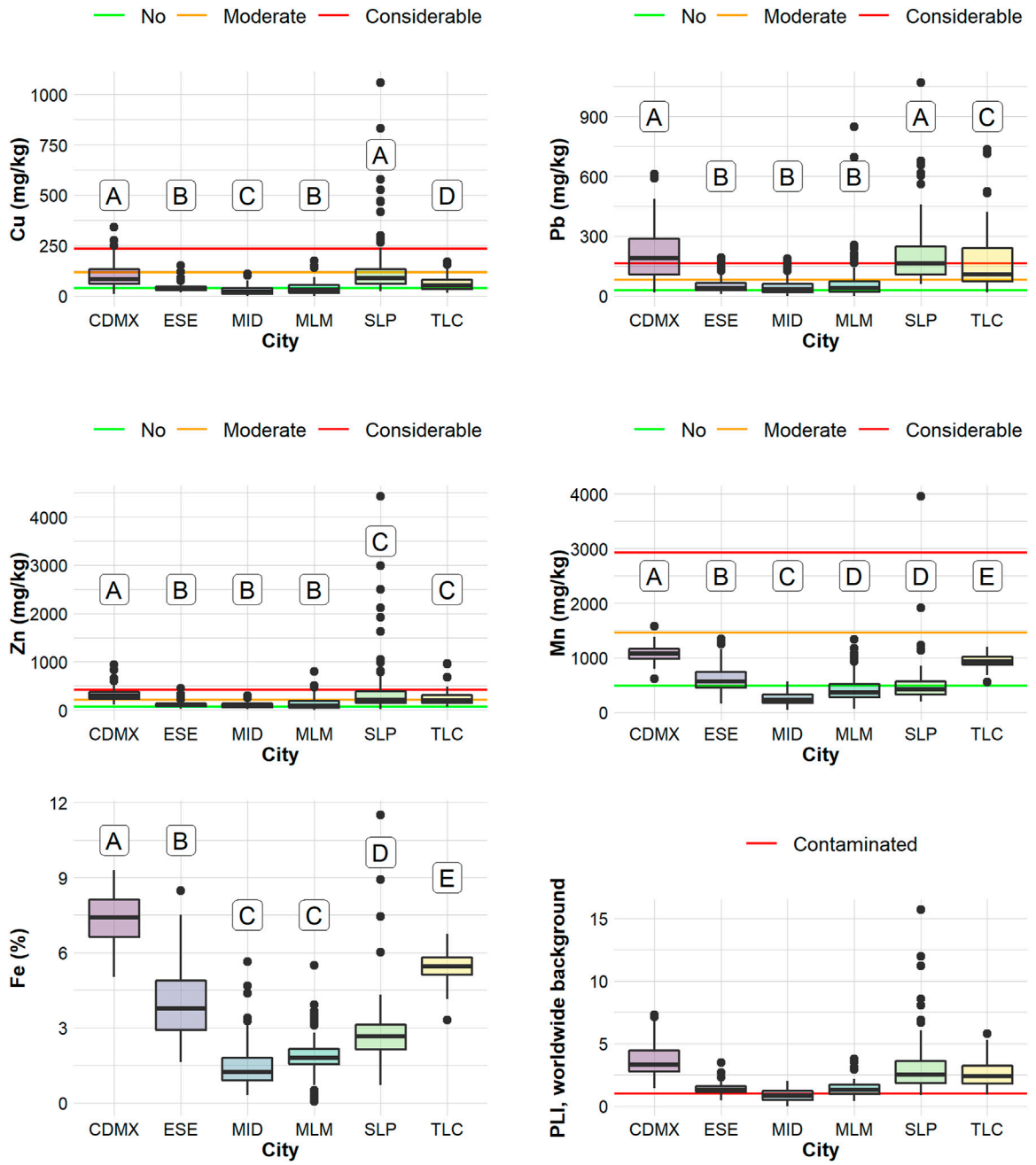

FIGURE 1 | Boxplots of the heavy metal concentrations. Different letters indicate significant differences. CDMX: Mexico City, ESE: Ensenada, MID: Mérida, MLM: Morelia, SLP: San Luis Potosí, TCL: Toluca. PLI: pollution load index. Horizontal lines represent the contamination levels using the background value established for soils worldwide (Kabata-Pendias 2011).

Previously, we did a systematic review to summarize the heavy metal concentrations in urban dust worldwide, considering 39 cities (Aguilera, Bautista, Goguitchaichvili, et al., 2021). This is a more efficient way to compare with multiple studies, instead of doing it one by one. Compared to the median values of that review, Cu (Mexico: 46.83 mg/kg, world: 83.4 mg/kg) and Zn (Mexico: 149.9 mg/kg, world: 280.7 mg/kg) had a lower median in the Mexican cities analyzed in this study. While the median Fe concentration in Mexico was higher than that reported for the world (Mexico: 30,600 mg/kg, world: 22,103 mg/kg).

By cities, the median Fe concentrations in CDMX, Ensenada, Toluca, and SLP were higher than those reported worldwide (Aguilera, Bautista, Goguitchaichvili, et al., 2021). In addition, in CDMX and Toluca the medians of Mn and Pb were also higher than those reported worldwide (Aguilera, Bautista, Goguitchaichvili, et al., 2021). In SLP, the median Pb

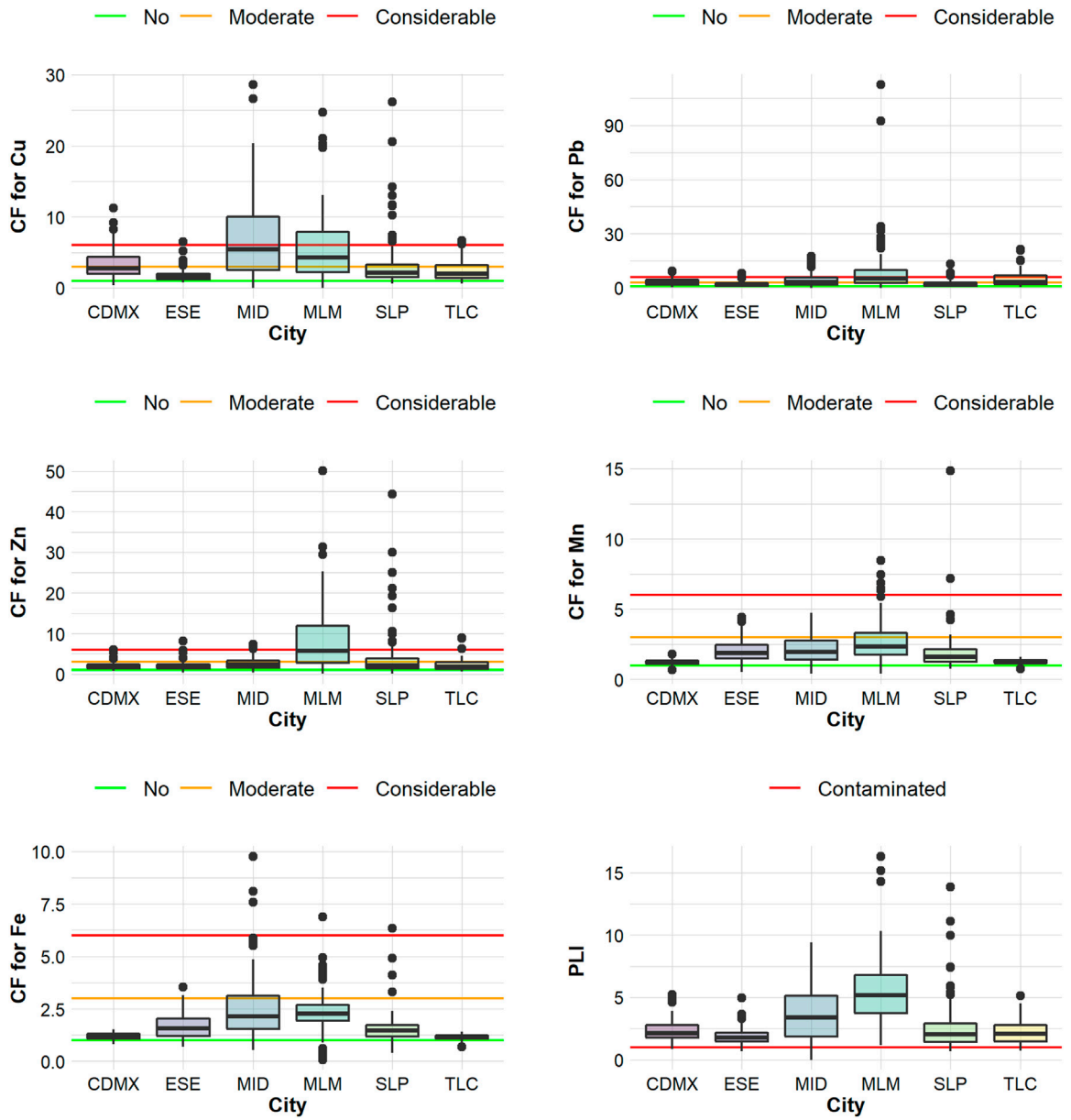

FIGURE 2 | Box plots of the contamination factors (CF), using decile 1 of each city as the background value. CDMX: Ciudad de México, ESE: Ensenada, MID: Mérida, MLM: Morelia, SLP: San Luis Potosí, TCL: Toluca. PLI: pollution load index. Horizontal lines represent the contamination levels.

concentration exceeded the world median While in Morelia and Mérida the median concentrations of all metals were lower than those of the world.

3.1 Most Polluted Cities

When the background value established for soils worldwide was considered (Kabata-Pendias 2011), all cities were contaminated, except for Mérida, since 75% of the data had a PLI greater than one (**Figure 1**). The median PLI decreased in the order CDMX > SLP > Toluca > Morelia–Ensenada > Mérida. It should be remembered that this indicates a general pattern of contamination by Cu, Pb, Zn, and Mn; Fe was not considered because there is no reported background value. This same order was maintained in the specific case of Cu, Pb, and Zn concentrations, with significant differences; particularly for Cu and Pb, SLP accompanied CDMX as the most polluted city. However, there were variations in the level of contamination for Mn and Fe by the city, the order was CDMX > Toluca > Ensenada > SLP > Morelia-Mérida (**Figure 1**).

On the other hand, when we estimated the level of contamination using decile 1 of each city as background values, the results changed. The cities with the lowest concentrations (Mérida and Morelia), and therefore the least contaminated using as a background value the one established for

soils worldwide, became the most polluted (**Figure 2**). When comparing the results of both background values, we observe that Morelia and Mérida were the most susceptible cities to changes in their level of pollution.

Morelia and Mérida turned out to be the most polluted cities because deciles 1 of heavy metals in both cities were very low (**Supplementary Table S3**), while deciles 1 of CDMX, Toluca, and SLP were high. The values of the first decile of Morelia were between 3 (the case of Mn) and 5.5 (the case of Cu) times lower than the background values of soils worldwide; while, in CDMX, the values of the first decile were approximately double the background values of soils worldwide, except for Cu, which was very similar to the first decile.

The differences observed by the use of both background values highlight the problem that has been discussed for decades, when a general background value is used all local variations are ignored, while when particular background values are used for each site, all local differences are emphasized (Hakanson 1980). In this study it was clear that the concentrations of CDMX, SLP, and Toluca were higher than those of Morelia or Mérida, however, the local background values of these last two cities were so small that they turned out to be the most contaminated when compared.

Another point to consider was the fact that the analytical technique (ICP-OES) with which Morelia concentrations were obtained was more sensitive than that used in all the other cities (XRF-ED). For this reason, lower values could have been detected in Morelia.

It is noteworthy that the contamination of Pb and Cu in the largest city in Mexico (CDMX) was comparable to that of a metallurgical city (SLP). Metallurgical and mining activities are among the main emitters of heavy metals into the environment (Tapia et al., 2018; Li et al., 2015), however, a large number of minor sources (vehicles, industries, garbage incineration, etc.) in urbanization (CDMX) can lead to a similar level of contamination.

While it is a common idea that the largest or most populated cities should be the most polluted, this is not necessarily true. The population decreased in the order CDMX > Toluca > SLP > Mérida > Morelia > Ensenada (INEGI Instituto Nacional de Estadística y Geografía 2014). Mérida was the fourth most populated city; however, it was the least polluted, considering the global background value. SLP was the third most populated city, but its level of contamination by Pb and Cu was comparable to that of CDMX (the most populated). Ensenada was the least populated city, but its concentrations of Mn and Fe were higher than those of SLP, Morelia, and Mérida. At the global level, Aguilera et al. (2021) did not find a correlation between the number of inhabitants and the concentrations of heavy metals. At the local level, in CDMX, no relationship was found (Aguilera, Bautista-Hernández, et al., 2021). However, other studies have found this relationship (Acosta et al., 2015; Trujillo-González et al., 2016).

Among the cities of the Neovolcanic Belt (Morelia, Toluca, CDMX; **Supplementary Material**), there were significant differences in the level of contamination, CDMX was the most contaminated city by Cu, Pb, Zn, Mn, and Fe with significant differences from Toluca, while Morelia was the least contaminated; therefore, pollution must be caused by human activities, rather than natural causes.

Fe and Mn may be sharing the same sources, they are considered as elements of natural or mixed origin (Dehghani et al., 2016). Zn and Cu may also be sharing similar sources, some of which may be the same as for Pb, while the latter metal could have other sources.

In CDMX it has been recognized that the main sources of Cu, Pb, and Zn in urban dust could be related to vehicular traffic (Aguilera, Bautista-Hernández, et al., 2021; Aguilera, Bautista, Gutiérrez-Ruiz, et al., 2021). In SLP, the main source of Cu and Zn is the metallurgical complex and to a lesser extent the industrial park, Pb could have the same sources, in addition to vehicular traffic (Aguilera et al., 2019). In Toluca, the main sources of Pb can be the combustion processes of food waste, paper, plastics, textiles, rubber, wood, and metal smelting; other sources, other than combustion, from these industries; as well as the old Pb deposit from leaded gasoline (Ávila-Pérez et al., 2019).

Little information is available on possible sources of heavy metals in the environment in Ensenada and Morelia. In Ensenada, using a bioindicator (mussel *Mytilus californianus*), it has been observed that Pb concentrations are affected by anthropic activities, in this study it was thought that Pb reached the mussel through the atmospheric deposition (Muñoz-Barbosa, Gutiérrez-Galindo, and Flores-Muñoz 2000). In Morelia, it was found that the highest concentrations of Zn in soils were located in primary roads with significant differences for the other roads. In addition, the concentrations of Mn, Pb, and Fe exceeded the maximum limits of the Mexican regulations for soils (Carranza et al., 2015), called NOM-147 (SEMARNAT 2007).

In Mérida, Cu, Zn, and Pb have been associated with vehicular traffic, because the highest concentrations have been found in the historic center and on primary roads. When observing the dust particles under a microscope, spherical particles of anthropic origin with these associated metals were found (Aguilar et al., 2021).

3.1.1 Potential Ecological Risk

The PER was below 150 for practically all cities; therefore, there is no potential ecological risk due to the concentrations of Cu, Pb, Mn, and Zn, together, in urban dust. Only two sites in SLP had a moderate potential ecological risk ($150 < PER \leq 300$) and one more site had a considerable risk ($300 < PER \leq 600$). The values of the medians of the PER decreased in the order CDMX > SLP > Toluca > Ensenada > Morelia > Mérida (**Figure 3**). Pb was the metal that most contributed to the PER in all cities, representing 67.3% of the PER in CDMX, 49.3% in Ensenada, 58.1% in Mérida, 55.1% in Morelia, 66.8.1% in SLP, and 64.1% in Toluca.

Even when no potential ecological risk was found due to Cu, Pb, Mn, and Zn, in the urban dust of the studied cities, it is important to remember that this index is the addition of the individual risks of each metal, as in this study only three metals could be analyzed, the risk may be lower than in other cities where more metals were considered (Yesilkanat et al., 2021). Therefore, if more metals were analyzed in Mexican cities, the ecological risk would change.

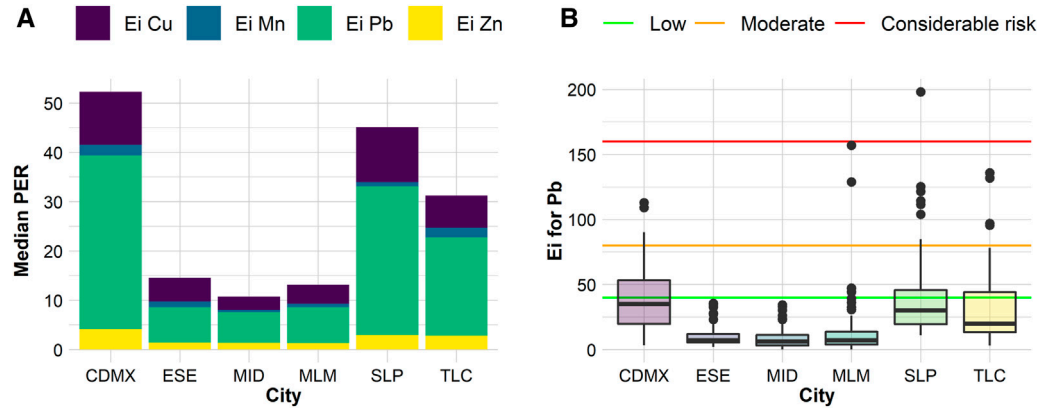

FIGURE 3 | In the **(A)**, the value of the median potential ecological risk (PER), divided according to the contribution of each of the metals risk factors (Ei). In the **(B)**, box plots of lead risk factors (Ei) for each studied city. CDMX: Mexico City, ESE: Ensenada, MID: Mérida, MLM: Morelia, SLP: San Luis Potosí, TCL: Toluca.

Pb alone did represent a potential ecological risk, according to the ecological risk factor (Ei). In more than 25% of sites of CDMX, SLP and Toluca a moderate risk was found, in some sites of these cities, a considerable risk was found, and only in one SLP site was a high risk (**Figure 3**). This result differs from that found in other studies where several cities were analyzed, in those cases different metals contributed the most to the ecological risk (Jahandari 2020; Yesilkanat et al., 2021). In fact, in the present work, Pb alone represents a moderate ecological risk in more than a quarter of the sampling sites of CDMX, SLP, and Toluca.

3.1.2 Human Health Risk

The main route of exposure to heavy metals was ingestion. The risk to human health was 10 times higher for children than for adults. Pb was the only metal that represented a non-carcinogenic risk for the health of children in the cities of CDMX, SLP, and Toluca since its HI was greater than one in ~25% of the sampling sites (**Figure 4**). Children are the most susceptible due to their hand-to-mouth habits and rapid growth rates (Kamali, Omidvar, and Kazemzadeh 2013).

Some points to consider are 1) the fact that the total concentrations of Pb were used to calculate the health risk indices, therefore the risk is being overestimated, it is necessary to use the bioavailable concentrations (Huang. 2016); 2) on the other hand, only the risk represented by urban dust is being considered, while that from other sources such as water, food, air, soil, and glazed ceramic also has its contribution to the total risk of this metal for the human health (Li et al., 2017); and 3) the effect that may have the combination of Pb with other metals and pollutants is still unknown.

Chronic exposure to an HI greater than 0.1 (1E-01) has been reported to trigger many ailments (Jadoon et al., 2018). In this sense, Fe represented a risk of generating ailments in children in all cities, since they all had HI greater than 0.1 (1E-01), in some sampling points; in CDMX and Toluca this happened for the entire city; in Ensenada, it happened in 87% of the cases and in SLP 46% of the cases had an HI greater than 0.1 (1E-01). In Morelia and Mérida, only the extreme values were in this situation. The Mn could also unleash health problems for children in all cities; especially in CDMX and Toluca, since their HI was greater than 0.1 in the entire city; in Ensenada, the HI was higher than 0.1 in 88% of the city, in SLP in 79%, in Morelia in 67% and Mérida in 29% of the city. In the case of Zn HI greater than 0.1 was only found in some sites of SLP; the same for Cu, together with one sampling point in CDMX. Cu and Zn were the metals that represented the least risk to human health.

Iron and manganese are generally not analyzed in heavy metal contamination studies, probably because they are not considered dangerous or relevant in the urban environment, however, that is not true (Kim, Lee, Seok et al., 2015; Kletetschka, Bazala, Takáč et al., 2021). We compared the mean HI for kids and adults in different cities and observed that HI for Fe commonly is higher than the one for other metals such as Cu and Zn (**Table 1**). In Mexico, the mean Fe HI for kids was higher than those reported in all the other cities. Black magnetite particles can be seen in the air filters of the air monitoring systems of Mexican cities. Mn has been analyzed only at sites where significant sources of this metal are known in advance (Menezes-Filho 2016; Rodrigues et al., 2018). The results of the present work indicated that it is important to include them and monitor their concentrations in cities. 04) (USEPA 2001).

In comparison with other cities (**Table 1**), the mean HI for Cu for kids was ten times higher than for Bandar-Abbas and Shiraz and the same for the other cities. For Zn were ten to twenty times lesser tan for the other cities. Mean Pb HI for kids in the six Mexican cities was higher than for Bandar-Abbas, lesser than for Düzce, and almost the same magnitude as for the rest of the cities. Mean Fe HI for kids in the six Mexican cities was higher than all the cities in comparison. Mn was higher than four of the six cities in comparison. The HIs for adults were similar but ten times lesser than for kids.

Pb was the only analyzed metal with the potential to generate cancer. However, the carcinogenic risk index (RI) indicated that this metal in urban dust does not represent a risk of developing cancer in any of the cities, the median value was 1.1E-9, which is below the accepted or tolerable risk (1E-06 a 1E-08 After

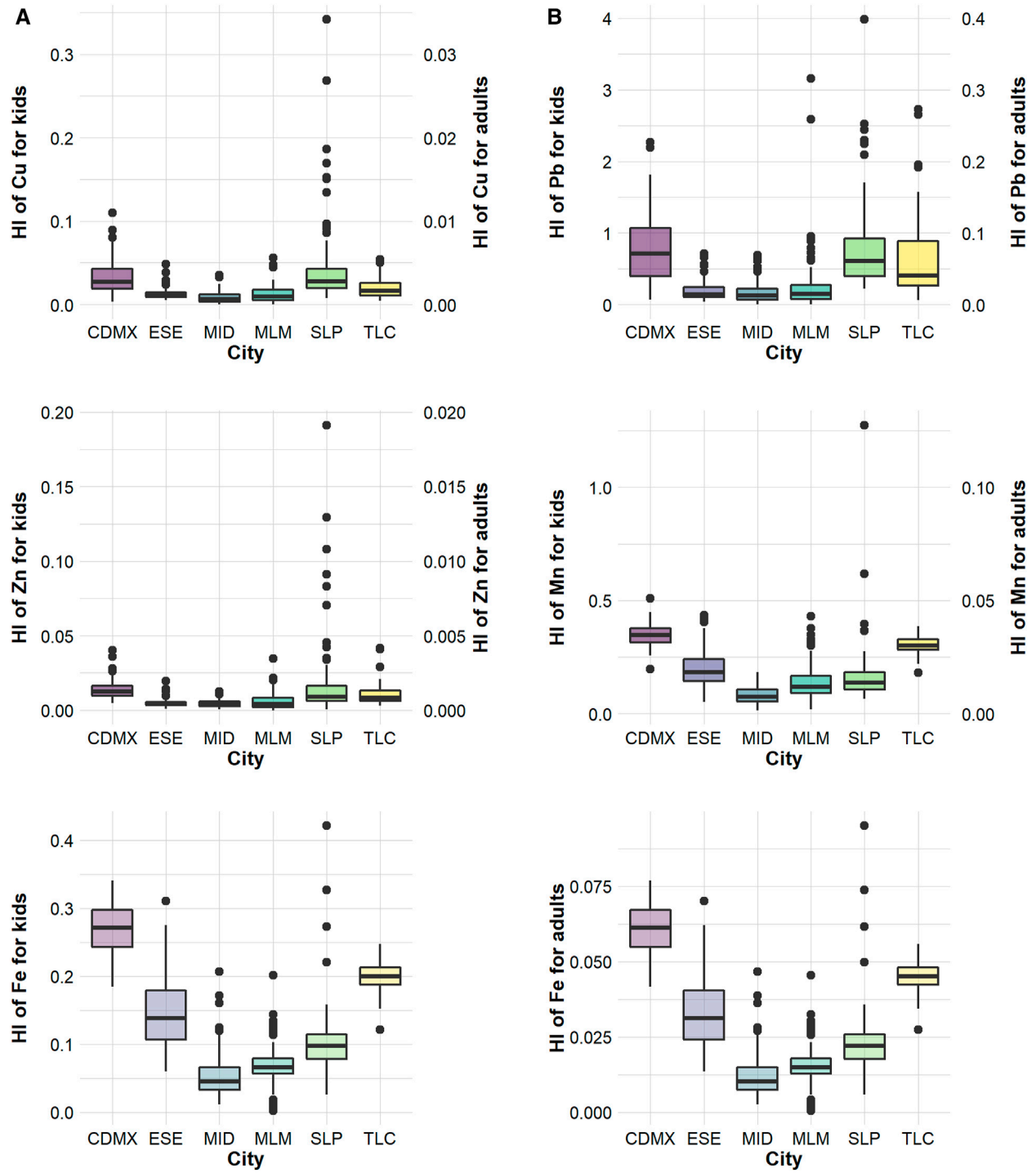

FIGURE 4 | Box plots of the human health risk indices (HI) for children **(A)** and adults **(B)**, of each heavy metal for Mexican cities. CDMX: Mexico City, ESE: Ensenada, MID: Mérida, MLM: Morelia, SLP: San Luis Potosí, TCL: Toluca.

analyzing the pollution and ecological and human health risk indices, we were able to observe that lead was the metal that causes the greatest concern in Mexican cities. Globally, Pb is also one of the metals of greatest concern, along with Cr (Aguilera, Bautista, Goguitchaichvili, et al., 2021). In the case of Mexico, practically in all cities, it is attributed the source of this metal in urban dust to vehicular traffic, however, it is also investigated how much the deposit of old Pb from leaded gasoline contributes (Ávila-Pérez et al., 2019).

TABLE 1 | Comparison of mean Hazard Index (HI) for the studied heavy metals in other cities around the world.

City	—	Cu	Fe	Mn	Pb	Zn	Authors
Bandar-Abbas, Iran	Kids	1.70E-03	9.91E-02	7.61E-02	4.34E-03	5.61E-03	Keshavarzi et al. (2018)
	Adults	7.10E-04	1.38E-02	1.05E-02	5.77E-04	7.46E-04	
Düzce, Turkey	Kids	1.60E-02	4.00E-02	4.10E-02	1.40E+00	7.40E-03	Taşpınar and Bozkurt (2018)
	Adults	2.00E-03	2.00E-02	1.10E-02	3.10E-01	9.40E-04	
Jeddah, Saudi-Arabia	Kids	4.47E-02	4.29E-02	1.70E-01	5.20E-01	2.09E-02	Shabbaj et al. (2018)
	Adults	5.25E-03	1.67E-02	3.35E-02	6.63E-02	2.57E-03	
Suzhou, China	Kids	1.20E-02	8.70E-02	1.40E-01	1.80E-01	1.10E-02	Lin et al. (2017)
	Adults	2.70E-03	5.30E-02	3.80E-02	3.10E-02	1.70E-03	
Shiraz, Iran	Kids	8.70E-03	1.21E-04	2.60E-03	2.23E-01	6.36E-03	Keshavarzi et al. (2015)
	Adults	9.00E-04	8.10E-06	1.70E-04	4.85E-02	7.70E-04	
Nanjing, China	Kids	1.09E-02	2.22E-02	2.24E-02	1.76E-01	1.00E-02	Hu et al. (2011)
	Adults	1.17E-03	2.38E-03	2.40E-03	1.88E-02	1.08E-03	
Mexican cities	Kids	2.23E-02	1.36E-01	2.01E-01	4.80E-01	9.51E-03	This study
	Adults	2.39E-03	3.08E-02	2.60E-02	5.17E-02	1.03E-03	

On the other hand, it is necessary to establish a monitoring system for heavy metals in the dust of the streets, soils, and plants of Mexican cities, as well as pollution indicators with proxy characteristics (easy analysis and low cost) that allow the analysis of thousands of dust samples to identify the sites of high concentration of heavy metals. In this sense, magnetic (Sánchez-Duque et al., 2015; Aguilera et al., 2020) and colorimetric (Cortés et al., 2015; Sanleandro et al., 2018; Aguilar et al., 2021) techniques are promising.

4 CONCLUSION

In this study, we highlighted the current situation in terms of heavy metal contamination in Mexican cities. When the proposed value for soils worldwide was considered as the background, all cities were contaminated, except for Mérida. However, Mérida and Morelia were the most polluted cities when a local background value was used (decile 1). For the metals Cu, Pb and Zn, the concentrations in the cities decreased in the order CDMX > San Luis Potosí > Toluca > Morelia-Ensenada > Mérida. In the particular case of Cu and Pb, SLP accompanied CDMX as the city with the highest concentrations. For the Mn and Fe, the order slightly changed: CDMX > Toluca > Ensenada > San Luis Potosí > Morelia-Mérida.

The largest and most industrialized cities were expected to have the highest concentrations of heavy metals; however, we did not know if this was proportional to the size and if this was the case for all metals. The results showed that contamination was not necessarily related to the number of inhabitants, a populated city like Mérida was the least contaminated; on the contrary, a sparsely populated city like Ensenada was more polluted by Mn and Fe than other more populated ones like San Luis Potosí, Morelia, and Mérida.

No potential ecological risk was found due to contamination by Cu, Pb, and Zn, in the urban dust of the studied cities. However, Pb was the metal that contributed the most to potential ecological risk in all cities. Furthermore, Pb alone did represent a moderate ecological risk in more than 25% of the CDMX, San Luis Potosí, and Toluca sites. Pb could also represent a health risk for the children in these cities. Additionally, chronic exposure to Fe and Mn could trigger many ailments or illnesses.

The analysis of the level of contamination and the possible ecological and human health risk of heavy metals in the dust of six Mexican cities, allowed us to identify that Pb is the metal that causes the greatest concern in the urban environment of Mexico. Therefore, it is important to pay attention to this metal and inquire more deeply about its sources and mitigation strategies.

DATA AVAILABILITY STATEMENT

The raw data supporting the conclusion of this article will be made available by the authors, without undue reservation.

AUTHOR CONTRIBUTIONS

Conceptualization: FB; methodology: CD, YA, DA, JC, AA, and RC; validation: FB, PQ, and AG; formal analysis: AA; resources: FB, PQ, and AG; writing-original draft: AA; writing-review and editing: FB, PQ, and AG; visualization: AA; supervision: FB; Project administration: FB; funding acquisition: FB and AG.

FUNDING

This research was funded by DGAPA Universidad Nacional Autónoma de México grant number IN208621 and SEP-CONACYT project 283135. The funding sources had no involvement in the design, collection, analysis, and interpretation of the data.

SUPPLEMENTARY MATERIAL

The Supplementary Material for this article can be found online at: https://www.frontiersin.org/articles/10.3389/fenvs.2022.854460/full#supplementary-material

REFERENCES

Ávila-Pérez, P., Ortiz-Oliveros, H. B., Zarazúa-Ortega, G., Tejeda-Vega, S., Villalva, A., and Sánchez-Muñoz, R. 2019. "Determining of Risk Areas Due to Exposure to Heavy Metals in the Toluca Valley Using Epiphytic Mosses as a Biomonitor." *J. Environ. Manage.* 241 (2018): 138–148. doi:10.1016/j.jenvman.2019.04.018

Acosta, J. A., Gabarrón, M., Faz, A., Martínez-Martínez, S., Zornoza, R., and Arocena, J. M. (2015). Influence of Population Density on the Concentration and Speciation of Metals in the Soil and Street Dust from Urban Areas. *Chemosphere* 134, 328–337. doi:10.1016/j.chemosphere.2015.04.038

Aguilar, Y., Bautista, F., Quintana, P., Aguilar, D., Trejo-Tzab, R., Goguitchaichvili, A., et al. (2021). Color as a New Proxy Technique for the Identification of Road Dust Samples Contaminated with Potentially Toxic Elements: The Case of Mérida, Yucatán, México. *Atmosphere* 12 (4), 483. doi:10.3390/atmos12040483

Aguilera, A., Bautista, F., Gutiérrez-Ruiz, M., Ceniceros-Gómez, A. E., Cejudo, R., and Goguitchaichvili, A. (2021b). Heavy Metal Pollution of Street Dust in the Largest City of Mexico, Sources and Health Risk Assessment. *Environ. Monit. Assess.* 193 (4), 193. doi:10.1007/s10661-021-08993-4

Aguilera, A., Armendariz, C., Quintana, P., García-Oliva, F., and Bautista, F. (2019). Influence of Land Use and Road Type on the Elemental Composition of Urban Dust in a Mexican Metropolitan Area. *Pol. J. Environ. Stud.* 28 (3), 1535–1547. doi:10.15244/pjoes/90358

Aguilera, A., Bautista-Hernández, D., Bautista, F., Goguitchaichvili, A., and Cejudo, R. (2021c). Is the Urban Form a Driver of Heavy Metal Pollution in Road Dust? Evidence from Mexico City. *Atmosphere* 12 (2), 266. doi:10.3390/atmos12020266

Aguilera, A., Morales, J. J., Goguitchaichvili, A., García-Oliva, F., Armendariz-Arnez, C., Quintana, P., et al. (2020). Spatial Distribution of Magnetic Material in Urban Road Dust Classified by Land Use and Type of Road in San Luis Potosí, Mexico. *Air Qual. Atmos. Health* 13 (8), 951–963. doi:10.1007/s11869-020-00851-5

Aguilera, A., Bautista, F., Goguitchaichvili, Avto., and Garcia-Oliva, F. (2021a). Health Risk of Heavy Metals in Street Dust. *Front. Biosci. (Landmark Edition)* 26 (9), 327–345. doi:10.2741/4896

Angeoletto, F., Essy, C., Ruiz Sanz, J. P., Silva, F. F. d., Albertin, R. M., and Santos, J. W. M. C. (2015). Ecología Urbana: La Ciencia Interdisciplinaria del Planeta Ciudad. *DQuestão* 13 (32), 6. doi:10.21527/2237-6453.2015.32.6-20

Carranza, D., Carmen, Ma. del., Israde Alcántara, Isabel., Bautista Zúñiga, Francisco., Gogichaishvili, Avto., Márquez Herrera, Ciro., et al. (2015). "Metales Pesados En Suelos Urbanos de Morelia. *Michoacán: Influencia de Los Usos de Suelo y Tipos de Vialidad." Ciencia Nicolaita* 0 (65), 120–138. doi:10.1017/CBO9781107415324.004

CONAPO, and SEDESOL (2012). Catálogo Sistema Urbano Nacional 2012. http://www.conapo.gob.mx/work/models/CONAPO/Resource/1539/1/images/PartesIaV.pdf.

Cortés, J. L., Bautista, Fr., Bautista, F., Quintana, P., Aguilar, D., and Goguichaishvili, A. (2015). "The Color of Urban Dust as an Indicator of Contamination by Potentially Toxic Elements: the Case of Ensenada, Baja California, Mexico," in Chapingo Serie Ciencias Forestales Y Del Ambiente *XXI (3)* (Mexico: Baja California), 255–266. doi:10.5154/r.rchscfa.2015.02.003

Dehghani, S., Moore, F., Keshavarzi, B., and HaleHale, B. A. (2016). Health Risk Implications of Potentially Toxic Metals in Street Dust and Surface Soil of Tehran, Iran. *Ecotoxicol Environ. Saf.* 136, 92–103. doi:10.1016/j.ecoenv.2016.10.037

Delgado, C., Bautista, F., Bautista, F., Gogichaishvili, A., Cortés, J. L., Quintana, P., et al. (2019). Identificación De Las Zonas Contaminadas Con Metales Pesados En El Polvo Urbano De La Ciudad De México. *Rev. Int. Contam. Ambie.* 35 (1), 81–100. doi:10.20937/RICA

Flores-Ramírez, R., Pérez-Vázquez, F. J., Pérez-Vázquez, S. E., Medellín-Garibay, S. E., Aldrete, A. C., Vallejo-Pérez, M. R., et al. (2018). Exposure to Mixtures of Pollutants in Mexican Children from Marginalized Urban Areas. *Ann. Glob. Health* 84 (2), 250–256. doi:10.29024/aogh.912

Hakanson, L. (1980). An Ecological Risk index for Aquatic Pollution control.a Sedimentological Approach. *Water Res.* 14 (8), 975–1001. doi:10.1016/0043-1354(80)90143-8

Helaluddin, A., Khalid, R. S., Alaama, M., and Abbas, S. A. (2016). Main Analytical Techniques Used for Elemental Analysis in Various Matrices. *Trop. J. Pharm. Res.* 15 (2), 427–434. doi:10.4314/tjpr.v15i2.29

Hu, X., Zhang, Y., Luo, J., Wang, T., Lian, H., and Ding, Z. (2011). Bioaccessibility and Health Risk of Arsenic, Mercury and Other Metals in Urban Street Dusts from a Mega-City, Nanjing, China. *Environ. Pollut.* 159 (5), 1215–1221. doi:10.1016/j.envpol.2011.01.037

Hua, L., Yang, X., Liu, Y., Tan, X., and Yang, Y. (2018). "Spatial Distributions, Pollution Assessment, and Qualified Source Apportionment of Soil Heavy Metals in a Typical Mineral Mining City in China. *Sustainability (Switzerland)* 10. doi:10.3390/su10093115

Huang, J.-h., Liu, W.-c., Zeng, G.-m., Li, F., Huang, X.-l., Gu, Y.-l., et al. (2016). An Exploration of Spatial Human Health Risk Assessment of Soil Toxic Metals under Different Land Uses Using Sequential Indicator Simulation. *Ecotoxicology Environ. Saf.* 129, 199–209. doi:10.1016/j.ecoenv.2016.03.029

Ihl, T., Bautista, F., Rubén Cejudo Ruíz, F., Delgado, M., Quintana Owen, P., Aguilar, Da., et al. (2015). "Concentration of Toxic Elements in Topsoils of the Metropolitan Area of Mexico City: A Spatial Analysis Using Ordinary Kriging and Indicator Kriging.". *Internacional de Contaminacion Ambiental* 31 (1), 47–62. http://www.scielo.org.mx/scielo.php?script=sci_abstract&pid=S0188-49992015000100004&lng=en&nrm=iso&tlng=en.

INEGI Instituto Nacional de Estadística y Geografía (2014). "Las Zonas Metropolitanas En México.". *Censos Económicos* 2014.

Jadoon, W. A., Khpalwak, W., Chidya, R. C. G., Abdel-Dayem, S. M. M. A., Takeda, K., Makhdoom, M. A., et al. (2018). Evaluation of Levels, Sources and Health Hazards of Road-Dust Associated Toxic Metals in Jalalabad and Kabul Cities, Afghanistan. *Arch. Environ. Contam. Toxicol.* 74 (1), 32–45. doi:10.1007/s00244-017-0475-9

Jahandari, A. (2020). Pollution Status and Human Health Risk Assessments of Selected Heavy Metals in Urban Dust of 16 Cities in Iran. *Environ. Sci. Pollut. Res.* 27 (18), 23094–23107. doi:10.1007/s11356-020-08585-8

Jayarathne, A., Egodawatta, P., Ayoko, G. A., and Goonetilleke, A. (2018). Intrinsic and Extrinsic Factors Which Influence Metal Adsorption to Road Dust. *Sci. Total Environ.* 618, 236–242. doi:10.1016/j.scitotenv.2017.11.047

Kabata-Pendias, Alina. (2011). *Trace Elements in Soils and Plants. CRC Press*. 4th ed. New York: Taylor & Francis. doi:10.1201/b10158-25

Kamali, M. R., Omidvar, A., Kazemzadeh, E., and Kazemzadeh, Ezatallah. (2013). 3D Geostatistical Modeling and Uncertainty Analysis in a Carbonate Reservoir, SW Iran. *J. Geol. Res.* 2013, 1–7. doi:10.1155/2013/687947

Keshavarzi, B., Abbasi, S., Moore, F., Mehravar, S., Sorooshian, A., Soltani, N., et al. (2018). Contamination Level, Source Identification and Risk Assessment of Potentially Toxic Elements (PTEs) and Polycyclic Aromatic Hydrocarbons (PAHs) in Street Dust of an Important Commercial Center in Iran. *Environ. Manage.* 62 (4), 803–818. doi:10.1007/s00267-018-1079-5

Keshavarzi, B., Tazarvi, Z., Rajabzadeh, M. A., and Najmeddin, A. (2015). Chemical Speciation, Human Health Risk Assessment and Pollution Level of Selected Heavy Metals in Urban Street Dust of Shiraz, Iran. *Atmos. Environ.* 119, 1–10. doi:10.1016/j.atmosenv.2015.08.001

Kim, G., Lee, H.-S., Seok Bang, J., Kim, B., Ko, D., and Yang, M. (2015). A Current Review for Biological Monitoring of Manganese with Exposure, Susceptibility, and Response Biomarkers. *J. Environ. Sci. Health C* 33 (2), 229–254. doi:10.1080/10590501.2015.1030530

Kletetschka, G., Bazala, R., Takáč, M., and Svecova, E. (2021). Magnetic Domains Oscillation in the Brain with Neurodegenerative Disease. *Sci. Rep.* 11, 714. doi:10.1038/s41598-020-80212-5

Lawrence, Roderick. J. (2003). "Human Ecology and its Applications.". *Landscape Urban Plann.* 65 (1–2), 31–40. doi:10.1016/S0169-2046(02)00235-9

Lewis, R. C., Meeker, J. D., Basu, N., Gauthier, A. M., Cantoral, A., Mercado-GarcíaPetersonMartha Maria Téllez-Rojo, A., et al. (2018). Urinary Metal Concentrations Among Mothers and Children in a Mexico City Birth Cohort Study. *Int. J. Hyg. Environ. Health* 221 (4), 609–615. doi:10.1016/j.ijheh.2018.04.005

Li, H.-H., Chen, L.-J., Yu, L., Guo, Z.-B., Shan, C.-Q., Lin, J.-Q., et al. (2017). Pollution Characteristics and Risk Assessment of Human Exposure to Oral Bioaccessibility of Heavy Metals via Urban Street Dusts from Different Functional Areas in Chengdu, China. *Sci. Total Environ.* 586, 1076–1084. doi:10.1016/j.scitotenv.2017.02.092

Li, K., Liang, T., Wang, L., and Yang, Z. (2015). Contamination and Health Risk Assessment of Heavy Metals in Road Dust in Bayan Obo Mining Region in Inner Mongolia, North China. *J. Geogr. Sci.* 25 (12), 1439–1451. doi:10.1007/s11442-015-1244-1

Liang, L., Wang, Z., and Li, J. (2019). The Effect of Urbanization on Environmental Pollution in Rapidly Developing Urban Agglomerations. *J. Clean. Prod.* 237, 117649. doi:10.1016/j.jclepro.2019.117649

Lin, M., Gui, H., Wang, Y., and Peng, W. (2017). Pollution Characteristics, Source Apportionment, and Health Risk of Heavy Metals in Street Dust of Suzhou, China. *Environ. Sci. Pollut. Res.* 24 (2), 1987–1998. doi:10.1007/s11356-016-7934-0

Lu, X., Wu, X., Wang, Y., Chen, H., Gao, P., and Fu, Y. (2014). Risk Assessment of Toxic Metals in Street Dust from a Medium-Sized Industrial City of China. *Ecotoxicology Environ. Saf.* 106, 154–163. doi:10.1016/j.ecoenv.2014.04.022

Marín Sanleandro, P., Sánchez Navarro, A., Díaz-Pereira, E., Bautista Zuñiga, F., Romero Muñoz, M., and Delgado Iniesta, M. (2018). Assessment of Heavy Metals and Color as Indicators of Contamination in Street Dust of a City in SE Spain: Influence of Traffic Intensity and Sampling Location. *Sustainability* 10 (11), 4105. doi:10.3390/su10114105

Menezes-Filho, J. A., Souza, K. O. F. d., Rodrigues, J. L. G., Santos, N. R. d., Bandeira, M. d. J., Koin, N. L., et al. (2016). Manganese and lead in Dust Fall Accumulation in Elementary Schools Near a Ferromanganese alloy Plant, Ng Lai Koin, Sérgio S. Do Prado Oliveira, Ana Leonor P. Campos Godoy, and Donna Mergler. *Environ. Res.* 148, 322–329. doi:10.1016/j.envres.2016.03.041

Muñoz-Barbosa, A., Gutiérrez-Galindo, E. A., and Flores-Muñoz, G. (2000). *Mytilus californianus* as an Indicator of Heavy Metals on the Northwest Coast of Baja California, Mexico. *Mar. Environ. Res.* 49 (2), 123–144. doi:10.1016/S0141-1136(99)00052-5

Perez-Vazquez, F. J., Flores-Ramirez, R., Ochoa-Martinez, A. C., Orta-Garcia, S. T., Hernandez-Castro, B., Carrizalez-Yañez, L., et al. (2015). Concentrations of Persistent Organic Pollutants (POPs) and Heavy Metals in Soil from San Luis Potosí, México. *Environ. Monit. Assess.* 187 (1), 4119. doi:10.1007/s10661-014-4119-5

Pérez-Vázquez, F. J., Flores-Ramírez, R., Catalina Ochoa-Martínez, A., Carrizales-Yáñez, L., Arturo Ilizaliturri-Hernández, Cesar., Moctezuma-González, J., et al. (2015). "Human Health Risks Associated with Heavy Metals in Soil in Different Areas of San Luis Potosí. *México." Hum. Ecol. Risk Assess. Int. J.* 7039 (September), 1–14. doi:10.1080/10807039.2015.1064760

Rastegari Mehr, M., Keshavarzi, B., Moore, F., Sharifi, R., Lahijanzadeh, A., Kermani, M., et al. (2017). Distribution, Source Identification and Health Risk Assessment of Soil Heavy Metals in Urban Areas of Isfahan Province, Iran. *J. Afr. Earth Sci.* 132, 16–26. doi:10.1016/j.jafrearsci.2017.04.026

Rodrigues, J. L. G., Araújo, C. F. S., dos Santosdos Santos, N. R., BandeiraBandeira, M. J., AnjosAnjos, A. L. S., CarvalhoCarvalho, C. F., et al. (2018). Airborne Manganese Exposure and Neurobehavior in School-Aged Children Living Near a Ferro-Manganese alloy Plant. *Environ. Res.* 167 (May), 66–77. doi:10.1016/j.envres.2018.07.007

Safiur Rahman, M., Khan, M. D. H., Jolly, Y. N., Kabir, J., Akter, S., and Salam, A. (2019). Assessing Risk to Human Health for Heavy Metal Contamination through Street Dust in the Southeast Asian Megacity: Dhaka, Bangladesh. *Sci. Total Environ.* 660 (April), 1610–1622. doi:10.1016/j.scitotenv.2018.12.425

Sánchez-Duque, A., Bautista, F., Goguitchaichvili, A., Cejudo-Ruiz, R., Alonso Reyes-López, J., Amílcar Solís-Domínguez, F., et al. (2015). "Evaluación de La Contaminación Ambiental a Partir Del Aumento Magnético En Polvos Urbanos. Caso de Estudio Para La Ciudad de Mexicali. *México." Mexicana de Ciencias Geológicas* 32 (3), 501–513.

SEMARNAT. (2007). NOM-147-SEMARNAT/SSA1-2004. Diario Oficial de La Federación. http://www.salud.gob.mx/unidades/cdi/nom/147ssa16.html.

Shabbaj, I., Alghamdi, A., Shamy, M, Hassan, S, Alsharif, M, and Khoder, M. 2018. Risk Assessment and Implication of Human Exposure to Road Dust Heavy Metals in Jeddah, Saudi Arabia." *Int. J. Environ. Res. Public Health* 15. doi:10.3390/ijerph15010036

Tapia, J. S., Valdés, J., Tchernitchin, A., Dorador, C., Bolados, A., and Harrod, C. (2018). Geologic and Anthropogenic Sources of Contamination in Settled Dust of a Historic Mining Port City in Northern Chile: Health Risk Implications. *"Geologic Anthropogenic Sourc. Contam. Settled Dust a Historic Mining Port City North. Chile: Health Risk Implications." PeerJ* 6, e4699. doi:10.7717/peerj.4699

Taşpınar, F., and Bozkurt, Z. (2018). "Heavy Metal Pollution and Health Risk Assessment of Road Dust on Selected Highways in Düzce. *Turkey." Environ. Forensics* 19 (4), 298–314. doi:10.1080/15275922.2018.1519736

Tomlinson, D. L., Wilson, J. G., Harris, C. R., and Jeffrey, D. W. (1980). "Problems in the Assessment of Heavy-Metal Levels in Estuaries and the Formation of a Pollution Index.". *Helgoländer Meeresuntersuchungen* 33 (1–4), 566–575. doi:10.1007/BF02414780

Trujillo-González, J. M., Torres-Mora, M. A., Keesstra, S., Brevik, E. C., and Jiménez-Ballesta, R. (2016). Heavy Metal Accumulation Related to Population Density in Road Dust Samples Taken from Urban Sites under Different Land Uses. *Sci. Total Environ.* 553, 636–642. doi:10.1016/j.scitotenv.2016.02.101

USEPA. (2001). U.S. Environmental Protection Agency. *Risk Assess. Guidance Superfund (Rags) Volume - A: Process Conducting Probabilistic Risk Assess. Appendix B* III, 02–002. http://www.epa.gov/sites/production/files/2015-09/documents/rags3adt_complete.pdf.

Yesilkanat, C. M., Mert, C, and Kobya, Y. 2021. "Spatial Characteristics of Ecological and Health Risks of Toxic Heavy Metal Pollution from Road Dust in the Black Sea Coast of Turkey." *Geoderma Regional* 25, e00388. doi:10.1016/j.geodrs.2021.e00388

Conflict of Interest: The authors declare that the research was conducted in the absence of any commercial or financial relationships that could be construed as a potential conflict of interest.

Publisher's Note: All claims expressed in this article are solely those of the authors and do not necessarily represent those of their affiliated organizations, or those of the publisher, the editors and the reviewers. Any product that may be evaluated in this article, or claim that may be made by its manufacturer, is not guaranteed or endorsed by the publisher.

frontiers | Frontiers in Environmental Science

ORIGINAL RESEARCH
published: 04 April 2022
doi: 10.3389/fenvs.2022.866427

Bioaccumulation and Risk Assessment of Potentially Toxic Elements in Soil-Rice System in Karst Area, Southwest China

Chunlai Zhang[1,2], *Xia Zou*[3]*, *Hui Yang*[2], *Jianhong Liang*[2] *and Tongbin Zhu*[2]

[1]School of Environmental Studies, China University of Geosciences, Wuhan, China, [2]Key Laboratory of Karst Dynamics, Ministry of Natural Resources and Guangxi, Institute of Karst Geology, Chinese Academy of Geological Sciences, Guilin, China, [3]School of Medical Laboratory, Guilin Medical University, Guilin, China

OPEN ACCESS

Edited by:
Johnbosco C. Egbueri, Chukwuemeka Odumegwu Ojukwu University, Nigeria

Reviewed by:
Johnson Agbasi, Chukwuemeka Odumegwu Ojukwu University, Nigeria
Andrew Hursthouse, University of the West of Scotland, United Kingdom

***Correspondence:**
Xia Zou
zx0205@126.com

Specialty section:
This article was submitted to Toxicology, Pollution and the Environment, a section of the journal Frontiers in Environmental Science

Received: 31 January 2022
Accepted: 23 February 2022
Published: 04 April 2022

Citation:
Zhang C, Zou X, Yang H, Liang J and Zhu T (2022) Bioaccumulation and Risk Assessment of Potentially Toxic Elements in Soil-Rice System in Karst Area, Southwest China. Front. Environ. Sci. 10:866427. doi: 10.3389/fenvs.2022.866427

The accumulation of potentially toxic elements (PTE) in a soil–rice system poses a significant issue of concern in agricultural soils, particularly in the polluted or high PTE geological background regions, such as karst areas. The source identification, bioaccumulation factors of PTE, and its health risk were investigated by correlation analysis, principal components analysis, and single/comprehensive assessments in a soil-rice system in Mashan County, Guangxi Province. The results showed that the mean contents of PTE in rice rhizosphere soil samples were higher than Guangxi surface soil, but lower than Mashan background. Of the samples, 84.21% have Cd content exceeding the soil environmental quality -- risk control standard for soil contamination of agricultural land in China (GB 15618-2018) risk screening value. The Nemerow comprehensive pollution index indicated that 21.05 and 26.32% of the soil samples were moderately and heavily polluted. The contents of pH-related exchangeable Ca, exchangeable Mg, and redox-related available Fe and available Mn in soil affected the bioaccumulation of PTE in rice. In all the rice samples, 55.26% of Cd and 31.58% of Pb exceed the maximum allowable value of contaminants in rice recommended by the national food safety standard for maximum levels of contaminants in foods in China (GB 2762-2017). The average targeted hazard quotient values (THQ) of PTE decreased in an order of As > Cd > Cr > Cu > Zn > Pb > Hg, and the degree of health risk it posed to the population was Children > Female > Male. The hazard index (HI) of all samples was greater than one due to all THQ_{As} and the THQ_{Cd} of more than half samples were above 1, which implied that the residents were exposed to non-carcinogenic risk by rice ingestion. Therefore, the PTE in the karst area with a high geological background can be absorbed and migrated by crops, leading to a greater health risk to humans, which should be paid attention to in future research and agricultural management.

Keywords: bioaccumulation, risk assessment, potentially toxic elements, soil-rice, karst

INTRODUCTION

With population growth and economic development, the natural process of slow release of heavy metals is accelerated, resulting in heavy metal pollution of soil, water, and the atmosphere (Bing et al., 2021; Savignan et al., 2021; Egbueri et al., 2022a). Heavy metals can accumulate in soil and dissolve into groundwater during leaching, resulting in groundwater and surface contamination of water (Ayejoto et al., 2022; Egbueri et al., 2022b). Heavy metal pollution in cropland soils is a global environmental issue of concern owing to its toxicological effects on soil-plant systems and humans (Bashir et al., 2018; Hou D. et al., 2020; Kukusamude et al., 2021). Cobalt (Co), copper (Cu), nickel (Ni), iron (Fe), manganese (Mn), zinc (Zn), molybdenum (Mo), and selenium (Se) are essential elements of the human body; still, they would cause health problems after years of insufficient intake or excessive intake of food exceeding the safety limit (Giri et al., 2020), while arsenic (As), cadmium (Cd), chromium (Cr), mercury (Hg), and lead (Pb) are nonessential to the human body, and these can cause health problems even at low contents (Giri et al., 2019; Jalili et al., 2020). Human exposure to heavy metals is through inhalation, oral ingestion, and skin absorption (Sanaei et al., 2021; Ayejoto et al., 2022; Egbueri et al., 2022b). Rice is the most widely consumed grain on the planet, with global rice production exceeding 740 million tons in 2014, with Asian countries such as China, Thailand, Japan, and Indonesia leading the way in global rice production (Hu et al., 2016). Rice is one of the most essential staple foods in China, particularly in southern areas. The average consumption of rice is 219 g/person/day, which is nearly 50% higher than the global average (Hu et al., 2016). Dietary intake of rice grown in soils with a high content of potentially toxic elements (PTE) exceeding the maximum allowable contaminant concentration could be a serious threat to human health (Chen et al., 2018; Mu et al., 2020). Previous studies revealed that the content of PTE in rice grains is mainly determined by soil physicochemical properties, element availability, and rice varieties (Li et al., 2019).

The content of PTE in rice grains is correlated with its corresponding soil (Baruah et al., 2021). Approximately 19.4% of farmland in China has been reported contaminated by PTE in 2014 (Qu et al., 2016), with higher contents of Cd and Pb distributed in northwest, south, and southwest China than elsewhere (Bing et al., 2021). Weathering of parent materials is a natural source of heavy metals in soils. High geological background characteristics of soil heavy metals have been found in karst areas such as Southwest China (Wen et al., 2020b; Tang et al., 2021; Yang et al., 2021b), the Indo-China Peninsula (Mallongi et al., 2022), and Europe (Savignan et al., 2021). The soil in the karst valley densely populated and concentrated in rural towns is strongly affected by anthropic activities. Soil heavy metals can be affected by wet and dry deposition of fossil fuel combustion, fertilizer and pesticide application, sewage irrigation, and improper disposal of waste (Egbueri et al., 2020; Egbueri et al., 2021b; Savignan et al., 2021). In addition, the combination of a high geological background of heavy metals and human activities makes crops in karst areas vulnerable to heavy metal pollution, which will affect future environmental sustainability and human health (Zhang et al., 2019; Zhang et al., 2021; Mallongi et al., 2022).

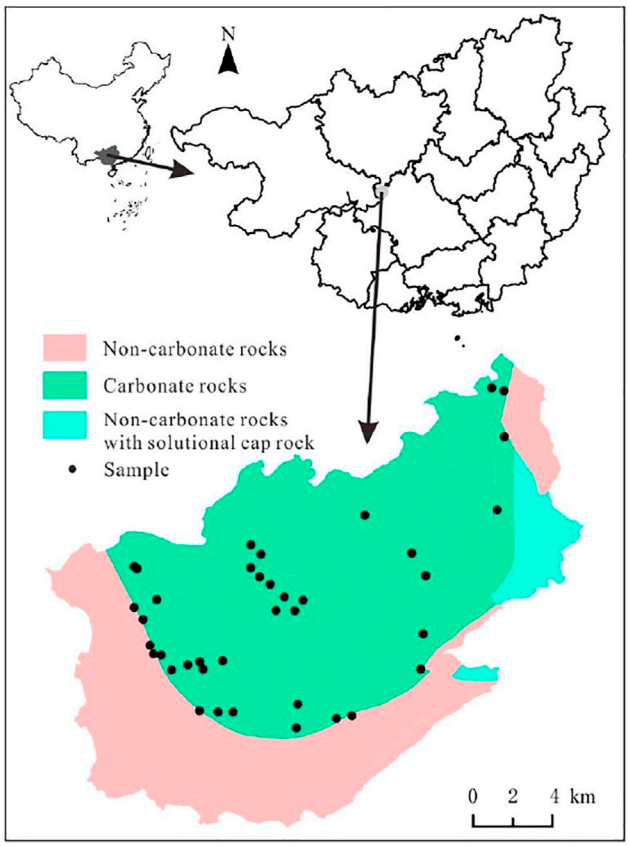

FIGURE 1 | Map of sampling sites and geological background.

Due to the enrichment of heavy metal elements in the carbonate weathering process and soil genesis, the resulting soil has significantly high contents of PTE (Wen et al., 2020b; Yang et al., 2021b). The first national pollutant survey reflected that the average contents of As, Cd, Cr, Cu, Hg, Ni, Pb, and Zn in the surface soils of Guangxi where karst is widely distributed were 2.0, 4.5, 1.6, 1.1, 2.6, 1.3, 1.4, and 1.4 times higher than that of China, respectively. Due to the limited arable land per capita, part of farmlands with a high heavy metal geological background in the karst area in Southwest China is still used to grow crops (Zhang et al., 2019).

Limestone soil developed from weathering of carbonate rocks may affect the accumulation of trace elements in the edible parts of crop plants (Wen et al., 2020a; Li et al., 2021; Tang et al., 2021; Zhang et al., 2021). Yang et al. (2021a) studied the excess rate and influencing factors of Cd in the soil-rice system in karst areas and proposed a new safety standard based on pH and soil Cd content. Soil carbonate in the karst area increased soil pH, and the adsorption of Cd by Fe/Mn oxide/hydroxide significantly reduced the bioavailability of soil Cd, and the excess rate of rice in the karst area was much lower than that in the non-karst area (Li et al., 2021). The limestone soil in the karst area is

calcium-rich and alkaline. Unfortunately, to the best of our knowledge, the effect of exchangeable Ca and Mg on the immobilization of heavy metals in the soil-rice system has not been reported yet. Therefore, the purposes of this study were to (1) evaluate the contents of 7 PTE (As, Cd, Cr, Cu, Hg, Pb, and Zn) in rice grains and rhizosphere soils of the karst area, identifying the source of heavy metals and understanding the influence of soil physicochemical properties related to pH and redox on the accumulation of PTE in the soil-rice system; and (2) assess the potential health (non-carcinogenic) risk of these PTE to children and adult through rice consumption.

MATERIALS AND METHODS

Study Area

The studied area is located west of Mashan County, Guangxi Province, China (**Figure 1**). This area is characterized by a mean annual rainfall of 1722.5 mm, with an annual average temperature of 21.8°C. The central part of the study area is characterized by thick limestone layers with dolomitic limestone intercalations. Soils are dominated by brown rendzina. The land use types are mainly shrubs in mountainous areas and abandoned farmland in depressions. Non-carbonate rocks, comprising sandstones and mudstones, are distributed to the west, south, and east of the study area. The land uses in this area mainly include secondary forests and reservoirs. The valley consists of Holocene clay and loamy sand sediments, distributed among the mountains, and the land uses include paddy fields, drylands, and villages. Agricultural activities are the source of income for residents in the study area. Cultivated land includes two-season rice, water and vegetable rotation, corn and orchards, etc. Excessive use of chemical fertilizers and pesticides to pursue higher yields may bring heavy metal pollution to the cultivated soil.

Samples

Thirty-eight groups of rice and rhizosphere soil samples were collected in early November 2017 (**Figure 1**). Field sampling was conducted according to a standardized sampling method (MLRPRC Ministry of Land and Resources of the People's Republic of China, 2016). At each sampling point, rice and rhizosphere soil were collected from four sub-spots within 20 m of the surrounding area and combined into a compositional sample, sealed, and transported with a plastic bag. After removing the debris and roots, the fresh soil sample was passed through a 2-mm nylon sieve to improve uniformity. Air-dried soil samples and polished rice were ground to a particle size of not more than 74 um for trace element analysis.

Laboratory Analysis

Contents of Cd, Cr, Cu, Pb, and Zn measuring were performed on inductively coupled plasma (ICP)-mass spectrometry (PerkinElmer Inc., United States, NexION 300) after digesting the soil samples with <0.074-mm particle size by HCl—HF—$HClO_4$—HNO_3 mixture, and rice sample digested by HNO_3–H_2O_2. After digesting by aqua regia, and reducting by potassium borohydride, As and Hg were determined by atomic fluorescence spectroscopy. Soil pH was determined at a 1:2.5 (w/v) soil/water ratio by a precision pH meter (PHS-3C) in the lab. The soil organic carbon (Corg) was determined through titration using the potassium dichromate oxidation–ferrous ammonium sulfate method. Exchangeable calcium (E_{Ca}) and magnesium (E_{Mg}) were leached with 1 mol/L ammonium acetate (pH = 7.0), and measured by ICP-emission spectrometry (PerkinElmer Inc., United States, OPTIMA 8300). The availably iron (A_{Fe}), copper (A_{Cu}), zinc (A_{Zn}), and manganese (A_{Mn}) were leached with leaching solution (0.1 mol/L hydrochloric acids for acid soil, and DTPA for calcareous soil). The leaching solution was determined by ICP-emission spectrometry. The available silicon (A_{Si}) was leached with 0.025 mol/L citric acid at 30°C for 5 h equilibrating, and the filtrate was taken for colorimetric comparison with silicon molybdenum blue. Standard materials of soil (GBW07417 for effective state analysis of soil elements, GBW07427 for total concentration analysis of soil elements) and rice (GSB-1 and GSB-23, both for total concentration analysis of rice elements) covered all studied elements and were tested among every ninth sample, revealing that the average analytical errors were about 5%.

PTE Contamination Assessment

Pollution Load Index and Potential Ecological Risk Index

The contamination factor (CF) has been used to assess the pollution level of trace elements in the soil since the 1980s (Tomlinson et al., 1980; Kowalska et al., 2018). The CF values of PTE in soil were calculated as follows:

$$CF_i = C_i / C_{REF_i} \quad (1)$$

where C_i and C_{Refi} are the contents of element "i" (mg/kg) in the soils and background value of the PTE in Mashan County, which was obtained from this study and a geochemical survey of land quality in 2016, respectively (**Table 1**).

Correspondingly, the pollution degree of a single element is grouped into four levels: low (CF < 1), moderate (1 ≤ CF < 3), equivalent (3 ≤ CF < 6), and extremely high (CF F 6) (Hakanson, 1980; Egbueri et al., 2021b; Egbueri and Agbasi, 2022).

To evaluate the overall degree of heavy metal contamination across all sampling sites, the pollution load index (PLI) was proposed to represent total pollution of all PTE in the soil, which is calculated as follows:

$$PLI = \sqrt[n]{CF_1 \times CF_2 \times \cdots \times CF_n} \quad (2)$$

where n is the total number of the studied PTE consisting of As, Cd, Cr, Cu, Hg, Pb, and Zn. The contamination degrees were further classified as PLI <1, 1 ≤ PLI <2, 2 ≤ PLI <3, and PLI ≥3, which indicated low, moderate, high, and very high contamination, respectively (Egbueri et al., 2021b).

The potential ecological factor (PEF) has been widely applied to assess the ecological risk of toxic PTE in soils (Hakanson, 1980; Gu et al., 2021). The PEF values are calculated as follows:

TABLE 1 | Descriptive analysis of the heavy metal contents in rhizosphere soil and rice samples.

Plantation type	Item	As	Cd	Cr	Cu	Hg	Pb	Zn
Soil (*N* = 38)	Min	1.75	0.22	35.50	12.10	0.07	15.00	47.30
	Max	20.72	7.72	177.00	45.80	0.34	57.80	324.00
	Mean	7.45	1.52	83.13	24.30	0.17	32.67	137.47
	SD	4.97	1.48	33.45	7.53	0.07	10.75	70.75
	CV (%)	66.76	97.35	40.24	30.99	37.55	32.89	51.47
	Skewness	1.186	2.466	1.066	0.947	0.882	0.779	0.983
	Kurtosis	0.463	7.851	0.734	0.858	0.215	0.255	0.527
	Soil background value	22.15	2.38	140.39	40.13	0.197	44.43	199.48
	Surface soil in Guangxi (Hou, 2020)	8	0.144	50	18	0.083	24	43
Rice (N = 38)	Min	0.06	0.01	0.03	1.15	0.00	0.01	10.20
	Max	0.21	1.04	1.54	14.10	0.01	0.60	21.10
	Mean	0.10	0.28	0.36	4.12	0.00	0.15	14.64
	SD	0.03	0.26	0.29	3.12	0.00	0.17	2.28
	CV(%)	30.26	92.88	80.18	75.87	31.57	109.21	15.56
	Skewness	1.621	1.358	2.083	1.772	0.106	1.146	0.665
	Kurtosis	3.356	1.521	6.781	2.821	-1.424	0.444	0.660

N is the number of samples (there are 22 Hg data in the rice sample); CV is the coefficient of variable; CV = SD/mean×100%; the units of elements are mg/kg.

$$PEF_i = Tr_i \times CF_i = Tr_i \times C_i / C_{REF_i} \quad (3)$$

where Tr_i is the biological toxicity coefficient for heavy metal i (10, 30, 2, 5, 40, 5, and one for As, Cd, Cr, Cu, Hg, Pb, and Zn, respectively) (Hakanson, 1980). The potential ecological risk index (RI) can be calculated by the following function:

$$RI = \sum_{i=1}^{n} PEF_i \quad (4)$$

The classification standards of ecological risks for PEF and RI are shown in **Supplementary Table S1**.

Nemeiro Comprehensive Pollution Index

Single pollution index (Pi) is calculated to assess heavy metal pollution in soils and rice as follows:

$$Pi = \frac{C_i}{S_i} \quad (5)$$

where C_i represents contents of the element i in the soil or rice sample, S_i represents contents of component i in risk screening values for soil contamination of agriculture land GB 15618-2018 (MEEPRC Ministry of Ecology and Environment of the People's Republic of China, 2018), or maximum levels of contaminants in foods GB 2762-2017 (NHFPCPRC and CFDA, National Health and Family Planning Commission and China Food and Drug Administration, 2017) in China, respectively. The risk screening values for soil and maximum levels of contaminants for rice were listed in **Supplementary Table S2**. As GB 2762-2017 only stipulates the content limits of As, Cd, Cr, Hg, and Pb in rice (**Supplementary Table S2**), these elements were assessed by Pi in this study. Soil or crop are polluted by metal i if Pi > 1 (Hu et al., 2017).

The Nemerow Comprehensive Pollution Index (NCPI) is simple in form and has good applicability. It is commonly used for heavy metal comprehensive pollution evaluation, and expressed as:

$$NCPI = \sqrt{\left(P_{i\,max}^2 + P_{i\,ave}^2\right)/2} \quad (6)$$

where Pimax and Piave represent the maximum and average Pi value of PTE, respectively. According to NCPI, five levels are used to classify the pollution level of PTE: clean (≤0.7), prevention (0.7 ~1.0), light pollution (1.0~2.0), moderate (2.0 ~3.0), and heavy pollution (>3.0) (Hu et al., 2017; Kowalska et al., 2018).

Bioaccumulation factor

The transfer ratio of PTE from soil to the crop could be quantified by bioaccumulation factor (BAF) (Kumar et al., 2019) as follows:

$$BAF_i = \frac{C_{i\,rice}}{C_{i\,soil}} \quad (7)$$

where $C_{i\,rice}$ and $C_{i\,soil}$ are the contents of element i in the rice and the corresponding rhizosphere soils, respectively.

Human Exposure and Risk Assessment

Health risk for three groups of people—children, adult women, and adult men—through rice consumption was evaluated by estimated daily intake (EDI), targeted hazard quotient (THQ), and hazard index (HI), as proposed by (USEPAU.S. Environmental Protection Agency, 1989)

$$EDI_i = (C_i \times DI)/BW \quad (8)$$

$$THQ_i = EDI_i / RfD_i \quad (9)$$

$$HI = \sum_{i=1}^{n} THQ_i \quad (10)$$

where EDI_i is the total daily exposure of element i [mg/(kg bodyweightday)], C_i is the content of i in polished rice (mg/kg), and DI is the recommended dose of rice intake for residents during 2013–2018 [0.25 and 0.40 kg/day for children and adults, according to the minimum and maximum recommended amounts of cereals by Chinese Nutrition Society (CNS Chinese Nutrition Society, 2021)]; BW is the body weight of children (9 years old), adult men and women,

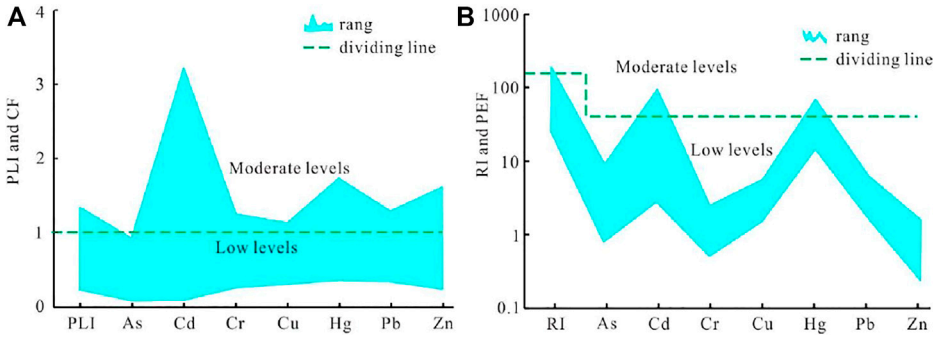

FIGURE 2 | Contamination levels **(A)** and potential ecological risk **(B)** of each PTE in the soils of the karst. The blue bands indicate the range of contamination factor (CF) and pollution load index (PLI) **(A)**, and potential ecological factor (PEF) and potential ecological risk index (RI) **(B)** of PTE in soils; and the green dotted line divides the low and moderate levels.

which are 30, 66.2, and 57.3 kg on average, respectively (Zuo et al., 2019). THQ_i is the ratio of element i between EDI and reference dose (RfDis). The RfD is considered safe for lifetime exposure to PTE and was enumerated in **Supplementary Table S3**. It may cause side effects to health when THQ >1. HI assumes that eating certain types of food may result in simultaneous exposure to multiple PTE. If HI < 1, harmful health effects are assumed to be unlikely to happen, while there are non-carcinogenic risks that could arise when HI > 1 (Zeng et al., 2015).

Data Analysis

Chemometric analysis including correlation analysis, unrotated principal component analysis, and varimax-rotated factor analysis were performed for source apportionment of soil PTE and risk assessment of soil-rice system by SPSS Statistics 18 (IBM, United States). Boxplots were performed by Origin 8.5 (Origin Lab, United States).

RESULTS AND DISCUSSION

Contents and Contamination Levels of PTE in the Soil

The statistical analysis results of PTE are exhibited in **Table 1**. On average, the contents of As, Cd, Cr, Cu, Hg, Pb, and Zn in soils were 7.45 ± 4.98, 1.53 ± 1.49, 83.13 ± 33.45, 24.3 ± 7.53, 0.18 ± 0.07, 32.67 ± 10.75, and 137.47 ± 70.75 mg/kg, respectively. Soil pH ranged from acidic (4.83) to alkaline (8.18). The results showed that the averaged contents of all PTE in soil samples were significantly lower than the corresponding local background values of Mashan County but higher than the background value of surface soil in Guangxi except for As (Hou Q. Y. et al., 2020) (**Table 1**). There were 6, 2, 2, 11, 6, and 7 in 38 samples of Cd, Cr, Cu, Hg, Pb, and Zn that exceeded the local background values.

The coefficient of variations (CV) of the PTE in the soils was, in a decreased order, Cd (97.35%), As (66.76%), Zn (51.47%), Cr (40.24%), Hg (37.55%), Pb (32.89%), and Cu (30.99%), respectively (**Table 1**), suggesting that Cd was obviously enriched in some soil samples, while Zn, Cr, Hg, Pb, and Cu were slightly enriched in some areas. In addition, results of the Kolmogorov-Smirnov test for normality also showed that all the studied soil element contents were skewed distributions.

PTE in almost all soil samples had a CF value below 3, except for one sample with CF_{Cd} of 3.24 (**Figure 2A**; **Table 2**), indicating that the contamination levels of PTE were low or slightly moderate (Kowalska et al., 2018). The average PLI value was 0.60 ± 0.27, and 5 out of 38 samples had a PLI value greater than 1, with the maximum value of 1.35. The relatively low PLI value indicated that the soil was mildly polluted due to the high geological background (Kowalska et al., 2018).

The PEF of soil samples was 3.37 ± 2.25, 19.24 ± 18.73, 1.18 ± 0.48, 3.03 ± 0.94, 35.59 ± 13.37, 3.68 ± 1.21, and 0.69 ± 0.35 for As, Cd, Cr, Cu, Hg, Pb, and Zn, respectively (**Figure 2B**). Only 3 samples of Cd and 11 samples of Hg had a moderate potential risk in the study area (**Figure 2B**). The RI values ranged from 23.70 to 190.30, with an average value of 66.77 ± 35.00, demonstrating that all soil samples were at a pollution-free level.

However, according to the risk screening values of As, Cd, Cr, Cu, Hg, Pb, and Zn stipulated in GB 15618-2018, the contents of Cd in 84.21% of soil samples were above the risk screening values, followed by Zn, with 10.53% of samples exceeding the risk screening values, while As, Cr, Cu, Hg, and Pb in paddy soils were lower than the guideline (**Figure 3**). NCPI of 21.05 and 26.32% soil samples showed moderate and heavy pollution (**Table 3**), which is common in karst areas (Wen et al., 2020b). With the increase of weathering intensity, the content of Fe/Al/Mn oxides, organic carbon, and clay minerals increases, and leads to the enrichment of Cd in soil (Wen et al., 2020b; Yang et al., 2021b).

Chemometric Analysis for Source Identification and Risk Assessment of PTE in Soil

Correlation Analysis

The correlation coefficients between soil pH, SOC, effective state, and heavy metals (As, Cd, Cr, Cu, Hg, Pb, and Zn) in the studied soils were calculated to study the influencing factors on the enrichment of heavy metals in soils (**Supplementary Table S4**). Contents of As, Cd, Cr, Cu, Hg, Pb, Zn, A_{Si}, and A_{Mn} in

TABLE 2 | Number of soil samples with PTE pollution assessed by contamination factor (CF) and pollution load index (PLI) in the study area.

Pollution level		As	Cd	Cr	Cu	Hg	Pb	Zn	PLI
Low degree	Number	38	32	36	36	27	32	31	33
	Percentage	100%	84.21%	94.74%	94.74%	71.05%	84.21%	81.58%	86.84%
Moderate degree	Number	0	5	2	2	11	6	7	5
	Percentage	0.00%	13.16%	5.26%	5.26%	28.95%	15.79%	18.42%	13.16%
Equivalent degree	Number	0	1	0	0	0	0	0	0
	Percentage	0.00%	2.63%	0.00%	0.00%	0.00%	0.00%	0.00%	0.00%

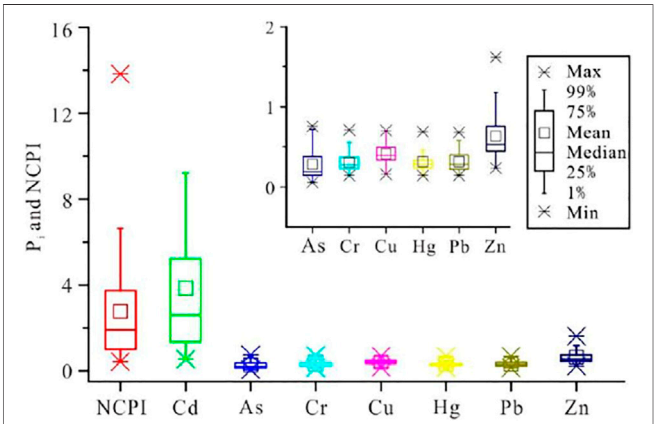

FIGURE 3 | Boxplots of heavy metal single pollution index (Pi) and Nemerow Comprehensive Pollution Index (NCPI) of soil in the study area.

soils were significantly positively correlated with each other ($p < 0.01$). High E_{Ca} and E_{Mg} content can increase the adsorption of heavy metal ions (Kokkinos et al., 2020), can also increase soil pH, and indirectly immobilize heavy metals (Hussain et al., 2021). The Corg was significantly positively correlated with Cd, Cu, Hg, and Pb, consistent with the results of previous studies (Mu et al., 2020; Zhang et al., 2021). Available Fe was significantly ($p < 0.01$) negatively correlated with pH, E_{Ca}, E_{Mg}, A_{Si}, and all studied PTE, but significantly positively correlated with A_{Cu} and A_{Zn}, indicating higher Fe availability in lower pH soils, similar to those reported for paddy soil in Bangladesh (Rahman et al., 2018) and India (Baruah et al., 2021). All the studied PTE were almost significantly negatively correlated with A_{Fe} in soils, which indicated that the activity of Fe is not conducive to the accumulation of heavy metals (Yu et al., 2016). The ferromanganese nodules have a strong ability to enrich heavy metals. The change of redox conditions results in the layered distribution of iron, manganese, and heavy metals in the nodules. Different mineral species in the nodules have different release and adsorption capacities of elements in the face of environmental changes, which results in different correlations (Frierdich and Catalano, 2012; Liu et al., 2021).

Principal Component Analysis

PCA can be used to identify potential sources of the PTE (Egbueri and Agbasi, 2022; Mallongi et al., 2022). The correlation coefficients of most variables in this area were relatively high, and common factors can be extracted from them; the corresponding probability P is close to 0, and the Kaiser-Meyer-Olkin test value is 0.831, which is suitable for PCA to establish an adequate understanding of the sources of heavy metals and other parameters in the analyzed samples. Results of the PCA are presented in **Table 4**. It can be seen from **Table 4** that the information of the sources of PTE can be represented by 3 PCs, and the 3 PCs can explain 86.6% of the total variables, indicating that the first three factors can reflect most of the information of all the data. It was clear that As, Cd, Cr, Cu, Hg, Pb, Zn, pH, A_{Si}, and A_{Fe} have significant loadings in PC1. This suggests that there may be a closer correlation between these parameters. The average content of all PTE did not exceed the local background value, and the excess rate was very low, indicating a main natural source of these PTE (Kowalska et al., 2018). They could be attributed to the weathering of carbonate minerals (Egbueri et al., 2021a). Various degrees of soil pollution of PTE were reported in the karst regions (Zhang et al., 2013). During the weathering and pedogenesis of heavy metal-rich carbonate rocks, alkaline Earth elements were leached, and heavy metals in soil were enriched by residues such as Fe/Mn oxides and clay minerals (Wen et al., 2020b). The carbonate rocks weathered soil characterized by high pH, high calcium carbonate, and soil organic matter content, which play an essential role in immobilizing PTE in soil (Guo et al., 2006; Zhao et al., 2010; Wang et al., 2015).

In PC2, significant loadings were observed on the A_{Cu}, Corg, A_{Zn}, and Cu (**Table 4**). Rice roots and straws are the main sources of organic matter in paddy soils. The enrichment coefficients of Cd, Cu, and Zn in the soil-rice system are relatively high. Previous studies believed that heavy metals mainly accumulated in the

TABLE 3 | Number of soil samples with PTE pollution assessed by Nemerow composite pollution index (NCPI) according to GB 15618-2018 in the study area.

	Clean	Precaution	Light pollution	Moderate	Heavy pollution
Number	4	5	11	8	10
Percent	10.53%	13.16%	28.95%	21.05%	26.32%

TABLE 4 | Data dimensionality reduction extractions.

Parameter	Unrotated principal components			Varimax-rotated factor loadings			Communality
	PC1	PC2	PC3	Factor 1	Factor 2	Factor 3	
As	0.928	–0.151	-0.115	0.771	0.550	–0.027	0.898
Cd	0.915	0.206	0.130	0.698	0.502	0.397	0.897
Cr	0.861	–0.125	–0.079	0.703	0.519	0.003	0.763
Cu	0.817	0.550	–0.069	0.807	0.138	0.552	0.975
Hg	0.921	0.033	0.076	0.696	0.564	0.228	0.855
Pb	0.916	0.121	–0.185	0.859	0.354	0.155	0.887
Zn	0.975	0.117	0.061	0.766	0.541	0.297	0.967
Corg	0.314	0.694	0.396	0.173	0.054	0.839	0.737
pH	0.904	–0.227	0.105	0.611	0.711	0.028	0.880
E_{Ca}	0.570	–0.466	0.607	0.010	0.953	0.051	0.911
E_{Mg}	0.697	–0.535	0.371	0.229	0.918	–0.113	0.909
A_{Si}	0.838	0.217	–0.407	0.944	0.121	0.098	0.915
A_{Mn}	0.639	0.059	–0.693	0.914	–0.085	–0.222	0.891
A_{Fe}	–0.824	0.407	–0.037	–0.547	–0.719	0.171	0.846
A_{Zn}	–0.635	0.557	0.148	–0.47	–0.576	0.427	0.736
A_{Cu}	–0.156	0.850	0.227	–0.071	–0.406	0.792	0.798
NCPI	0.780	0.468	0.190	0.613	0.319	0.621	0.863
PLI	0.990	0.107	-0.005	0.813	0.515	0.255	0.992
RI	0.980	0.115	0.070	0.764	0.551	0.302	0.979
Eigenvalue	12.238	2.942	1.520	8.365	5.547	2.788	
Variance %	64.412	15.482	7.998	44.026	29.193	14.674	
Cumulative %	64.412	79.894	87.893	44.026	73.219	87.893	

roots, and there was a good correlation between Corg and PTE. For instance, human activities such as water irrigation and application of fertilizers and pesticides may have a significant impact on the enrichment of metals in farmland (Yang et al., 2013). Thus, PC2 can be attributed to agricultural activity.

Furthermore, PC3 was noticed to have obvious loadings on A_{Mn} and E_{Ca} (**Table 4**), having a negative and positive loading, respectively. The variation showed differences in their origin or impact. As discussed above, E_{Ca} affects the mobility of heavy metals by buffering pH. While A_{Mn} was significantly positively correlated with organic matter and clay content, extremely significantly negatively correlated with pH and calcium carbonate content, and extremely significantly positively correlated with cation exchange capacity (Pu et al., 2010).

Varimax-Rotated Factor Analysis

The Varimax twiddle factors extracted in this study for soil heavy metal association and source identification are shown in **Table 4**. Similar to PCA, 86.6% of the information about the heavy metal data was explained by three-factor categories. Factor 1 has high loadings for As, Cd, Cr, Cu, Hg, Pb, Zn, pH, A_{Si}, A_{Fe}, PLI, and RI (**Table 4**). Combined with the fact that there are only individual quarries in the locality and no other industries, therefore, Factor 1 was judged to be the "weathering residual source". Meanwhile, the correlation between As, Cd, Cr, Hg, Pb, Zn, SPI, and RI in Factor 2 became stronger than in PC3. This observation seems to confirm that they may have the same origin. The extremely positive correlation of E_{Ca} and E_{Mg} with Factor 2 suggested the source of carbonate rock, the nearby limestone quarries. Furthermore, leaded gasoline, diesel combustion, fossil fuel burning, braking, and vehicular emission were potentially elevated PTE levels in the soil. Therefore, Factor 2 may be attributed to the mixture of mineral powder and fuel exhaust particles in the farmland soil in the form of dry and wet deposition. Moreover, recent studies found that several elements such as Zn, Cd, Pb, and As in alluvial deposits are related to their easily transportable forms (soluble forms) (Fonseca et al., 2021). Toxic elements in soils developed from carbonate rocks can also be transported and deposited in downstream alluvial plains (Hou Q. et al., 2020). Factor 3 explained about 14.674% of the total variance and was considered loaded for Corg, A_{Cu}, Cu, and A_{Zn} (**Table 4**), which is the same as PC2 related to agricultural resources. They can come from wastewater irrigation, fertilizer application, pesticides, organic manures, compost, and sewage sludges.

Contents and Risk Assessment of PTE in Rice

The mean contents of As, Cd, Cr, Cu, Hg, Pb, and Zn in rough rice were 0.10 ± 0.03, 0.28 ± 0.26, 0.36 ± 0.29, 4.12 ± 3.12, 0.0045 ± 0.0014, 0.15 ± 0.17, and 14.64 ± 2.28 mg/kg, respectively (**Table 1**; **Figure 4A**). The Pi of the As, Cd, Cr, Hg, and Pb of rice samples varied from 0.29 to 1.05, 0.03 to 5.20, 0.03 to 1.54, 0.01 to 0.35, and 0.03 to 3.00, respectively. The average Pi decreased in the order of Cd (1.38) >Pb (0.77) > As (0.52) > Cr (0.36) > Hg (0.13) (**Figure 4B**). In the present study, 55.26% of Cd (21 samples) and 31.58% of Pb (12 samples) were higher than the maximum allowable value of 0.2 mg/kg for cereal grains recommended by NHFPCPRC and CFDA, National Health and Family Planning Commission and China Food and Drug Administration (2017), respectively, and 15.79% (6 samples) of the samples had both Cd and Pb exceeding the maximum

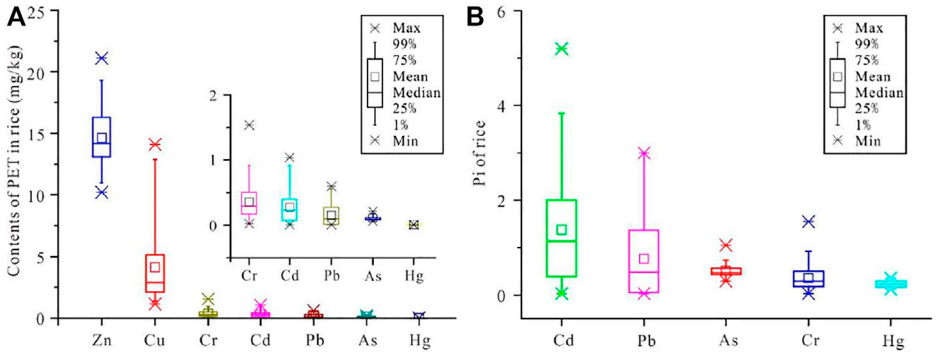

FIGURE 4 | Boxplots of heavy metal contents **(A)** and single pollution index (Pi) **(B)** of rice in the study area (mg/kg).

TABLE 5 | The number of samples with non-carcinogenic risk [targeted hazard quotient (THQ)≥1] caused by rice intake of different groups in the study area.

Groups		As	Cd	Cr	Cu	Hg	Pb	Zn
Child	Number	38	23	16	11	0	3	0
	Percentage	100%	60.53%	42.11%	28.95%	0%	7.89%	0%
Women	Number	38	22	12	8	0	2	0
	Percentage	100%	57.89%	31.58%	21.05%	0%	5.26%	0%
Men	Number	38	21	10	6	0	1	0
	Percentage	100%	55.26%	26.32%	15.79%	0%	2.63%	0%

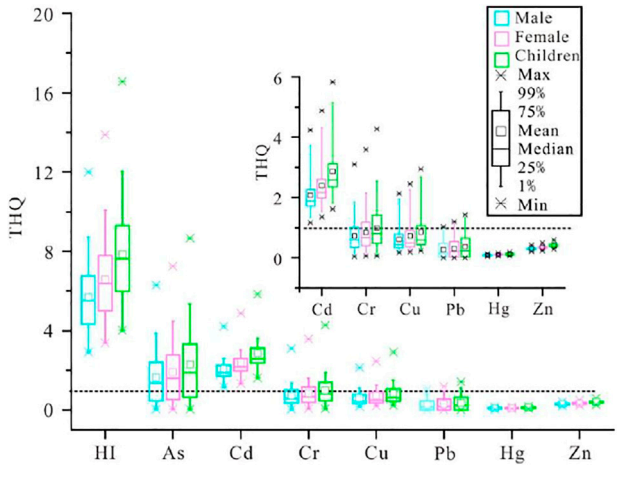

FIGURE 5 | Box plots of targeted hazard quotient (THQ) for individual heavy metals and hazard index (HI) of men, women, and children (horizontal dotted line indicates the threshold value of the hazard quotient).

allowable value. The exceedance rate of inorganic As and Cr was 2.6%. This is consistent with the low exceedance rates of As, Cr, and Hg in rice grain in the karst areas of Guangxi (Yang et al., 2021a). The excess rate of Pb in this study was relatively high but does not exceed the maximum allowable value in Yang et al. (2021a). The Cd in 26.67% (75 in total) of the rice samples exceeded the maximum allowable value in karst regions of Liujiang County, Guangxi, with the mean contents of 0.16 mg/kg (Tang et al., 2021). Even higher excessive rates were found in the karst area of Jinchengjiang, Guangxi, 95% (40 in total) of rice grains harvested from limestone soil had a Cd content that surpasses the maximum permissible concentration (Li et al., 2018). The CVs of PTE in rice decreased in an order of Pb (109.21%), Cd (92.88%), Cr (80.18%), Cu (75.87%), Hg (31.57%), As (30.26%), and Zn (15.56%) in this study. The high spatial heterogeneity of Cd may lead to different results of the exceeded rate in different areas.

Human Health Risk Assessments

The results of using EDI, THQ, and HI to assess the potential non-carcinogenic effect of long-term exposure to PTE of edible rice are shown in **Table 5** and **Figure 5**. The average EDIs of As, Cd, Cr, Cu, Hg, Pb, and Zn for inhabitants by consuming rice were 0.00062, 0.00166, 0.00216, 0.02487, 0.00002, 0.00191, and 0.08849 mg/(kg BWday) for men, and 0.00072, 0.00192, 0.00250, 0.02874, 0.00002, 0.00107, and 0.10223 mg/(kg BWday) for women, and 0.00086, 0.00230, 0.00298, 0.03430, 0.00004, 0.00128, and 0.12204 mg/(kg BWday) for children. The average THQ values of PTE decreased in an order of As (2.08) >Cd (1.66) >Cr (0.72) >Cu (0.62) >Zn (0.29) >Pb (0.27) >Hg (0.09) for men, As (2.4) >Cd (1.92) >Cr (0.83) >Cu (0.72) >Zn (0.34) >Pb (0.31) >Hg (0.1) for women, and As (2.86)>Cd (2.3) >Cr (0.99) >Cu (0.86) >Zn (0.41) >Pb (0.37) >Hg (0.12) for children. The EDIs and THQs values of the PTE decreased in the order of children > women > men owing to the increasing body weight. The dietary risk of Cd and As in children is the highest, and decreases with the increasing body weight. The same results were reported by Chen et al. (2018), Baruah et al. (2021), and Mallongi et al. (2022). Children are also at higher health risks

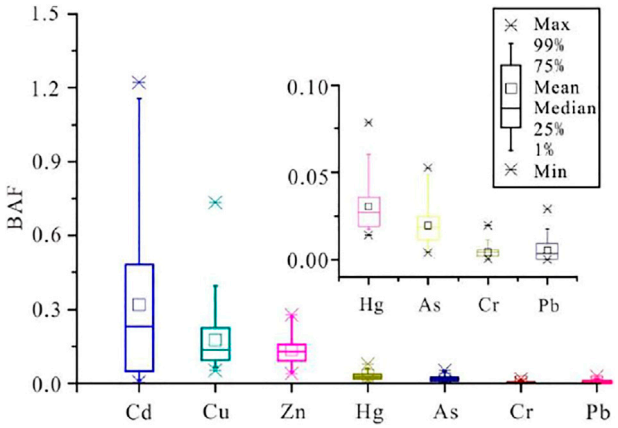

FIGURE 6 | The bioaccumulation factor (BAF) values of PTE in rice samples.

than adults by drinking substandard water. The HI, THQ_{As}, and the average THQ_{Cd} in all the samples were greater than 1 (**Figure 5**), indicating that residents suffer from non-carcinogenic risk by rice consumption. As and Cd were the biggest contributors to high HI. This is consistent with previous studies reporting that As and Cd intake of rice is the main contributor to health risks (Chen et al., 2018; Baruah et al., 2021; Tang et al., 2021). Given the high dietary Cd intake, effective agronomic measures should be considered to solve Cd pollution in the soil and reduce the transfer of Cd from the soil to edible crops (Hussain et al., 2021).

Influencing Factors of PTE Enrichment in Soil-Rice System

The BAF values of As, Cd, Cr, Cu, Hg, Pb, and Zn in rice were 0.02, 0.318, 0.005, 0.173, 0.030, 0.005, and 0.135, respectively, on average (**Figure 6**). The results are consistent with the fact that cadmium seems to prefer to be absorbed by the rice, although it is not an essential element. The average enrichment index for Cd, Zn, and Cu was 0.269, 0.160, and 0.083 in a soil–rice system in Wenling, Zhejiang Province, respectively, and varied significantly with heavy metals in paddy fields (Zhao et al., 2010). Cd can form a complex with plant peptide transporters; thus, it can be transported to the rice grains (Rizwan et al., 2012). Cd^{2+} could replace Ca^{2+} more easily than other PTE owing to their similar ion radius and same valence, and Cd would be transported actively into the grain through the Ca channel, while other PTEs could only be transported passively (Kim et al., 2002; Chang et al., 2014).

To determine the relationship between the PTE in rice and the corresponding rhizosphere soils, correlation analysis was performed. There was a certain correlation of PTE between rice and soil (**Supplementary Table S5**). The concentrations of Cd ($p < 0.01$), Hg ($p < 0.01$), Pb ($p < 0.01$), and Zn ($p < 0.01$) in soil correlated positively with As in rice, and the concentrations of As ($p < 0.01$), Cr ($p < 0.05$), Hg ($p < 0.05$), Pb ($p < 0.05$), and Zn ($p < 0.05$) in soil correlated positively with Hg in rice, indicating that these elements in soil promoted the accumulation of As and Hg in rice grains. However, the correlation of other heavy metals in rice and soil was not significant, even A_{Cu} was not significantly correlated with Cu in rice, indicating that the accumulation of heavy metals in the soil-rice system was also affected by other factors. Heavy metals are absorbed by soil organic matter and reduce the accumulation of heavy metals in crops. For example, the Hg content of rice, $lgBAF_{Hg}$, and $lgBAF_{Zn}$ are negatively correlated with Corg (**Supplementary Table S5**). But the high Corg content will also increase the accumulation of As in rice (Norton et al., 2013). This study also found a significant positive correlation between As in rice and Corg in soil (**Supplementary Table S5**). Content of As, Cd, and Zn in rice and their lgBAF were significantly negatively correlated with pH, E_{Ca}, and E_{Mg} in soil, respectively, at different confidence levels (except that Cd was not significantly correlated with E_{Ca}) (**Supplementary Table S5**). Soil pH affects the dissolution of heavy metals, especially in acidic rice fields; low pH may result in increased solubility and high availability of heavy metals in rice. High exchangeable calcium and magnesium content can increase soil pH and indirectly immobilize heavy metals (Hussain et al., 2021), and also promote the adsorption capacity of heavy metals (Kokkinos et al., 2020), leading to negatively correlated results. However, the correlation between Hg in rice and elements in the soil is opposite to them. Hg in rice was significantly positively correlated with pH, E_{Ca}, and E_{Mg} in soil, but significantly negatively correlated with A_{Fe}, A_{Zn}, and A_{Cu} (**Supplementary Table S5**). Meanwhile, Cd and Zn in rice were significantly positively correlated with A_{Fe}, A_{Zn}, and A_{Cu}; lgBAF of As, Cd, and Zn were significantly positively correlated with A_{Fe} and A_{Zn} (**Supplementary Table S5**). This is consistent with previous reports that decreased rhizosphere Fe and Cd concentrations resulted in lower Cd concentrations in rice (Zhang et al., 2018). Iron is an essential and important element in plants, and the chemical properties and pathways into rice of Fe and Cd are similar, resulting in their high correlation in crops (Sharma et al., 2004; Chen et al., 2017; Liu et al., 2017). Changes in the redox environment affect the dissolution and bioavailability of heavy metals with different irrigation methods. Concentrations of iron oxides change due to redox changes in paddy fields, so it is reasonable that Fe oxide was significantly and positively correlated with BAF of As, Cd, and Zn since heavy metals may release from stable Fe oxide bound fraction which would increase the availability of heavy metals to rice. The correlation of A_{Mn}, A_{Fe}, and lgBAF of heavy metals can also be traced back to their correlation with heavy metal content in soil (**Supplementary Tables S5 and S4**), which may be related to changes in pH and redox conditions affecting the formation and evolution of iron-manganese nodules. Significantly negative correlations between A_{Si} and $lgBAF_{As}$, $lgBAF_{Cd}$, $lgBAF_{Hg}$, and $lgBAF_{Zn}$ indicate that Si can effectively alleviate the bioaccumulation of PTE (**Supplementary Table S5**), as suggested by a previous study (Li et al., 2018). In natural environments, soil properties such as pH, CEC, redox potential, minerals (phosphates, metal

hydroxides, metal oxides, and clays), and SOM jointly affect the BCF of PTE (Ata-Ul-Karim et al., 2020). Future studies are recommended to investigate the interactions between soil properties to gain a comprehensive understanding of the bioavailability of PTE in soil-crop systems. For farmers, the use of unqualified mineral fertilizers or excessive use of pesticides should be avoided. Although the excess rate of As in soil and rice was very low, its non-carcinogenic risk to humans is high, so organic fertilizers should be used with caution to reduce the risk of As enrichment in rice. Meanwhile, attention should be paid to soil acidity and alkalinity, as well as the impact of irrigation methods on the accumulation of heavy metals in rice.

CONCLUSION

The average concentration of all studied PTE in rhizosphere soil of rice samples was below the local background value of Mashan County, but higher than the background value of surface soil in Guangxi except for As. Results of contaminant risk assessment using background values as reference values indicated a low-risk status. However, Cd in 84.21% of the samples exceeded the risk screening value of GB 15618-2018, and 21.05 and 26.32% of the samples were moderately and heavily polluted in the NCPI assessment. Weathering of parent rocks and alluvial deposits are the major source of heavy metals in soils, while fossil fuel combustion and agricultural activities also contribute to the accumulation of soil PTE. Cd in 55.26% and Pb in 31.58% of rice samples exceed the maximum allowable value of rice of China. The high excessive rate of Cd and Pb could be attributed to their high bioaccumulation factor and high content in the soil. Residents may be exposed to As and Cd through rice consumption, resulting in significant non-carcinogenic health risks, especially children. Health risks caused by excessive consumption of wild heavy metal-enriched rice should be avoided. Residents are expected to apply appropriate agricultural products and irrigation methods to mitigate the risk of PTE enrichment in rice, and future research should place a high value on rice cultivars and bioavailability of PTE in agricultural soils in the karst areas.

DATA AVAILABILITY STATEMENT

The raw data supporting the conclusion of this article will be made available by the authors, without undue reservation.

AUTHOR CONTRIBUTIONS

XZ had the original ideas, designed the research, and acquired financial support for the project leading to this publication. CZ collected the sample, carried out the data analysis, and prepared the original draft. HY, JL, and TZ analyzed data for figures and tables, and helped to prepare the original draft. All authors contributed to manuscript development and edited the final version.

FUNDING

This study was funded by the Natural Science Foundation of Guangxi (2017GXNSFBA198090), the Guangxi Science and Technology Base and Talent Project (AD20297090), Guangxi Key Science and Technology Innovation Base on Karst Dynamics (KDL and Guangxi202209), China Geological Survey (DD20160324-03), and Guilin Science and Technology Project (2020010403).

SUPPLEMENTARY MATERIAL

The Supplementary Material for this article can be found online at: https://www.frontiersin.org/articles/10.3389/fenvs.2022.866427/full#supplementary-material

REFERENCES

Ata-Ul-Karim, S. T., Cang, L., Wang, Y., and Zhou, D. (2020). Effects of Soil Properties, Nitrogen Application, Plant Phenology, and Their Interactions on Plant Uptake of Cadmium in Wheat. *J. Hazard. Mater.* 384, 121452. doi:10.1016/j.jhazmat.2019.121452

Ayejoto, D. A., Agbasi, J. C., Egbueri, J. C., and Echefu, K. I. (2022). Assessment of Oral and Dermal Health Risk Exposures Associated with Contaminated Water Resources: an Update in Ojoto Area, Southeast Nigeria. *Int. J. Environ. Anal. Chem.*, 1–21. doi:10.1080/03067319.2021.2023515

Baruah, S. G., Ahmed, I., Das, B., Ingtipi, B., Boruah, H., Gupta, S. K., et al. (2021). Heavy Metal(loid)s Contamination and Health Risk Assessment of Soil-rice System in Rural and Peri-Urban Areas of Lower Brahmaputra valley, Northeast India. *Chemosphere* 266, 129150. doi:10.1016/j.chemosphere.2020.129150

Bashir, S., Hussain, Q., Akmal, M., Riaz, M., Hu, H., Ijaz, S. S., et al. (2018). Sugarcane Bagasse-Derived Biochar Reduces the Cadmium and Chromium Bioavailability to Mash Bean and Enhances the Microbial Activity in Contaminated Soil. *J. Soils Sediments* 18, 874–886. doi:10.1007/s11368-017-1796-z

Bing, H., Qiu, S., Tian, X., Li, J., Zhu, H., Wu, Y., et al. (2021). Trace Metal Contamination in Soils from Mountain Regions across China: Spatial Distribution, Sources, and Potential Drivers. *Soil Ecol. Lett.* 3, 189–206. doi:10.1007/s42832-021-0080-8

Chang, C. Y., Yu, H. Y., Chen, J. J., Li, F. B., Zhang, H. H., and Liu, C. P. (2014). Accumulation of Heavy Metals in Leaf Vegetables from Agricultural Soils and Associated Potential Health Risks in the Pearl River Delta, South China. *Environ. Monit. Assess.* 186, 1547–1560. doi:10.1007/s10661-013-3472-0

Chen, H., Yang, X., Wang, P., Wang, Z., Li, M., and Zhao, F.-J. (2018). Dietary Cadmium Intake from rice and Vegetables and Potential Health Risk: A Case Study in Xiangtan, Southern China. *Sci. Total Environ.* 639, 271–277. doi:10.1016/j.scitotenv.2018.05.050

Chen, Z., Tang, Y.-T., Zhou, C., Xie, S.-T., Xiao, S., Baker, A. J. M., et al. (2017). Mechanisms of Fe Biofortification and Mitigation of Cd Accumulation in rice (Oryza Sativa L.) Grown Hydroponically with Fe Chelate Fertilization. *Chemosphere* 175, 275–285. doi:10.1016/j.chemosphere.2017.02.053

CNS Chinese Nutrition Society (2021). *Scientific Research Report on Dietary Guidelines for Chinese Residents*. Beijing. (in Chinese).

Egbueri, J. C., and Agbasi, J. C. (2022). Data-driven Soft Computing Modeling of Groundwater Quality Parameters in Southeast Nigeria: Comparing the

Performances of Different Algorithms. *Environ. Sci. Pollut. Res.* doi:10.1007/s11356-022-18520-8

Egbueri, J. C., Ayejoto, D. A., and Agbasi, J. C. (2022a). Pollution Assessment and Estimation of the Percentages of Toxic Elements to Be Removed to Make Polluted Drinking Water Safe: a Case from Nigeria. *Toxin Rev.*, 1–15. doi:10.1080/15569543.2021.2025401

Egbueri, J. C., Enyigwe, M. T., and Ayejoto, D. A. (2022b). Modeling the Impact of Potentially Harmful Elements on the Groundwater Quality of a Mining Area (Nigeria) by Integrating NSFWQI, HERisk Code, and HCs. *Environ. Monit. Assess.* 194, 150. doi:10.1007/s10661-022-09789-w

Egbueri, J. C., Ezugwu, C. K., Unigwe, C. O., Onwuka, O. S., Onyemesili, O. C., and Mgbenu, C. N. (2021a). Multidimensional Analysis of the Contamination Status, Corrosivity and Hydrogeochemistry of Groundwater from Parts of the Anambra Basin, Nigeria. *Anal. Lett.* 54, 1–31. doi:10.1080/00032719.2020.1843049

Egbueri, J. C., Mgbenu, C. N., Digwo, D. C., and Nnyigide, C. S. (2021b). A Multi-Criteria Water Quality Evaluation for Human Consumption, Irrigation and Industrial Purposes in Umunya Area, southeastern Nigeria. *Int. J. Environ. Anal. Chem.*, 1–25. doi:10.1080/03067319.2021.1907360

Egbueri, J. C., Ukah, B. U., Ubido, O. E., and Unigwe, C. O. (2020). A Chemometric Approach to Source Apportionment, Ecological and Health Risk Assessment of Heavy Metals in Industrial Soils from Southwestern Nigeria. *Int. J. Environ. Anal. Chem.*, 1–19. doi:10.1080/03067319.2020.1769615

Fonseca, R., Pinho, C., Albuquerque, T., and Araújo, J. (2021). Environmental Factors and Metal Mobilisation in Alluvial Sediments-Minas Gerais, Brazil. *Geosciences* 11 (3), 110. doi:10.3390/geosciences11030110

Frierdich, A. J., and Catalano, J. G. (2012). Distribution and Speciation of Trace Elements in Iron and Manganese Oxide Cave Deposits. *Geochimica et Cosmochimica Acta* 91, 240–253. doi:10.1016/j.gca.2012.05.032

Giri, S., Mahato, M. K., Bhattacharjee, S., and Singh, A. K. (2020). Development of a New Noncarcinogenic Heavy Metal Pollution index for Quality Ranking of Vegetable, rice, and Milk. *Ecol. Indicators* 113, 106214. doi:10.1016/j.ecolind.2020.106214

Giri, S., Singh, A. K., and Mahato, M. K. (2019). Monte Carlo Simulation-Based Probabilistic Health Risk Assessment of Metals in Groundwater via Ingestion Pathway in the Mining Areas of Singhbhum Copper belt, India. *Int. J. Environ. Health Res.* 30, 447–460. doi:10.1080/09603123.2019.1599101

Gu, X., Xu, L., Wang, Z., Ming, X., Dang, P., Ouyang, W., et al. (2021). Assessment of Cadmium Pollution and Subsequent Ecological and Health Risks in Jiaozhou Bay of the Yellow Sea. *Sci. Total Environ.* 774, 145016. doi:10.1016/j.scitotenv.2021.145016

Guo, X., Zhang, S., Shan, X.-q., Luo, L., Pei, Z., Zhu, Y.-G., et al. (2006). Characterization of Pb, Cu, and Cd Adsorption on Particulate Organic Matter in Soil. *Environ. Toxicol. Chem.* 25, 2366–2373. doi:10.1897/05-636R.1

Hakanson, L. (1980). An Ecological Risk index for Aquatic Pollution control.a Sedimentological Approach. *Water Res.* 14, 975–1001. doi:10.1016/0043-1354(80)90143-8

Hou, D., O'Connor, D., Igalavithana, A. D., Alessi, D. S., Luo, J., Tsang, D. C. W., et al. (2020a). Metal Contamination and Bioremediation of Agricultural Soils for Food Safety and Sustainability. *Nat. Rev. Earth Environ.* 1, 366–381. doi:10.1038/s43017-020-0061-y

Hou, Q., Yang, Z., Yu, T., You, Y., Dou, L., and Li, K. (2020b). Impacts of Parent Material on Distributions of Potentially Toxic Elements in Soils from Pearl River Delta in South China. *Sci. Rep.* 10, 17394. doi:10.1038/s41598-020-74490-2

Hou, Q. Y., Yang, Z. F., Yu, T., Xia, X. Q., Cheng, H. X., and Zhou, G. H. (2020c). *Soil Geochemical Parameters in China*. Beijing: Geological Publishing House.

Hu, B., Jia, X., Hu, J., Xu, D., Xia, F., and Li, Y. (2017). Assessment of Heavy Metal Pollution and Health Risks in the Soil-Plant-Human System in the Yangtze River Delta, China. *Ijerph* 14, 1042. doi:10.3390/ijerph14091042

Hu, Y., Cheng, H., and Tao, S. (2016). The Challenges and Solutions for Cadmium-Contaminated Rice in China: A Critical Review. *Environ. Int.* 92-93, 515–532. doi:10.1016/j.envint.2016.04.042

Hussain, B., Ashraf, M. N., Shafeeq-ur-Rahman, R., Abbas, A., Li, J., and Farooq, M. (2021). Cadmium Stress in Paddy fields: Effects of Soil Conditions and Remediation Strategies. *Sci. Total Environ.* 754, 142188. doi:10.1016/j.scitotenv.2020.142188

Jalili, C., Kazemi, M., Taheri, E., Mohammadi, H., Boozari, B., Hadi, A., et al. (2020). Exposure to Heavy Metals and the Risk of Osteopenia or Osteoporosis: a Systematic Review and Meta-Analysis. *Osteoporos. Int.* 31, 1671–1682. doi:10.1007/s00198-020-05429-6

Kim, Y.-Y., Yang, Y.-Y., and Lee, Y. (2002). Pb and Cd Uptake in rice Roots. *Physiol. Plantarum* 116, 368–372. doi:10.1034/j.1399-3054.2002.1160312.x

Kokkinos, E., Chousein, C., Simeonidis, K., Coles, S., Zouboulis, A., and Mitrakas, M. (2020). Improvement of Manganese Feroxyhyte's Surface Charge with Exchangeable Ca Ions to Maximize Cd and Pb Uptake from Water. *Materials* 13, 1762. doi:10.3390/ma13071762

Kowalska, J. B., Mazurek, R., Gąsiorek, M., and Zaleski, T. (2018). Pollution Indices as Useful Tools for the Comprehensive Evaluation of the Degree of Soil Contamination-A Review. *Environ. Geochem. Health* 40, 2395–2420. doi:10.1007/s10653-018-0106-z

Kukusamude, C., Sricharoen, P., Limchoowong, N., and Kongsri, S. (2021). Heavy Metals and Probabilistic Risk Assessment via rice Consumption in Thailand. *Food Chem.* 334, 127402. doi:10.1016/j.foodchem.2020.127402

Kumar, S., Prasad, S., Yadav, K. K., Shrivastava, M., Gupta, N., Nagar, S., et al. (2019). Hazardous Heavy Metals Contamination of Vegetables and Food Chain: Role of Sustainable Remediation Approaches - A Review. *Environ. Res.* 179, 108792. doi:10.1016/j.envres.2019.108792

Li, C., Yang, Z., Yu, T., Hou, Q., Liu, X., Wang, J., et al. (2021). Study on Safe Usage of Agricultural Land in Karst and Non-karst Areas Based on Soil Cd and Prediction of Cd in rice: A Case Study of Heng County, Guangxi. *Ecotoxicology Environ. Saf.* 208, 111505. doi:10.1016/j.ecoenv.2020.111505

Li, D., Li, W., Lu, Q., Li, Y., Li, N., Xu, H., et al. (2018). Cadmium Bioavailability Well Assessed by DGT and Factors Influencing Cadmium Accumulation in rice Grains from Paddy Soils of Three Parent Materials. *J. Soils Sediments* 18, 2552–2561. doi:10.1007/s11368-018-1950-2

Li, D., Wang, L., Wang, Y., Li, H., and Chen, G. (2019). Soil Properties and Cultivars Determine Heavy Metal Accumulation in rice Grain and Cultivars Respond Differently to Cd Stress. *Environ. Sci. Pollut. Res.* 26, 14638–14648. doi:10.1007/s11356-019-04727-9

Liu, C., Massey, M. S., Latta, D. E., Xia, Y., Li, F., Gao, T., et al. (2021). Fe(II)-induced Transformation of Iron Minerals in Soil Ferromanganese Nodules. *Chem. Geology.* 559, 119901. doi:10.1016/j.chemgeo.2020.119901

Liu, H., Zhang, C., Wang, J., Zhou, C., Feng, H., Mahajan, M. D., et al. (2017). Influence and Interaction of Iron and Cadmium on Photosynthesis and Antioxidative Enzymes in Two rice Cultivars. *Chemosphere* 171, 240–247. doi:10.1016/j.chemosphere.2016.12.081

Mallongi, A., Astuti, R. D. P., Amiruddin, R., Hatta, M., and Rauf, A. U. (2022). Identification Source and Human Health Risk Assessment of Potentially Toxic Metal in Soil Samples Around Karst Watershed of Pangkajene, Indonesia. *Environ. Nanotechnology, Monit. Manage.* 17, 100634. doi:10.1016/j.enmm.2021.100634

MEEPRC Ministry of Ecology and Environment of the People's Republic of China (2018). *Risk Control Standard for Soil Contamination of Agriculture Land*. Beijing: MEEPRC

MLRPRC Ministry of Land and Resources of the People's Republic of China (2016). *Specification of Land Quality Geochemical Assessment*. Beijing: Geological Publishing House

Mu, T., Zhou, T., Li, Z., Hu, P., Luo, Y., Christie, P., et al. (2020). Prediction Models for rice Cadmium Accumulation in Chinese Paddy fields and the Implications in Deducing Soil Thresholds Based on Food Safety Standards. *Environ. Pollut.* 258, 113879. doi:10.1016/j.envpol.2019.113879

NHFPCPRC and CFDA, National Health and Family Planning Commission and China Food and Drug Administration (2017). *National Standard for Food Safety: Limit of Contaminants in Food*. Beijing: NHFPCPRC and CFDA

Norton, G. J., Adomako, E. E., Deacon, C. M., Carey, A.-M., Price, A. H., and Meharg, A. A. (2013). Effect of Organic Matter Amendment, Arsenic Amendment and Water Management Regime on rice Grain Arsenic Species. *Environ. Pollut.* 177, 38–47. doi:10.1016/j.envpol.2013.01.049

Pu, Y. L., Long, G. F., Gou, W. P., and Liu, S. Q. (2010). Status of Soil Available Manganese in Tibet and its Affecting Factors. *J. SW China Nor.Univer.Natural Sci. Edition* 35, 163. doi:10.13718/j.cnki.xsxb.2010.06.026

Qu, C., Shi, W., Guo, J., Fang, B., Wang, S., Giesy, J. P., et al. (2016). China's Soil Pollution Control: Choices and Challenges. *Environ. Sci. Technol.* 50, 13181–13183. doi:10.1021/acs.est.6b05068

Rahman, M. S., Biswas, P. K., Al Hasan, S. M., Rahman, M. M., Lee, S. H., Kim, K.-H., et al. (2018). The Occurrences of Heavy Metals in farmland Soils and Their

Propagation into Paddy Plants. *Environ. Monit. Assess.* 190, 201. doi:10.1007/s10661-018-6577-7

Rizwan, M., Meunier, J.-D., Miche, H., and Keller, C. (2012). Effect of Silicon on Reducing Cadmium Toxicity in Durum Wheat (Triticum Turgidum L. Cv. Claudio W.) Grown in a Soil with Aged Contamination. *J. Hazard. Mater.* 209-210, 326–334. doi:10.1016/j.jhazmat.2012.01.033

Sanaei, F., Amin, M. M., Alavijeh, Z. P., Esfahani, R. A., Sadeghi, M., Bandarrig, N. S., et al. (2021). Health Risk Assessment of Potentially Toxic Elements Intake via Food Crops Consumption: Monte Carlo Simulation-Based Probabilistic and Heavy Metal Pollution index. *Environ. Sci. Pollut. Res.* 28, 1479–1490. doi:10.1007/s11356-020-10450-7

Savignan, L., Lee, A., Coynel, A., Jalabert, S., Faucher, S., Lespes, G., et al. (2021). Spatial Distribution of Trace Elements in the Soils of South-Western France and Identification of Natural and Anthropogenic Sources. *Catena* 205, 105446. doi:10.1016/j.catena.2021.105446

Sharma, S. S., Kaul, S., Metwally, A., Goyal, K. C., Finkemeier, I., and Dietz, K.-J. (2004). Cadmium Toxicity to Barley (Hordeum Vulgare) as Affected by Varying Fe Nutritional Status. *Plant Sci.* 166, 1287–1295. doi:10.1016/j.plantsci.2004.01.006

Tang, M., Lu, G., Fan, B., Xiang, W., and Bao, Z. (2021). Bioaccumulation and Risk Assessment of Heavy Metals in Soil-Crop Systems in Liujiang Karst Area, Southwestern China. *Environ. Sci. Pollut. Res.* 28, 9657–9669. doi:10.1007/s11356-020-11448-x

Tomlinson, D. L., Wilson, J. G., Harris, C. R., and Jeffrey, D. W. (1980). Problems in the Assessment of Heavy-Metal Levels in Estuaries and the Formation of a Pollution index. *Helgolander Meeresunters* 33, 566–575. doi:10.1007/BF02414780

USEPA U.S. Environmental Protection Agency (1989). "Risk-assessment Guidance for Superfund," in *Human Health Evaluation Manual. Part A. Interim Report (Final)* (Washington: Office of Emergency and Remedial Response), Vol. 1.

Wang, C., Li, W., Yang, Z., Chen, Y., Shao, W., and Ji, J. (2015). An Invisible Soil Acidification: Critical Role of Soil Carbonate and its Impact on Heavy Metal Bioavailability. *Sci. Rep.* 5, 12735. doi:10.1038/srep12735

Wen, Y., Li, W., Yang, Z., Zhang, Q., and Ji, J. (2020b). Enrichment and Source Identification of Cd and Other Heavy Metals in Soils with High Geochemical Background in the Karst Region, Southwestern China. *Chemosphere* 245, 125620. doi:10.1016/j.chemosphere.2019.125620

Wen, Y., Li, W., Yang, Z., Zhuo, X., Guan, D.-X., Song, Y., et al. (2020a). Evaluation of Various Approaches to Predict Cadmium Bioavailability to rice Grown in Soils with High Geochemical Background in the Karst Region, Southwestern China. *Environ. Pollut.* 258, 113645. doi:10.1016/j.envpol.2019.113645

Yang, Q., Yang, Z., Filippelli, G. M., Ji, J., Ji, W., Liu, X., et al. (2021b). Distribution and Secondary Enrichment of Heavy Metal Elements in Karstic Soils with High Geochemical Background in Guangxi, China. *Chem. Geology.* 567, 120081. doi:10.1016/j.chemgeo.2021.120081

Yang, Q., Yang, Z., Zhang, Q., Liu, X., Zhuo, X., Wu, T., et al. (2021a). Ecological Risk Assessment of Cd and Other Heavy Metals in Soil-rice System in the Karst Areas with High Geochemical Background of Guangxi, China. *Sci. China Earth Sci.* 64, 1126–1139. doi:10.1007/s11430-020-9763-0

Yang, S., Zhou, D., Yu, H., Wei, R., and Pan, B. (2013). Distribution and Speciation of Metals (Cu, Zn, Cd, and Pb) in Agricultural and Non-agricultural Soils Near a Stream Upriver from the Pearl River, China. *Environ. Pollut.* 177, 64–70. doi:10.1016/j.envpol.2013.01.044

Yu, H.-Y., Li, F.-B., Liu, C.-S., Huang, W., Liu, T.-X., and Yu, W.-M. (2016). "Iron Redox Cycling Coupled to Transformation and Immobilization of Heavy Metals: Implications for Paddy Rice Safety in the Red Soil of South China," in *Advances in Agronomy*. Editor D. L. Sparks (Academic Press), 279–317. doi:10.1016/bs.agron.2015.12.006

Zeng, F., Wei, W., Li, M., Huang, R., Yang, F., and Duan, Y. (2015). Heavy Metal Contamination in Rice-Producing Soils of Hunan Province, China and Potential Health Risks. *Ijerph* 12, 15584–15593. doi:10.3390/ijerph121215005

Zhang, B., Liu, L., Huang, Z., Hou, H., Zhao, L., and Sun, Z. (2021). Application of Stochastic Model to Assessment of Heavy Metal(loid)s Source Apportionment and Bio-Availability in rice fields of Karst Area. *Sci. Total Environ.* 793, 148614. doi:10.1016/j.scitotenv.2021.148614

Zhang, C., Li, Z., Yang, W., Pan, L., Gu, M., and Lee, D. (2013). Assessment of Metals Pollution on Agricultural Soil Surrounding a lead-zinc Mining Area in the Karst Region of Guangxi, China. *Bull. Environ. Contam. Toxicol.* 90, 736–741. doi:10.1007/s00128-013-0987-6

Zhang, Q., Zhang, L., Liu, T., Liu, B., Huang, D., Zhu, Q., et al. (2018). The Influence of Liming on Cadmium Accumulation in rice Grains via Iron-Reducing Bacteria. *Sci. Total Environ.* 645, 109–118. doi:10.1016/j.scitotenv.2018.06.316

Zhang, Z., Zhang, Q., Tu, C., Zhang, J., Lin, C., Fang, H., et al. (2019). Effects on Heavy Metals in Karst Region Soil and the Enrichment Characteristics of Rice-Rape Rotation. *Pol. J. Environ. Stud.* 28, 4485–4493. doi:10.15244/pjoes/99242

Zhao, K., Liu, X., Xu, J., and Selim, H. M. (2010). Heavy Metal Contaminations in a Soil-rice System: Identification of Spatial Dependence in Relation to Soil Properties of Paddy fields. *J. Hazard. Mater.* 181, 778–787. doi:10.1016/j.jhazmat.2010.05.081

Zuo, T.-T., Li, Y.-L., He, H.-Z., Jin, H.-Y., Zhang, L., Sun, L., et al. (2019). Refined Assessment of Heavy Metal-Associated Health Risk Due to the Consumption of Traditional Animal Medicines in Humans. *Environ. Monit. Assess.* 191, 171. doi:10.1007/s10661-019-7270-1

Conflict of Interest: The authors declare that the research was conducted in the absence of any commercial or financial relationships that could be construed as a potential conflict of interest.

Publisher's Note: All claims expressed in this article are solely those of the authors and do not necessarily represent those of their affiliated organizations, or those of the publisher, the editors, and the reviewers. Any product that may be evaluated in this article, or claim that may be made by its manufacturer, is not guaranteed or endorsed by the publisher.

frontiers | Frontiers in Environmental Science

ORIGINAL RESEARCH
published: 14 June 2022
doi: 10.3389/fenvs.2022.909858

An Integrated Approach in the Assessment of the Vlasina River System Pollution by Toxic Elements

Sanja Sakan[1]*, *Aleksandra Mihajlidi-Zelić*[1], *Sandra Škrivanj*[2], *Stanislav Frančišković-Bilinski*[3] and *Dragana Đorđević*[1]

[1]Centre of Excellence in Environmental Chemistry and Engineering, Institute of Chemistry, Technology and Metallurgy, University of Belgrade, Belgrade, Serbia, [2]Faculty of Chemistry, University of Belgrade, Belgrade, Serbia, [3]Ruđer Bošković Institute, Division for Marine and Environmental Research, Zagreb, Croatia

Increasing pollutant levels in surface water are a very important problem in developing countries. In Serbia, the largest rivers are transboundary rivers that cross the border already polluted. Taking this into account, evaluation of the distribution characteristics, ecological risk, and sources of toxic elements in river water and surface sediments in the watercourses of the Vlasina watershed is of great significance for the protection of water resources in Serbia. A total of 17 sediment and 18 water samples were collected and analyzed by Inductively Coupled Plasma—Optical Emission spectrometry (ICP-OES) and Inductively Coupled Plasma—Mass spectrometry (ICP-MS) to determine micro- and macroelements contents. The geo-accumulation index (I_{geo}) was applied to determine and classify the magnitude of toxic element pollution in this river sediment. The contents of the studied toxic elements were below water and sediment quality guidelines. For studied river water, results of principal component analysis (PCA) indicated the difference in behavior of Cr, Mn, Ni, Cu, and As and V, respectively. Cluster analysis (CA) classified water samples according to As and Cu content. The PCA results revealed that lead in river sediments had different behavior than other elements and can be associated mainly with anthropogenic sources. According to the degree of I_{geo}, the majority of sediments in the Vlasina region were uncontaminated regarding studied toxic elements. The origin of elements is mostly from natural processes such as soil and rock weathering.

Keywords: Vlasina river, trace elements, spatial distribution, chemometric methods, pollution, surface water, integrated approach

OPEN ACCESS

Edited by:
Antonije Onjia,
University of Belgrade, Serbia

Reviewed by:
Dejan Krčmar,
University of Novi Sad, Serbia
Fikret Ustaoğlu,
Giresun University, Turkey
Snezana Dragovic,
University of Belgrade, Serbia

***Correspondence:**
Sanja Sakan
ssakan@chem.bg.ac.rs
sanja.sakan@ihtm.bg.ac.rs

Specialty section:
This article was submitted to Toxicology, Pollution and the Environment, a section of the journal Frontiers in Environmental Science

Received: *31 March 2022*
Accepted: *29 April 2022*
Published: *14 June 2022*

Citation:
Sakan S, Mihajlidi-Zelić A, Škrivanj S, Frančišković-Bilinski S and Đorđević D (2022) An Integrated Approach in the Assessment of the Vlasina River System Pollution by Toxic Elements. Front. Environ. Sci. 10:909858. doi: 10.3389/fenvs.2022.909858

INTRODUCTION

The sediment environmental compartment is a heterogeneous natural matrix of materials (Carrillo et al., 2021). Unfortunately, great pollution of rivers and sediments has been noticed recently. Monitoring of sediment contaminants and assessment of sediment quality is usually carried out with the objectives of determining the extent to which the sediments are either a source or a sink for contaminants and evaluating the effects of these contaminants on the environment of the investigated water body. Bearing this in mind, analysis of sediments provides an efficient tool for water-quality management. There are numerous challenges in the management of contaminated sediments, and there are no easy solutions.

Anthropogenic activities have increased the concentrations of pollutants in our environment. One of the significant pollutants are potentially toxic elements (PTEs), and they can easily bind to sediments. The majority of toxic elements are quickly deposited in the sediment after entering rivers, and their concentration in the sediment is much higher than in the water body of riverine systems (Huang et al., 2020). The trace elements can be toxic at high concentrations. Due to their resistance to degradation, trace elements could continue to exist in the environment for a long time (Haris et al., 2017). Since trace elements are not biodegradable, they have a hazardous effect on the ecological balance in aquatic ecosystems (Baran et al., 2019). Toxic elements in the environment can be of natural, geogenic origin, such as rock weathering with subsequent dissolution of metals in rivers (Looi et al., 2013). Still, the portions of metal emitted by natural processes such as volatilization, deposition from mineral rock, and weathering of bedrock are small (Rodríguez et al., 2015). Sediments do not permanently binds metal although they are some of the endmost sinks for metals input into the aquatic environment (Jahan and Strezov, 2018). Since remobilization can happen long after the initial input, it is essential to understand the toxic properties of contaminants in order to assess the risks associated with contamination.

For the identification of pollution problems, it is necessary to distinguish anthropogenic contributions from natural sources. In the past few years, applying pollution index-based approaches (contamination factor, enrichment factor, geoaccumulation index, toxic risk index, pollution load index, potential ecological risk, biogeochemical index, etc.) and multivariate statistical methods (cluster analysis, principal component analysis, factor analysis, and discriminant analysis) in riverine environments has become a very important and significant combination of methods in assessing the degree of pollution (Radomirović et al., 2021). Chemometric methods are statistical analyses of measured data, but pollution indexes are used for quantification of pollution and they are calculated as ratios of measured and background contents of elements. Pollution indices are widely considered as tools to quantify the degree of total metal pollution and assess the ecological risk of metals in sediments and soils (Ustaoğlu et al., 2020; Ustaoğlu and Islam, 2020; Carrillo et al., 2021; Ustaoğlu 2021; Yüksel et al., 2021). Multivariate statistical approaches have been successfully used in environmental studies to identify the interrelationships between the measured data (Sakan et al., 2009; Thuong et al., 2013; Mihajlidi-Zelić et al., 2015; Dević et al., 2016; Varol et al., 2021), in order to detect sources of pollution and relationships between sampling sites and toxic element contents (Radomirović et al., 2020; Đorđević et al., 2021). Chemometric methods provide powerful tools for the modelling and interpretation of large, environmental, multivariate data sets generated within environmental monitoring programmes (Peré-Trepat et al., 2006) and, for that reason, are used in many studies.

Therefore, for a comprehensive evaluation of the quality of river sediments and quantification of pollution content, different methods should be integrated, and complementary approaches that combine sediment quality guidelines, geoaccumulation index, and statistical analysis should be applied. Since the river water system is dynamic with highly variable short- and long-term properties, analysis of sediment is very important in assessing the status of pollution in the river system.

In the previous period, accidental water pollution in Serbia was recorded (Sakan et al., 2009; Sakan et al., 2011; Dević et al., 2016), causing the destruction of wildlife in the watercourses. Taking into account that mountain rivers in Serbia are generally considered unpolluted, research involving an assessment of their ecochemical status and defining the degree of pollution would have great significance for Serbia as well as for the wider region.

In this manuscript, different approaches have been applied in the ecochemical study of the river sediments of Vlasina and the rivers in its basin. The objectives of this manuscript were to: 1) determine the distribution of micro- and macroelements; 2) assess the degree of contamination with PTEs using different methods; 3) identify the interrelationships between the studied elements and localities; and 4) identify possible sources of pollution using chemometric methods. Since this type of research has not been done in the investigated area so far, the obtained data will be of great importance both for researchers engaged in the research of river systems and the population living in this area.

MATERIALS AND METHODS

Site Description

Vlasina is a river in southeastern Serbia. The spring is below the Vlasina lake dam. The most important tributaries are: Lužnica (Ljuberađa), the Tegošnička River and the Pusta River. Other tributaries are the Gradska River and the Bistrička River. The length of Vlasina is about 70 km, and eventually it flows into the South Morava as a right tributary, 10 km downstream from Vlasotince. Because of its mountain environment and because of the lack of industrial polluters, Vlasina is considered one of the cleanest rivers in Serbia. In recent years, in the surroundings of Vlasina basin, some anthropogenic emission sources have appeared, which can change the environmental status of this basin. For example, foreign investors are planning to open several mines upstream (Crna Trava, Čemernik) and it is very important to know the history of Vlasina basin water pollution.

The pedological composition of the territory of Vlasina is characterized by diversity, although due to the influence of pedogenic factors (rocks, vegetation, climate, and water), a certain zonation in the distribution of land is observed (Marjanović 2000). The area of Vlasina is characterized by exceptional biodiversity and autochthonous biosystems. Climatic factors, as well as geological, geomorphological, and pedological characteristics of the terrain, lead to the development of interesting flora and fauna in this area. This entire area is covered by forests, degraded forests, pastures, and agricultural crops. In the Vlasotince plain, around the river Vlasina, river sediment—alluvial is rich in humus, and as such, it is suitable for growing agricultural crops. Fertile land, vast pastures, and a favorable climate provide good opportunities for agriculture (Savić, 2019). One of the main activities of the inhabitants of

TABLE 1 | Content of element in mineral resources in Leskovac (L) and Vranje (V) Neogene basin (ppm).

	Co	Cu	Ba	Sr	Ti	As	Ni	Cd	Zn	Pb	Be
L_1[a]	3.66	5.80	442	511	1,674	5.28	nd	nd	nd	nd	nd
L_2	14.4	9.20	nd	nd	2,867	nd	57.2	nd	nd	nd	nd
L_3	3.92	nd	441	nd	1735	2.70	nd	nd	nd	nd	nd
L_4	6.14	5.22	390	396	2,280	nd	nd	nd	nd	nd	nd
L_5	16.2	21.0	752	nd	3,148	11.0	nd	<0.80	nd	nd	nd
L_6	16.6	49.2	nd	136	4,563	14.2	29.0	nd	63.8	30.8	nd
V_1	7.89	nd	1,170	337	2,176	nd	nd	nd	nd	nd	7.57
V_2	8.46	nd	1,220	370	2,598	nd	nd	nd	nd	29.6	4.81
V_3	8.40	13.7	1,051	500	2,528	nd	nd	0.10	nd	nd	nd
V_4	9.35	10.7	816	317	2,928	nd	nd	0.21	nd	nd	nd
V_5	4.17	nd	nd	133	2,237	nd	14.3	0.21	nd	nd	nd

[a]*L_1, light gray tuff; L_2, tufite sandstones and fine-grained sands; L_3, ocher darker tuffaceous sandstone; L_4, pale gray tuffites (carbonate lake phase); L_5, volcanic rock; L_6, marl; V_1, Volcanoclastic sedimentary breccias; V_2, Lithoclastic and vitroclastic tuff; V_3, light brown tuff; V_4, sandy tuff; V_5, Sediments of the carbonate lake facies; nd, no data.*

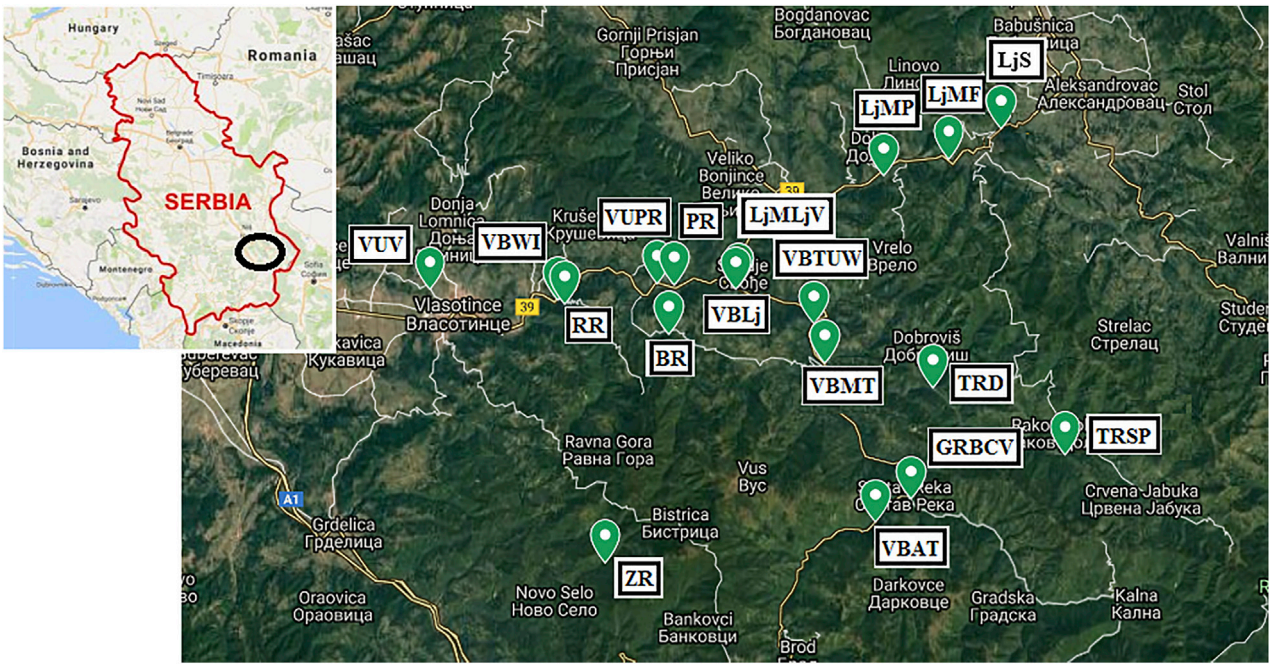

FIGURE 1 | Sampling locations: **VBAT**—Vlasina (before receiving any tributary); **GRBCV**—Gradska river (before its confluence with Vlasina); **VBMT**—Vlasina (upstream of the confluence with Tegošnička river); **TRSP**—Tegošnička river (stone pit); **TRD**—Tegošnička river (near village Dobroviš); **VBTUW**—Vlasina (downstream of the confluence with Tegošnička river, near village Gornji Orah); **LjMF**—Ljuberađa (middle course); **LjMP**—Ljuberađa (measuring profile); **LjMLjV**—Ljuberađa, (confluence with Vlasina); **VBLj**—Vlasina (after receiving Ljuberađa); **PR**—Pusta river; **VUPR**—Vlasina (downstream of the confluence with Pusta river); **BR**—Bistrička river; **RR**—Rastavnica river; **VBWI**—Vlasina (upstream of the intake for water supply); **VUV**—Vlasina (downriver from Vlasotince); **ZR**—Zelenička river.

Vlasina is mountain agriculture: mountain cattle breeding—raising small (sheep) and large cattle (cattle and horses) and mountain agriculture—growing mountain cereals (rye, barley, and oats) and potatoes. Arable agricultural land of lower quality occupies a significant area: arable land dominates the hills, orchards are around the houses, meadows are on the slopes along forest belts and in the stream valleys (GLP 2012). On the slightly undulating and hilly terrain of the Vlasotinac vineyards, vertisol is widespread. Vlasotince is also the center of the wine-growing region (Čvoro and Golubović 2001). The branch of the economy that has been developing in recent years in this micro-region is tourism (Savić, 2019).

Geological Characteristics of the Researched Area

The research area belongs to the area of the metallocene zone Mačkatica-Blagodat-Karamanica. The Vlasina complex represents its upper metamorphic complex. The largest part of this series is made up of crystalline shards of low metamorphism.

TABLE 2 | List of samples in Vlasina region.

ID	Sampling site	GPS coordinates
VBAT	Vlasina (before receiving any tributary)	N 42.893, E 22.329
GRBCV	Gradska river (before its confluence with Vlasina)	N 42.901, E 22.347
VBMT	Vlasina (upstream of the confluence with Tegošnička river)	N 42.949, E 22.306
TRSP	Tegošnička river (stone pit)	N 42.917, E 22.420
TRD	Tegošnička river (near village Dobroviš)	N 42.940, E 22.357
VBTUW	Vlasina (downstream of the confluence with Tegošnička river, near village Gornji Orah)	N 42.962, E 22.300
LjS	Ljuberađa (spring)	N 43.030, E 22.388
LjMF	Ljuberađa (middle course)	N 43.020, E 22.364
LjMP	Ljuberađa (measuring profile)	N 43.014, E 22.334
LjMLjV	Ljuberađa, (confluence with Vlasina)	N 42.975, E 22.264
VBLj	Vlasina (after receiving Ljuberađa)	N 42.974, E 22.263
PR	Pusta river	N 42.976, E 22.233
VUPR	Vlasina (downstream of the confluence with Pusta river)	N 42.977, E 22.225
BR	Bistrička river	N 42.959, E 22.231
RR	Rastavnica river	N 42.969, E 22.182
VBWI	Vlasina (upstream of the intake for water supply)	N 42.971, E 22.178
VUV	Vlasina (downriver from Vlasotince)	N 42.974, E 22.117
ZR	Zelenička river	N 42.879, E 22.200

It is a sediment-vulcanogenous formation metamorphosed under the conditions of the facies of green shale. The most important groups of rocks consist of mica-chlorite parashale of various varieties and mica-poor orthochlorites, which are very similar to metabasites. In addition, smaller masses of serpentinite appear (Simić 2001). The most represented rock complexes are the metamorphic rocks (49.31% of the total surface area), while the rest of the basin is mostly covered by the tertiary clastic sediments and Mesozoic carbonate rocks (Durlević et al., 2019).

In **Table 1** are shown the contents of elements in mineral resources in the Leskovac and Vranje Neogene basins (Kasalica et al., 2021) and only elements with elevated and anomalous values in relation to the mean content for sedimentary rocks are given.

Sample Collection

Water and sediment samples of the river Vlasina and its tributaries (Gradska River, Tegošnička River, Ljuberađa, Pusta River, Bistrička River, Rastavnica) and Zelenička River were collected in August 2018 at 18 sites (**Figure 1**). Both river water and sediment samples were taken at all sampling sites, excluding sampling site Ljuberađa (spring). At Ljuberađa (spring) sampling site, only water samples were taken. The goal was to examine the influence of main tributaries on potentially toxic elements (PTEs) content in the Vlasina River. Therefore, we chose the sampling sites of tributaries in the vicinity of the mouth and in the Vlasina River. A list of collected river water and sediment samples is shown in **Table 2**.

Water grab samples were collected at around 10 cm under the surface into the high-density polyethylene bottles. Samples were filtered through 0.2 μM nylon syringe filters, acidified with HNO_3 to a pH below 2 and stored at 4°C until analysis (Thuong et al., 2015).

Sediment samples were collected with a plastic spatula (Sakan et al., 2007; Patel et al., 2018; Đorđević et al., 2021). Plastic shovels were used to collect sediment samples from shallow waters (Kemble et al., 1994), as well as to avoid metal contamination (Patel et al., 2018). After sampling, the sediment was packed in polyethylene bottles and transported to the laboratory. In the process of preparation for analysis, stones and plant debris were removed from the samples, and the precipitate was homogenized by mixing the sample with a plastic spoon in the laboratory. In this paper, we decided to work with air-dried samples, which is also recommended in the literature (Arain et al., 2008; Jamali et al., 2009). Samples were air dried for 8 days before analysis (Arain et al., 2008; Jamali et al., 2009).

Chemical Analysis

Sediment samples were analyzed by the optimized BCR (Community Bureau of Reference) three-step sequential extraction procedure (Passos et al., 2010; Sutherland 2010; Sakan et al., 2016). This manuscript considered results for the total amounts of the extracted elements. The total amounts of elements are defined as the sum of the element contents in the three fractions plus the aqua-regia extractable content of the residue (Facchinelli et al., 2001; Sakan et al., 2007). This method results in concentrations normally referred to as "pseudo-total," "total extractable amount," or "sequentially extractable amount," as the silicates are not completely destroyed (Facchinelli et al., 2001).

Determination of Element Concentrations and Quality Control

Element concentrations in the water and extracts obtained at each of BCR extraction step were determined using techniques of Inductively Coupled Plasma—Optical Emission spectrometry (Thermo Scientific ICP-OES iCap 6500 Duo) and Inductively Coupled Plasma—Mass spectrometry (Thermo Scientific ICP-MS iCap Q). The analytical data quality was controlled by using laboratory quality assurance and quality control methods, including the use of standard operating procedures, calibration with standards, and analysis of both reagent blanks and replicates (Sakan et al., 2016). The blank solutions were prepared in the same

way as the samples during the extraction procedure. Sediment data in this study are reported on a dry weight mg kg^{-1} basis.

The quality of data was assessed by estimations of accuracy and precision. The accuracy and precision of the obtained results were checked by analyzing sediment reference material (BCR 701) for three-step sequential extraction. Acceptable accuracy (80–120%) and precision (≤20%) of metals was achieved for all steps of sequential extraction (**Supplementary Table S1**).

Determination of Magnetic Susceptibility

Magnetic susceptibility (MS) was measured using a magnetic susceptibility meter SM30. This is a small device, which is highly sensitive and therefore can measure sediments and rocks with an extremely low level of magnetic susceptibility. Also, it is very important to note that it can distinctly measure diamagnetic materials such as limestone, quartz, and even water. The sensitivity of the SM30 device is 1 SI × 10^{-7} SI units, which is about 10 times better than the sensitivity of the majority of other instruments. It operates on frequency of 8 kHz, measurement time is less than 5 s, operating temperature is −20–50 °C. It has an 8 kHz LC oscillator with a large size pick-up coil as a sensor. The frequency of oscillation is measured when the coil is put on the surface of the measured sample and when the coil is removed tens of cm away from the sample.

To assure as much precise data as possible, each sample was measured in triplicate and the mean value was taken as the final result of measurement.

Statistical Analysis

In this study, principal component analysis (PCA) and cluster analysis (CA) were applied. PCA is an advanced algorithm for exploration of data that can identify patterns in the data structure and discover a transformed representation of data that highlights these patterns. Cluster analysis (CA) is an unsupervised pattern recognition approach that groups data/objects into clusters based on their similarities or dissimilarities. Correlation, principal component, and cluster analysis were performed using IBM SPSS 21 software.

Contamination Assessment Methods

In this manuscript, the index of geoaccumulation (I_{geo}) has been applied to assess the metal pollution in the sediment samples. This determination equation was introduced by Müller (1979). The equation used for the calculation of I_{geo} was as follows: $I_{geo} = \log_2 (C_n/1.5 \cdot B_n)$, where C_n—the measured concentration of heavy metals in the studied sediment and B_n—the geochemical background value. In this manuscript, element contents in soil from the Vlasina region were used as background values. Soil samples were collected near the river Vlasina and its tributaries. The data for soil content near the watercourses of Vlasina watershed, which were used for the calculations in this study, is shown in Sakan et al. (2021). Background contents of elements were calculated for each element as the 75th percentiles of the frequency distribution of the data—soil content (Dos Santos and Alleoni, 2013). The I_{geo} is typically divided into seven grades: $I_{geo} < 0$: uncontaminated/unpolluted; $I_{geo} = (0–1)$: unpolluted/moderately; $I_{geo} = (1–2)$: moderately; $I_{geo} = (2–3)$: moderately/heavily; $I_{geo} = (3–4)$: heavily; $I_{geo} = (4–5)$: heavily/extremely and $I_{geo} > 5$: extremely. The factor 1.5 is the background matrix factor due to lithogenic effects (Haris et al., 2017).

RESULTS AND DISCUSSION

Concentration of Studied Elements in Water and Water Quality

The concentration values of 21 elements (Zn, Ni, Cu, Cr, Pb, Cd, Al, B, Ba, Be, Ca, Co, Fe, K, Mg, Mn, Na, Sr, Ti, V, and As) in the water of rivers in the Vlasina region and detection limits are shown in **Supplementary Table S2**, while basic statistical parameters are shown in **Table 3**. The content of Hg in water was under the detection limit on all sampling sites.

The relative abundance of major metals in studied river waters was Ca > Mg > Na > K (**Table 3**, **Supplementary Table S2**). Regarding trace elements, concentrations of Pb, Cd, Ti, and B in all water samples were below the detection limits, and the mean concentrations of other trace elements decreased in the order of Sr > Ba > Al > Fe > As > Zn > Cu > V > Ni > Mn > Cr > Be > Co (**Table 3**, **Supplementary Table S2**).

The spatial distribution of elements regarding studied rivers is presented on maps produced by ArcGIS (**Supplementary Figures S1–S3**). Spatial variability was generally not very pronounced, although, similar spatial concentration patterns can be noticed for Ca, Mg, Sr and As with higher concentrations in Ljuberađa River and Tegošnička River, for K and V with higher concentrations in Tegošnička River, Ljuberađa River and in the most downriver samples of Vlasina River, for Fe, Mn, Cr with higher concentrations in the most downriver samples of Vlasina River, and for Ni and Cu with higher concentrations in Gradska River, Tegošnička River, Vlasina (after receiving Ljuberađa) and in the most downriver samples of Vlasina River (**Supplementary Figures S1–S3**; **Supplementary Table S2**).

Element concentrations in river water samples were compared with surface and drinking water quality standards and the results of other river water quality studies, as presented in **Tables 3**, **4**. The concentrations of all measured regulated elements (Zn, Ni, Cu, Cr, Pb, Cd, Al, B, Ba, Be, Ca, Fe, K, Mg, Mn, Na, and As) in the investigated rivers of the Vlasina region were below recommended and prescribed limit values (**Table 4**).

Compared to less polluted rivers and rivers polluted by industrial discharges and mining activities in Serbia and the world (**Table 3**), element concentrations in this study were lower than those found in other studies.

Content of Studied Elements in Sediment and Comparison With Similar Results and Sediment Standards for Risk Elements

The content of 23 examined elements (Zn, Ni, Cu, Cr, Pb, Cd, Al, B, Ba, Be, Ca, Co, Fe, K, Mg, Mn, Na, Sr, Ti, V, As, Cd, Li) in sediments is shown in Supplementary Table 3 and **Figure 2**, while the mean, median, SD, minimum and maximum values of elements in the examined sediments are presented in **Table 5**. The content of Hg in river sediments was below the detection

TABLE 3 | Descriptive statistics for studied elements (μg/L) and comparison with other rivers.

	This study				Low polluted	Low polluted	Polluted by industrial wastes, coal combustion	Polluted by mining activities
	Min	Max	Average	SD	Velika Morava, Serbia Dević et al. (2016)	Karasu River,Turkey Varol et al. (2021)	Huaihe River, China Wang et al. (2017)	Tinto River, Spain Olías et al. (2020)
Zn	<DL[a]	6.4	0.81	1.83	45.15	25.4	10,504.1	45,000
Ni	0.028	0.486	0.281	0.142	4	5.7	46.19	218
Cu	<DL	1.05	0.420	0.335	18.17	2.6	52.32	29,000
Cr	0.021	0.194	0.091	0.053	1.2	1.7	23.08	42
Cd	<DL	<DL	/	/	0.05	1.18	61.74	144
Pb	<DL	<DL	/	/	0.37	0.9	154.96	166
Al	<DL	11.92	2.35	3.14		68	552.86	166,000
B	<DL	<DL	/	/				
Ba	4.13	19.02	9.62	3.85			132.46	15
Be	<DL	0.15	0.09	0.04				
Ca	3,918	46,650	27,650	14,221				63,000
Co	<DL	0.036	0.016	0.010				890
Fe	<DL	10.91	2.2	3.31		75	440.65	377,000
K	<DL	912	401	377				1,600
Mg	865	7,634	4,739	1734			12.03	178,000
Mn	<DL	0.574	0.143	0.153		9.7	49.02	16,000
Na	1831	577	3,301	1,031				34,000
Sr	32.3	190.3	98.4	56.4				
Ti	<DL	<DL	/	/				
V	0.106	0.568	0.391	0.124				
As	0.236	7.13	1.31	1.71	5.88	2.2		374

[a]*DL, detection limit (values are shown in* ***Supplementary Table S2****).*

TABLE 4 | Comparison of water quality in the present study with water quality standards.

	This study	Fresh water		Drinking water			
		European Commission (2013); Government of Republic of Serbia (2014)		Government of Republic of Serbia (2019)	WHO (2017)	European Commission (2020)	USEPA (2022)
		MAC[a]	AA[b]	MAC[a]	GV[c]	PV[d]	MAC[a]
Zn (μg/L)	<DL—6.40			3,000	3,000		
Ni (μg/L)	0.028—0.486	34	4	20	70	20	
Cu (μg/L)	<DL—1.05			2000	2000	2000	1,300
Cr (μg/L)	0.021—0.194			50	50	50	100
Cd (μg/L)	<DL	<0.45 (H < 40)[e] 0.45 (H = 40-50) 0.6 (H = 50-100) 0.9 (H = 100-200) 1.5 (H ≥ 200)	<0.08 (H < 40)[e] 0.08 (H = 40-50) 0.09 (H = 50-100) 0.15 (H = 100-200) 0.25 (H ≥ 200)	3	3	5	5
Pb (μg/L)	<DL	14	1.2	10	10	10	15
Al (μg/L)	<DL—11.92			200		200	
B (μg/L)	<DL			1,000	2,400	1,500	
Ba (μg/L)	4.13—19.02			700	1,300		2000
Be (μg/L)	<DL—0.15				10		4
Ca (mg/L)	3.92—46.6			200			
Fe (μg/L)	<DL—10.91			300		200	
K (mg/L)	<DL—0.912			12			
Mg (mg/L)	0.865—7.63			50			
Mn (μg/L)	<DL—0.574			50		50	
Na (mg/L)	1.83—5.48			200		200	
As (μg/L)	0.236—7.13			10	10	10	10

[a]*MAC, maximum allowable concentration.*
[b]*AA, annual average.*
[c]*GV, guideline value.*
[d]*PV, parametric value.*
[e]*H—water hardness (mg/L* $CaCO_3$*).*

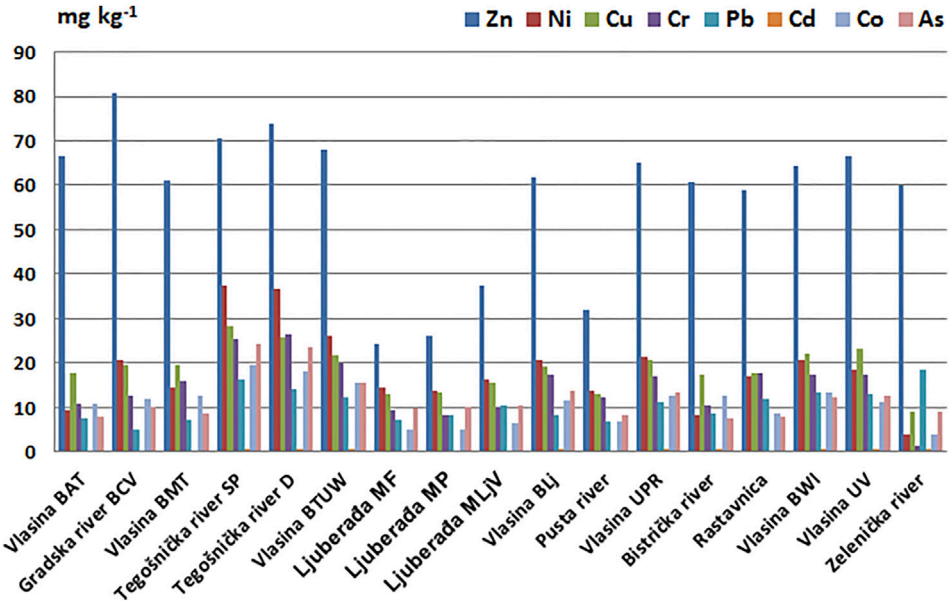

FIGURE 2 | Content of studied elements (Zn, Ni, Cu, Cr, Pb, Cd, Co, and As) in sediment.

limit in all samples. The spatial distribution of studied elements for sediment is presented in **Supplementary Figures S1–S4**. Geochemical maps of the trace metals were created using ArcGIS. No significant spatial variability of potentially toxic elements in sediments was observed. The results of microelement content in studied river sediments decreased in the following order: Al > Mn > Ti > Zn > Ba > V > Cu > Ni > Cr > Li > As > Sr > Co > Pb > B > Be > Cd. The results of the mean content of macroelements in sediment were in order: Ca > Fe > Mg > Si > K > Na.

The total content of the studied elements, extracted from the sediments at the examined site, was compared with the limit and remediation values prescribed by the "Regulation on limit values for pollutants in surface and ground waters and sediments and the deadlines for their achievement" (Regulation—Government of the Republic of Serbia, 2012) for the preliminary risk assessment. In addition, the obtained results were also compared with sediment quality guidelines (SQGs) of the numerical indices: threshold effect concentration (TEC) and probable effect concentration (PEC). The TEC represents the concentration below which harmful effects are unlikely to be observed, and the PEC indicates the concentration above which harmful effects are likely to be observed. These values were used to assess the potential hazard to organisms with regard to the content of trace elements in the sediments using MacDonald et al. (2000). We also compared our results with the values for element concentrations in the continental crust (Wedepohl, 1995) and with similar results for river sediments in Serbia and the world.

The results of the comparison of toxic elements' total extracted content with similar results for river sediments in Serbia and the world indicate that the contents of Zn, Ni, Cu, Cr, Pb, Cd, and As are much lower compared to the results from China, Serbia, and Dravinja (Slovenia). It was noticed that the contents of Cd and As in the sediments of Vlasina are similar to those in Dravinja. Mean values for As and maximum values for Ni are higher than TEC but lower than PEL values. The sediment samples with element concentrations between TEC and PEC values are potentially non-toxic, but the frequency of their toxicity occurrence is higher than for TEC values and yet lower than for PEC (MacDonald et al., 2000). The contents of Cd and As are higher than the average crust value; Cr and Ni are lower; while the contents of Zn, Cu, and Pb were similar to the crust contents. The Cr and Ni contents are lower than the crust values because the applied extraction agents do not completely destruct the silicates since hydrofluoric acid was not used. The slightly higher content of Cd and As in some sediments indicates the possible existence of additional sources of these elements in relation to geochemical processes in nature. Comparison of the contents of other examined elements (**Table 5**) with crust values indicates that the contents of Al, B, Ba, Be, Co, Fe, K, Li, and Na are mostly similar or slightly lower than the crust values, which is most likely due to incomplete destruction of silicates, while at some localities an increased content of Ca and Mg was observed, which indicates an increased content of carbonates in the examined localities.

The obtained results indicate that the contents of regulated toxic and potentially toxic elements in sediment samples are lower than the maximum allowable concentrations (Regulation—Government of the Republic of Serbia, 2012).

Correlation Analysis—Water

A correlation analysis was performed in order to examine the relationships between elements (**Supplementary Table S4**). At significance level 0.01, correlations were found between all major metals (Ca, K, Mg, Na), all major metals and V, and Ca and Sr with As. Regarding trace elements, correlations at significance level 0.01 were found for Ba-Ni and Ni-Cu. At significance level

TABLE 5 | Descriptive statistics for total element content (mg kg^{-1}) in sediment.

	Mean[a]	Median[a]	SD[a]	Min[a]	Max[a]	X[b]	Y[c]	Z[d]	P[e]	R[f]	P[g]	M[h]	R[i]	C[j]
Zn	57.5	61.6	16.9	24.1	80.6	257.2	125.2	342.5	135	121	459	430	720	65
Ni	18.4	16.8	19.2	3.93	37.4	36.29	36.0	83.19	34	22.7	48.6	44	210	56
Cu	18.6	19.2	4.95	9.10	28.4	71.29	49.9	78.02	39	31.6	149	110	190	25
Cr	14.7	15.8	6.28	1.44	26.4	59.7	103.9	53.62	91	43.4	111	240	380	126
Pb	10.5	10.3	3.62	5.14	18.4	102.5	213.8	67.67	35	35.8	128	310	530	14.8
Cd	0.44	0.43	0.08	0.32	0.60	23.31	0.70	2.43	0.403	0.99	4.98	6.4	12	0.1
As	12.1	10.2	5.03	7.49	24.2	98.38	17.88	19.0	11	9.79	33	42	55	1.7
Al	7,550	7,902	2,215	4,334	11,552	nd[#]	nd	nd	nd	nd	nd	nd	nd	79,600
B	0.75	0.47	0.61	0.21	2.48	nd	nd	nd	nd	nd	nd	nd	nd	11
Ba	34.9	33.1	9.98	22.6	57.6	nd	nd	nd	449	nd	nd	nd	nd	584
Be	0.54	0.54	0.10	0.31	0.76	nd	nd	1.36	nd	nd	nd	nd	nd	2.4
Ca	232,225	113,971	287,783	8,192	853,656	nd	nd	39,806	nd	nd	nd	nd	nd	38,500
Co	10.9	11.6	4.55	3.89	19.7	16.97	17.4	18.40	nd	nd	nd	nd	nd	24
Fe	30,009	33,375	9,991	14,381	43,302	nd	44,800	40,281	nd	nd	nd	nd	nd	43,200
K	633	636	120	329	902	nd	nd	nd	nd	nd	nd	nd	nd	21,400
Li	13.7	12.8	5.61	4.96	26.1	nd	nd	nd	nd	nd	nd	nd	nd	18
Mg	7,276	6,995	3,954	2,592	15,576	nd	nd	nd	nd	nd	nd	nd	nd	22,000
Mn	535	588	225	155	838	nd	2,500	1,113	nd	nd	nd	nd	nd	716
Na	55.8	52.7	25.0	28.0	101	nd	nd	nd	nd	nd	nd	nd	nd	23,600
Si	907	892	244	449	1,517	nd	nd	nd	nd	nd	nd	nd	nd	28,800
Sr	11.0	9.73	7.04	2.74	29.1	nd	nd	nd	nd	nd	nd	nd	nd	333
Ti	384	455	253	58.8	809	nd	9,300	nd	nd	nd	nd	nd	nd	4,010
V	25.3	28.8	9.21	11.8	37.4	nd	nd	87.34	91	nd	nd	nd	nd	98

*In percent.
#nd means—no data.
[a]This study.
[b]Zhuzhou Reach-Tunca river sediment, South China, mean values (Huang et al., 2020).
[c]Anning river sediment, SW china, mean values, Wang et al. (2018).
[d]River sediment—Serbia—mean values (Sakan et al., 2011; Sakan et al., 2017).
[e]Dravinja river, Eastern Slovenia, mean values (Mezga et al., 2021).
[f]TEC (threshold effect concentration)—MacDonald et al. (2000).
[g]PEL (probable effect concentration)—MacDonald et al. (2000).
[h]MAV, maximum allowable value (Government of Republic of Serbia, 2012).
[i]RV, remediation value (Government of Republic of Serbia, 2012).
[j]Element concentrations in the Continental Crust—K.H. Wedepohl, (1995).

0.05, correlations were found for the following pairs of trace elements: Ba-K, Ba-Cr, Ba-Mn, Cr-Mn, Cr-Ni, Mn-Ni, Ni-As (negative), Cu-As (negative).

Correlation Analysis—Sediment

The results of correlation analysis for the studied elements extracted from sediment are presented in **Supplementary Table S5**. The existence of positive correlations between most of the examined elements can be noticed, which may indicate their dominant geochemical origin. Of all the toxic elements, Pb stands out significantly, being the only one that is positively correlated with Cd, As, and Ba. Calcium is negatively correlated with elements that represent silicates (Al, Ti) and oxides (Fe, Mn), which is a consequence of the fact that they are competitive substrates. The existence of carbonate rocks has been shown in the studied area. Many elements show significant correlations with Mg, Li, Al, and Ti, but not with K. This could be an indication of magmatic rock presence in the studied area. According to elemental correlations, the most probable explanation is that present magmatic rocks are mostly acidic rocks, with prevailing albite and anorthite content, while sanidine $(K,Na)Si_3O_8$, orthoclase KSi_3O_8, and microcline KSi_3O_8 are most probably not present, or at least not in higher quantities. The highly positive correlation of Fe and Mn with trace elements indicates that Fe and Mn oxides/hydroxides play an important role in controlling the behavior of trace element pollution in sediments. Many authors have suggested that metals are efficiently adsorbed and co-precipitated with iron and manganese oxides/hydroxides (Al-Mur et al., 2017; Baran et al., 2019). All studied potentially toxic elements, except lead, were positively correlated with aluminum. The positive correlations of Al and Fe with PTEs in sediments indicate that these elements originate from lithogenic sources (Lima et al., 2022).

Correlation Analysis Between Mass Spectrometry and Studied Element Content in Sediment

The correlations between magnetic susceptibility (MS) and 23 studied elements in Vlasina sediments are presented in **Table 6**. As it can be seen, 10 elements show positive correlations while 13 elements show negative correlations with MS. None of the elements show very high correlation, which might be supported by our finding that Vlasina sediments are not under significant anthropogenic influence. That is, contrary to cases

TABLE 6 | Vlasina sediments—correlations between MS and studied elements.

	Zn	Ni	Cu	Cr	Pb	Al	B	Ba	Be	Ca	Co
MS	0.17	–0.20	0.12	–0.05	0.17	0.05	–0.21	0.13	–0.03	–0.27	0.07
	Fe	**K**	**Li**	**Mg**	**Mn**	**Na**	**Si**	**Sr**	**Ti**	**V**	**As**
MS	0.07	–0.01	–0.28	–0.19	0.10	–0.31	–0.22	–0.28	0.20	0.21	–0.25

**Marked correlations are significant at* p < *.05000.*

TABLE 7 | Varimax rotated component matrix for selected trace elements in the studied river water.

	Component	
	1	**2**
V	0.082	**0.883**
Cr	**0.795**	0.009
Mn	**0.810**	0.278
Ni	**0.840**	–0.166
Cu	**0.721**	–0.342
As	**–0.581**	**0.573**
Eigenvalues	2.86	1.33
% of variance	47.61	22.16
Cumulative %	47.61	69.78

Extraction method: Principal component analysis. Rotation method: Varimax with Kaiser normalization. Bold values represent significant loadings.

where significant anthropogenic influence was observed, like in the Kupa River drainage basin (Croatia), where very high positive correlations of MS with some elements exist (Frančišković-Bilinski et al., i2014, 2017; Sakan et al., 2020).

In Vlasina sediments highest positive correlations of MS are with V, Ti, Pb, Zn and a bit weaker correlations with Ba and Cu. Other elements have much weaker correlations with MS than these. It is known that reaction of V with cations of heavy metals, such as copper, lead, uranium, and zinc, forms epigenetic vanadate minerals in the oxidized zones of base-metal deposits (Kelley et al., 2017), so it could be assumed that this could be the natural source of these elements in the Vlasina region. Also, it is known that some altered titanium-rich syenite (igneous rock similar to granite) intrusions might contain high concentrations of vanadium, so this could explain MS correlations with V and Ti.

Principal Component Analysis—Water

Trace elements containing up to 10% of values below the detection limit (Ni, Cu, Cr, Mn, V, As) were included in PCA. The Kaiser–Meyer–Olkin (KMO) and the Bartlett sphericity tests were performed to examine the validity of PCA. The KMO value was 0.779 and the significant level of the Bartlett sphericity test was 0.02. In this study, as a result of PCA, initially 6 components were extracted. According to the Kaiser criterion, the first two components with initial eigenvalues larger than 1 were retained and subjected to varimax rotation. The results of PCA are shown in **Table 7** and **Figure 3A**. Two components explained 69.78% of the total variance of the original data set (**Table 7**).

Component 1, which explained 47.61% of the total variance, had high positive loadings for Cr, Mn, Ni, and Cu, and moderate negative loadings for As (**Table 7**). As it can be noticed in **Supplementary Table S4**, significant positive correlations were found for Ni and Cu (r = 0.634, $p < 0.01$), Cr and Mn (r = 0.587, $p < 0.05$), Cr and Ni (r = 0.549, $p < 0.05$), and Mn and Ni (r = 0.559, $p < 0.05$). Also, As showed significant negative correlations with Cu (r = - 0.531, $p < 0.05$) and Ni (r = - 0.496, $p < 0.05$). Component 2 accounted for 22.16% of the total variance and had a high positive loading for V and a moderate positive loading for As.

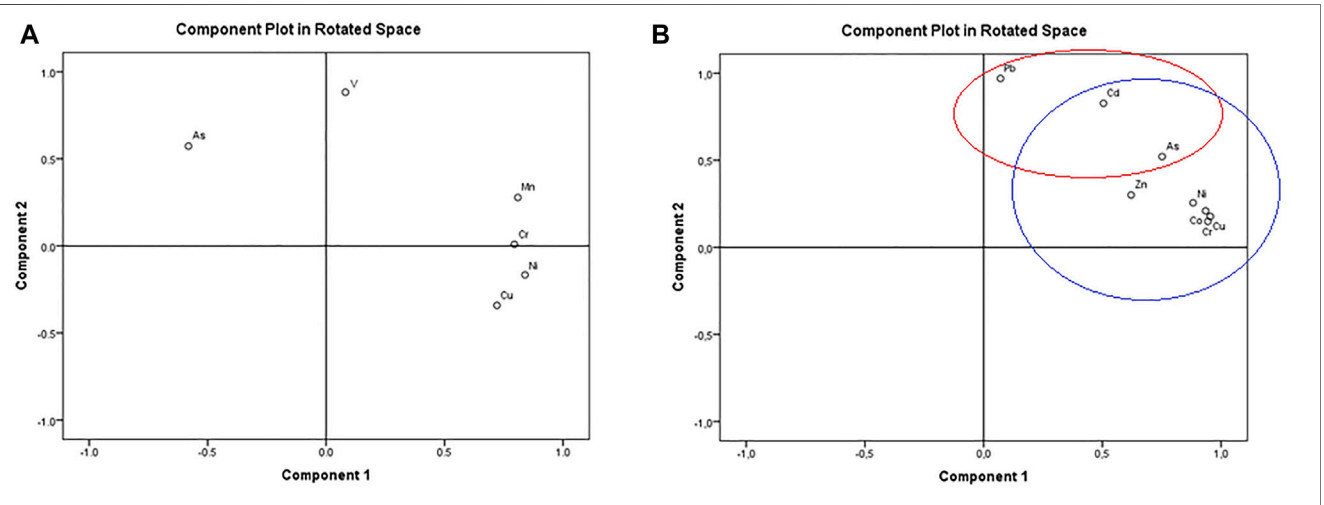

FIGURE 3 | PCA (R mode) for trace elements in water **(A)** and sediment **(B)**.

TABLE 8 | Varimax rotated component matrix for selected trace elements in the studied sediments.

	Component	
	1	2
Zn	**0.621**	0.301
Ni	**0.882**	0.256
Cu	**0.955**	0.178
Cr	**0.945**	0.149
Pb	0.071	**0.970**
Cd	**0.505**	**0.827**
Co	**0.935**	0.210
As	**0.752**	**0.521**
Eigenvalues	5.604	1.215
% of variance	70.049	15.183
Cumulative %	70.049	85.232

Extraction method: Principal component analysis. Rotation method: Varimax with Kaiser normalization. Bold values represent significant loadings.

The results of PCA suggest that different processes/sources contribute to concentrations of Cr, Mn, Ni, Cu, and also to concentrations of As and V in the studied waters.

Principal Component Analysis—Sediment

Principal component analysis showed that two principal components with an eigenvalue > 1 exist (**Figure 3B**; **Table 8**). Component 1 accounts for 70.049% of the variation and includes Ni, Zn, Cu, Cr, Cd, Co, and As. The obtained results suggested that these elements had a dominant geological source. Therefore, they may have been derived from natural processes such as soil erosion and rock weathering. This hypothesis is also supported by previous studies (Huang et al., 2020; Sakan et al., 2021). In Huang et al. (2020), it is shown that Cr, Ni, and Co may have derived from natural processes such as soil erosion and rock weathering. In Sakan et al. (2021), it is shown that the binding sites of microelements such as Co, Ni, Cr, and Cu in soils from the Vlasina region could be shales, as well as ultrabasites-basites and serpentinites. Erosive processes of various intensities affect most of the Vlasina River basin. The watercourses in the Vlasina basin are almost all torrents, and Tegošnica is among them. As a consequence of erosive processes and torrents, the soil is destroyed, which reduces its fertility and a huge amount of water is lost due to its sudden runoff.

Component 2 accounts for 15,183% of the variation and includes Pb, Cd, and As. The results show that the origin of lead is completely different in relation to the origin of Ni, Zn, Cu, Cr, and Co, while As and Cd are related to both components. It is possible to conclude that the content of Pb is mainly affected by human activities. Given that Cd and As are associated with both components, it is possible to assume that, in addition to the natural sources, anthropogenic sources of these elements are also important. Arsenic and cadmium are widely found in the environment (Perera et al., 2016). It can be found in the literature that use of agricultural chemicals has been indicated as the main anthropogenic source of As and Cd pollution in aquatic environments (Perera et al., 2016). Mickovski Stefanović (2012) showed that the sources of cadmium in the soil are mineral fertilizers, while lead and arsenic in general are derived from lead-arsenate ($PbAsO_4$), which is used in orchards to control insects.

Cluster Analysis—Water

In the present study, hierarchical cluster analysis in the Q-mode (classification of sampling sites) was performed.

The results of cluster analysis (CA) are presented in a dendrogram in **Figure 4**. Samples were divided into three main groups–clusters which mostly differed in concentrations of As and Cu. Cluster 1 included samples of Tegošnička River, Ljuberađa River, samples of the Vlasina River downstream of each of these rivers and downstream of the Pusta River, and the Bistrička River. The majority of water samples in cluster 1 were characterized by higher concentrations of As than samples in cluster 2, and most of the samples had lower concentrations of Cu. Cluster 2 contained samples of the Vlasina River upstream of the confluence with the Tegošnička River, Gradska River, Pusta River, Rastavnica River, and the most downstream samples of the Vlasina River. These river water samples mainly had higher concentrations of Cu and lower concentrations of As, compared to samples in cluster 1. Cluster 3 comprised one sample, the Zelenička River, the only studied river that is not a tributary of the Vlasina River. With the exception of Ni, the Zelenička River is characterized by lower concentrations of trace elements.

Cluster Analysis—Sediment

A cluster analysis (CA) was performed to classify sampling sites in the Vlasina River watershed. All the sites were divided into three groups (**Figure 5**): group (1) includes all samples of Vlasina (UPR, BWI, UV, BTUW; BLj, BMT, and BAT), Rastavnica, Gradska River and Bistrička River; group (2) consists of the two subclusters: (2a) Tegošnička and Pusta River, and (2b) all three samples of Ljuberađa and group (3) includes one site, Zelenička River.

Group (1): In the samples that make up this group, i.e., cluster 1, no increased content of studied toxic elements was found. Considering that this group consists of all sediment samples from the Vlasina River and its three tributaries (Rastavnica, Gradska Reka, and Bistrička Reka), we can assume that the examined river sediments forming the first cluster have a similar geochemical composition and are not significantly exposed to anthropogenic pollution.

Group (2): in the samples of the Tegošnička River, an increased content of Zn, Ni, Cu, Cr, Pb, Cd, Co, As and Fe was observed in relation to other sediments, while an increased content of Fe was also observed in the Pusta River. An increased content of calcium was observed in the samples of Ljuberađa, which may be the reason for the separation of these samples from the others. In Perović (2019), it was shown that within the cracked and karstified limestones in the area of eastern Serbia, there are significant accumulations of groundwater, which are discharged through karst springs withvariable yield, and one of those springs is Ljuberađa. No increased content of other elements was noticed in the sediment samples from Ljuberađa. At the Tegošnička River site, one sample was taken near the quarry, which explains the grouping of these samples with Ljuberađa samples within the

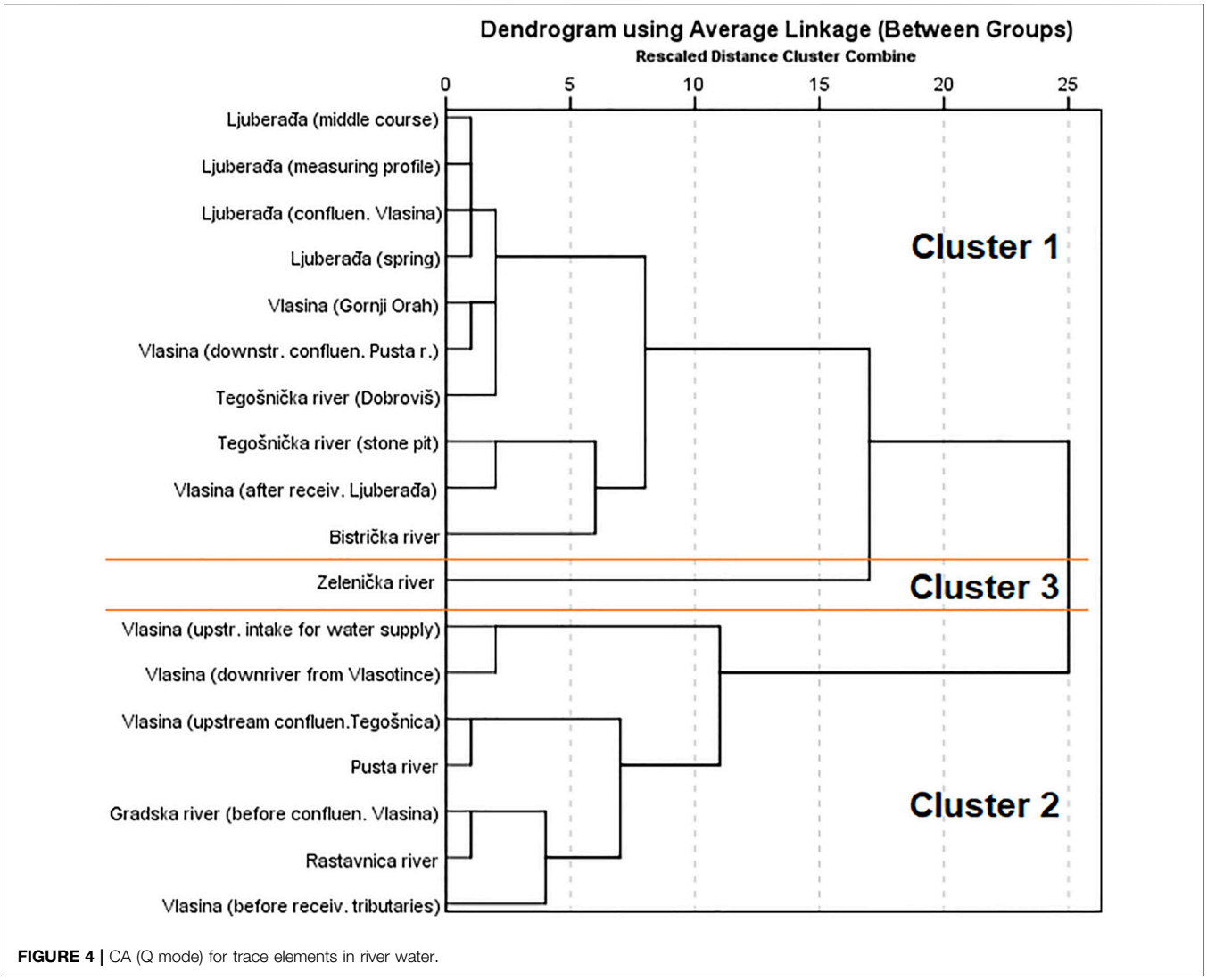

FIGURE 4 | CA (Q mode) for trace elements in river water.

same cluster. The increased content of calcium that represents carbonates in certain sediments can be explained by the existence of tertiary clastic sediments and mesozoic carbonate rocks in the river basins, as shown in Durlević et al. (2019).

Group (3) is characterized by low concentrations of Ni, Cu, Cr, Co, and Fe, suggesting that most elements in sediments from the Zelenička River had a geological origin. The separation of this river into a special group indicates that this river differs significantly from Vlasina and other rivers in its basin in terms of geological and chemical composition.

Index of Geoaccumulation

The calculated I_{geo} values for Zn, Ni, Cu, Cr, Pb, Cd, and As are shown in **Figure 6**. The majority of investigated sediments were in class 0 (background concentration) with the exception of samples from the Tegošnička River (one sample is near the stone pit and the other sample is near the village Dobroviš) for As and Ni, which were in class 1 (unpolluted to moderately polluted). It has been shown in the literature (Smedley and Kinniburgh, 2001) that most common silicate minerals contain around 1 mg kg^{-1} or less As and carbonate minerals usually contain less than 10 mg kg^{-1}. Since arsenic may be sorbed to the edges of clays and on the surface of calcite (Goldberg and Glaubig, 1988), higher mobility of arsenic can be expected in areas with high carbonate content. For nickel, process of adsorption on the calcite surface (Zachara et al., 1991) and coprecipitation with calcite (Alvarez 2019) was already described in literature. Lakshtanov and Stipp, (2007) reported that interaction of calcite with Ni controls its distribution in calcareous environments. Increased carbonate content in the Tegošnička River is expected given the nearby stone pit. In general, the values obtained for I_{geo} indicate that the sediments in the Vlasina region were uncontaminated regarding the studied elements. Negative I_{geo} values for most soils indicated that there was no contamination. Therefore, the origin of elements is mostly from natural processes such as soil and rock weathering.

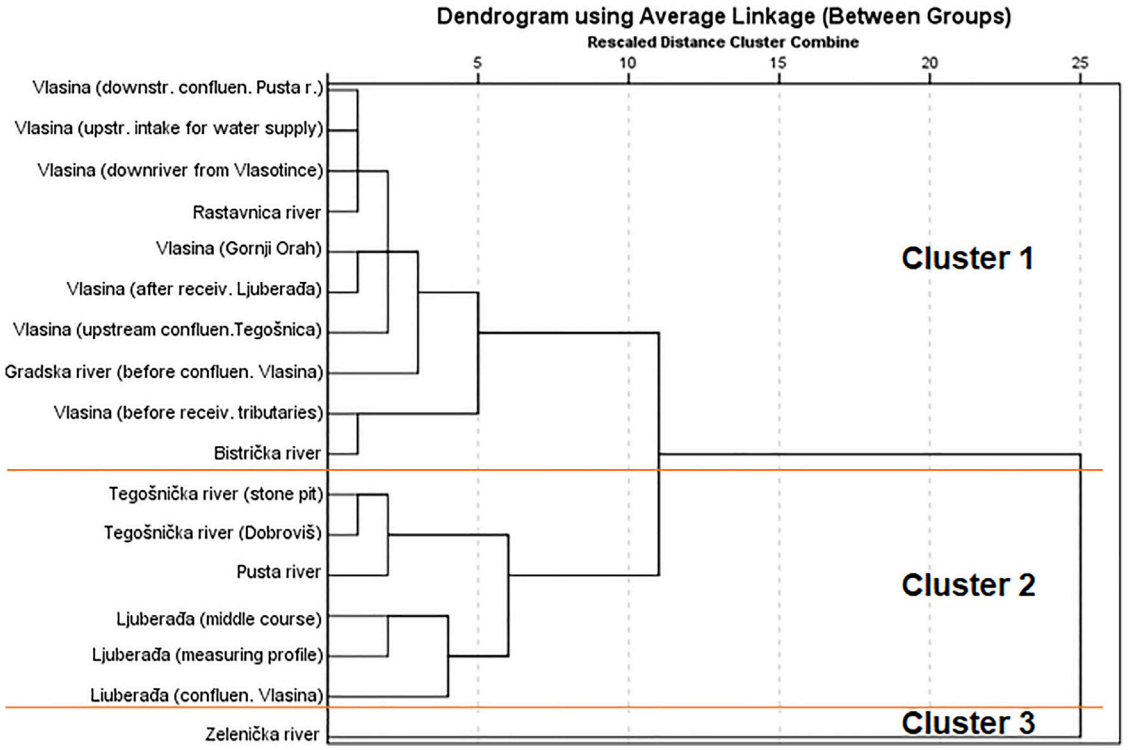

FIGURE 5 | CA (Q mode) for trace elements in river sediment.

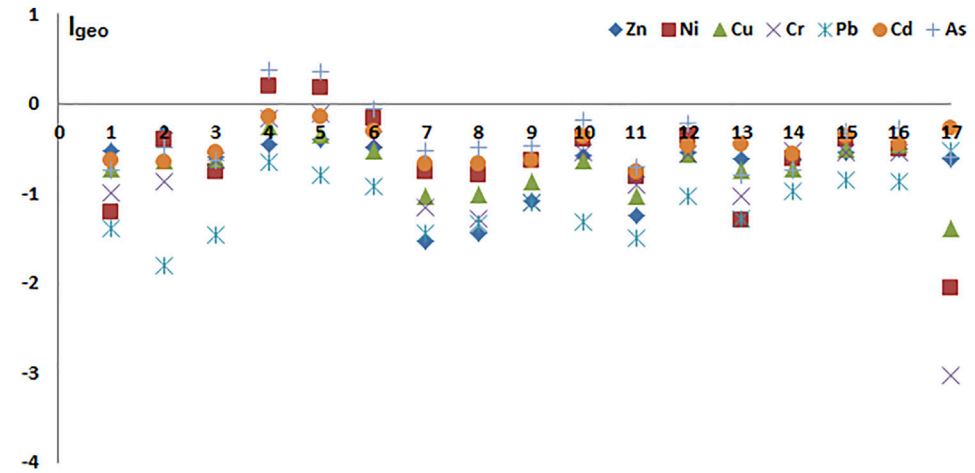

FIGURE 6 | Distribution of studied elements enrichment based on I_{geo} in sediment: **1**—Vlasina (before receiving any tributary); **2**—Gradska river (before its confluence with Vlasina); **3**—Vlasina (upstream of the confluence with Tegošnička river); **4**—Tegošnička river (stone pit); **5**—Tegošnička river (near village Dobroviš); **6**—Vlasina (downstream of the confluence with Tegošnička river, near village Gornji Orah); **7**—Ljuberađa (middle course); **8**—Ljuberađa (measuring profile); **9**—Ljuberađa, (confluence with Vlasina); **10**—Vlasina (after receiving Ljuberađa); **11**—Pusta river; **12**—Vlasina (downstream of the confluence with Pusta river); **13**—Bistrička river); **14**—Rastavnica river; **15**—Vlasina (upstream of the intake for water supply); **16**—Vlasina (downriver from Vlasotince); **17**—Zelenička river.

CONCLUSION

In this study, the water and sediments of rivers in the Vlasina region were analyzed to assess the current state of pollution with toxic elements. No significant spatial variability of potentially toxic elements in water and sediments was observed.

The concentrations of all measured regulated elements in the investigated rivers of the Vlasina region were below

recommended and prescribed limit values. Differences in the distribution of some elements in water and sediment are a consequence of the fact that the water samples constitute a snapshot of chemicals in the water, while surface sediments retain longer-term records.

The existence of positive correlations between most of the examined elements in sediments may indicate their dominant geochemical origin. The positive correlations of Al and Fe with PTEs in sediments indicate that these elements originate from lithogenic sources. The obtained results showed the great importance of carbonates for the mobility and binding of As and Ni in environments with increased calcium and magnesium content.

The results of PCA suggest that different processes/sources contribute to concentrations of Cr, Mn, Ni, Cu, and also to concentrations of As and V in the studied waters. Based on the obtained PCA results for sediments, it is possible to conclude that Ni, Zn, Cu, Cr, Cd, Co, and As had a dominant geological source, and the origin of lead is completely different in relation to the other elements. Since As and Cd are related to both components, it can be assumed that, in addition to natural, anthropogenic sources of these elements are also important.

In general, the values obtained for I_{geo} indicate that the sediments in the Vlasina region were uncontaminated regarding the studied elements. Negative I_{geo} values for most sediments indicated that there was no contamination. The results of magnetic susceptibility support our finding that Vlasina sediments are not under significant anthropogenic influence.

The obtained results confirmed the assumption that the Vlasina is one of the cleanest rivers in Serbia, as well as its tributaries. In view of this, as well as the major problems that exist with the pollution of river flows, all necessary measures should be taken to protect this river, as well as to continue monitoring the status of pollution in these river systems.

The combination of chemometric approaches and pollution indices is useful for assessment of the pollution status of toxic elements, but magnetic susceptibility measurement is better for more polluted areas.

DATA AVAILABILITY STATEMENT

The original contributions presented in the study are included in the article/**Supplementary Material**; further inquiries can be directed to the corresponding author.

AUTHOR CONTRIBUTIONS

All the authors listed have made a substantial, direct, and intellectual contribution to the work and approved it for publication.

FUNDING

The authors would like to thank the Ministry of Education, Science and Technological Development of the Republic of Serbia (Grant No: 451-03-68/2022-14/200026) for financial support.

SUPPLEMENTARY MATERIAL

The Supplementary Material for this article can be found online at: https://www.frontiersin.org/articles/10.3389/fenvs.2022.909858/full#supplementary-material

REFERENCES

Al-Mur, B. A., Quicksall, A. N., and Al-Ansari, A. M. A. (2017). Spatial and Temporal Distribution of Heavy Metals in Coastal Core Sediments from the Red Sea, Saudi Arabia. *Oceanologia* 59 (3), 262–270. doi:10.1016/j.oceano.2017.03.003

Alvarez, M. C. C. (2019). *Nickel Isotope Fractionation during Adsorption on the Calcite Surface and Coprecipitation with Calcite. Mineralogy*. [dissertation thesis]. Toulouse: Université Paul Sabatier. [Toulouse III], English. NNT : 2019TOU30047.

Arain, M. B., Kazi, T. G., Jamali, M. K., Jalbani, N., Afridi, H. I., and Baig, J. A. (2008). Speciation of Heavy Metals in Sediment by Conventional, Ultrasound and Microwave Assisted Single Extraction Methods: A Comparison with Modified Sequential Extraction Procedure. *J. Hazard. Mater.* 154, 998–1006. doi:10.1016/j.jhazmat.2007.11.004

Baran, A., Tarnawski, M., Koniarz, T., and Szara, M. (2019). Content of Nutrients, Trace Elements, and Ecotoxicity of Sediment Cores from Rożnów Reservoir (Southern Poland). *Environ. Geochem. Health* 41, 2929–2948. doi:10.1007/s10653-019-00363-x

Carrillo, K. C., Drouet, J. C., Rodríguez-Romero, A., Tovar-Sánchez, A., Ruiz-Gutiérrez, G., and Viguri Fuente, J. R. (2021). Spatial Distribution and Level of Contamination of Potentially Toxic Elements in Sediments and Soils of a Biological Reserve Wetland, Northern Amazon Region of Ecuador. *J. Environ. Manag.* 289, 112495. doi:10.1016/j.jenvman.2021.112495

Čvoro, J., and Golubović, P. (2001). *Geography of Yugoslavia*. Niš: University of Niš, Faculty of Science.

Dević, G., Sakan, S., and Đorđević, D. (2016). Assessment of the Environmental Significance of Nutrients and Heavy Metal Pollution in the River Network of Serbia. *Environ. Sci. Pollut. Res.* 23, 282–297. doi:10.1007/s11356-015-5808-5

Đorđević, D., Sakan, S., Trifunović, S., Škrivanj, S., and Finger, D. (2021). Element Content in Volcano Ash, Soil and River Sediments of the Watershed in the Volcanic Area of South Iceland and Assessment of Their Mobility Potential. *Water* 13, 1928. doi:10.3390/w13141928

Dos Santos, S. N., and Alleoni, L. R. F. (2013). Reference Values for Heavy Metals in Soils of the Brazilian Agricultural Frontier in Southwestern Amazônia. *Environ. Monit. Assess.* 185, 5737–5748. doi:10.1007/s10661-012-2980-7

Durlevic, U., Momcilovic, A., Curic, V., and Dragojevic, M. (2019). Gis Application in Analysis of Erosion Intensity in the Vlasina River Basin. *B Serbian Geogr.* 99 (2), 17–36. doi:10.2298/gsgd1902017d

European Commission (2013). Directive 2013/39/EU of the European Parliament and of the Council of 12 August 2013 Amending Directives 2000/60/EC and 2008/105/EC as Regards Priority Substances in the Field of Water Policy. *Off. J. Eur. Union* L226, 1–17.

European Commission (2020). Directive (EU) 2020/2184 of the European Parliament and of the Council of 16 December 2020 on the Quality of Water Intended for Human Consumption. *Off. J. Eur. Union, L* 435, 1–62.

Facchinelli, A., Sacchi, E., and Mallen, L. (2001). Multivariate Statistical and GIS-Based Approach to Identify Heavy Metal Sources in Soils. *Environ. Pollut.* 114, 313–324. doi:10.1016/s0269-7491(00)00243-8

Frančišković-Bilinski, S., Bilinski, H., Scholger, R., Tomašić, N., and Maldini, K. (2014). Magnetic Spherules in Sediments of the Karstic Dobra River (Croatia). *J. Soils Sediments* 14, 600–614. doi:10.1007/s11368-013-0808-x

Frančišković-Bilinski, S., Bilinski, H., Maldini, K., Milović, S., Zhang, Q., and Appel, E. (2017). Chemical and Magnetic Tracing of Coal Slag Pollutants in Karstic River Sediments. *Environ. Earth Sci.* 76, 476. doi:10.1007/s12665-017-6792-5

GLP (2012). *General Regulation Plan for the Settlement of Vlasina Stojkovićeva*. Surdulica: Municipal Administration of the Municipality of Surdulica.

Goldberg, S., and Glaubig, R. A. (1988). Anion Sorption on a Calcareous, Montmorillonitic Soil-Arsenic. *Soil Sci. Soc. Am. J.* 52, 1297–1300. doi:10.2136/sssaj1988.03615995005200050015x

Government of Republic of Serbia (2012). Regulation on Limit Values for Pollutants in Surface and Ground Waters and Sediments and the Deadlines for Their Achievement. *Off. Gaz. Rep.* Serbia No 50/12.

Government of Republic of Serbia (2014). Regulation on Limit Values for Priority and Priority Hazardous Substances that Pollute the Surface Waters and Deadlines for Their Achievement. *Off. Gaz. Rep.* Serbia No 24/14.

Government of Republic of Serbia (2019). Regulation on Hygienic Quality of Drinking Water. *Off. Gaz. Rep.* Serbia No 42/98, 44/99 and 28/19.

Hans Wedepohl, K. (1995). The Composition of the Continental Crust. *Geochimica Cosmochimica Acta* 59, 1217–1232. doi:10.1016/0016-7037(95)00038-2

Haris, H., Looi, L. J., Aris, A. Z., Mokhtar, N. F., Ayob, N. A. A., Yusoff, F. M., et al. (2017). Geo-accumulation Index and Contamination Factors of Heavy Metals (Zn and Pb) in Urban River Sediment. *Environ. Geochem. Health* 39, 1259–1271. doi:10.1007/s10653-017-9971-0

Huang, Z., Liu, C., Zhao, X., Dong, J., and Zheng, B. (2020). Risk Assessment of Heavy Metals in the Surface Sediment at the Drinking Water Source of the Xiangjiang River in South China. *Environ. Sci. Eur.* 32, 23. doi:10.1186/s12302-020-00305-w

Jahan, S., and Strezov, V. (2018). Comparison of Pollution Indices for the Assessment of Heavy Metals in the Sediments of Seaports of NSW, Australia. *Mar. Pollut. Bull.* 128, 295–306. doi:10.1016/j.marpolbul.2018.01.036

Jamali, M. K., Kazi, T. G., Arain, M. B., Afridi, H. I., Jalbani, N., Kandhro, G. A., et al. (2009). Speciation of Heavy Metals in Untreated Sewage Sludge by Using Microwave Assisted Sequential Extraction Procedure. *J. Hazard. Mater.* 163, 1157–1164. doi:10.1016/j.jhazmat.2008.07.071

Kasalica, V., Jovanović, J., and Bojić, Z. (2021). *Annual Report on the Annex to the Project Mineragenetic Characteristics and Potential of the Neogene Basins of Serbia for 2021. Republic of Serbia, Geologocal Survey of Serbia*. Belgrade, Serbia.

Kelley, K. D., Scott, C., Polyak, D. E., and Kimball, B. E. (2017). in *Critical Mineral Resources of the United States—Economic and Environmental Geology and Prospects for Future Supply*. Editors K. J. Vanadium, J. H. DeYoungJr., R. R. Seal, and D. C. Bradley (Reston, Virginia: U.S. Geological Survey Professional Paper 1802), U1–U36. March Accessed 02, 2022). doi:10.3133/pp1802U

Kemble, N. E., Brumbaugh, W. G., Brunson, E. L., Dwyer, F. J., Ingersoll, C. G., Monda, D. P., et al. (1994). Toxicity of Metal-Contaminated Sediments From the Upper Clark Fork River, Montana to Aquatic Invertebrates and Fish in Laboratory Exposures. *Environ. Toxicol. Chem.* 13, 1985–1997. doi:10.1016/j.envpol.2014.10.014

Lakshtanov, L. Z., and Stipp, S. L. S. (2007). Experimental Study of Nickel(II) Interaction with Calcite: Adsorption and Coprecipitation. *Geochimica Cosmochimica Acta* 71, 3686–3697. doi:10.1016/j.gca.2007.04.006

Lima, M. W. d., Pereira, W. V. d. S., Souza, E. S. d., Teixeira, R. A., Palheta, D. d. C., Faial, K. d. C. F., et al. (2022). Bioaccumulation and Human Health Risks of Potentially Toxic Elements in Fish Species from the Southeastern Carajás Mineral Province, Brazil. *Environ. Res.* 204, 112024. doi:10.1016/j.envres.2021.112024

Looi, L. J., Aris, A. Z., Wan Johari, W. L., Md. Yusoff, F., and Hashim, Z. (2013). Baseline Metals Pollution Profile of Tropical Estuaries and Coastal Waters of the Straits of Malacca. *Mar. Pollut. Bull.* 74, 471–476. doi:10.1016/j.marpolbul.2013.06.008

MacDonald, D. D., Ingersoll, C. G., and Berger, T. A. (2000). Development and Evaluation of Consensus-Based Sediment Quality Guidelines for Freshwater Ecosystems. *Archives Environ. Contam. Toxicol.* 39, 20–31. doi:10.1007/s002440010075

Marjanović, T. D. (2000). *Vlasina Basin (Natural Features, Water Management Problems and the Idea for Their Solution)*. Vlasotince: Informativni list Vlasina, 3–76.

Mezga, K., Dolenec, M., Šram, D., and Vrhovnik, P. (2021). Potentially Toxic Elements in the Dravinja River Sediments7 (Eastern Slovenia). *Geol* 35 (2), 141–150. doi:10.46763/geol21352141m

Mickovski Stefanović, V. Ž. (2012). *The Impact of Genotype and Locality on the Dynamic of Accumulation Heavy Metals in Wheat Vegetative Organs*. [dissertation thesis]. Belgrade (Serbia): University of Belgrade.

Mihajlidi-Zelić, A., Đorđević, D., Relić, D., Tošić, I., Ignjatović, Lj., Stortini, M. A., et al. (2015). Water-soluble Inorganic Ions in Urban Aerosols of the Continental Part of Balkans (Belgrade) during the Summer - Autumn (2008). *Open Chem.* 13 (1), 245–256. doi:10.1515/chem-2015-0010

Müller, G. (1979). Schwermetalle in den Sedimenten des RheinsVera¨nderungen seit 1971. *Umschau* 79, 778–783.

Olías, M., Cánovas, C. R., Macías, F., Basallote, M. D., and Nieto, J. M. (2020). The Evolution of Pollutant Concentrations in a River Severely Affected by Acid Mine Drainage: Río Tinto (SW Spain). *Minerals* 10, 598. doi:10.3390/min10070598

Passos, E. d. A., Alves, J. C., dos Santos, I. S., Alves, J. d. P. H., Garcia, C. A. B., and Spinola Costa, A. C. (2010). Assessment of Trace Metals Contamination in Estuarine Sediments Using a Sequential Extraction Technique and Principal Component Analysis. *Microchem. J.* 96, 50–57. doi:10.1016/j.microc.2010.01.018

Patel, P., Raju, N. J., Reddy, B. C. S. R., Suresh, U., Sankar, D. B., and Reddy, T. V. K. (2018). Heavy Metal Contamination in River Water and Sediments of the Swarnamukhi River Basin, India: Risk Assessment and Environmental Implications. *Environ. Geochem. Health* 40, 609–623. doi:10.1007/s10653-017-0006-7

Peré-Trepat, E., Olivell, L., Ginebreda, A., Caixach, J., and Tauler, R. (2006). Chemometrics Modelling of Organic Contaminants in Fish and Sediment River Samples. *Sci. Tot. Environ.* 371, 223–237. doi:10.1016/j.scitotenv.2006.04.005

Perera, P. C. T., Sundarabarathy, T. V., Sivananthawerl, T., Kodithuwakku, S. P., and Edirisinghe, U. (2016). Arsenic and Cadmium Contamination in Water, Sediments and Fish Is a Consequence of Paddy Cultivation: Evidence of River Pollution in Sri Lanka. *Achiev. Life Sci.* 10, 144–160. doi:10.1016/j.als.2016.11.002

Perović, M. (2019). *Impact Assessment and Regional Specificities of Hydrogeochemical Conditions on the Transformation of Nitrogenous Compounds in Groundwater*. [dissertation thesis]. Novi Sad (Serbia): University of Novi Sad.

Radomirović, M., Ćirović, Ž., Maksin, D., Bakić, T., Lukić, J., Stanković, S., et al. (2020). Ecological Risk Assessment of Heavy Metals in the Soil at a Former Painting Industry Facility. *Front. Environ. Sci.* 8, 560415. doi:10.3389/fenvs.2020.560415

Radomirović, M., Mijatović, N., Vasić, M., Tanaskovski, B., Mandić, M., Pezo, L., et al. (2021). The Characterization and Pollution Status of the Surface Sediment in the Boka Kotorska Bay, Montenegro. *Environ. Sci. Pollut. Res.* 28, 53629–53652. doi:10.1007/s11356-021-14382-8

Rodríguez, M. J. A., De Arana, C., Ramos-Mir, J. J., Gil, C., and Boluda, R. (2015). Impact of 70 Years Urban Growth Associated With Heavy Metal Pollution. *Environ. Pollut.* 196, 156–163. doi:10.1016/j.envpol.2014.10.014

Sakan, S., Gržetić, I., and Đorđević, D. (2007). Distribution and Fractionation of Heavy Metals in the Tisa (Tisza) River Sediments. *Env. Sci. Poll. Res. Int.* 14 (4), 229–236. doi:10.1065/espr2006.05.304

Sakan, S. M., Đorđević, D. S., Manojlović, D. D., and Predrag, P. S. (2009). Assessment of Heavy Metal Pollutants Accumulation in the Tisza River Sediments. *J. Environ. Manag. Manage.* 90, 3382–3390. doi:10.1016/j.jenvman.2009.05.013

Sakan, S., Đorđević, D., Dević, G., Relić, D., Anđelković, I., and Đuričić, J. (2011). A Study of Trace Element Contamination in River Sediments in Serbia Using Microwave-Assisted Aqua Regia Digestion and Multivariate Statistical Analysis. *Microchem. J.* 99 (2), 492–502. doi:10.1016/j.microc.2011.06.027

Sakan, S., Popović, A., Anđelković, I., and Đorđević, D. (2016). Aquatic Sediments Pollution Estimate Using the Metal Fractionation, Secondary Phase Enrichment Factor Calculation, and Used Statistical Methods. *Environ. Geochem. Health* 38, 855–867. doi:10.1007/s10653-015-9766-0

Sakan, S., Sakan, N., Anđelković, I., Trifunović, S., and Đorđević, D. (2017). Study of Potential Harmful Elements (Arsenic, Mercury and Selenium) in Surface Sediments from Serbian Rivers and Artificial Lakes. *J. Geochem. Explor.* 180, 24–34. doi:10.1016/j.gexplo.2017.06.006

Sakan, S., Frančišković-Bilinski, S., Đorđević, D., Popović, A., Škrivanj, S., and Bilinski, H. (2020). Geochemical Fractionation and Risk Assessment of Potentially Toxic Elements in Sediments from Kupa River, Croatia. *Water* 12, 2024. doi:10.3390/w12072024

Sakan, S., Mihajlidi Zelić, A., Škrivanj, S., Frančišković Bilinski, S., Bilinski, H., and Đorđević, D. (2021). "Toxic Elements in Soils from Vlasina Region," in Proceeding of the 3rd International and 15th National Congress Soils for Future Under Global Challenges, Sokobanja, Serbia, September 2021 (Belgrade: Serbian Society of Soil Science, Book of Proceedings), 79–86.

Simić, M. (2001). *Metallogeny of Mačkatica-Blagodat-Karamanica Zone*. Belgrade: Geo Institute, Special Editions of, Book 28. (in Serbian).

Savić, M. (2019). *Regional-geographical Overview of Vlasina and Krajina*. [master work]. Niš (Serbia): University of Niš.

Smedley, P. L., and Kinniburgh, D. G. (2001). *Source and Behaviour of Arsenic in Natural Waters*. Wallingford, Oxon OX10 8BB, U.K: British Geological Survey. Available from: https://www.Source_and_behaviour_of_arsenic_in_natur.pdf (Accessed March 03, 2022).[

Sutherland, R. A. (2010). BCR-701: A Review of 10-years of Sequential Extraction Analyses. *Anal. Chim. Acta* 680, 10–20. doi:10.1016/j.aca.2010.09.016

Thuong, N. T., Yoneda, M., Ikegami, M., and Takakura, M. (2013). Source Discrimination of Heavy Metals in Sediment and Water of to Lich River in Hanoi City Using Multivariate Statistical Approaches. *Environ. Monit. Assess.* 185, 8065–8075. doi:10.1007/s10661-013-3155-x

Thuong, N. T., Yoneda, M., Shimada, Y., and Matsui, Y. (2015). Assessment of Trace Metal Contamination and Exchange between Water and Sediment Systems in the to Lich River in Inner Hanoi, Vietnam. *Environ. Earth Sci.* 73, 3925–3936. doi:10.1007/s12665-014-3678-7

USEPA (2022). *National Primary Drinking Water Regulations*. Available from: https://www.epa.gov/ground-water-and-drinking-water/national-primary-drinking-water-regulations#Inorganic (Accessed March 27, 2022).

Ustaoğlu, F. (2021). Ecotoxicological Risk Assessment and Source Identification of Heavy Metals in the Surface Sediments of Çömlekci Stream, Giresun, Turkey. *Environ. Forensics* 22, 130–142. doi:10.1080/15275922.2020.1806148

Ustaoğlu, F., and Islam, M. S. (2020). Potential Toxic Elements in Sediment of Some Rivers at Giresun, Northeast Turkey: A Preliminary Assessment for Ecotoxicological Status and Health Risk. *Ecol. Indic.* 113, 106237. doi:10.1016/j.ecolind.2020.106237

Ustaoğlu, F., Tepe, Y., and Aydin, H. (2020). Heavy Metals in Sediments of Two Nearby Streams from Southeastern Black Sea Coast: Contamination and Ecological Risk Assessment. *Environ. Forensics* 21, 145–156. doi:10.1080/15275922.2020.1728433

Varol, M., Karakaya, G., and Sünbül, M. R. (2021). Spatiotemporal Variations, Health Risks, Pollution Status and Possible Sources of Dissolved Trace Metal(loid)s in the Karasu River, Turkey. *Environ. Res.* 202, 111733. doi:10.1016/j.envres.2021.111733

Wang, J., Liu, G., Liu, H., and Lam, P. K. S. (2017). Multivariate Statistical Evaluation of Dissolved Trace Elements and a Water Quality Assessment in the Middle Reaches of Huaihe River, Anhui, China. *Sci. Total Environ.* 583, 421–431. doi:10.1016/j.scitotenv.2017.01.088

Wang, X., Shi, Z., Shi, Y., Ni, S., Wang, R., Xu, W., et al. (2018). Distribution of Potentially Toxic Elements in Sediment of the Anning River Near the REE and V-Ti Magnetite Mines in the Panxi Rift, SW China. *J. Geochem. Explor.* 184, 110–118. doi:10.1016/j.gexplo.2017.10.018

WHO (2017). *Guidelines for Drinking-Water Quality: Fourth Edition Incorporating the First Addendum*. Geneva: World Health Organization.

Yüksel, B., Ustaoğlu, F., Tokatli, C., and Islam, M. S. (2021). Ecotoxicological Risk Assessment for Sediments of Çavuşlu Stream in Giresun, Turkey: Association between Garbage Disposal Facility and Metallic Accumulation. *Environ. Sci. Pollut. Res.* 29, 17223–17240. doi:10.1007/s11356-021-17023-2

Zachara, J. M., Cowan, C. E., and Resch, C. T. (1991). Sorption of Divalent Metals on Calcite. *Geochimica Cosmochimica Acta* 55, 1549–1562. doi:10.1016/0016-7037(91)90127-q

Conflict of Interest: The authors declare that the research was conducted in the absence of any commercial or financial relationships that could be construed as a potential conflict of interest.

Publisher's Note: All claims expressed in this article are solely those of the authors and do not necessarily represent those of their affiliated organizations, or those of the publisher, the editors, and the reviewers. Any product that may be evaluated in this article, or claim that may be made by its manufacturer, is not guaranteed or endorsed by the publisher.

frontiers | Frontiers in Environmental Science

ORIGINAL RESEARCH
published: 23 June 2022
doi: 10.3389/fenvs.2022.916916

Chemometric Optimization of Solid-Phase Extraction Followed by Liquid Chromatography-Tandem Mass Spectrometry and Probabilistic Risk Assessment of Ultraviolet Filters in an Urban Recreational Lake

*Jelena Lukić[1], Jelena Radulović[2], Milica Lučić[1], Tatjana Đurkić[3] and Antonije Onjia[3]**

[1]Innovation Center of the Faculty of Technology and Metallurgy, Belgrade, Serbia, [2]Anahem Laboratory, Belgrade, Serbia, [3]Faculty of Technology and Metallurgy, University of Belgrade, Belgrade, Serbia

OPEN ACCESS

Edited by:
Zhi-Feng Chen, Guangdong University of Technology, China

Reviewed by:
Hideo Okamura, Kobe University, Japan
Waldemar Studziński, Bydgoszcz University of Science and Technology, Poland

***Correspondence:**
Antonije Onjia
onjia@tmf.bg.ac.rs

Specialty section:
This article was submitted to Toxicology, Pollution and the Environment, a section of the journal Frontiers in Environmental Science

Received: *10 April 2022*
Accepted: *02 June 2022*
Published: *23 June 2022*

Citation:
Lukić J, Radulović J, Lučić M, Đurkić T and Onjia A (2022) Chemometric Optimization of Solid-Phase Extraction Followed by Liquid Chromatography-Tandem Mass Spectrometry and Probabilistic Risk Assessment of Ultraviolet Filters in an Urban Recreational Lake. Front. Environ. Sci. 10:916916. doi: 10.3389/fenvs.2022.916916

Solid-phase extraction (SPE) of eleven ultraviolet filters (UVFs): benzophenone-1 (BP-1); benzophenone-3 (BP-3); benzophenone-4 (BP-4); isoamyl p-methoxycinnamate (IAMC), homosalate (HMS); 4-hydroxybenzophenone (4-HB); 4-methylbenzylidene camphor (4-MBC); octocrylene (OC); octyl dimethyl-p-aminobenzoate (OD-PABA); 2-ethylhexyl-4-methoxycinnamate (EHMC); and avobenzone (AVO), has been optimized using Plackett-Burman design, Box-Behnken design, and Derrindzer desirability function. Of the six SPE variables studied, the most influencing is the type of eluent followed by pH and the methanol content in the rinsing solvent. A method with good analytical performance was obtained by applying optimal SPE conditions and liquid chromatography-tandem mass spectrometry (LC-MS/MS), with the method detection limit ranging from 0.1 to 5 ng/L, recovery from 44% to 99%, and relative standard deviation (RSD) within 19%. This method was used to analyze the content of UVFs in an urban lake (Sava Lake, Serbia). UVFs occurrence, geostatistical distribution, and associated environmental risk are highly dependent on recreational activities. The average concentrations of UVFs ranged from 0.3 to 113 ng/L, and the most present substance was EHMC, followed by 4-MBC and BP-3. The spatial distribution of the risk quotient (RQ = 0.04–1.7) inside the lake is highly correlated with the number of people bathing and swimming. Human exposure through the dermal pathway is higher than ingestion for most UVFs. Monte Carlo simulation of probabilistic risk assessment estimated the percentile P10, P50, P90 of 12.7; 17.3; 47.5 and 20.1; 27.6; 77.5 ng/kg·day for total human exposure of adults and children, respectively. The sensitivity analysis revealed that the health risk estimate depends mostly on the content of EHMC, HMS, and 4-MBC, while the most influential exposure variables were human body weight and skin surface area. There is no serious concern to human health due to UVFs in the short term; however, a high ecological risk in some parts of the lake is estimated.

Keywords: sunscreen, Monte Carlo, Plackett-Burman, Box-Behnken, Derringer desirability, spatial distribution, risk quotient, SWIMODEL

1 INTRODUCTION

Ultraviolet filters (UVF) are used to protect the human skin from harmful UV radiation and are added to various skin treatment products (Kunze et al., 2021; Kwon and Choi, 2021). However, some UVFs, especially if applied in large quantities, can cause side effects, such as various allergies, dermatitis, and adverse effects on hormonal receptors, nervous system, and reproductive functions (Huang et al., 2021).

Concentrations of individual UVFs in sunscreen preparations are at the level of several percent, and the European Commission (EC No 1223, 2009) has set limit/reference values for individual organic UVFs in the range of 2%–10% (except for drometrizole trisiloxane 15%). UVFs are used daily, and their use is exceptionally high during the summer months (Fagervold et al., 2019), which leads to the release of vast amounts of these substances into the environment (Ma et al., 2016).

Unfortunately, UVFs have been proved to pose a high risk for many aquatic organisms (Carve et al., 2021). Different UVFs affect the environment differently (Labille et al., 2020). Some UVFs tend to accumulate in living cells, affecting reproduction, and increasing mortality in benthic organisms, small fish, and sizeable newborn fish (Carve et al., 2021). This suggests that the presence of UVFs in the water should be considered with great concern.

A significant proportion of UVFs enters the environment through sewage effluents (Wang et al., 2021), which may further contaminate the surface water and groundwater (Li et al., 2020a). In addition, one of the ways of polluting the environment water with UVFs is rinsing the skin during swimming (Teo et al., 2015). Therefore, the presence of UVF needs to be investigated in water at the wastewater treatment plants and in the vicinity of beaches.

Numerous studies have been recently conducted on the occurrence and fate of UVFs in coastal aquatic systems, such as seawater and wastewater (Cadena-Aizaga et al., 2022), corals (Tashiro and Kameda, 2013; Mitchelmore et al., 2021), surface water (Kameda et al., 2011; Tsui et al., 2014), marine water and sediment (Sánchez Rodríguez et al., 2015; Allinson et al., 2018; Mitchelmore et al., 2019), lake sediments (Kaiser et al., 2012), beach sediments (Astel et al., 2020), river sediment (Huang et al., 2016), and fish (Balmer et al., 2005).

Sava Lake in Belgrade (Serbia) is a typical urban lake that is used for recreation such as swimming, sailing, fishing, and diving. In the summer months, there are several thousand people at the lake daily, and it is expected that a large amount of UVFs will be released into the lake water. However, the recreational activities are not evenly distributed along the lake, i.e., there are parts of the lake where there is a big crowd with people sunbathing and swimming and parts of the lake without such activities. Consequently, the different spatial distribution of potential water contaminants is expected.

Risk assessment studies have shown an increased ecological risk due to UVFs in recreational locations and that it depends on the intensity of application of sunscreen products (Teo et al., 2015). Keeping in mind that the concentrations of different UVFs in waters are different and each UVF has a different distribution, the probabilistic approach to risk assessment in swimming water has recently become irreplaceable (Astuti et al., 2022; Dehghani et al., 2022). Compared to the deterministic one, this approach gives a complete picture of the risk estimate, considering that individual UVFs concentrations differ temporarily and spatially (Tsui et al., 2015). In addition to the distribution of UVF concentrations, the distribution of the exposure parameters influencing the risks should not be neglected.

Several analytical methods can be used to quantify the UVFs traces in water. When UVF concentrations are very low, the most optimal technique for sample preparation is solid-phase extraction (SPE) (Allinson et al., 2018; Cadena-Aizaga et al., 2020). This technique enables high degrees of preconcentration, which is why it is the most commonly used technique for analyzing trace level organics in water. In order to get the best analytical performance, the SPE process needs to be optimized (Silva et al., 2013; Chávez-Moreno et al., 2018). As for the instrumental measurement itself, two techniques are predominantly used to measure UVFs. One is gas chromatography with tandem mass spectrometry (GC-MS/MS) (da Silva et al., 2015; Huang et al., 2016; Ramos et al., 2019), which has a huge potential for identification and selectivity in separation. Another technique is liquid chromatography with tandem mass spectrometry (LC-MS/MS) (Li et al., 2020b; Chiriac et al., 2020; Cadena-Aizaga et al., 2022), which is characterized by exceptional sensitivity and is very suitable for the analysis of low-volatile and degradable UVFs.

The main objectives of this work were to optimize the SPE sample preparation prior to LC-MS/MS, investigate the occurrence and spatial distribution of different UVFs in recreational water of an urban city lake, and assess potential environmental risk using a probabilistic approach.

2 MATERIAL AND METHODS

2.1 Study Area and Sampling

The Sava Lake (**Figure 1**), better known as Ada Ciganlija, is a tributary of the Sava River. The lake was formed about 50 years ago. The length of the lake is about 4.4 km, the average width is 250 m, and the average depth is 4.5 m (Trbojević et al., 2021). The lake volume is about 4 million m^3, and the area is approximately 1.0 km^2. On the left side, there is a small fenced pool connected to the Sava River, from which water is pumped into the Sava Lake, while on the right side, water is discharged from the lake into the Čukarica stream. This artificially ensures water flows through the lake.

Sampling was performed in a one-time sampling campaign conducted in August 2021, at the peak of the recreational season. The population of swimmers/bathers on Sava Lake at the time of sampling was about a thousand people. A total of 28 grab samples were taken along the coast and in the middle of Sava Lake. The samples were taken 10 cm below the water surface, stored at 4 °C, and analyzed within 24 h. All water samples were collected in amber glass bottles (volume 0.5 L). Prior to the LC-MS/MS® measurement, all samples were subjected to SPE on Oasis®

FIGURE 1 | Sampling location - Sava Lake (Serbia).

TABLE 1 | Plackett-Burman design values for SPE variables.

Variable	Coded value		
	−1	**0**	**1**
PH	2	5	8
V_e, mL	5	10	15
Eluent	CH_3OH	CH_3CN	EtOAc
V_s, mL	50	100	150
%MeOH	0	5	10
V_r, mL	5	10	15

Subscript: e, eluent; s, sample; r - rinsing.

HLB 6 ml Vac Cartridges with 100 mg sorbent per cartridge (Waters Corp., Milford, MA, United States).

2.2 Sample Preparation

A two-step statistical approach was employed to optimize several variables that affect the SPE sample preparation of UVFs. The variables, such as the type of eluent, percentage of methanol in the rinsing solution (%MeOH), initial pH value, the sample volume (V_s), the rinsing solution volume (V_r), and eluent volume (V_e), were screened by applying Plackett–Burman design (PBD) and were optimized further by central composite design (CCD). The variable and their coded values for PBD are listed in **Table 1**. PBD experiments, consisting of 15 runs, have been performed according to **Supplementary Tables S1, S2**, while the subsequent CCD experimental runs are listed in **Supplementary Table S3**.

The effect of pH on the UVFs extraction from sample solution was studied within the range of 2–8, using 0.1 M HCl and 0.1 M NaOH for pH adjustment. Spiked samples were made by dissolving standard mixture solutions of 1.0 µg/ml each UVF in water. After adjusting the initial pH values of the samples, the conditioning of the SPE cartridge was started. A 5 ml volume of the eluent was applied to the cartridges, followed by 5 ml of deionized water whose pH was adjusted to the same value as the pH of the sample to be applied. The sample application was made at approximately 1.0 ml/min flow rate. After applying the sample, the cartridges were washed with a rinsing solution and dried for 10 min. The elution was performed with the selected type of the eluent and its optimized volume. The eluted extracts were evaporated under a stream of nitrogen and reconstituted with 0.5 ml of methanol. All samples were filtered with a 0.22 µm PTFE syringe filter.

2.3 Liquid Chromatography-Tandem Mass Spectrometry Measurement

A Thermo Fisher Scientific (Waltham, United States) LC-MS/MS system comprised of a Dionex Ultimate 3000 liquid chromatograph fitted with an Accucore™ aQ C-18 column (10 cm length, 2.1 mm I.D., particle size 2.6 µm) and LTQ XL linear ion trap mass spectrometer operating in the electrospray ionization (ESI) mode. Mass spectra of analytes were processed by an Xcalibur Ver. 3.0 software. A 10 µL volume of the SPE prepared extract was injected into the LC-MS/MS system. LC mobile phase composition and MS/MS operating parameters are given in **Supplementary Tables S4, S5**.

2.4 Data Analysis

First, the experimental results were processed by descriptive statistics, Pearson correlation, and the Ryan-Joiner normality test. Then, the log-transformed concentration data were subjected to hierarchical cluster analysis (HCA) using Ward linkage and Euclidean distance. Finally, geostatistical distribution analysis was based on the ordinary kriging

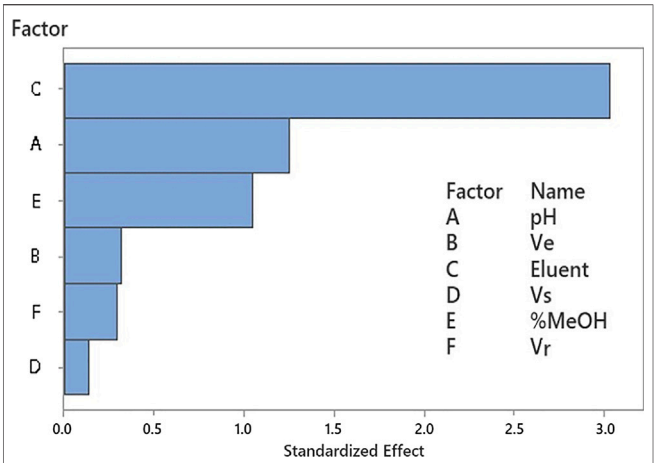

FIGURE 2 | Pareto plot of PBD screening SPE variables.

method, and results were mapped in the polygon representing Sava Lake.

The ecological risk associated with UVFs in the Sava Lake was assessed based on the risk quotient (RQ), which is the ratio between a measured concentration (C) and a predicted no-effect concentration (PNEC), as described in **Eq. 1**:

$$\sum RQ = \sum_{i=1}^{n} (C_i / PNEC_i) \quad (1)$$

Human exposure to UVFs through ingestion and dermal pathways has been evaluated by following the US EPA SWIMODEL exposure assessment model (Li et al., 2020b; Dehghani et al., 2022). Accordingly, the calculation formulas are given in **Eqs 2**, **3**, while the exposure parameters and their values used for risk assessment are listed in **Table 2** and **Supplementary Tables S6, S7**.

$$D_{ing} = (C_i \cdot IR \cdot ST \cdot SF \cdot BI) / (AT \cdot BW) \quad (2)$$

$$D_{derm} = (DA \cdot SA \cdot SF) / (AT \cdot BW) \quad (3)$$

Monte Carlo simulation and sensitivity analysis have been made with the following run preferences: the number of trials is 1000, the confidence level is 95%, and the initial seed value of 999.

3 RESULTS AND DISCUSSION

3.1 Optimization of SPE of Ultraviolet Filters From Water

3.1.1 Plackett–Burman Design Screening

Since all UVFs are simultaneously subjected to the SPE process, additional efforts should be made to obtain an optimal response that would include all individual responses. Thus, considering that we have 11 UVFs, an aggregate response that includes the individual responses for all analytes simultaneously is used here.

The most commonly used cumulative response in analytical measurements is the desirability function (D) proposed by Derringer and Suich (1980), which represents the geometric mean estimated as a product of the individual desirabilities (d_i) weighted by their individual coefficients (r_i) (**Eq. 4**). In this case, no difference in weights for individual responses was assumed, so the D values were calculated taking into account all UVFs equally. Therefore, the values for d_i have been maximized and ranged from 0 to 1, while the r_i values were fixed ($r_i = 1$).

$$D = \left(\prod_{i=1}^{n} d_i^{ri} \right)^{1/\sum ri} \quad (4)$$

The results of the screening design are given in the form of a Pareto plot in **Figure 2**. It shows that the parameter of the most significant influence is the type of SPE eluting solvent. Besides, a considerable influence is also noticed for %MeOH and pH, while other parameters have much less impact on the SPE process. The main effects plot for the tested analytes (**Supplementary Figure S1**) revealed that in addition to the type of solvent, recoveries are positively affected by increasing the parameters V_e and V_s. Conversely, the increase in the values of the parameters %MeOH, pH, and V_r affect the response negatively.

In the second step, ethyl acetate (EtOAc) was selected as an eluent, and the percentage of methanol (%MeOH) in the rinsing solvent and the sample pH value were selected as variables for the CCD optimization.

3.1.2 Central Composite Design Optimization

The initial pH of the sample and %MeOH have been optimized according to CCD in the experimental domain for pH = 2–8 and %MeOH = 2%–8%. **Figure 3** shows the response surface plot for optimization of pH and %MeOH. The response was fitted to a second-order polynomial model represented by the following regression equation:

$$D = -1.239 + 0.404 \cdot pH + 0.362 \cdot \%MeOH - 0.007 \cdot pH \cdot \%MeOH - 0.036 \cdot pH^2 - 0.034 \cdot \%MeOH^2 \quad (5)$$

Final SPE conditions were obtained by optimizing the D value (**Figure 3**). As a result, a maximum D value of 0.67 was obtained for %MeOH of 4.8% and pH = 5.1. Finally, the global optimum for SPE of all UVFs was selected for the following values of variables: the extraction volume of 150 ml of aqueous sample, pH of the sample set at 5.1, and 15 ml aqueous solution with 4.8%MeOH to rinse the cartridge, and 15 ml EtOAc for elution. These conditions were used to prepare water samples from Sava Lake for the analysis of UVFs by the LC-MS/MS method.

3.2 Validation of SPE-LC-MS/MS Method

The optimized SPE sample preparation was accompanied by LC-MS/MS measurement. The LC-MS/MS method was previously optimized, which included optimizing the HPLC mobile phase (Vasiljević et al., 2004), tuning the MS instrument, finding optimal m/z and values, and CID value optimization (Grujić et al., 2009). The optimal LC-MS/MS parameters are given in **Supplementary Tables S4, S5**. Typical LC-MS/MS

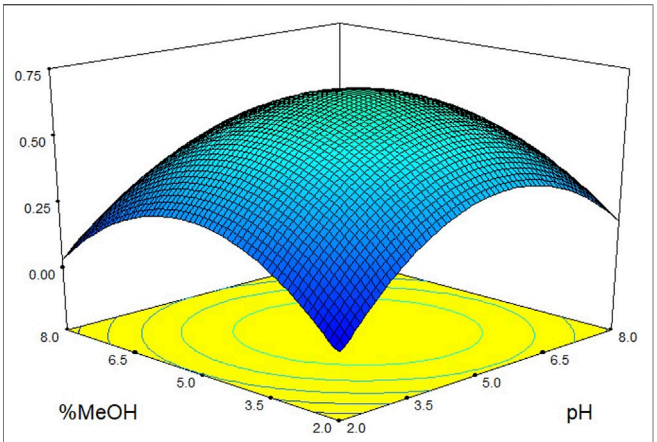

FIGURE 3 | Response surface plot of CCD optimization of UVFs.

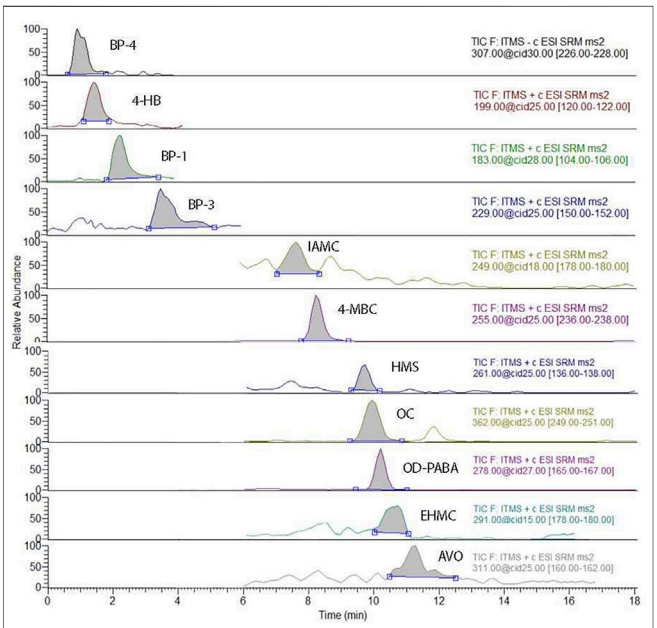

FIGURE 4 | LC-MS/MS chromatograms of UVFs in a real water sample (no. 20) from Sava Lake.

chromatograms for eleven UVFs detected in Sava Lake water are shown in **Figure 4**. **Supplementary Figures S2–S31** present the LC-MS/MS chromatograms for all samples, blank and a standard mixture.

In order to assess the analytical performances of the method, the method detection limits (MDL), average recovery (R), and relative standard deviation (RSD) were determined. Clean surface water, in which the analyzed UVFs were not detected, was used to make spiked samples and construct matrix-matched calibration lines at nine concentration levels for the UVFs mixture. The calibration range was 0.1–300 ng/L. For each UVF, the linear correlation coefficient was greater than 0.995. The obtained MDL, R, and RSD values are listed in **Supplementary Table S8**. MDLs, estimated as three times the signal-to-noise ratio, range from 0.01 to 4.4 ng/L. Recovery studies were performed at 1.0, 10, and 100 ng/L concentration levels. Average recoveries for 11 analytes range from 44% to 99%. Six replicates were used to investigate repeatability at the mentioned concentration levels, and RSDs values within ±19% were obtained.

3.3 Occurrence of Ultraviolet Filters in Recreational Lake Water

Descriptive statistics, along with the distribution parameters, are presented in **Table 3**. The concentration profile of most of the tested UVFs in the studied Sava Lake shows a log-normal distribution skewed to the right, which is shown by positive values for skewness. All skewness values are greater than 1.0, except for BP-1, BP-3, and 4-HB. These three UVFs have negative kurtosis, indicating platykurtic distributions, i.e., flatter tails. Mean values of UVFs substances in the investigated water were different in different parts of the lake. The obtained concentrations range from 0.09 ng/L for IAMC to 584 ng/L for EHMC. The highest average concentration was detected for EHMC at 113 ng/L, and the least present UVFs detected were IAMC and OD-PABA, with average concentrations of 0.3 ng/L and 0.4 ng/L, respectively. These two UVFs were detected only in parts of the lake where human recreational activity (swimming/bathing) is intense, while the other nine UVFs were detected in all samples. Total mean concentrations of UVFs decrease in the following order: EHMC > 4-MBC > BP-3 > OC > AVO > 4-HB > HMS > BP-4 > BP-1 > OD-PABA > IAMC.

The content of these UVFs in Sava Lake water varies significantly, so it is somewhat inconvenient to compare it with other recreational waters. However, one may conclude that the level of concentrations obtained is in the range of concentrations in other cited studies, including coastal marine water: 0.07–172 μg/L (Cadena-Aizaga et al., 2022), n.d.–3730 ng/L, n.d.–1298 ng/L, n.d.–341 ng/L (Kwon and Choi, 2021), swimming pool water: up to 1500 μg/L (Mokh et al., 2021), n.d.–289 ng/L (Li et al., 2020b), lake water: <2–35 ng/L (Balmer et al., 2005), drinking and river water: 44–105 ng/L (da Silva et al., 2015), and municipal wastewater: 0.1–19 μg/L (Balmer et al., 2005), n.d.–400 ng/L (Wang et al., 2021), 621–951 ng/L (Wu et al., 2018).

Pearson correlation matrix (**Supplementary Table S9**) reveals a strong association between UVFs. Only OD-PABA concentrations are not related to other UVFs. The highest correlation coefficient of 0.969 was found for the pair EHMC and AVO, while the smallest one was estimated for the pair BP-1 and OD-PABA (0.102). In general, it can be concluded that there is a large intercorrelation between UVFs. **Figure 5** shows a dendrogram obtained by hierarchical cluster analysis (HCA). The relationship between the groups of tested samples and UVFs is obvious. Four clusters (I, II, III, and IV) were identified. This grouping can be attributed to the different spatial distribution of sampling points and the difference in the amount of UVFs in sunscreen products and how they are

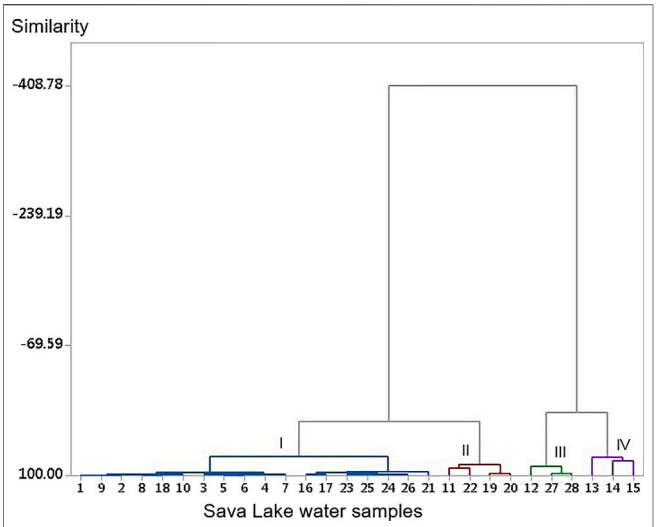

FIGURE 5 | Dendrogram of water samples from Sava Lake.

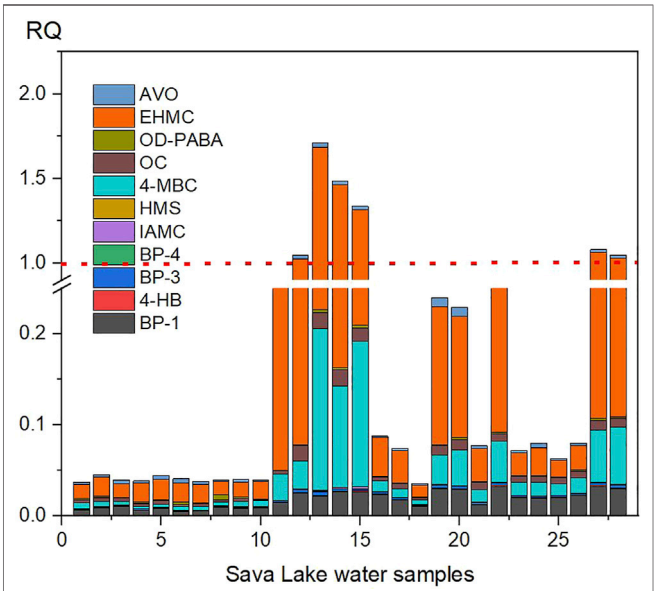

FIGURE 6 | Contribution of individual UVFs to total RQ.

applied. Namely, sunscreen products are usually composed of a combination of UVFs to ensure the broadest protection.

3.4 Environmental Risk Assessment

3.4.1 Deterministic Approach

RQs for individual UVFs were obtained by dividing C_i obtained in this study by PNECs values (**Supplementary Table S10**), which are collected after the literature survey (Lukić et al., 2021). The risk classification was based on risk ranking criteria in which RQ < 0.01; 0.01 < RQ < 0.1; 0.1 < RQ < 1; and RQ > 1, are "Unlikely to pose risk"; "Low risk"; "Medium risk" and "High risk", respectively (Ma et al., 2016).

Contributions of individual UVFs to total RQ are presented in **Figure 6**. It is noticeable that the greatest contribution to RQ is made by the presence of EHMC, followed by 4-MBC and BP-1. The share of other UVFs in total RQ can be almost neglected. The estimated minimum, average and maximum RQs values are 0.4, 0.35 and 1.7, respectively. There are two groups of samples in which the RQ values exceed 1. The first group comprises samples that highly exceed one and are marked 13–15, while the second group includes samples numbered 12, 27, and 28, slightly above 1. In conclusion, both sample groups represent locations with a high ecological risk.

The geostatistical distribution of risk in Sava Lake was made based on calculated RQs from the measured values, which were used to perform ordinary kriging interpolation on the entire lake area (Radomirović et al., 2020). **Figure 7** shows that in several places close to the lake beach, the RQs are elevated in comparison to the middle of the lake. Several hotspots have been identified (A, B, C, D), which correlate with the intensity of human activities at the site.

In area A, samples 12, 13, 14, and 15 are located, while samples 27 and 28 are in area B. These samples show RQ ˃ 1 (**Figure 6**) and are classified in clusters III and IV in the dendrogram (**Figure 5**). Samples 19 and 20 are in area D, and sample 22 represents sampling point C. This distribution reflects the intensity of human activity at the lake. Most people and swimmers/bathers are located on the beach and in the water in area A, then an area at point B. At locations C and D, there are beaches with significantly fewer people. In the middle of the lake, as well as at the left and right edges, water contamination with UVFs is significantly lower.

3.4.2 Monte Carlo Simulation and Sensitivity Analysis

Since UVFs concentrations are not uniformly distributed across the lake, a probabilistic approach to human exposure is expected to provide a more realistic assessment than a point estimate (Astuti et al., 2022; Dehghani et al., 2022). Given that the exposure parameters also have their distributions, individual risks and cumulative risk will also follow some distributions. Namely, the exposure parameters AT and BI are fixed points, SF and ST have triangle distribution, while BW and SA follow a log-normal distribution. PNEC, Log Kow, and MW are analyte-specific fixed-values (**Table 2**, **Supplementary Tables S6, S7**). Concentrations of individual UVFs have been fitted to estimate the best distribution. All UVFs concentrations follow a log-normal distribution, except BP-4, which is best fitted with the Webuill curve.

Monte Carlo simulation of human exposure was applied to UVFs in Sava Lake. According to the SWIMMER model, humans may be exposed to UVFs through inhalation, digestion, and dermal pathway. While inhalation is less likely to be a significant route due to the low volatility of UVFs (Lu et al., 2017), the other two are expected to be the important exposure routes of UVFs to humans. The accidental ingestion and dermal absorption of UVFs were calculated from **Eqs 2**, **3**. The exposure parameters listed in **Table 2** were used to estimate the human dose for adults and children (age

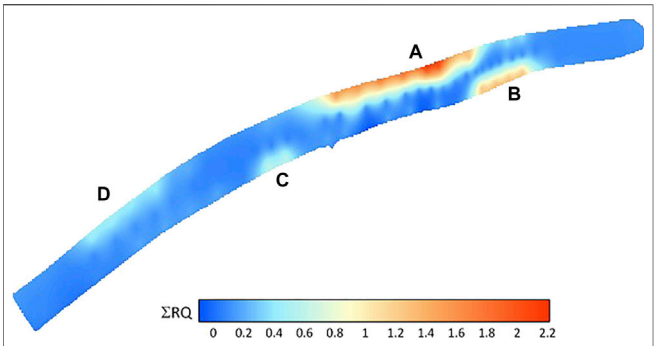

FIGURE 7 | Geostatistical distribution of ΣRQ in Sava Lake.

TABLE 2 | Parameters and values used for risk assessment.

Exposure parameter	Adult	Children	Distribution
Ingestion rate (L/h) (IR)	0.025	0.05	LN
Swimming frequency (event/year) (SF)	120	120	T
Swimming time (h/event) (ST)	1.3	1.7	T
Body weight (kg) (BW)	71.75	48.2	LN
Skin surface area (cm^2) (SA)	18150	14200	LN
Averaging time (d) (AT)	365	365	P
Bioavailability (BI)	100	100	P

LN, log-normal; T, triangle; P, fixed point.

TABLE 3 | Descriptive statistics of UVFs in Sava Lake (ng/L).

UVF	Mean	RSD	Min	Max	S	K
BP-1	5.0	2.6	1.5	9.2	0.2	−1.4
4-HB	6.6	2.5	2.4	12	0.5	−0.6
BP-3	35	19	11	82	0.8	−0.3
BP-4	8.2	6.9	1.4	25	1.0	0.2
IAMC	0.3	0.3	0.09	1.5	2.2	5.0
HMS	8.4	11	1.1	40	1.7	1.7
4-MBC	63	91	5.6	354	2.3	4.8
OC	23	16	4.2	58	1.1	0.2
OD-PABA	0.4	0.3	0.13	1.7	2.4	7.8
EHMC	113	183	5.1	584	1.6	0.9
AVO	15	16	2.6	55	1.4	0.6

S, skewness (unitless); K, kurtosis (unitless).

11–14 years). The Monte Carlo calculation results are presented in **Supplementary Table S11**.

Human exposure through the dermal pathway poses a higher risk compared to ingestion for most UVFs, except for BP-1, BP-3, BP-4 and 4-HB. **Figure 8** shows the human exposure distribution for adults and children and the corresponding sensitivity risk analysis. The histograms for the total exposure dose show the simulated ΣD_a and ΣD_c in 90% (the 90 of the estimated percentile) for the adult and children groups of 47.5 and 77.5 ng/kg·day, respectively. This indicates that children are much more at risk due to UVFs exposure than adults because of their lower body-weight/skin

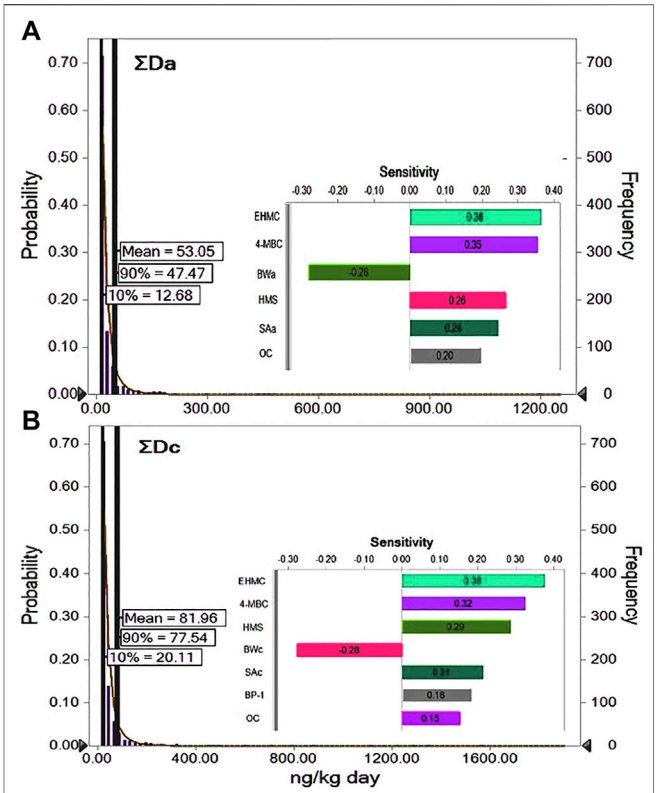

FIGURE 8 | Probability and sensitivity analysis of different groups exposed to UVFs: **(A)** adults; **(B)** children.

surface ratio. Anyway, the lack of reference dose (R_fD) values prevents the explicit expression of the health risk index. Instead, the UVFs exposure can be compared to similar substances, i.e., parabens for which there is R_fD of 10 mg/kg·BW/day (Li et al., 2021) proposed by the Joint Expert Committee on Food Additives (JECFA) of Food and Agriculture Organization of the United Nations (FAO) and World Organization (WHO). Based on this comparison, it can be concluded that there is a negligible risk to human health for the estimated UVFs doses (ng/kg·day) (Li et al., 2020B). Thus, the concentrations of these compounds in Sava Lake water can be considered acceptable, except at a few hotspot locations. Anyhow, there are concerns that UVFs will affect human health in the long term either through their influence or from harmful organic substances that may arise as products of their degradation.

4 CONCLUSION

SPE may be efficiently step-wise optimized using screening and response surface designs. It is a reliable sample preparation technique, which, coupled with LC-MS/MS, represents a suitable analytical tool for UVFs in surface water. Among 11 popular UVFs, EHMC, 4-MBC, and BP-3 were most abundant in

the studied recreational lake. It was shown that recreational activities greatly influenced the occurrence of UVFs, their spatial distribution, and potential environmental risk. UVFs are significantly present near the coast, i.e., close to the beach. Nevertheless, the RQ values exceeded one at several locations in the lake. The incidental ingestion is a minor route to human exposure to most UVFs. Monte Carlo simulation of risk estimated 63% higher percentiles for total human exposure of children compared to adults. In addition, the sensitivity identified the most influential variables as the content of EHMC, HMS, and 4-MBC, along with two exposure parameters, human body weight and skin surface area. In general, except for the high ecological risk in some parts of the lake, UVFs in studied recreational lake water posed no concern to human health in the short term.

DATA AVAILABILITY STATEMENT

The original contributions presented in the study are included in the article/**Supplementary Material**, further inquiries can be directed to the corresponding author.

AUTHOR CONTRIBUTIONS

JL: methodology, investigation, and writing–original draft. JR: resources and validation. ML: formal analysis and visualization. TĐ: supervision, project administration, and funding acquisition. AO: conceptualization, software, writing–review and editing.

FUNDING

This research was supported by the Ministry of Education, Science and Technological Development of the Republic of Serbia (Grants 451-03-68/2022-14/200287 and 451-03-68/2022-14/200135).

SUPPLEMENTARY MATERIAL

The Supplementary Material for this article can be found online at: https://www.frontiersin.org/articles/10.3389/fenvs.2022.916916/full#supplementary-material

REFERENCES

Allinson, M., Kameda, Y., Kimura, K., and Allinson, G. (2018). Occurrence and Assessment of the Risk of Ultraviolet Filters and Light Stabilizers in Victorian Estuaries. *Environ. Sci. Pollut. Res.* 25, 12022–12033. doi:10.1007/s11356-018-1386-7

Astel, A., Stec, M., and Rykowska, I. (2020). Occurrence and Distribution of UV Filters in Beach Sediments of the Southern Baltic Sea Coast. *Water* 12, 3024. doi:10.3390/w12113024

Astuti, R. D. P., Mallongi, A., Choi, K., Amiruddin, R., Hatta, M., Tantrakarnapa, K., et al. (2022). Health Risks from Multiroute Exposure of Potentially Toxic Elements in a Coastal Community: A Probabilistic Risk Approach in Pangkep Regency, Indonesia. *Geomatics, Nat. Hazards Risk* 13, 705–735. doi:10.1080/19475705.2022.2041110

Balmer, M. E., Buser, H.-R., Müller, M. D., and Poiger, T. (2005). Occurrence of Some Organic UV Filters in Wastewater, in Surface Waters, and in Fish from Swiss Lakes. *Environ. Sci. Technol.* 39, 953–962. doi:10.1021/es040055r

Cadena-Aizaga, M. I., Montesdeoca-Esponda, S., Torres-Padrón, M. E., Sosa-Ferrera, Z., and Santana-Rodríguez, J. J. (2020). Organic UV Filters in Marine Environments: An Update of Analytical Methodologies, Occurrence and Distribution. *Trends Environ. Anal. Chem.* 25, e00079. doi:10.1016/j.teac.2019.e00079

Cadena-Aizaga, M. I., Montesdeoca-Esponda, S., Sosa-Ferrera, Z., and Santana-Rodríguez, J. J. (2022). Occurrence and Environmental Hazard of Organic UV Filters in Seawater and Wastewater from Gran Canaria Island (Canary Islands, Spain). *Environ. Pollut.* 300, 118843. doi:10.1016/j.envpol.2022.118843

Carve, M., Nugegoda, D., Allinson, G., and Shimeta, J. (2021). A Systematic Review and Ecological Risk Assessment for Organic Ultraviolet Filters in Aquatic Environments. *Environ. Pollut.* 268, 115894. doi:10.1016/j.envpol.2020.115894

Chávez-Moreno, C. A., Hinojosa-Reyes, L., Ruiz-Ruiz, E. J., Hernández-Ramírez, A., and Guzmán-Mar, J. L. (2018). Optimization of Solid-phase Extraction of Parabens and Benzophenones in Water Samples Using a Combination of Plakett-Burman and Box-Behnken Designs. *J. Sep. Sci.* 41, 4488–4497. doi:10.1002/jssc.201800796

Chiriac, F. L., Paun, I., Pirvu, F., Pascu, L. F., Niculescu, M., and Galaon, T. (2020). Liquid Chromatography Tandem Mass Spectrometry Method for Ultra-trace Analysis of Organic UV Filters in Environmental Water Samples. *Rev. Chim.* 71, 92–99. doi:10.37358/RC.20.1.7818

da Silva, C. P., Emídio, E. S., and de Marchi, M. R. R. (2015). The Occurrence of UV Filters in Natural and Drinking Water in São Paulo State (Brazil). *Environ. Sci. Pollut. Res.* 22, 19706. doi:10.1007/s11356-015-5174-3

Dehghani, M., Shahsavani, S., Mohammadpour, A., Jafarian, A., Arjmand, S., Rasekhi, M. A., et al. (2022). Determination of Chloroform Concentration and Human Exposure Assessment in the Swimming Pool. *Environ. Res.* 203, 111883. doi:10.1016/j.envres.2021.111883

Derringer, G., and Suich, R. (1980). Simultaneous Optimization of Several Response Variables. *J. Qual. Technol.* 12, 214–219. doi:10.1080/00224065.1980.11980968

EC No 1223 (2009). Regulation (EC) No 1223/2009 of the European Parliament and of the Council of 30 November 2009 on Cosmetic Products. *Official Journal of the European Union L.* 342, 59.

Fagervold, S. K., Rodrigues, A. S., Rohée, C., Roe, R., Bourrain, M., Stien, D., et al. (2019). Occurrence and Environmental Distribution of 5 UV Filters during the Summer Season in Different Water Bodies. *Water. Air. Soil Pollut.* 230, 172. doi:10.1007/s11270-019-4217-7

Grujić, S., Vasiljević, T., and Laušević, M. (2009). Determination of Multiple Pharmaceutical Classes in Surface and Ground Waters by Liquid Chromatography-Ion Trap-Tandem Mass Spectrometry. *J. Chromatogr. A* 1216, 4989–5000. doi:10.1016/j.chroma.2009.04.059

Huang, W., Xie, Z., Yan, W., Mi, W., and Xu, W. (2016). Occurrence and Distribution of Synthetic Musks and Organic UV Filters from Riverine and Coastal Sediments in the Pearl River Estuary of China. *Mar. Pollut. Bull.* 111, 153–159. doi:10.1016/j.marpolbul.2016.07.018

Huang, Y., Law, J. C.-F., Lam, T.-K., and Leung, K. S.-Y. (2021). Risks of Organic UV Filters: a Review of Environmental and Human Health Concern Studies. *Sci. Total Environ.* 755, 142486. doi:10.1016/j.scitotenv.2020.142486

Kaiser, D., Wappelhorst, O., Oetken, M., and Oehlmann, J. (2012). Occurrence of Widely Used Organic UV Filters in Lake and River Sediments. *Environ. Chem.* 9, 139. doi:10.1071/EN11076

Kameda, Y., Kimura, K., and Miyazaki, M. (2011). Occurrence and Profiles of Organic Sun-Blocking Agents in Surface Waters and Sediments in Japanese Rivers and Lakes. *Environ. Pollut.* 159, 1570–1576. doi:10.1016/j.envpol.2011.02.055

Kunze, G., Schlifke, A., Jackson, E., Hefner, N., Berg, K., and Vollhardt, J. (2021). A Novel, Benchmark-Centered, Eco-Impact Rating System for Sunscreens and Sunscreen Formulation Design. *Front. Environ. Sci.* 9, 727404. doi:10.3389/fenvs.2021.727404

Kwon, B., and Choi, K. (2021). Occurrence of Major Organic UV Filters in Aquatic Environments and Their Endocrine Disruption Potentials: A Mini-review. *Integr. Environ. Assess Manag.* 17, 940–950. doi:10.1002/ieam.4449

Labille, J., Catalano, R., Slomberg, D., Motellier, S., Pinsino, A., Hennebert, P., et al. (2020). Assessing Sunscreen Lifecycle to Minimize Environmental Risk Posed by Nanoparticulate UV-Filters - A Review for Safer-By-Design Products. *Front. Environ. Sci.* 8, 101. doi:10.3389/fenvs.2020.00101

Li, X., Tian, T., Shang, X., Zhang, R., Xie, H., Wang, X., et al. (2020a). Occurrence and Health Risks of Organic Micro-pollutants and Metals in Groundwater of Chinese Rural Areas. *Environ. Health Perspect.* 128, 107010. doi:10.1289/EHP6483

Li, Y., Chen, L., Li, H., Peng, F., Zhou, X., and Yang, Z. (2020b). Occurrence, Distribution, and Health Risk Assessment of 20 Personal Care Products in Indoor and Outdoor Swimming Pools. *Chemosphere* 254, 126872. doi:10.1016/j.chemosphere.2020.126872

Li, C., Zhao, Y., Liu, S., Yang, D., Ma, H., Zhu, Z., et al. (2021). Exposure of Chinese Adult Females to Parabens from Personal Care Products: Estimation of Intake via Dermal Contact and Health Risks. *Environ. Pollut.* 272, 116043. doi:10.1016/j.envpol.2020.116043

Lu, J., Mao, H., Li, H., Wang, Q., and Yang, Z. (2017). Occurrence of and Human Exposure to Parabens, Benzophenones, Benzotriazoles, Triclosan and Triclocarban in Outdoor Swimming Pool Water in Changsha, China. *Sci. Total Environ.* 605-606, 1064–1069. doi:10.1016/j.scitotenv.2017.06.135

Lukić, J., Rvović, S., Đurkić, T., and Onjia, A. (2021). Procena Ekološkog Rizika Usled Prisustva Organskih UV Filtera U Vodi I Sedimentima. *Ecologica* 28, 325–330. doi:10.18485/ecologica.2021.28.102.26

Ma, B., Lu, G., Liu, F., Nie, Y., Zhang, Z., and Li, Y. (2016). Organic UV Filters in the Surface Water of Nanjing, China: Occurrence, Distribution and Ecological Risk Assessment. *Bull. Environ. Contam. Toxicol.* 96, 530–535. doi:10.1007/s00128-015-1725-z

Mitchelmore, C. L., He, K., Gonsior, M., Hain, E., Heyes, A., Clark, C., et al. (2019). Occurrence and Distribution of UV-Filters and Other Anthropogenic Contaminants in Coastal Surface Water, Sediment, and Coral Tissue from Hawaii. *Sci. Total Environ.* 670, 398–410. doi:10.1016/j.scitotenv.2019.03.034

Mitchelmore, C. L., Burns, E. E., Conway, A., Heyes, A., and Davies, I. A. (2021). A Critical Review of Organic Ultraviolet Filter Exposure, Hazard, and Risk to Corals. *Environ. Toxicol. Chem.* 40, 967–988. doi:10.1002/etc.4948

Mokh, S., Nassar, R., Berry, A., Doumiati, S., Taha, M., Ezzeddine, R., et al. (2021). Chromatographic Methods for the Determination of a Broad Spectrum of UV Filters in Swimming Pool Water. *Environ. Sci. Pollut. Res.* 29, 18605–18616. doi:10.21203/rs.3.rs-284258/v1

Radomirović, M., Ćirović, Ž., Maksin, D., Bakić, T., Lukić, J., Stanković, S., et al. (2020). Ecological Risk Assessment of Heavy Metals in the Soil at a Former Painting Industry Facility. *Front. Environ. Sci.* 8, 560415. doi:10.3389/fenvs.2020.560415

Ramos, S., Homem, V., and Santos, L. (2019). Simultaneous Determination of Synthetic Musks and UV-Filters in Water Matrices by Dispersive Liquid-Liquid Microextraction Followed by Gas Chromatography Tandem Mass-Spectrometry. *J. Chromatogr. A* 1590, 47–57. doi:10.1016/j.chroma.2019.01.013

Sánchez Rodríguez, A., Rodrigo Sanz, M., and Betancort Rodríguez, J. R. (2015). Occurrence of Eight UV Filters in Beaches of Gran Canaria (Canary Islands). An Approach to Environmental Risk Assessment. *Chemosphere* 131, 85–90. doi:10.1016/j.chemosphere.2015.02.054

Silva, C. P. D., Emídio, E. S., and Marchi, M. R. R. D. (2013). UV Filters in Water Samples: Experimental Design on the SPE Optimization Followed by GC-MS/MS Analysis. *J. Braz. Chem. Soc.* 24, 1433. doi:10.5935/0103-5053.20130182

Tashiro, Y., and Kameda, Y. (2013). Concentration of Organic Sun-Blocking Agents in Seawater of Beaches and Coral Reefs of Okinawa Island, Japan. *Mar. Pollut. Bull.* 77, 333–340. doi:10.1016/j.marpolbul.2013.09.013

Teo, T. L. L., Coleman, H. M., and Khan, S. J. (2015). Chemical Contaminants in Swimming Pools: Occurrence, Implications and Control. *Environ. Int.* 76, 16–31. doi:10.1016/j.envint.2014.11.012

Trbojević, I. S., Popović, S. S., Milovanović, V. V., Predojević, D. D., Subakov Simić, G. V., Jakovljević, O. S., et al. (2021). Substrate Type Selection in Diatom Based Lake Water Quality Assessment. *Knowl. Manag. Aquat. Ecosyst.* 21, 12. doi:10.1051/kmae/2021022

Tsui, M. M. P., Leung, H. W., Wai, T.-C., Yamashita, N., Taniyasu, S., Liu, W., et al. (2014). Occurrence, Distribution and Ecological Risk Assessment of Multiple Classes of UV Filters in Surface Waters from Different Countries. *Water Res.* 67, 55–65. doi:10.1016/j.watres.2014.09.013

Tsui, M. M. P., Leung, H. W., Kwan, B. K. Y., Ng, K.-Y., Yamashita, N., Taniyasu, S., et al. (2015). Occurrence, Distribution and Ecological Risk Assessment of Multiple Classes of UV Filters in Marine Sediments in Hong Kong and Japan. *J. Hazard. Mater.* 292, 180–187. doi:10.1016/j.jhazmat.2015.03.025

Vasiljević, T., Onjia, A., Čokeša, Đ., and Laušević, M. (2004). Optimization of Artificial Neural Network for Retention Modeling in High-Performance Liquid Chromatography. *Talanta* 64, 785–790. doi:10.1016/j.talanta.2004.03.032

Wang, S., Huo, Z., Gu, J., and Xu, G. (2021). Benzophenones and Synthetic Progestin in Wastewater and Sediment from Farms, WWTPs and Receiving Surface Water: Distribution, Sources, and Ecological Risks. *RSC Adv.* 11, 31766–31775. doi:10.1039/D1RA05333G

Wu, M.-h., Li, J., Xu, G., Ma, L.-d., Li, J.-j., Li, J.-s., et al. (2018). Pollution Patterns and Underlying Relationships of Benzophenone-type UV-Filters in Wastewater Treatment Plants and Their Receiving Surface Water. *Ecotoxicol. Environ. Saf.* 152, 98–103. doi:10.1016/j.ecoenv.2018.01.036

Conflict of Interest: The authors declare that the research was conducted in the absence of any commercial or financial relationships that could be construed as a potential conflict of interest.

Publisher's Note: All claims expressed in this article are solely those of the authors and do not necessarily represent those of their affiliated organizations, or those of the publisher, the editors, and the reviewers. Any product that may be evaluated in this article, or claim that may be made by its manufacturer, is not guaranteed or endorsed by the publisher.

frontiers | Frontiers in Environmental Science

ORIGINAL RESEARCH
published: 13 July 2022
doi: 10.3389/fenvs.2022.910234

Bacterial Cadmium-Immobilization Activity Measured by Isothermal Microcalorimetry in Cacao-Growing Soils From Colombia

Daniel Bravo *

Laboratory of Soil Microbiology & Calorimetry, Corporación Colombiana de Investigación Agropecuaria Agrosavia, Centro de Investigación Tibaitatá Km 14 Vía Bogotá-Mosquera, Mosquera, Colombia

In cacao farms, the presence of cadmium (Cd) is a major issue for commercialization, particularly for countries such as Colombia. Cadmium-tolerant bacteria (CdtB) are an important functional group of microorganisms with a potential for bioremediation strategies. Cd immobilization activity by CdtB can be accurately measured by isothermal microcalorimetry (IMC). In this study, the metabolic capacity of an entire CdtB community in cacao farm soils from three cacao-producing districts of Colombia, with and without the addition of Cd was measured using IMC. The differences between the observed peaks in metabolic activity related to Cd immobilization were analysed to determine whether activation of CdtB populations occurred when Cd content was increased. The thermograms from Santander soil samples have a major metabolic activity of the CdtB community compared to peaks of maximal heat-flow in the samples from Antioquia and Arauca. IMC showed differences in Cd immobilization ratios of the soil samples of 0.11–0.30 mg kg^{-1} h^{-1} at 25°C over 12 days of thermal monitoring. Furthermore, the amplicons of *cadA* and *smt* genes from the soil samples allow elucidation of possible metabolic mechanisms used by CdtB soil populations. The gene amplification confirmed the existence of CdtB populations related to both bioweathering and biochelating metabolic capacities. Scanning electron microscope (SEM) images supported the existence of otavite biologically induced by CdtB naturally. A Pearson correlation analysis was made between kinetical growth parameters and thermodynamic data. Besides, a PCA was performed between CdtB *cadA* gene copies, soil pH and SOM indicating the effect of CdtB in Cd translocation. Thus, it is concluded that the combination of Cd immobilization ratios obtained using isothermal microcalorimetry, the molecular basis of metabolic immobilization, and SEM imagery could act as a useful toolkit to identify CdtB populations for bioremediation strategies in contaminated cacao farms. The research importance of this study is the use of combined tools for quantitative IMC measurements to identify and assess Cd metabolic capacities of CdtB populations in soil, *in situ*, as a new proxy for CdtB assessment in cacao-growing soils.

Keywords: isothermal microcalorimetry (IMC), cadmium-tolerant bacteria (CdtB), cadmium, cacao (*Theobroma cacao* L.), metabolic activity, cocoa soils

OPEN ACCESS

Edited by:
Juan Manuel Trujillo-González, University of the Llanos, Colombia

Reviewed by:
Suzana Dimitrijevic-Brankovic, University of Belgrade, Serbia
Milan Momčilović, University of Belgrade, Serbia

***Correspondence:**
Daniel Bravo
dbravo@agrosavia.co

Specialty section:
This article was submitted to Toxicology, Pollution and the Environment, a section of the journal Frontiers in Environmental Science

Received: *01 April 2022*
Accepted: *24 June 2022*
Published: *13 July 2022*

Citation:
Bravo D (2022) Bacterial Cadmium-Immobilization Activity Measured by Isothermal Microcalorimetry in Cacao-Growing Soils From Colombia. Front. Environ. Sci. 10:910234. doi: 10.3389/fenvs.2022.910234

1 INTRODUCTION

Cadmium (Cd) is a non-essential element for almost all life systems, including humans, plants and some microorganisms (Himeno and Aoshima, 2019; Satarug, 2019). It is considered a heavy metal because is an element that have a high atomic weight and a density at least 5 times greater than that of water (Tchounwou et al., 2012) and due to its toxicity that imposes a human health risk particularly when it enters into the food chain. The European Union (EU) introduced a regulation in 2019 that indicates maximum levels of Cd in chocolates and cocoa-derivatives. This regulation can negatively affect the cacao exportations of producer countries, including Colombia, where some hotspots of high Cd content have been found in some cacao producing areas (Bravo et al., 2021). Therefore, several mechanisms of remediation are being studied to minimize Cd content throughout the cacao production chain. One understudied remediation strategy is bioremediation using Cd-tolerant bacteria (CdtB). This is an important strategy as the bioavailability and mobility of heavy metals in soils and sediments are controlled by their adsorption in soils through components such as microorganisms (Groenenberg and Lofts, 2014). **Table 1** summarizes some studies using bacteria for soil bioremediation techniques.

CdtB are a non-phylogenetically related group of bacteria with the exceptional capacity of metabolize Cd and using it as source of energy (Bravo and Braissant, 2022). Their metabolic capacity may vary depending on the soil type, the soil Cd content as well as other soil characteristics (Bravo et al., 2018). The co-metabolism has been noted in this functional group, because the expression of Cd immobilization capacity is also related to P and K solubilization capacities. This has been highlighted in previous studies with CdtB isolated from cacao-growing farms in Colombia (Bravo et al., 2018). However, to date, the metabolic activity of these soil bacterial populations has not been assessed *in situ* in relation to the bioweathering of Cd into non-soluble forms such as secondary otavite.

The isothermal microcalorimetry method (IMC), is a sensitive and non-destructive approach to assess bacterial metabolic activity (Braissant et al., 2010) and could be useful to monitor the metabolic ratios of Cd immobilization in soil. This technique, in combination with methods to determine viability, vitality and metabolic rates of microorganisms could be an excellent proxy to assess overall Cd metabolism (Bravo et al., 2018; Braissant et al., 2020). Besides, the amplification of genes related to Cd immobilization is a first step to know if CdtB population are present in the bacterial community. The *CadA* and *smt* genes have been highlighted as an important resource to estimate the presence of CdtB (Bravo and Braissant, 2022).

In previous studies in Central and South America (Chavez et al., 2015; Gramlich et al., 2018; Engbersen et al., 2019; Ramtahal et al., 2019), including Colombia (Gil et al., 2022), physical and chemical soil parameters, such as soil pH, soil organic matter (SOM) and the Cd values in soils have been identified as having a major influence on the final content of Cd in cacao beans. However, the role *in situ* of CdtB in translocation rates of the metal from soil to crop hast not been studied.

This study aims to compare the IMC thermograms of CdtB in soils with 1) a molecular tool, the PCR amplification of genes *CadA* and *smt,* related to Cd immobilization of the soils used; 2) a visualization tool, the scanning electron microscope (SEM) imagery of the soil samples assessed, and 3) the use of reference CdtB strains to compare the Cd tolerance with each method. Moreover, the inclusion of soil parameters such as soil pH, SOM, average soil Cd values and average cacao bean Cd values, will allow an increase in our understanding on the role of CdtB with the Cd translocation from soils to the cacao beans, from which chocolate is made.

2 MATERIALS AND METHODS

2.1 Study Area

The soil samples were collected from cacao-growing farms located in three cacao districts in Colombia. The districts were Antioquia, Arauca and Santander. The location districts were selected due to their high production and the economic importance of cacao in Colombia. **Figure 1** shows the location of sampling sites. Each sample consisted of a composite sample made by mixing soil samples from 20 farms within each of the

TABLE 1 | Summary of significant studies using bioremediation techniques in agricultural soils.

Bacteria	Crop/Niche	Bioremediation Technique	Cd Immobilized [mg kg^{-1}]	References
Microbacterium sp. D2-2	*Andropogon gayanus*	mixture of chitin, peat and microbial biomass	222.22[a]	Long et al. (2021)
Bacillus sp. C9-3	*Andropogon gayanus*	mixture of chitin, peat and microbial biomass	163.96[a]	Long et al. (2021)
Pseudomonas putida	paddy soils	mixture of goethite, humid acid and microbial biomass	4.68[b]	Qu et al. (2021)
Desulfobacter spp.	farmland forming soil of greenockite/ hawleyite	ZnS biomineralization	0.25[b]	Liu et al. (2020)
Alcaligenes eutrophus CH34	paddy soils	Chemisorption	5[b]	Diels et al. (1995)
Enterobacter sp. CdtB41	cacao (*Theobroma cacao* L.)	bioweathering of Cd binding Zn	2.5[b]	Bravo et al. (2018)
C. taiwanensis DSM 17343	Rice (*Oryza sativa*)	Bioweathering	0.5[b]	Siripornadulsil et al. (2014)

[a]*Natural Cd content in soil.*
[b]*Spiked Cd content in steady-state experiments.*

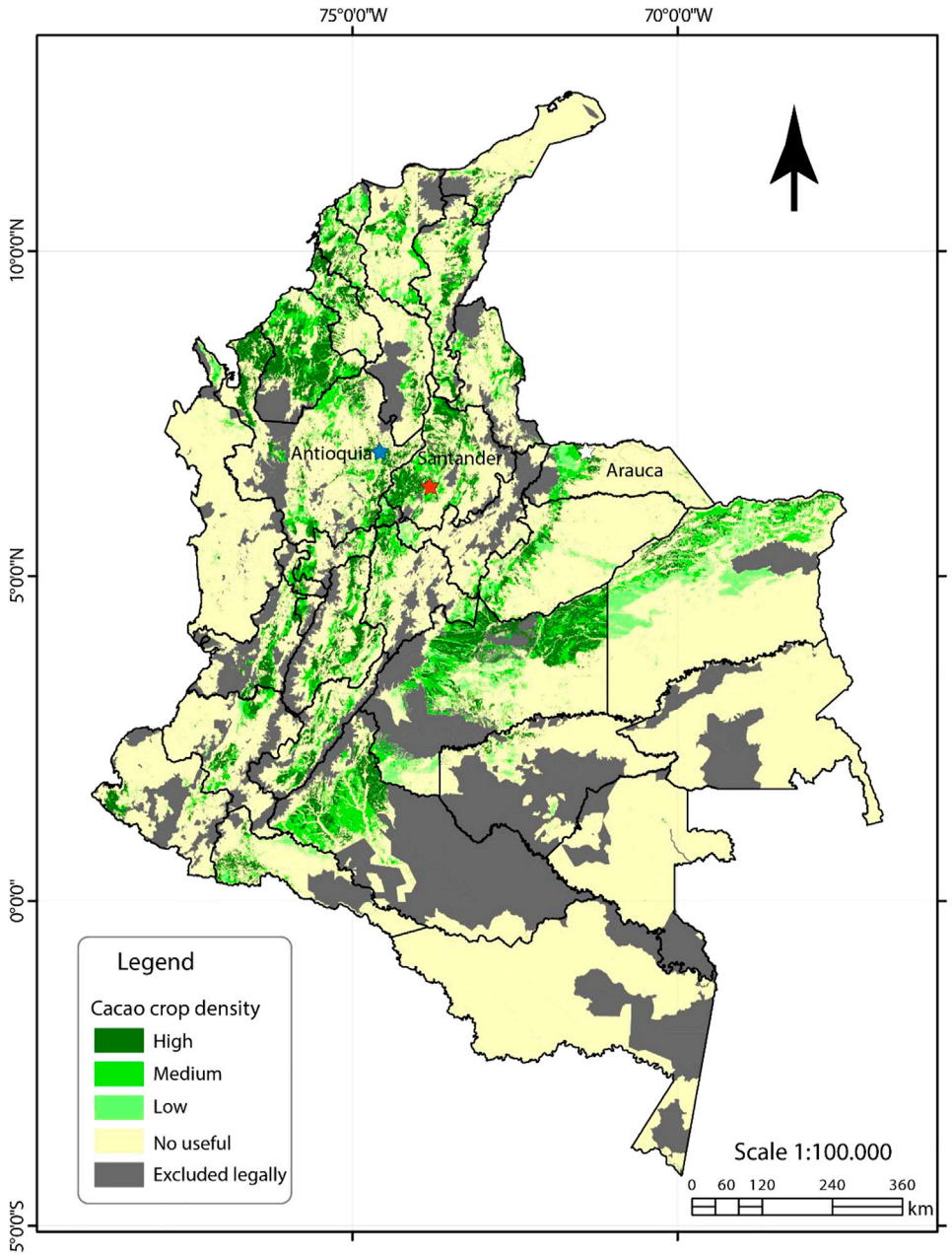

FIGURE 1 | Locations of the assessed composite soil samples. Each composite soil sample was compiled based on the sampling of 20 cacao-growing farms at each location. Therefore, a representativeness was assured for each location, selected for its traditional land uses for cacao production and high yielding of fine flavour and aroma beans. In Antioquia district, the blue star included 20 samples from cacao-farms located in San Roque and Yolombó municipalities as part of the middle Magdalena mountain-system. The soil samples from the 20 assessed farms in Arauca are represented by a white star and are located in the municipality of Arauquita. In Santander, the 20 soil samples of farms assessed represented by a red star belongs to farms located in both San Vicente de Chucurí and El Carmen de Chucuri municipalities, as part of the Montaña Santandereana in the east cordilleras mountain-system. Adapted from UPRA's map 2019.

three districts. The soil type from Antioquia farms were classified as soils belong to the subgroup *Oxic Dystrudepts* of Inceptisols (Gil et al., 2022). The soil type of cacao farms sampled from Arauca were classified as *Typic Endoaquepts* of Inceptisols (Bravo and Benavides-Erazo, 2020). Moreover, the soil type observed in the 20 farms assessed in Santander district were classified as Entisols (Bravo et al., 2018). Two kg of composite samples were formed by collecting 0.4 kg of soil in a zip bag taken at 30 cm of soil depth and at 70 cm around five cacao trunks, distributed in zig-zag, in the centre of the farm. Quantification of Cd soil content and Cd in beans was conducted previously in these farms (Bravo et al., 2021). One set of soil samples was measured with 'natural Cd content' and the other set of the same samples was 'spiked' with 1 mg kg^{-1} of $CdCl_2$. This is

necessary in order to exhibit increased metabolic capacities of CdtB in soil samples, especially for IMC measurements. The samples were collected and transported and the assays were done at the Tibaitatá Research Centre of the Corporación Colombiana de Investigacion Agropecuaria–Agrosavia, in Mosquera, Colombia. The soil samples from each location were used for several experimental approaches detailed below.

2.2 IMC Measurement

For calorimetric assessment, the soil samples were sieved to avoid roots and particles bigger than 0.2 mm, therefore, a sieve with filter of 0.2 mm particle size was used in sterile conditions with a new sieve for each sample. Five grams of soil was added to glass ampoules of 20 mL. The samples were diluted in 10 mL of Mergeay medium (Bravo et al., 2018). The same amount of sample was amended with 10 mL of Mergeay medium containing 6 mg L^{-1} of $CdCl_2$ (Sigma Aldrich, IL, United States). The amendment was included to excite both fast- and slow-growing CdtB populations. The samples were stirred with an electric stirring device adapted for mixing the soil samples with the media, which is constructed with a rotating stick and a stirring motor (TA Instruments, Delaware, United States; see http://www.tainstruments.com/wp-content/uploads/TAM-AIR-brochure.pdf, page 7). The stirring was at a constant of 80 rpm during all the thermal monitoring. This increases the heat-flow signal for target bacterial populations. The ampoules were inserted into the channels of a TAM Air 8 channels isothermal microcalorimeter (TA Instruments, Delaware, United States). The thermal monitoring was performed at 25°C for 12 days. This time is sufficient to perceive heat-flow from both, fast- and slow-growing CdtB populations.

2.3 Cadmium Immobilization

In parallel with the calorimetric experiment, a batch experiment was conducted to assess the Cd immobilization capacity of the CdtB populations from the soil samples. Five grams of the same soil samples were diluted in 500 mL of Mergeay medium amended with 6 mg L^{-1} of $CdCl_2$. The samples were incubated at 25°C and shaken at 200 rpm for 12 days. Samples were taken at each 4 h. The strain *Cupriavidus taiwanensis* DSM17343 was used as positive control. The strain was grown in 500 mL of Mergeay liquid medium amended with the same concentration of Cd. *Escherichia coli* K12 DSM498 was used as a negative control which has been recognized as a non-tolerant Cd bacterium. To calculate the Cd immobilization ratios the pseudo-total Cd values were quantified in the subsamples and the controls. Cd was quantified by inductive coupled plasma with optical emission spectrometry (ICP-OES) in the supernatant. The digestion of samples and the conditions for ICP readings were carried out according to a previous methodology reported (Bravo et al., 2018). The residual Cd values were considered as the fraction of Cd that was not metabolized by CdtB in the soil sample or in the bacterial biomass, respectively.

2.4 *CadA* and *smt* Genes

To assess the presence of genes related to Cd immobilization, PCR amplifications of *CadA* and *smt* genes from soil samples were performed. The amplicons used were designed for CdtB populations. The primers used for *CadA* were Primer 1 forward: 5′AARACIGGIACIYTIACIAARGGIG3′, and Primer 2 reverse 5′GIGCRTCRTTIACICCRTCICCIA3'. The primers for *smt* were: primer 1, smt1, forward: 5′GAT CGA CGT TGC AGA GAC AG 3′ and primer 2, smt2, reverse: 5′GAT CGA GGG CGT TTT GAT AA 3'. These primers were designed from a consensus of available data (Naz et al., 2005; Aryal, 2020). The fragments obtained for *CadA* and *smt* genes were between 300 and 370 bp, respectively. The PCR was done using a master mix of, with a gold master mix solution (Qiagen, Germany), according to a previous study (Bravo et al., 2015). As a positive control the gene was amplified from DNA extracted from the strain *C. taiwanensis* reported previously as CdtB (Siripornadulsil and Siripornadulsil, 2013). Real-time quantitative PCR reactions were performed on an iCycler IQ5 real-time PCR System using the iQ SYBR Green supermix System (Bio-Rad, Hercules, CA, United States). The qPCR was performed in triplicate. The amplification of *CadA* gene in a final volume of work of 10 µL was carried out. Two µL of the diluted DNA from soil were mixed with 0.25 µL of the primers above-mentioned (final concentration of 1.25 µM). Five µL of SYBR green PCR kit (Qiagen, Germany) was included. The mix was diluted to 10 µL adding RNAase-free nanopure water. The qPCR program was a per previous work (Bravo et al., 2013). A standard curve and *Ct* values were obtained with dilutions of known copy numbers of the target gene from DNA from the positive control strain *C. taiwanensis* DSM17343.

2.5 SEM Measurement

To visualize the CdtB active in soil samples, a SEM imagery was performed. The samples were taken when maximal peaks of heat-flow were observed during IMC experiments. The SEM was carried out using a protocol previously reported for bacteria visualization (Páez-Vélez et al., 2019). An aluminium support was used for fixing the samples with an exposure time of 50s. A quantification of the metal and other related ions were done in spectra performed with energy dispersive X-ray spectroscopy (EDS) coupled to the SEM, using the equipment JEOL JSM-6490LV (JEOL, Tokyo, Japan). The scanning electron microscope was equipped with an Oxford INCA PentaFetX3 EDS detector. The range of visualization was screened through the slide of 2 cm^2 and the images were taken in a range between 0.2–7 µm. Magnification scales were included on each micrography.

2.6 Soil Parameters and Cd Determinations

Soil pH was measured in each sample. The soil pH was assessed with a pH meter (Toledo, Spain) according to a previous method (Gil et al., 2022). The soil organic matter was quantified by atomic absorption spectrometry (Agilent Technologies, CA, United States). The method to estimate the percent of SOM was also previously reported (Bravo et al., 2021). Cd content in leaves and in cacao-beans (fermented and dried) was quantified with ICP-OES according to a methodology established previously (Rodríguez Giraldo et al., 2022), at the laboratory of chemistry of Agrosavia, C.I. Tibaitatá, in Mosquera, Colombia.

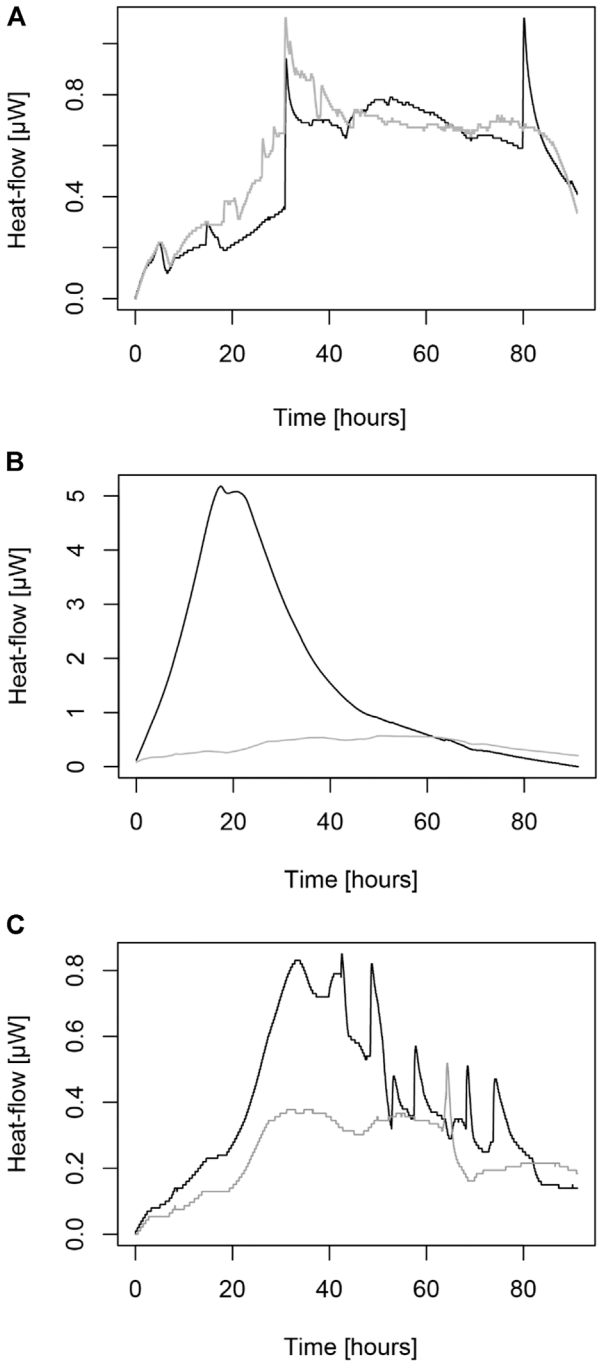

FIGURE 2 | Thermograms of IMC showing the heat-flow of Cd metabolic activity in soils. **(A)** the heat-flow of soils from Antioquia. **(B)** the heat-flow of soils from Arauca. **(C)** the heat-flow of soils from Santander. Grey lines correspond to samples with natural Cd content. Black lines correspond to the metabolic activity of samples amended with 1 mg kg^{-1} of Cd.

2.7 Data Analysis

The IMC data was used to integrate the heat-flow into heat in Joules. Once integrated, the data were fitted with the Gompertz equation of bacterial growth (Zwietering et al., 1991; Braissant et al., 2013). This equation was used to estimate the growth rate (μ), the maximal growth rate (μ_{max}), the adaptation phase lambda (λ), the time to reach the maximum peak of heat-flow (TTP) and the maximum heat produced (Q_{max}). With the Cd immobilization test, it was possible to estimate the Cd immobilization ratio (Cd_{imm}) (Bravo et al., 2018) in the soil samples assessed.

For all the experimental setups, three replicates were considered for each treatment and the data are shown as mean values. A Pearson correlation was performed between the kinetical growth parameters and the thermodynamic parameters. A PCA corelation analysis was performed to see if the gene amplification of *CadA* is related to soil pH and SOM, and to elucidate if the CdtB populations have an influence on Cd values found in soils and cacao beans.

3 RESULTS AND DISCUSSION

3.1 How IMC Improve Our Knowledge on Functional Activity in Soils

Three composite soil samples were used to study the metabolic activity of Cd immobilization due to CdtB metabolism. The thermograms from **Figure 2** show the differences between the metabolic fluxes of Cd, particularly when the CdtB populations are excited due to spiking with Cd in a soluble form, with $CdCl_2$. In natural Cd conditions even if high Cd values have been found in some hotspots in Colombia (i.e., in some farms from Santander or Arauca), much more activity is found in soil samples spiked with exogenous Cd soluble solution than in natural Cd in soils. Interestingly, when Cd was amended in all samples a second peak of heat-flows appears after 96 h, showing the metabolic flux of slow-growing CdtB. In samples where no Cd was added, only the first peak occurring at 24–48 h is attributed to the metabolic rates related to Cd use by fast-growing CdtB.

Table 2 shows both the kinetical growth and the thermodynamic parameters obtained by IMC after fitting the Gompertz equation (Zwietering et al., 1991) into the edited data. Interestingly, both sets of parameters show the metabolic capacity of CdtB populations *in situ*, with a Cd_{imm} from 0.16 to 0.30 mg $kg^{-1}h^{-1}$. **Figure 3** shows a high correlation between the heat-flow and the maximum heat released by the soil samples both for natural Cd content and amended with 1 mg kg^{-1} Cd. The coefficient of determination is higher in natural conditions than those amended with Cd. However, it is highlighted that in both cases, the coefficient of determination is high enough for field samples measured by IMC. This has been also observed in previous metabolic measurements in a metabolic pathway related to C sequestration (Bravo et al., 2011; Bravo et al., 2015). Likewise, **Figure 4** shows a correlation between the maximum growth rate (μ_{max}) and the adaptation phase (λ) of CdtB exposed to natural Cd content or the amendment with Cd. This correlation shows two conditions. One condition, when CdtB are exposed to high adaptation phases and low growth. The other condition, when CdtB expresses a fast adaptation phase and a major maximum growth rate. The second condition might be of use for selecting viable cultures of CdtB to propose for bioremediation processes of Cd in cacao soils. The use of IMC

TABLE 2 | The kinetical growth and the thermodynamic parameters found in the assessed composite soil samples from Antioquia, Santander and Arauca. The parameters were calculated fitting the Gompertz equation with the edited data obtained from the heat-flow over time (thermograms), by IMC.

	Soil Sample	λ [h^{-1}]	μ [h^{-1}]	μ_{max} [h^{-1}]	TTP [h^{-1}]	Q_{max} [J]	Cd_{imm} [mg $kg^{-1}h^{-1}$]	*p*-value
Natural Cd 2.2 mg kg^{-1}	Antioquia	3.00 ± 0.003	1.40 ± 0.002	1.60 ± 0.003	36.00 ± 0.001	0.13 ± 0.002	0.16 ± 0.002	0.998
	Arauca	2.00 ± 0.008	0.02 ± 0.001	0.03 ± 0.002	58.00 ± 0.002	0.02 ± 0.001	0.11 ± 0.001	0.996
	Santander	2.80 ± 0.002	0.38 ± 0.006	0.41 ±0.004	33.00 ± 0.003	0.10 ± 0.001	0.12 ± 0.001	0.997
Cd spike 1 mg kg^{-1}	Antioquia	3.00 ± 0.004	1.80 ± 0.008	1.90 ± 0.003	79.00 ± 0.002	0.15 ± 0.001	0.30 ± 0.003	0.998
	Arauca	20.00 ± 0.006	5.20 ± 0.005	5.40 ± 0.004	17.00 ± 0.004	0.50 ±0.003	0.21 ± 0.005	0.999
	Santander	3.10 ± 0.005	1.30 ± 0.004	1.80 ± 0.007	43.00 ± 0.003	0.12 ± 0.002	0.25 ± 0.002	0.998

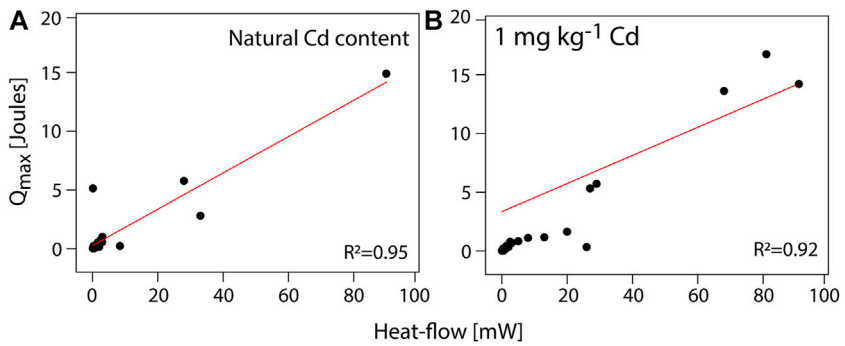

FIGURE 3 | A Pearson correlation between heat-flow and the maximum heat obtained by IMC of composite soil samples exposed to **(A)** natural Cd content and **(B)** an amendment with 1 mg kg^{-1} $CdCl_2$ ($p \leq 0.005$).

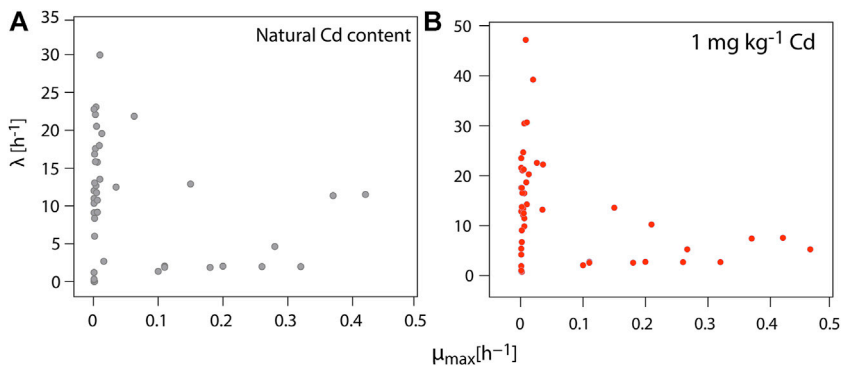

FIGURE 4 | A Pearson correlation between the maximum growth rate and the adaptation phase of the CdtB populations into the composite soil samples, when exposed to **(A)** natural Cd content and **(B)** an amendment with 1 mg kg^{-1} of $CdCl_2$. The kinetic growth parameters were calculated after fitting the edited data with the Gompertz equation ($p \leq 0.005$).

in soil samples with natural Cd content, or in amendment with soluble source of Cd is an important tool to select specific CdtB populations, because fluctuations in energy availability can alter microbial activity related to Cd (Hart and Gorman-Lewis 2021), and thus, the capacity to adapt it to enriched soils where a bioremediation process needs to be settable.

This study highlights, the IMC method to characterize the metabolic activity of soil samples with natural content or spiked with Cd. With the heat-flow it is possible to fit a mathematical equation based on heat production. This feature is the main thermodynamic condition to access kinetical growth parameters of total microbial community, exhibiting the CdtB populations. It is worth mentioning, that spiked samples increase the growth rates, as well as the Q_{max} values. This is related to the increasing Cd immobilization capacity. It has been observed that CdtB have the property to increase in biomass (i.e., from 0.03 to 5.40 h^{-1} in Araucan sample) when increasing concentrations of Cd appears in the surroundings (i.e., from 0.11 to 0.21 mg kg^{-1} in Araucan sample). This has not been well documented before. Furthermore, it is pointed out that, the adaptation phase increase when soil

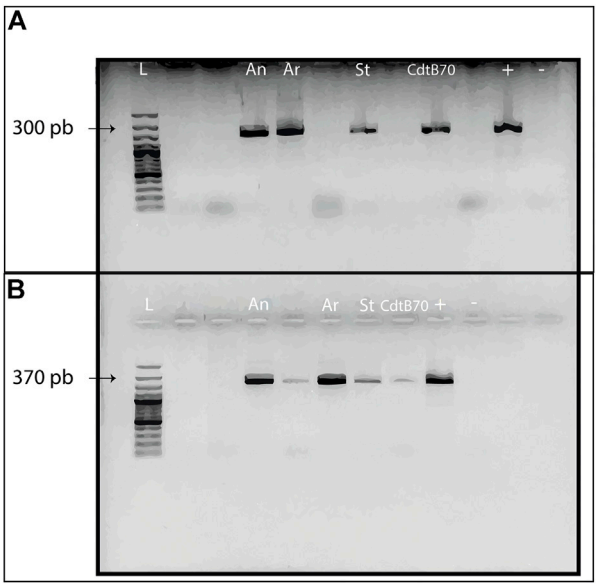

FIGURE 5 | PCR amplifications of genes implied in Cd immobilization through the bioweathering pathway. **(A)**. *CadA* amplicons from composite soil samples. **(B)**. *smt* amplicons from the assessed soil samples. Conventions: L = Ladder; CdtB70 = CdtB strain from Santander, Colombia; + = Positive control strain *Cupriavidus taiwanensis* DSM17343; - = Negative control, ultra-nanopure sterile H_2O with dimer-primers.

samples were spiked with Cd. This could be related to the time the CdtB needs to make the metabolic switch from a minimum to a high toxic level of the metal in soil. This is also supported by changes observed with the TTP parameter where three major changes were observed when soil was spiked: 1) passing from fast to later peaks of metabolic activity; 2) increasing the signal of metabolic peaks and 3) yielding greater metabolic peaks that otherwise could not be possible to observe (see **Figures 2A,C**). Regarding the spiked soil samples, the first peak corresponds most likely to direct Cd consumption by faster growth rates of CdtB (i.e., Bacilli-like), due to availability of highly soluble forms of Cd, such as the most frequently bioavailable Cd^{2+} (Meter et al., 2019), which is the major Cd source added to the soil. The second peak could represent either the use of Cd by bacteria with slower growth rates (e.g., *Streptomyces*-like or actinomycetes-like) or the consumption of a less accessible pool of Cd, such as colloids of Fe/Mn oxides and phyllosilicates (Muehe et al., 2013; Bravo et al., 2018).

3.2 Cd Immobilization Capacity of CdtB in Soil

The parallel batch experiment to IMC shows that autochthonous populations of CdtB in composite soil samples from Antioquia exhibited major Cd immobilization capacities (0.30 mg kg^{-1}) compared to those from Santander (0.25 mg kg^{-1}) and Arauca (0.21 mg kg^{-1}) after 12 days of incubation. It is important to mention that at this stage, the immobilization capacity was measured without any other mechanism to enhance the metabolic capacity. Therefore, a selection of microorganisms and the design of inoculums with high performance in formulated environments might increase the metabolic activity assessed in this study.

The soil samples were used to amplify two genes involved in Cd immobilization. **Figure 5** shows the PCR amplification of genes *CadA* and *smt*. The bands correspond to the amplification of several populations with the gene present in soils. Even if the amplification does not mean that all the populations that have these genes are active, the brightness and width of the bands indicate a good concentration of the genes within the whole community of the composite soil samples. *CadA* gene is implied in cation pump exchange at periplasmic level, where internalization through the bioweathering pathway is the first step towards biological induction of $CdCO_3$ or secondary otavite (Bravo and Braissant, 2022). Likewise, *smt* gene is involved in the regulation of ATPase dependant on reduction of Cd from soluble forms such as chlorates, or sulphates present in soil that CdtB transforms into non-soluble and geostable forms. The amplification of the *smt* and *CadA* genes is of note because they are related to metabolic pathways where the energy activation (ATPase systems) is needed, which could be expressed by the activation of the *cad* operon. The P-type ATPase efflux system causes transport of the metal by ATP hydrolysis, so the reaction is considered endothermic, due to the need for energy to hydrolyse ATP (Bravo and Braissant, 2022). This implies that the presence of these genes from CdtB populations in the assessed soil samples requires energy, which is confirmed by the endothermic reactions observed in **Figure 2**, and the last values of **Figure 3**, particularly when Cd is amended.

3.3 Bioweathering of Cd by CdtB in Soils: From Soluble to Sequestered Forms

Using scanning electron microscopy with energy dispersive spectroscopy (SEM/EDS) it was possible to visualize the presence of CdtB in samples where $CdCl_2$ was amended to excite CdtB populations over the whole bacterial community. The presence of Cd^+ and CO^- as precursor of $CdCO_3$ were detected in EDS spectra. These are known to be biologically induced. **Figure 6** shows the presence of CdtB in samples from each spiked composite soil sample. The figure highlights the presence of several morphologies and shapes of CdtB populations, which are indicated with an asterisk in the microphotographs and $CdCO_3$, indicated with white arrows. It is assumed that the observed morphotype corresponds to the target populations. It is worth mentioning that the Cd content at the concentration added, negatively affects the growth of any microorganism not-tolerant to the metal (Bravo et al., 2018), therefore, the observed morphologies corresponds exclusively to CdtB. Furthermore, with the SEM/EDS system it was possible to examine micro-scale features of the soil samples with Cd. The EDS system make enough magnification possible to detect Cd chemical elemental composition. As pointed out in **Figure 6**, on the surface of the tested soil samples Cd was detected with carbonate aggregations in each sampled assessed with higher presence of C and O atoms at the samples. Thus, the inclusion of

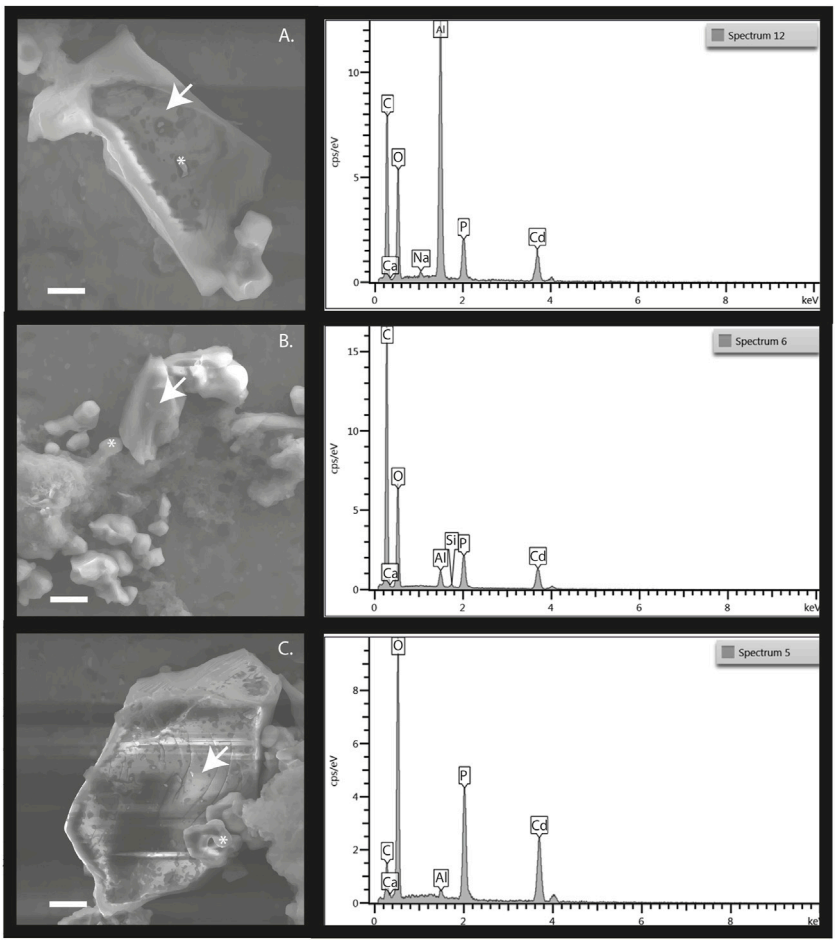

FIGURE 6 | SEM-EDS of composite soil samples from **(A)**. Antioquia, **(B)**. Arauca and **(C)**. Santander. The micrographs shown the presence of CdtB and the presence of cadmium carbonate or otavite ($CdCO_3$). The white arrows point out the aggregates microbiologically induced. The presence of CdtB is highlighted by white asterisks. the EDS spectra show a greater presence of C, O ions, and the presence of Cd in all cases.

this technology to the IMC technique allows an increase in our existing capacity to provide evidence of Cd bioweathering of total CdtB community, using a complete testing package, including metabolic capacities in surface soil micro-particle analysis, such as in this case, in field cacao evaluations.

The PCA is shown in **Figure 7**. The PCA suggest that Cd in cacao beans is well explained by the factors assessed in this paper. The soil samples were clustered by location. The scale shows the Cd content in cacao beans as a reference variable. According to the scree plot, the percentage of explained variances was 61.1% on principal component 1 (see **Supplementary Figure S1**). Interestingly, Cd in soils is more related to soil *CadA*, soil pH, and SOM than Cd in cacao beans. This indicates that the presence of some genes could have more interaction in some soil Cd than others.

Another important variable to have into account is the type soil related with Cd immobilization capacity of CdtB. In this study three soil origin were confirmed. The soil type from Antioquia belong to the subgroup *Oxic Dystrudepts* of Inceptisols with some presence of Cd-like rocky types mainly in the forms of "Antioqueño Batholites" (Gil et al., 2022). The soil type of cacao farms from Arauca were Typic *Endoaquepts* of Inceptisols, with low levels of clay content (1.15%), SOM (less than 3%), and lower patchy parent material in alluvial sediments in farms nears to the rivers (Bravo and Benavides-Erazo, 2020). Moreover, the soil type observed in farms of Santander were Entisols made from the *Umir formation*, which is a lithostratigraphic unit, with high clay content around 85%, SOM of 5–20% and high heterogenous presence of Cd-rocky types mainly granitoids and some spots of shales, that have been detected in the central zone of Santander district (Bravo et al., 2018). Therefore, the relationship between the origin of soil with the chemical properties, may have an influence in the CdtB Cd immobilization capacity because the changes in soil type exert changes in potential capacity of phenotypic capacities of CdtB community due to the soil pH, clay content, the SOM percentage and the distribution of Cd, as mentioned previously. Nonetheless, **Figure 7** shows that, even if pH is a well correlated variable to Cd in soil, there are other not directly related factors, such as the Cd content in cacao beans, which it has been also suggested by other authors (Argüello et al., 2019). This study supports the

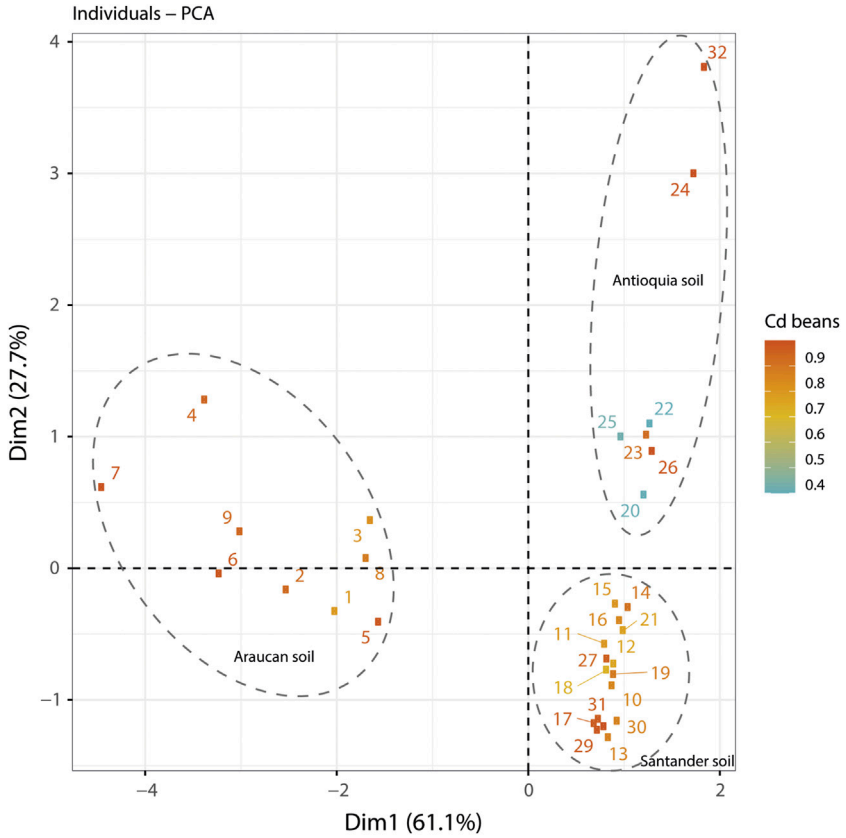

FIGURE 7 | A PCA analysis of soil samples from Antioquia, Arauca and Santander. The scree plot suggested that 61.1% of the explained variances were observed in dimension 1. The origin of soil samples was clustered into each assessed location. The scale shown the Cd content in cacao beans as reference variable.

observation where more Cd in soils correlate with less in cacao beans, however, it also suggests that the presence of CdtB might have an influence on Cd geoaccumulation and Cd translocation factors, when the metabolic activity of microorganisms tolerant to the metal is included.

3.4 Cd: The Geoaccumulation Index (I_{geo})

The geoaccumulation index (I_{geo}) was introduced by Müller in 1969 (Muller, 1969) and refers to the assessment of the degree of heavy metal (including Cd) enrichment due to 1) anthropogenic pollution, 2) the geochemical background values at the location and 3) the effect of natural diagenesis (Bravo and Braissant, 2022). Since the I_{geo} takes into account Cd measured in the rhizospheric zone, the sum of the three components explains the Cd content. The anthropogenic contribution can be calculated by the Cd input of fertilizers, manure or compost elements, mining, industry and petroleum extraction. In the soils collected from farms in Santander, the presence of coal mines might be an important form of Cd input. In soils collected from Arauca, petroleum refineries are nearby the cacao farms. The main anthropogenic factor influencing Cd input to the cacao system it seems to be due to P-like fertilizers with values greater than 60 mg kg^{-1} Cd (Bravo et al., 2022). However, it is likely that anthropogenic pollution is of minor importance.

Interestingly, there are strong differences between the geochemical background values from soil samples to each assessed district. Santander is known to have some hotspots of high Cd background in the soil (Bravo et al., 2021) with some spots of shales (Bravo et al., 2018), while soil samples from Antioquia (Gil et al., 2022) are rich in Batholite. This geological background is important due to the sedimentary process resulting in outcroppings that migrates from the subsoils (mainly by capillary fringe fractures) to the topsoil (mainly in the vadose zone).

On the contrary, soils from Arauca had lower values of Cd, supported by a lower geochemical background. However, the effect of natural diagenesis of Cd mobilized by the river and found in sediments, combined with phosphorites (Bravo et al., 2018), seems to be the key for faster release of available Cd at that location.

To this, it is important to add the translocation factor or TF of plants (Wiesler, 2012), especially in the case of the hyperaccumulator plant *Theobroma cacao* L. (Kirkham, 2006). The TF is the ratio of the Cd found in plant tissue and total Cd value found in soil (Roslan et al., 2016). The TF factor is particularly useful when it is compared to the pseudo-total Cd from soils with available Cd from plant tissue. Combining this with the I_{geo}, could improve the understanding on the origins of

pseudototal Cd in soils, where the available fraction is recovered. In this, the role of CdtB is intriguing, because the bacterial metabolic pathways might induce a trade-off between solubilizing or weathering Cd in the cacao-soil system. Therefore, both the I_{geo} and the TF should take into account the role of CdtB in rhizosphere of cacao plants.

3.5 CdtB as Critical Factor in Cd Accumulation

This study suggests that the combination of Cd_{imm} ratios obtained using isothermal microcalorimetry, the molecular basis of metabolic immobilization, and SEM imagery could be seen as a useful toolkit to select CdtB populations for bioremediation in contaminated cacao farms. The accumulation of Cd in cacao is cyclic, and therefore, depends on translocation fluxes from the underground to the topsoil, thus, the rhizosphere of cacao is an area of high Cd movement. It is worth mentioning, that not all the Cd found in subsoil, is retrieved in the cacao beans via root system. It has been estimated that approximately 60% of Cd in the cacao-growing soils is related to the acid-soluble fraction and bound to organic matter (Chavez et al., 2016), that might enter in some soil types, the roots as part of the so-called 'available Cd' and finally into the food chain. But how much of Cd could be regulated in the rhizosphere modifying the percent available into non-soluble forms of the heavy metal? The answer is in the metabolic activity of CdtB and its regulatory capacity of edaphic conditions in the surrounding soil.

In a recent review, it has been demonstrated that CdtB participate in at least seven known metabolic pathways that affect the Cd content in soil (Bravo and Braissant, 2022). The metabolic condition regardless of the availability of Cd, is excited by CdtB present in soil. How can we increase this metabolic capacity to kick-off bioremediation strategies in order to tackle Cd entry into the food chain? One key point in the bioremediation is the bioaugmentation of CdtB so that the biomass concentration is great enough to deal with high values of Cd, including the phytoavailable and the aqueous-phase fractions. But this is just the first step. It is necessary to go in deep into the metabolic mechanisms that rule CdtB via bioweathering, biochelation, or even by biosorption, or the metabolic pathway they are capable to exhibit. A compromise between the design of new culture media adapted to the CdtB metabolic capacities and increasing biomass production, could be a second stage in the strategy. However, at that point, there remain a set of questions that need to be addressed. For instance, what is the effect of the bioaugmentation of CdtB populations on the ecology of the cacao-soil system? or what is the effect of the bioaugmented microbial biomass applied in cacao-growing soils on the nutrition cycling of cacao plantation? Moreover, does the applicability of CdtB for bioremediation in other cacao growing areas around the world remain effective?

These questions require more researchers in bioremediation, to make the necessary probes that cover enough criteria to obtain a bioformulation that meets with the standards required to generate successful remediation. This focus has started in Colombia, however a joint-effort research project in cooperation between Colombia, Ecuador and Costa Rica allows inclusion of the bioremediation strategy as one of the proposed applications in field semi-controlled experiments. This approach could be also applied to other heavy metal pollution issues in cacao. For instance, the main issue in terms of heavy metals in Brazilian cacao plantations is not cadmium but lead. The presence of Pb-tolerant bacteria could be useful to explore using the chemometric approach here proposed. Interestingly, in all the above-mentioned stages, the IMC in combination with molecular tools and visualization of the probes, might yield high quality information to allow more detailed research in the bioremediation of complexes systems such as that found in a cacao plantation.

4 CONCLUSION

This study demonstrates the use of data from a combination of technical tools including isothermal microcalorimetry, to assess metabolic Cd immobilization capacity from total CdtB community in cacao-growing soils. This study highlighted the IMC method to characterize the metabolic activity of soil samples with natural Cd or spiked with it. This allows observation of differences between the metabolic fluxes of Cd, particularly when slow-growing CdtB populations (more likely of actinomycetes-like class) were excited with $CdCl_2$ after 48 h of thermal monitoring, where a less accessible pool of Cd is found. The kinetic growth and thermodynamic parameters derived from IMC data are important criteria to recognize and select potential bioremediation populations with highly correlated factors such as heat-flow with maximum heat (Q_{max}) as well as the maximum growth rate and lambda.

The IMC combined with Cd immobilization test confirmed that the CdtB community in Antioquian soil samples have major Cd immobilization rates ($0.30\ mg\ kg^{-1}$) compared to the other sites sampled. The thermograms of IMC confirmed a major metabolic flux of Cd with the presence of major peaks of activity in both natural- and spiked-Cd soil samples. The presence of both, *CadA* and *smt* genes supported the metabolic mechanisms that CdtB uses to be a bioweathering pathway. IMC confirmed this pathway since both are endothermic reactions due to the regulation of ATPase dependant mechanisms that bind Cd into geostable forms. Likewise, the SEM/EDS imagery show the presence of both autochthonous CdtB populations and $CdCO_3$ confirmed by the EDS spectroscopy. These results support the evidence of a bioweathering process occurring due to the metabolic activity observed by IMC.

The PCA performed suggested correlations between Cd in cacao beans with some key parameters in cacao-growing soils, such as *CadA*, pH and SOM. The soil type and origin influences the variation of these soil parameters into each set of soil samples from the three cacao-growing districts assessed in this study. The correlation between Cd in soils with Cd in beans was discussed in two main processes by which CdtB might have

an influence: the Cd geoaccumulation index (I_{geo}) and the translocation factor TF in cacao plants.

In conclusion, the geomicrobiological aspects of the presence of total community of CdtB was possible to described using a chemometric approach. This study supports the idea that the role of CdtB is underestimated and is a key critical factor in Cd accumulation in cacao-growing farms. The combination of IMC with other molecular, statistical and theoretical tools could be seen as a useful toolkit for the chemometric approach for bioremediation of contaminated cacao farms. To expand the applicability of this approach, broad field-based experiments should be included in cacao plantations in other countries with the same issue.

DATA AVAILABILITY STATEMENT

The datasets presented in this article are not readily available because the raw data supporting the conclusions of this article will be made available by the authors, once requested officially to Agrosavia intellectual property department. Requests to access the datasets should be directed to dbravo@agrosavia.co.

AUTHOR CONTRIBUTIONS

DB contributed to collecting the data, performing the experiments, editing and analysing the data, writing the manuscript and editing the final version.

FUNDING

This research was supported by the project 'SGR Cacao Arauca - Contribuir mitigación niveles cadmio cacao', through the Grant 1001450. The long name of the project is 'Implementación de estrategias agroforestales y vinculación de avances en el manejo agronómico y poscosecha de nuevos clones, para mejorar la productividad y calidad del cacao en el departamento de Arauca' with the SGR Grant BPIN 2018000100148. This project was also in part supported by the project: Multi-agency cocoa platform for Latin America and the Caribbean 'Cocoa 2030-2050,' with the grant ATN/RF-17235-RG. The opinions expressed in this publication are exclusively those of the authors and do not necessarily reflect the point of view of FONTAGRO, its Board of Directors, or the countries it represents.

ACKNOWLEDGMENTS

I gratefully acknowledge the "Ministerio de Agricultura y Desarrollo Rural (MADR)" for their generous financial support of this study. I wish to thank to the Corporación Colombiana de Investigación Agropecuaria (AGROSAVIA) for technical support. Soil samples were collected according to the Colombian Resolution No. 1466 of 3rd December 2014, by which Agrosavia has a collecting permit of biological diversity sampling for non-commercial and scientific research purposes. I would also like to thank to Dr. Rachel Atkinson from Alliance Bioversity-CIAT, in Lima, Perú, for scientific discussions and proofreading this manuscript. To the reviewers of this manuscript for their generous comments and contributions for improvement.

SUPPLEMENTARY MATERIAL

The Supplementary Material for this article can be found online at: https://www.frontiersin.org/articles/10.3389/fenvs.2022.910234/full#supplementary-material

REFERENCES

Argüello, D., Chavez, E., Lauryssen, F., Vanderschueren, R., Smolders, E., and Montalvo, D. (2019). Soil Properties and Agronomic Factors Affecting Cadmium Concentrations in Cacao Beans: A Nationwide Survey in Ecuador. *Sci. Total Environ.* 649, 120–127. doi:10.1016/j.scitotenv.2018.08.292

Aryal, M. (2020). A Comprehensive Study on the Bacterial Biosorption of Heavy Metals: Materials, Performances, Mechanisms, and Mathematical Modellings. *Rev. Chem. Eng.* 36, 1–40. doi:10.1515/revce-2019-0016

Braissant, O., Wirz, D., Göpfert, B., and Daniels, A. U. (2010). Use of Isothermal Microcalorimetry to Monitor Microbial Activities. *FEMS Microbiol. Lett.* 303, 1–8. doi:10.1111/j.1574-6968.2009.01819.x

Braissant, O., Bonkat, G., Wirz, D., and Bachmann, A. (2013). Microbial Growth and Isothermal Microcalorimetry: Growth Models and Their Application to Microcalorimetric Data. *Thermochim. Acta* 555, 64–71. doi:10.1016/j.tca.2012.12.005

Braissant, O., Astasov-Frauenhoffer, M., Waltimo, T., and Bonkat, G. (2020). A Review of Methods to Determine Viability, Vitality, and Metabolic Rates in Microbiology. *Front. Microbiol.* 11, 547458–547525. doi:10.3389/fmicb.2020.547458

Bravo, D., and Benavides-Erazo, J. (2020). The Use of a Two-Dimensional Electrical Resistivity Tomography (2D-ERT) as a Technique for Cadmium Determination in Cacao Crop Soils. *Appl. Sci.* 10, 1–16. doi:10.3390/app10124149

Bravo, D., and Braissant, O. (2022). Cadmium-tolerant Bacteria: Current Trends and Applications in Agriculture. *Lett. Appl. Microbiol.* 74, 311–333. doi:10.1111/lam.13594

Bravo, D., Braissant, O., Solokhina, A., Clerc, M., Daniels, A. U., Verrecchia, E., et al. (2011). Use of an Isothermal Microcalorimetry Assay to Characterize Microbial Oxalotrophic Activity. *FEMS Microbiol. Ecol.* 78, 266–274. doi:10.1111/j.1574-6941.2011.01158.x

Bravo, D., Martin, G., David, M. M., Cailleau, G., Verrecchia, E., and Junier, P. (2013). Identification of Active Oxalotrophic Bacteria by Bromodeoxyuridine DNA Labeling in a Microcosm Soil Experiments. *FEMS Microbiol. Lett.* 348 (2), 103–111.

Bravo, D., Braissant, O., Cailleau, G., Verrecchia, E., and Junier, P. (2015). Isolation and Characterization of Oxalotrophic Bacteria from Tropical Soils. *Arch. Microbiol.* 197, 65–77. doi:10.1007/s00203-014-1055-2

Bravo, D., Pardo-Díaz, S., Benavides-Erazo, J., Rengifo-Estrada, G., Braissant, O., and Leon-Moreno, C. (2018). Cadmium and Cadmium-tolerant Soil Bacteria in Cacao Crops from Northeastern Colombia. *J. Appl. Microbiol.* 124, 1175–1194. doi:10.1111/jam.13698

Bravo, D., Leon-Moreno, C., Martínez, C. A., Varón-Ramírez, V. M., Araujo-Carrillo, G. A., Vargas, R., et al. (2021). The First National Survey of Cadmium in Cacao Farm Soil in Colombia. *Agronomy* 11, 1–18. doi:10.3390/agronomy11040761

Bravo, D., Santander, M., Rodriguez, J., Escobar, S., Gideon, R., and Atkinson, R. (2022). 'From Soil to Chocolate Bar': Identifying Critical Steps in the Journey of Cadmium in a Colombian Cacao Plantation. *Food Addit. Contam. Part A* 39, 949–963. Accepted. doi:10.1080/19440049.2022.2040747

Chavez, E., He, Z. L., Stoffella, P. J., Mylavarapu, R. S., Li, Y. C., Moyano, B., et al. (2015). Concentration of Cadmium in Cacao Beans and its Relationship with Soil Cadmium in Southern Ecuador. *Sci. Total Environ.* 533, 205–214. doi:10.1016/j.scitotenv.2015.06.106

Chavez, E., He, Z. L., Stoffella, P. J., Mylavarapu, R. S., Li, Y. C., and Baligar, V. C. (2016). Chemical Speciation of Cadmium: An Approach to Evaluate Plant-Available Cadmium in Ecuadorian Soils under Cacao Production. *Chemosphere* 150, 57–62. doi:10.1016/j.chemosphere.2016.02.013

Diels, L., Dong, Q., Lelie, D., Baeyens, W., and Mergeay, M. (1995). The Czc Operon of Alcaligenes Eutrophus CH34: from Resistance Mechanism to the Removal of Heavy Metals. *J. Indust. Microbiol.* 14, 142–153. doi:10.1007/bf01569896

Engbersen, N., Gramlich, A., Lopez, M., Schwarz, G., Hattendorf, B., Gutierrez, O., et al. (2019). Cadmium Accumulation and Allocation in Different Cacao Cultivars. *Sci. Total Environ.* 678, 660–670. doi:10.1016/j.scitotenv.2019.05.001

Gil, J. P., López-Zuleta, S., Quiroga-Mateus, R. Y., Benavides-Erazo, J., Chaali, N., and Bravo, D. (2022). Cadmium Distribution in Soils, Soil Litter and Cacao Beans: a Case Study from Colombia. *Int. J. Environ. Sci. Technol.* 19, 2455–2476. doi:10.1007/s13762-021-03299-x

Gramlich, A., Tandy, S., Gauggel, C., López, M., Perla, D., Gonzalez, V., et al. (2018). Soil Cadmium Uptake by Cocoa in Honduras. *Sci. Total Environ.* 612, 370–378. doi:10.1016/j.scitotenv.2017.08.145

Groenenberg, J. E., and Lofts, S. (2014). The Use of Assemblage Models to Describe Trace Element Partitioning, Speciation, and Fate: A Review. *Environ. Toxicol. Chem.* 33, 2181–2196. doi:10.1002/etc.2642

Hart, C., and Gorman-Lewis, D. (2021). Energetics of Acidianus Ambivalens Growth in Response to Oxygen Availability. *Geobiology* 19 (1), 48–62.

Himeno, S., and Aoshima, K. (2019). *Cadmium Toxicity: New Aspects in Human Disease, Rice Contamination, and Cytotoxicity*. Okayama, Japan: Springer.

Kirkham, M. B. (2006). Cadmium in Plants on Polluted Soils: Effects of Soil Factors, Hyperaccumulation, and Amendments. *Geoderma* 137, 19–32. doi:10.1016/j.geoderma.2006.08.024

Liu, Y., Wang, J., Li, P., Xie, Y., Xie, H., Xie, T., et al. (2020). Bioconversion of High-concentration Chelated Cd to nano-CdS Photocatalyst by Sulfate-reducing Bacteria. *J. Chem. Technol. Biotechnol.* 95, 3003–3011. doi:10.1002/jctb.6461

Long, J., Yu, M., Xu, H., Huang, S., Wang, Z., and Zhang, X.-X. (2021). Characterization of Cadmium Biosorption by Inactive Biomass of Two Cadmium-Tolerant Endophytic Bacteria Microbacterium Sp. D2-2 and Bacillus Sp. C9-3. *Ecotoxicology* 30, 1419–1428. doi:10.1007/s10646-021-02363-z

Meter, A., Atkinson, R., and Laliberte, B. (2019). *Cadmium in Cacao from Latin America and the Caribbean. A Review of Research and Potential Mitigation Solutions*. Lima, Peru: CIAT-Bioversity International.

Muehe, E. M., Obst, M., Hitchcock, A., Tyliszczak, T., Behrens, S., Schröder, C., et al. (2013). Fate of Cd during Microbial Fe(III) Mineral Reduction by a Novel and Cd-Tolerant *Geobacter* Species. *Environ. Sci. Technol.* 47, 14099–14109. doi:10.1021/es403365w

Muller, G. (1969). Index of Geoaccumulation in Sediments of the Rhine River. *Geojournal* 2, 108–118.

Naz, N., Young, H. K., Ahmed, N., and Gadd, G. M. (2005). Cadmium Accumulation and DNA Homology with Metal Resistance Genes in Sulfate-Reducing Bacteria. *Appl. Environ. Microbiol.* 71, 4610–4618. doi:10.1128/aem.71.8.4610-4618.2005

Páez-Vélez, C., Rivas, R. E., and Dussán, J. (2019). Enhanced Gold Biosorption of *Lysinibacillus Sphaericus* CBAM5 by Encapsulation of Bacteria in an Alginate Matrix. *Metals* 9, 1–10. doi:10.3390/met9080818

Qu, C., Chen, W., Fein, J. B., Cai, P., and Huang, Q. (2021). The Role of Interfacial Reactions in Controlling the Distribution of Cd within Goethite–humic Acid–bacteria Composites. *J. Hazard Mater.* 405, 1–9. doi:10.1016/j.jhazmat.2020.124081

Ramtahal, G., Umaharan, P., Hanuman, A., Davis, C., and Ali, L. (2019). The Effectiveness of Soil Amendments, Biochar and Lime, in Mitigating Cadmium Bioaccumulation in *Theobroma Cacao* L. *Sci. Total Environ.* 693, 1–11. doi:10.1016/j.scitotenv.2019.07.369

Rodríguez Giraldo, Y., Rodriguez Sánchez, E., Torres, L. G., Montenegro, A. C., and Pichimata, M. A. (2022). Development of Validation Methods to Determine Cadmium in Cocoa Almond from the Beans by ICP-MS and ICP-OES. *Talanta Open* 5, 1–6. doi:10.1016/j.talo.2021.100078

Roslan, N. A., Syed Ismail, S., and Praveena, S. M. (2016). The Transfer Factor of Cadmium in Fern Leaves and its Potential Health Risk. *Asia Pac Environ. Occup. Health J.* 2, 48–57.

Satarug, S. (2019). "Cadmium Sources and Toxicity," in *Toxics*. (Basel, Switzerland: MDPI).

Siripornadulsil, S., and Siripornadulsil, W. (2013). Cadmium-tolerant Bacteria Reduce the Uptake of Cadmium in Rice: Potential for Microbial Bioremediation. *Ecotoxicol. Environ. Saf.* 94, 94–103. doi:10.1016/j.ecoenv.2013.05.002

Siripornadulsil, S., Thanwisai, L., and Siripornadulsil, W. (2014). Changes in the Proteome of the Cadmium-Tolerant Bacteria Cupriavidus Taiwanensis KKU2500-3 in Response to Cadmium Toxicity. *Can. J. Microbiol.* 60, 121–131. doi:10.1139/cjm-2013-0713

Tchounwou, P. B., Yedjou, C. G., Patlolla, A. K., and Sutton, D. J. (2012). Heavy Metal Toxicity and the Environment. *Exp. Suppl.* 101, 133–164. doi:10.1007/978-3-7643-8340-4_6

Wiesler, F. (2012). "Chapter 9 - Nutrition and Quality," in *Marschner's Mineral Nutrition of Higher Plants*. Editor P. Marschner. Third Edition (San Diego: Academic Press), 271–282. doi:10.1016/b978-0-12-384905-2.00009-1

Zwietering, M. H., de Koos, J. T., Hasenack, B. E., de Witt, J. C., and van't Riet, K. (1991). Modeling of Bacterial Growth as a Function of Temperature. *Appl. Environ. Microbiol.* 57, 1094–1101. doi:10.1128/aem.57.4.1094-1101.1991

Conflict of Interest: The author declares that the research was conducted in the absence of any commercial or financial relationships that could be construed as a potential conflict of interest.

Publisher's Note: All claims expressed in this article are solely those of the authors and do not necessarily represent those of their affiliated organizations, or those of the publisher, the editors and the reviewers. Any product that may be evaluated in this article, or claim that may be made by its manufacturer, is not guaranteed or endorsed by the publisher.

frontiers | Frontiers in Environmental Science

ORIGINAL RESEARCH
published: 08 August 2022
doi: 10.3389/fenvs.2022.939860

Ecological–Health Risk of Antimony and Arsenic in *Centella asiatica*, Topsoils, and Mangrove Sediments: A Case Study of Peninsular Malaysia

Chee Kong Yap[1], Wen Siang Tan[2,3], Wan Hee Cheng[4]*, Wan Mohd Syazwan[1], Noor Azrizal-Wahid[1], Kumar Krishnan[4], Rusea Go[1], Rosimah Nulit[1], Mohd. Hafiz Ibrahim[1], Muskhazli Mustafa[1], Hishamuddin Omar[1], Weiyun Chew[5], Franklin Berandah Edward[6], Hideo Okamura[7], Khalid Awadh Al-Mutairi[8], Salman Abdo Al-Shami[9], Moslem Sharifinia[10], Mehrzad Keshavarzifard[10], Chen Feng You[11], Alireza Riyahi Bakhtiari[12], Amin Bintal[13], Hesham M. H. Zakaly[14,15], Takaomi Arai[16], Abolfazl Naji[17,18], Muhammad Saleem[19], Mohd Amiruddin Abd Rahman[20], Ghim Hock Ong[4], Geetha Subramaniam[4] and Ling Shing Wong[4]*

[1]Department of Biology, Faculty of Science, Universiti Putra Malaysia, Serdang, Malaysia, [2]Laboratory of Vaccines and Biomolecules, Institute of Bioscience, Universiti Putra Malaysia, Serdang, Malaysia, [3]Department of Microbiology, Faculty of Biotechnology and Biomolecular Sciences, Universiti Putra Malaysia, Serdang, Malaysia, [4]Faculty of Health and Life Sciences, INTI International University, Nilai, Malaysia, [5]Centre for Pre-University Study, MAHSA University, Jenjarom, Malaysia, [6]Natural Resources and Environment Board, Kuching, Malaysia, [7]Graduate School of Maritime Sciences, Faculty of Maritime Sciences, Kobe University, Kobe, Japan, [8]Department of Biology, Faculty of Science, University of Tabuk, Tabuk, Saudi Arabia, [9]Indian River Research and Education Center, IFAS, University of Florida, Fort Pierce, FL, United States, [10]Shrimp Research Center, Iranian Fisheries Science Research Institute, Agricultural Research, Education and Extension Organization (AREEO), Bushehr, Iran, [11]Department of Earth Sciences, National Cheng-Kung University, Tainan, Taiwan, [12]Department of Environmental Sciences, Faculty of Natural Resources and Marine Sciences, Tarbiat Modares University, Noor, Iran, [13]Fisheries and Marine Science Faculty, Universitas Riau, Riau, Indonesia, [14]Physics Department, Faculty of Science, Al-Azhar University, Assuit Branch, Egypt, [15]Institute of Physics and Technology, Ural Federal University, Yekaterinburg, Russia, [16]Environmental and Life Sciences Programme, Faculty of Science, Universiti Brunei Darussalam, Gadong, Brunei Darussalam, [17]Department of Fisheries, Faculty of Marine Science and Technology, University of Hormozgan, Bandar Abbas, Iran, [18]Leibniz Centre for Tropical Marine Research (ZMT), Bremen, Germany, [19]Department of Pathology, School of Medicine and Health Sciences, University of North Dakota, Grand Forks, ND, United States, [20]Department of Physics, Faculty of Science, Universiti Putra Malaysia, Serdang, Malaysia

OPEN ACCESS

Edited by:
Johnbosco C. Egbueri,
Chukwuemeka Odumegwu Ojukwu University, Nigeria

Reviewed by:
Chinanu Unigwe,
Federal University, Nigeria
Noverita Sprinse Vinolina,
Universitas Sumatera Utara, Indonesia
Daniel A. Ayejoto,
University of Ilorin, Nigeria

***Correspondence:**
Chee Kong Yap
yapchee@upm.edu.my
Wan Hee Cheng
wanhee.cheng@newinti.edu.my

Specialty section:
This article was submitted to Toxicology, Pollution and the Environment, a section of the journal Frontiers in Environmental Science

Received: 09 May 2022
Accepted: 22 June 2022
Published: 08 August 2022

Citation:
Yap CK, Tan WS, Cheng WH, Syazwan WM, Azrizal-Wahid N, Krishnan K, Go R, Nulit R, Ibrahim MH, Mustafa M, Omar H, Chew W, Edward FB, Okamura H, Al-Mutairi KA, Al-Shami SA, Sharifinia M, Keshavarzifard M, You CF, Bakhtiari AR, Bintal A, Zakaly HMH, Arai T, Naji A, Saleem M, Abd Rahman MA, Ong GH, Subramaniam G and Wong LS (2022) Ecological–Health Risk of Antimony and Arsenic in Centella asiatica, Topsoils, and Mangrove Sediments: A Case Study of Peninsular Malaysia. Front. Environ. Sci. 10:939860. doi: 10.3389/fenvs.2022.939860

The current study assessed the ecological–health risks of potentially toxic arsenic (As) and antimony (Sb) in the vegetable *Centella asiatica*, topsoils, and mangrove sediments sampled from Peninsular Malaysia. The As concentrations ranged from 0.21 to 4.33, 0.18 to 1.83, and 1.32 to 20.8 mg/kg dry weight, for the leaves, stems, and roots of the vegetable, respectively. The ranges of Sb concentrations were 0.31–0.62, 0.12–0.35, and 0.64–1.61 mg/kg dry weight, for leaves, stems, and roots of the vegetable, respectively. The children's target hazard quotient (THQ) values indicated no non-carcinogenic risks of As and Sb in both leaves and stems, although children's THQ values were higher than those in adults. The calculated values of estimated weekly intake were lower than established provisional tolerable weekly intake of As and Sb for both children and adult consumers. The carcinogenic risk (CR) values of As for children's intake of leaves and stems of vegetables showed more public concern than those of adults. The levels of Sb and As in the topsoils were generally higher (although not significantly) than those in the mangrove sediments, resulting in a higher geoaccumulation index, contamination factor and ecological risk, hazard index, THQ, and CR values. This indicated that the

anthropogenic sources of Sb and As originated from the land-based activities before reaching the mangrove near the coast. The CR of As signifies a dire need for comprehensive ecological–health risks exposure studies, as dietary intake involves more than just vegetable consumption. Therefore, risk management for As and Sb in Malaysia is highly recommended. The present findings of the ecological–health risks of As and Sb based on 2010–2012 samples can be used as an important baseline for future reference and comparison.

Keywords: ecological risk, health risk, arsenic and antimony, soil and sediment pollution, Peninsular Malaysia

INTRODUCTION

Reports on antimony (Sb) and arsenic (As) sources in Malaysia are scarce. In the central area of Sarawak, for example, Sb mineralization was found along the Lalang Fault Zone (Yeap et al., 1996), which also marks the boundary between the Upper Cretaceous Layar Member and the Eocene to Paleocene Kapit Member, both of which are part of the Belaga Formation. Pereira et al. (1994) also reported the use of soil geochemistry in the Buffalo Reef area, Kuala Medang, Pahang, to find Sb–Au mineralization. Recently, the concentrations of mineral-forming and trace elements including As and Sb were examined by Sia and Abdullah, (2012) in coal and coal ashes of the Balingian coalfield in Sarawak, Malaysia. However, the ecological and health effects of Sb and As in Malaysian soils were not addressed in the aforementioned studies.

In general, potentially toxic metals in the environmental media have received substantial concerns due to human health risk potentials (Egbueri et al., 2019; Ukah et al., 2019; Egbueri et al., 2020; Omeka et al., 2022). Murphy et al. (1989) developed risk assessment methodologies for two chronic As-contaminated soil exposure pathways: inhalation of fugitive dust emissions over a lifetime and unintentional soil/house dust intake. There is a wealth of knowledge about inorganic As oral toxicity, and several effects have been recorded, both non-carcinogenic and carcinogenic in nature. Fatigue, gastrointestinal complaints, irregular heart rhythm, bruises, and reduced nerve function can all occur due to ingestion (ATSDR, 2007). Other non-carcinogenic toxic effects due to As exposure include peripheral vascular diseases such as cyanosis, gangrene, and a condition known as "blackfoot disease" (Tseng et al., 2007). Oral ingestion of inorganic As has also been associated with an increased risk of cancer in the skin, liver, bladder, and lungs (Mandal, 2017). Bhattacharya et al. (2007) undertook a complete assessment of As in the environment, emphasizing the necessity for remediation of As-polluted groundwater, considering the carcinogenic toxicological effects on human health. According to Zhang et al. (2020), the combined effect of As in the atmosphere and groundwater may greatly worsen both the carcinogenic and non-carcinogenic effects associated with As pollution.

Sb is regarded as a valuable metal due to its vast range of applications, including catalysts, flameproof materials, ammunition, and bearings (Smichowski 2008; Reimann et al., 2010; Li et al., 2018; Wang et al., 2018). According to Zhou et al. (2015), based on projection scenarios employing the worldwide Sb emission inventory for 1995–2010, the global Sb emissions are expected to grow by a factor of two between 2010 and 2050. Sb is now recognized as a global pollutant, and it has recently sparked global concern (Muhammad et al., 2021; Chang et al., 2022). Sb has gradually become one of the prime hazardous elements of environmental interest due to anthropogenic activities' elevated input (Kawamoto and Morisawa, 2003; Casado et al., 2007; Qi et al., 2011a). Environmental concerns of Sb in soils have been identified in Chinese coal mines (Qi et al., 2011a). *In vitro* and *In vivo* Sb, like As, is known to be a genotoxic element. However, little is known about the transfer of Sb from the environment to humans and its health risk (Wu et al., 2011; Muhammad et al., 2021). In the Yodo River basin, Kawamoto and Morisawa, (2003) investigated the distribution of Sb in the river water environment, which included water, sediment, aquatic vegetation, and fish. They found that the biota in the Yodo River basin had elevated Sb levels. Sb pollution in soils is a significant environmental issue, and it is critical to understand how Sb migrates and transforms in soils (Mu et al., 2022). To acquire a better picture of the environmental risk caused by Sb, Serafimovska et al. (2013) investigated the distribution of Sb and its species in soil fractions. According to Mu et al. (2022), Sb is geochemically stable in soil due to its high presence in the residue fractions.

Wilson et al. (2010) reviewed the environmental chemistry of inorganic Sb in soils and compared and contrasted their findings with those of As. Sb is a hazardous trace element primarily linked to As (Shtangeeva et al., 2011). Due to its greater mobility in the soil than Pb, this metal is thought to provide a greater long-term risk than Pb (Tschan et al., 2010). Nevertheless, knowledge concerning the biogeochemical properties of Sb is relatively limited compared to other frequent hazardous elements (Shtangeeva et al., 2011). Although Sb and As are generally comparable in biogeochemical behavior; discrepancies in regulating variables impacting their mobility and bioavailability in soils were evident and warrant further investigation (Chang et al., 2022). In some mineralized soils, Sb can be found in high amounts. Sb's action in plants is poorly understood (Hajiani et al., 2015). Casado et al. (2007) investigated the extent of Sb and As pollution, their bioavailability in mining-affected grassland soils, and their concentrations in plant aboveground sections. Humans can be exposed to excessive levels of As and Sb via ingestion of polluted soil, dust, or food plants, which leads to serious health risks (Clemente, 2013; Muhammad et al., 2021). Furthermore, the food chain is a

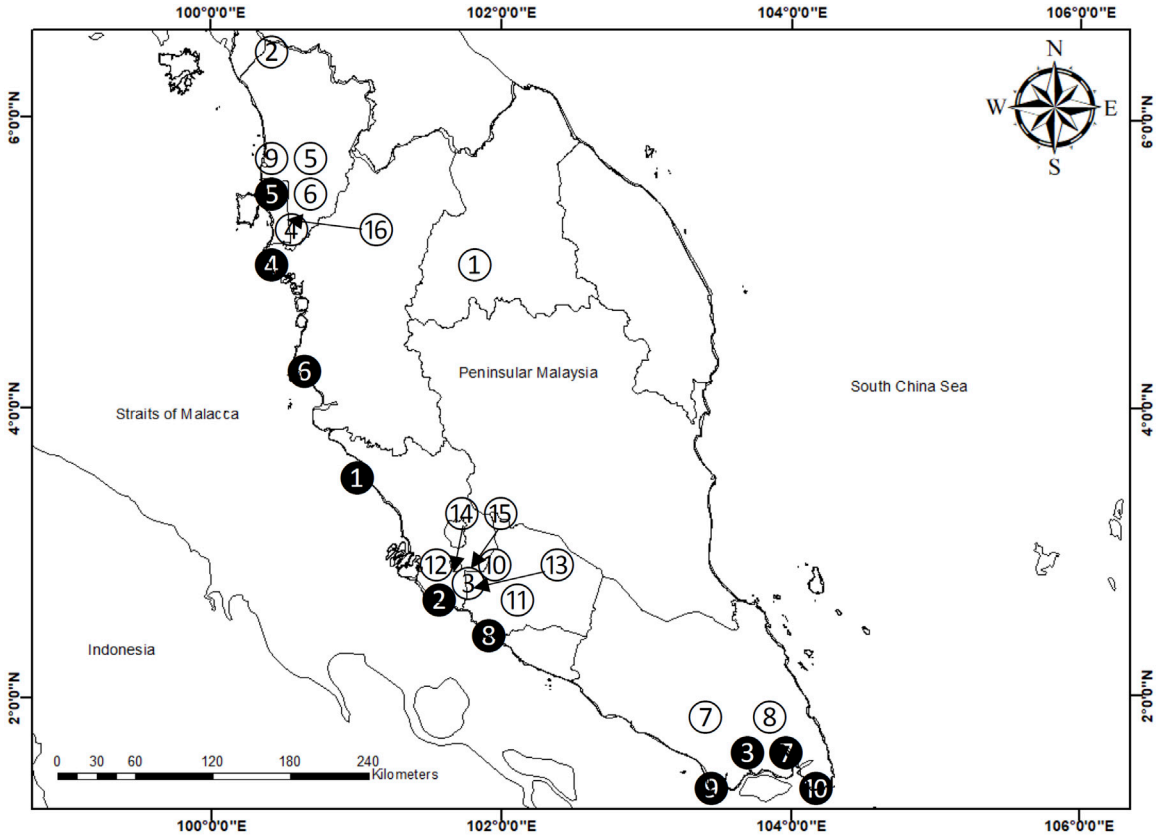

FIGURE 1 | Map showing the sampling sites in Peninsular Malaysia (See **Supplementary Table S1**). Note: numbers in black circles (1-10) are sampling sites (M1–M10 in **Supplementary Table S1**) for mangrove sediments without collection of *Centella asiatica*; numbers in white circles (1-12) are sampling sites (S1–S12 in **Supplementary Table S1**) for *C. asiatica* with habitat topsoils; and numbers in white circles (13–16) are sampling sites (S12–S16 in **Supplementary Table S1**) for topsoils only.

primary route for harmful substances to enter living creatures (Dubey et al., 2014). Tschan et al. (2009a) demonstrated that plants might absorb a considerable amount of Sb while appearing healthy.

Despite the growing concern about the ecological–health risks of As and Sb found in edible plants and mineralized topsoils, there is an acute lack of baseline knowledge regarding this aspect in Malaysia, or elsewhere in the Southeast Asia region. The vegetable plant *Centella asiatica* was selected given its reputation for being a good biomonitor of metals (Rainbow and Phillips, 1993; Ong, 2011; Ong, 2013). The aim of this study, therefore, was to assess the ecological–health risks of As and Sb in *C. asiatica*, topsoils, and mangrove sediments from Peninsular Malaysia.

2 MATERIALS AND METHODS

2.1 Study Area Description

In the present study, the mangrove sediments were collected from 10 sampling sites along the west coast of Peninsular Malaysia. These sites are flanked by a coastal fringe of mangrove forest, primarily in the vicinity of the residential area, hydroelectric power plant, fishing villages, shipping areas, tourism spots, fish and shrimp farms, and industrial area. The sampling seasons ranged from March to June 2012, between the seasons of the first inter-monsoonal period and the Southwest monsoon (Britannica, 2022). *C asiatica* plants, together with their habitat topsoils were collected from 12 sampling sites in Peninsular Malaysia. These sites are located near the residential area, agricultural areas such as oil palm plantation, industrial areas, highways, seaports, shop lots, and roadsides. The sampling seasons ranged from May to June 2010 during the Southwest monsoon season (Britannica, 2022).

2.2 Sampling

Samples of the plant *C. asiatica* and their habitat topsoils were collected between March and June 2010, while the mangrove sediments were collected from the west coast between March and June 2012, from Peninsular Malaysia (**Figure 1**; **Supplementary Table S1**). Plant samples were collected from three parts: leaves, stems, and roots, while soils and sediments of the top 0–5 cm layer were collected.

2.3 Neutron Activation Analysis

The leaves, stems, and roots from five plants were pooled for the analysis of As and Sb. Plants, topsoils, and mangrove sediment samples were dried at 65°C until the constant dry weight was achieved (approximately 5 days). Homogeneity of the dried samples was achieved by grinding them into a powder using an electronic agate homogenizer. The homogenous powder (0.15–0.20 g) of samples was manually shaken and sieved with a 63-μm siever placed into polyethylene vials. These polyethylene vials were heat-sealed until analysis.

Sb and As were analyzed using the TRIGA MARK II reactor at the Malaysian Nuclear Agency, Bangi, Selangor, Malaysia. Neutron flux of 4–5 × 10^{12} n/cm^2 was used for long irradiation of Sb as its half-life is 60.9 days. Following the irradiation, the samples were allowed to cool for a while using closed-end coaxial high purity germanium detectors (Model GC3018 CANBERRA Inc and Model GMX 20180, EG4G ORTEC Nuclear Instrument) and its related electronics. Counting of cooling time ranged from 3 to 6 days, and the lifetime counting for Sb was 3,600 s (IAEA-TECDOC-1360, 2003).

For quality control and quality assurance, acid-washed apparatus was used to avoid external contamination. The Certified Reference Material (CRM) IAEA-SOIL-7 was prepared under identical conditions and used as quality control for each batch. The CRM used for this study was IAEA-SOIL-7 for quality control purposes where the recovery of Sb was 73.58% (certified: 1.70 ± 0.09 mg/kg dry weight; measured: 1.25 ± 0.27 mg/kg dry weight), while the As recovery was 89.25% (certified: 13.40 ± 0.67 mg/kg dry weight; measured: 11.96 ± 2.16 mg/kg dry weight). To achieve greater sensitivity, precision, and accuracy of the analysis, we used a detection limit of 0.001 mg/g for As and Sb by NAA.

2.4 Data Treatment

2.4.1 Geoaccumulation Index

The geoaccumulation index (I_{geo}) is determined by using the following formula (**Eq. (1)**) (Muller, 1969):

$$Igeo = Log10\left(\frac{Cn}{1.5 \times Bn}\right) \quad (1)$$

where

C_n = concentration of element;
B_n = concentrations of background reference for Sb (0.31 mg/kg dry weight) and As (2.00 mg/kg dry weight) by Wedepohl (1995);
Factor 1.5 = background matrix correction factor due to lithogenic effects. The pollution intensities of I_{geo} were based on Muller (1969): "unpolluted" (<0); "unpolluted to moderately polluted" (0–1); "moderately polluted" (1–2); "moderately to strongly polluted" (2–3); "strongly polluted" (3–4); "strongly to very strongly polluted" (4–5); and "very strongly polluted" (>5).

2.4.2 Ecological Risk Assessment of Topsoils and Mangrove Sediments

Ecological risk (ER) of the individual element is an informative index reflecting the effects and toxicity of an element to the environment (Hakanson, 1980; Wang et al., 2018). First, the contamination factor (CF) is calculated as in **Eq. 2** (Hakanson, 1980):

$$CF = \frac{Cs}{Cn} \quad (2)$$

where CF = contamination factor of the element; Cs = the investigated metals in the soils or sediments; Cn = the background values for Sb and As by Wedepohl (1995).

Later, the ER is defined as the formula shown in **Eq. 3** (Hakanson, 1980):

$$ER = Tr \times CF \quad (3)$$

The toxic coefficient (Tr) for As was calculated as 10 based on Hakanson (1980). Since the Tr for Sb was not provided by Hakanson (1980), the Sb Tr was adopted from Wang et al. (2018) (7.0 mg/kg), which was calculated based on Hakanson's principles.

Classifications based on Hakanson (1980) for CF are: "low contamination" (CF < 1); "mild contamination" (1 ≤ CF < 3); "considerable contamination" (3 ≤ CF < 6); and "high contamination" (CF ≥ 6). Classifications of the values of ER are (Hakanson 1980): "minimal potential ecological risk" (ER < 40); "mild potential ecological risk" (40 ≤ ER < 80); "considerable potential ecological risk" (80 ≤ ER < 160); "high potential ecological risk" (160 ≤ ER < 320); and "very high ecological risk" (ER ≥ 320).

2.5 Human Health Risk Assessments of *Centella asiatica*

For human health risk assessment (HHRA), the conversion factor (0.10) was applied to convert the dry weight (DW)-based data of As and Sb in leaves and stems of *C. asiatica* into wet weight (WW)-based data. To estimate the HHRA, three assessments were carried out, namely:

(a) Target hazard quotient

The estimated daily intake (EDI) and target hazard quotient (THQ) of elements were calculated to evaluate the once or long-term possible hazardous exposure to metals from eating edible leaves and stems of *C. asiatica* (USEPA, 1989) by the Peninsular Malaysian population. First, the EDI is calculated using the formula (**Eq. 4**):

$$EDI = \frac{Mc \times \text{consumption rate}}{\text{body weight}} \quad (4)$$

where Mc is the concentrations of the element (mg/kg wet weight; after converted from dry weight-based data) in leaves and stems of *C. asiatica*. The body weights were 17 kg and 69.2 kg for children and adults, respectively (Nurul Izzah et al., 2012; Chong et al., 2017), while the consumption rates were 17.0 and 34.0 g/day for children and adults, respectively (Chong et al., 2017).

Second, the THQ is calculated based on **Eq. 5**:

$$THQ = \frac{EDI}{RfD} \quad (5)$$

The oral reference portion (RfD) was compared with the EDIs (μg/kg wet weight/day) of metals in vegetables. The RfD (μg/kg wet weight/day) values used in this study were based on USEPA regional screening level (USEPA, 2022) for Sb (0.40) and As (0.30).

(b) Comparisons between estimated weekly intake and provisional tolerable weekly intake

The Joint FAO/WHO Expert Committee on Food Additives (JECFA) considered As at its 33rd meeting (FAO/WHO, 1989) and confirmed its earlier evaluation by establishing a provisional tolerable weekly intake (PTWI) of 15 μg/kg body weight. Therefore, the present study used the PTWI of 15 μg/kg body weight for As (FAO/WHO, 1989). Thus, the As PTWI values for 17 and 69.2 kg body weights for children and adults in Malaysia are equivalent to 255 and 1,038 μg/week, respectively.

For Sb, based on the WHO (2017) and ATSDR (2019), which was initially based on drinking water quality guidelines (0.02 mg/L) for Sb and compounds (WHO, 2017), the tolerable daily intake (TDI) for Sb was recommended as 6 μg/kg/body weight. Therefore, 7 days of Sb TDI was calculated as 42 μg/kg/body weight. An adult with a body weight of 69.2 kg would have a PTWI of 2,906 μg/week, while a child with a body weight of 17 kg would have a PTWI of 714 μg/week.

In order to evaluate the risk exposure from *C. asiatica* consumption, the estimated weekly intake (EWI) values of Sb and As are calculated as follows using **Eq. 6**:

$$EWI = EDI \times 7 \quad (6)$$

where EDI = [estimated daily intake calculated in **Eq. 1**] × 7 (number of days in a week). The comparison between calculated EWI and established PTWI limits for children and adults will reveal if the EWI values are lower than the established PTWI values.

(c) Carcinogenic risk of As in *Centella asiatica*

The incremental probability of an individual developing cancer during a lifetime is determined by the cancer risks (CRs) for As. For example, a CR of 1.0×10^{-4} indicates a probability of 1 in 10,000 individuals developing cancer (USEPA, 1989). The CR of As in the leaves and stems of *C. asiatica* was calculated by multiplying the average daily intake of As (in μg/kg/day over a lifetime) with a cancer slope factor (SF) according to Eq. (7).

$$CR = \left(\frac{EDI}{1000}\right) \times SF \quad (7)$$

Here, the SF actor for As after oral exposure has been set to 1.50 $(mg/kg/day)^{-1}$ by the USEPA (2022). According to USEPA methods, cancer risk lower than 1.0×10^{-6} is considered to be "negligible," $>1.0 \times 10^{-4}$ is considered "unacceptable," and in the range from 1.0×10^{-6} to 1.0×10^{-4} is considered "acceptable" (USEPA, 1989).

2.6 Human Health Risk Assessment of Topsoils and Sediments

(a) Non-carcinogenic risks of As and Sb

The non-carcinogenic risk (NCR) of As and Sb to humans was measured by HHRA of topsoils and sediments via three exposure pathways: ingestion, inhalation, and skin contact based on the guidelines and Exposure Factors Handbook of the US Environmental Protection Agency (USEPA, 1986, 1989, 1997, 2001). The average daily doses (ADDs) (mg/kg day) of As and Sb through ingestion (ADD_{ing}), inhalation (ADD_{inh}), and dermal contact (ADD_{der}) for both children and adults are calculated by using **Eqs. 8–10** as follows:

$$ADD_{ing} = C_{soil}\left(\frac{IngR \times EF \times ED}{BW \times AT}\right) \times 10^{-6} \quad (8)$$

$$ADD_{inh} = C_{soil}\left(\frac{InghR \times EF \times ED}{PEF \times BW \times AT}\right) \quad (9)$$

$$ADD_{der} = C_{soil}\left(\frac{SA \times AF \times ABS \times EF \times ED}{BW \times AT}\right) \times 10^{-6} \quad (10)$$

where ADD_{ing}, ADD_{inh}, and ADD_{der} are the daily amounts of exposure to As and Sb (mg/kg day) through ingestion, inhalation, and dermal contact, respectively. In this study, NCR values of As and Sb were assessed by using the hazard quotient (HQ) and hazard index (HI) (Chabukdhara and Nema, 2013; Qing et al., 2015). The definition, exposure factors, and reference values used to estimate the intake values and health risks of As and Sb in topsoils and sediments are presented in **Supplementary Table S2**.

The HQ is the proportion of the ADD of a metal to its reference dose (RfD) for the three exposure pathway(s) (USEPA, 1989), as shown in **Eq. 11**:

$$HQ = \frac{ADD}{RfD} \quad (11)$$

The RfD (mg/kg day) is the maximum daily dose of As and Sb from three exposure pathways for both children and adults, which will not pose significant risks of adverse effects on sensitive individuals throughout the course of their lives. ADD values lower than the RfD value (HQ ≤ 1) indicate no hazardous health effects, while higher ADD values than RfD values (HQ > 1) indicate potential hazardous health effects (USEPA, 1986, 2001). Despite substantial uncertainties, HQ values above 1 are regarded as an indicator of the potential risk of hazardous health effects to certain exposed individuals (USEPA, 1989).

(b) Carcinogenic risk of As in topsoils and sediments

The HHRA of topsoils and sediments was utilized to measure CR of As to humans by means of three exposure pathways, namely, ingestion, inhalation, and skin contact since the SF values were established for the three pathways for As but not for Sb (Cao et al., 2014; USEPA, 2022).

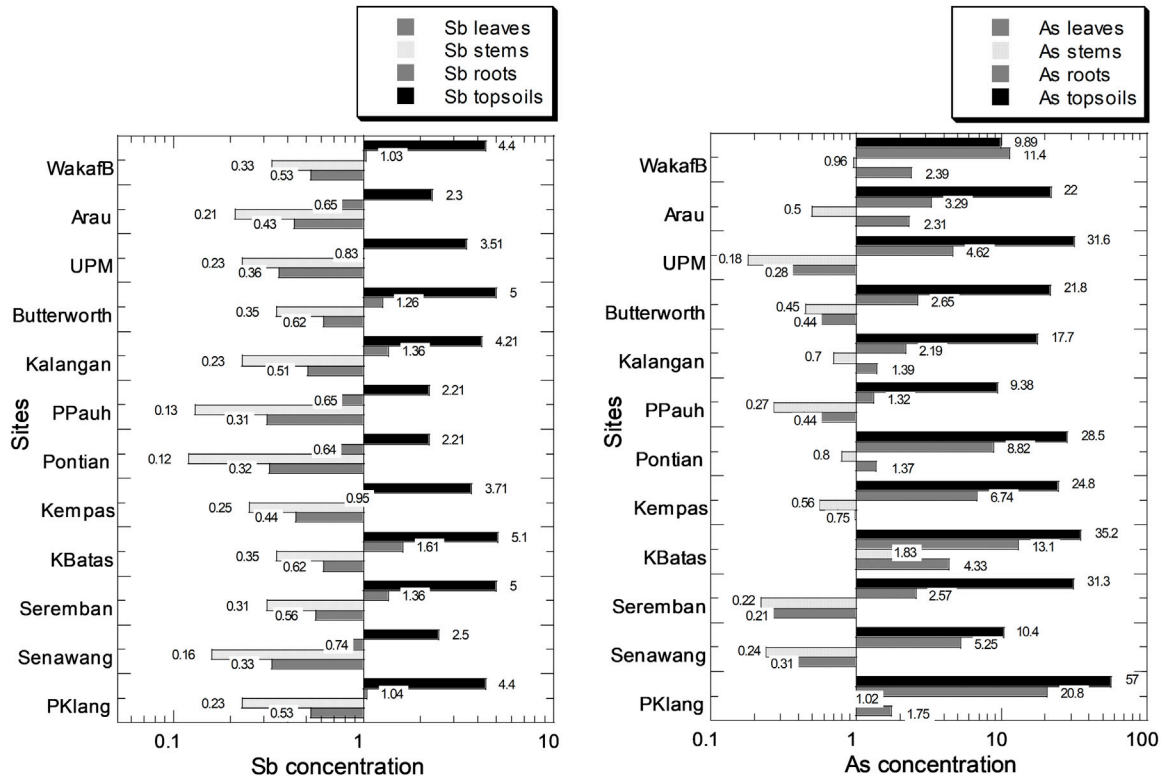

FIGURE 2 | Mean concentrations (mg/kg dry weight) of Sb and As in leaves, stems, and roots of *Centella asiatica* and their habitat topsoils collected from 12 sampling sites (indicated by numbers in white circles (1–12) in **Figure 1**; S1–S12 in **Supplementary Table S1**) in Peninsular Malaysia. The *X*-axes are based on a logarithmic scale.

The CR was calculated by multiplying the average daily intake of As (in μg/kg/day over a lifetime) with an SF according to **Eq. 12**. The CR was estimated as the incremental probability of an individual developing cancer over a lifetime. For example, a CR of 1.0×10^{-4} indicates a probability of 1 in 10,000 individuals developing cancer (USEPA, 1989).

$$CR = \left(\frac{ADD}{1000}\right) \times SF \quad (12)$$

For both children and adults, the SF for As after oral exposure has been set to 1.5 $(mg/kg/day)^{-1}$ by the USEPA (USEPA, 1989; Cao et al., 2014; USEPA, 2022). For inhalation and dermal contact pathways, they were 15.1 $(mg/kg/day)^{-1}$ and 3.66 $(mg/kg/day)^{-1}$, respectively (Cao et al. (2014). According to USEPA's categories, a cancer risk lower than 1.0×10^{-6} is considered to be "negligible," $>1.0 \times 10^{-4}$ is considered "unacceptable," and in the range from 1.0×10^{-6} to 1.0×10^{-4} is considered "acceptable" (USEPA, 1989).

2.7 Statistical Analysis

KaleidaGraph (Version 3.08, Synergy Software, Eden Prairie, MN, United States) was utilized to obtain the overall statistics of the data and to create the graphical bar charts in this study.

3 RESULTS

3.1 Concentrations of Sb and As in *Centella asiatica* and Their Habitat Topsoils

Figure 2 and **Supplementary Table S3** show the levels of As and Sb. The As concentrations (mg/kg dry weight) ranged from 0.21 to 4.33, 0.18 to 1.83, and 1.32 to 20.8 for the leaves, stems, and roots of *C. asiatica*, respectively. The ranges of Sb concentrations (mg/kg dry weight) were 0.31–0.62, 0.12–0.35, and 0.64–1.61, for leaves, stems, and roots of *C. asiatica*, respectively. The As and Sb levels followed the order of roots > leaves > stems.

3.2 Health Risk Assessments of Sb and As in *Centella asiatica*

Figure 3 and **Supplementary Table S4** show the EDI values in the leaves and stem for both children and adults. The values of Sb EDI for children and adults in the leaves ranged from 3.10×10^{-2} to 6.20×10^{-2} and 1.50×10^{-3} to 3.10×10^{-2}, respectively. The values of Sb EDI in the stems ranged from 1.20×10^{-2} to 3.50×10^{-2} and 6.00×10^{-3} to 1.70×10^{-2}, for children and adults, respectively (**Supplementary Table S4**). The values of As EDI for children and adults in the leaves ranged from 2.10×10^{-2} to 4.33×10^{-1} and 1.00×10^{-2} to 2.13×10^{-1}, respectively. The values of As

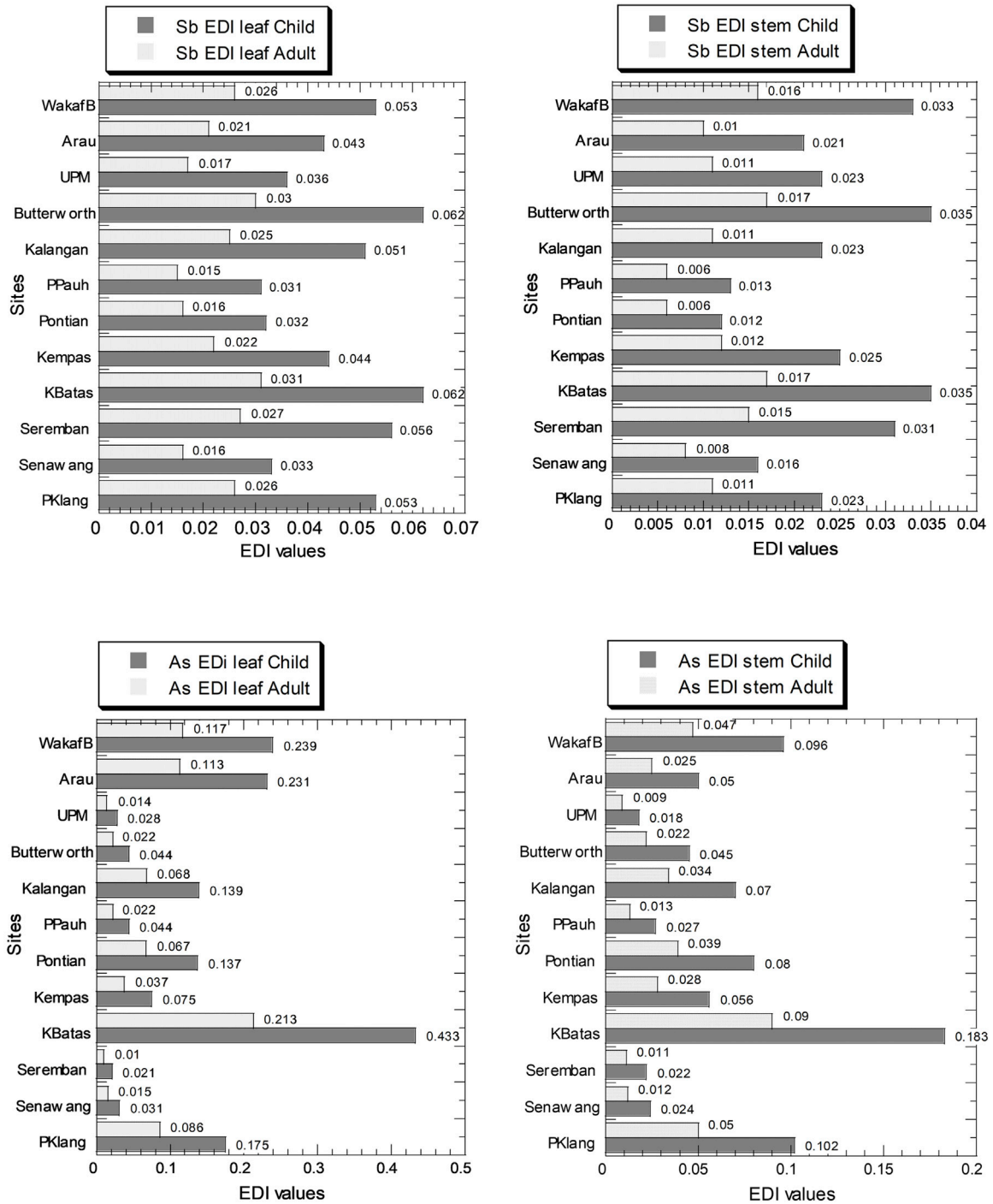

FIGURE 3 | Estimated dietary intake (EDI) values (μg/kg wet weight/day) of Sb and As in the leaves and stems of *Centella asiatica* collected from 12 sampling sites (numbers in white circles (1–12) in **Figure 1**; S1–S12 in **Supplementary Table S1**) in Peninsular Malaysia. The *X*-axes are based on a linear scale.

EDI in the stems ranged from 1.80×10^{-2} to 1.83×10^{-1} and 9.00×10^{-3} to 9.00×10^{-2}, for children and adults, respectively (**Supplementary Table S4**).

For Sb and As, the values of THQ in the leaves and stem in both children and adults are presented in **Figure 4**, and **Supplementary Table S5**. The values of Sb THQ for children and adults in the leaves ranged from 7.90×10^{-2} to 1.55×10^{-1} and 3.90×10^{-2} to 7.60×10^{-2}, respectively. The values of Sb THQ for children and adults in the stems ranged from 2.90×10^{-2} to 8.80×10^{-2} and 1.40×10^{-2} to 4.30×10^{-2},

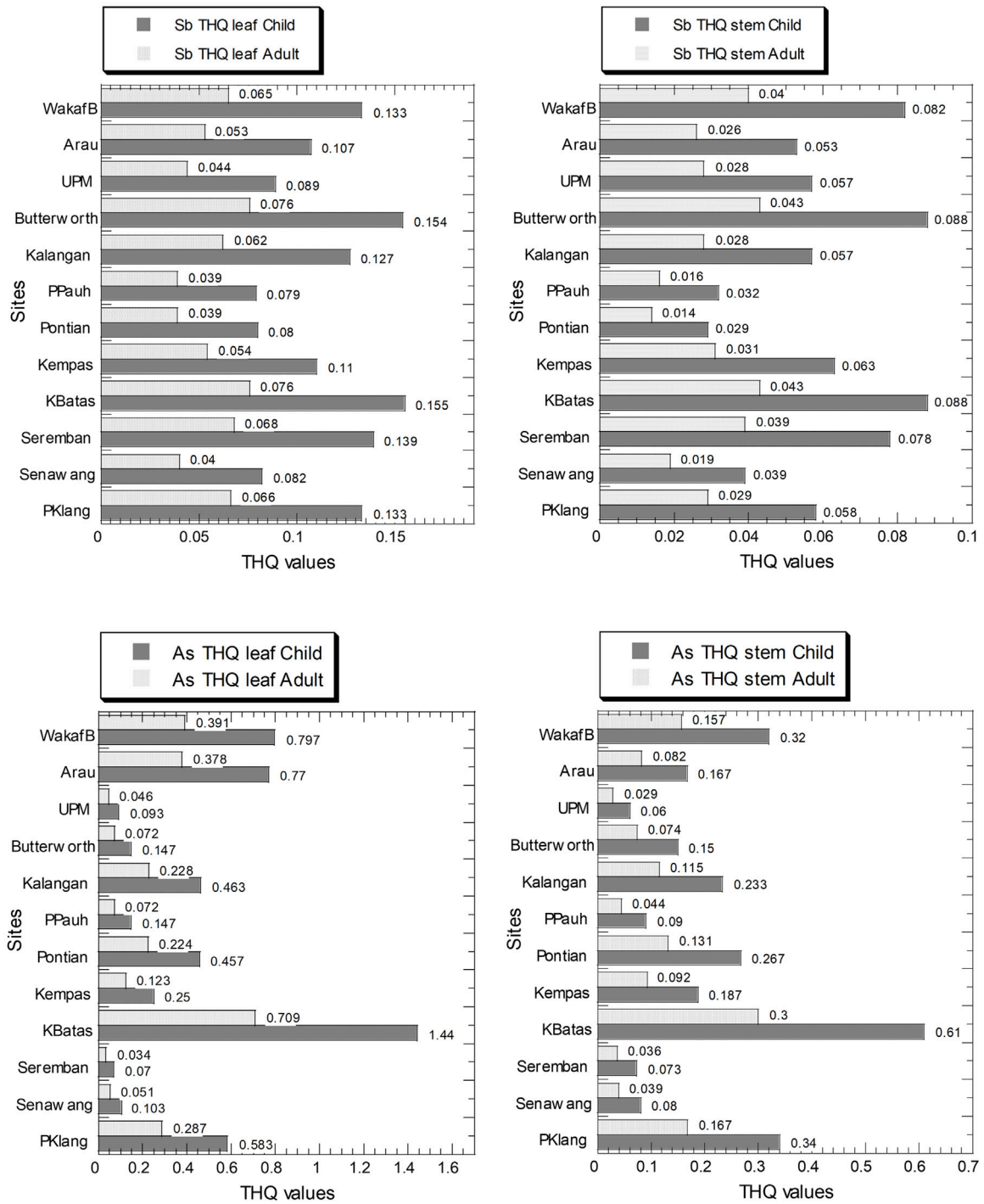

FIGURE 4 | Target hazard quotient (THQ) values (unitless) of As and Sb in the leaves and stems of *Centella asiatica* collected from 12 sampling sites (numbers in white circles (1–12) in **Figure 1**; S1–S12 in **Supplementary Table S1**) in Peninsular Malaysia. The *X*-axes are based on a linear scale.

respectively (**Supplementary Table S5**). The values of As THQ in the leaves ranged from 7.00×10^{-2} to 1.44 and 3.40×10^{-2} to 7.09×10^{-1}, for children and adults, respectively. The values of As THQ in the stems ranged from 6.00×10^{-2} to 6.10×10^{-1} and 2.90×10^{-2} to 3.00×10^{-1}, for children and adults, respectively (**Supplementary Table S5**).

Two major patterns can be identified. First, the children's THQ values in both leaves and stems were higher than those in

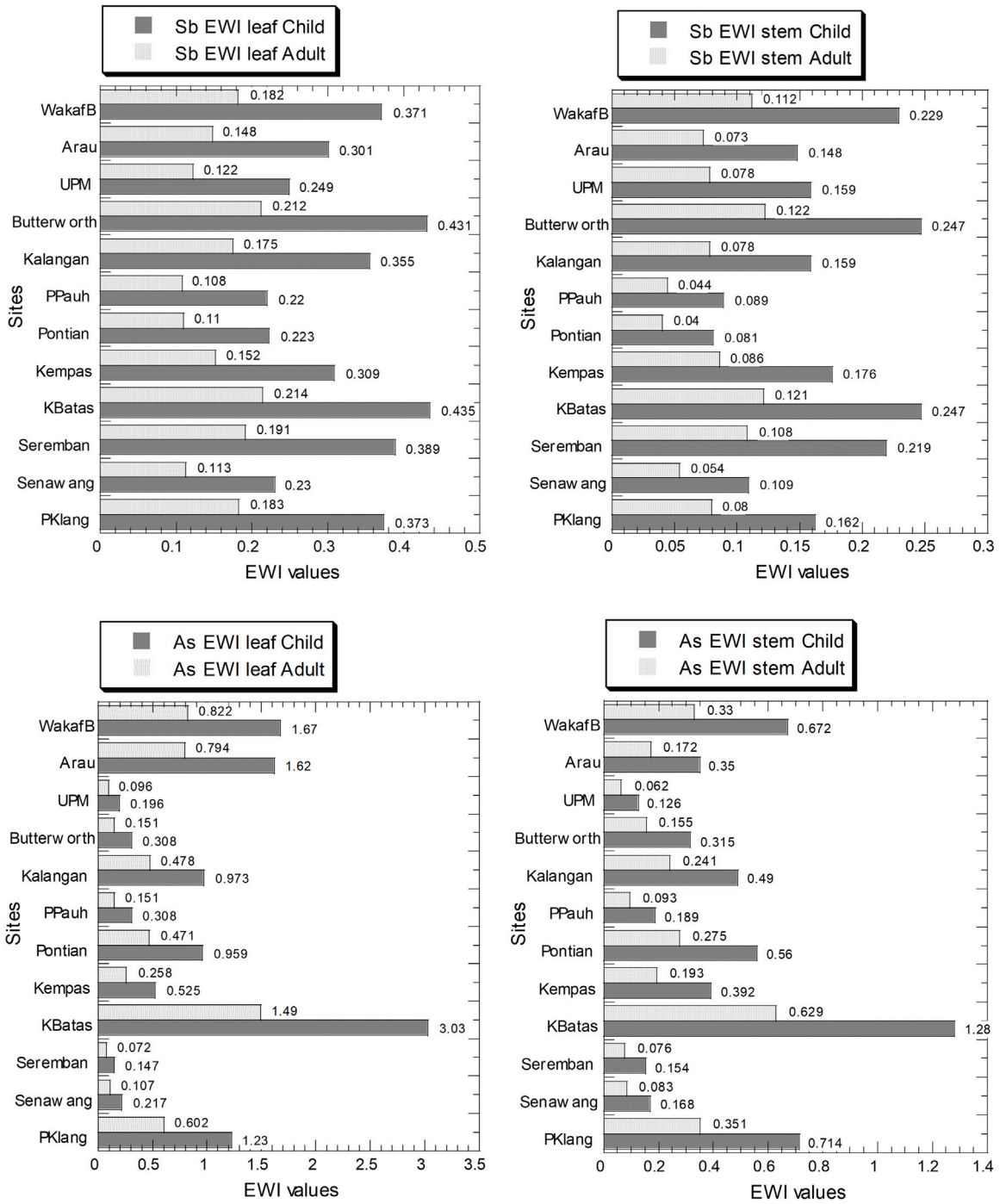

FIGURE 5 | Estimated weekly intake (EWI) values (μg/kg wet weight/week) of Sb and As in the leaves and stems of *Centella asiatica* collected from 12 sampling sites (numbers in white circles (1–12) in **Figure 1**; S1–S12 in **Supplementary Table S1**) in Peninsular Malaysia. The *X*-axes are based on a linear scale.

the adults. Second, all THQ values for Sb and As were below 1.0, except for As in children consuming the leaves collected from Kepala Batas (KBatas) in northwest Peninsular Malaysia.

Figure 5 and **Supplementary Table S6** show the values of EWI for Sb and As in the leaves and stems in both children and adults. The values of Sb EWI for children and adults in the leaves ranged from 2.20×10^{-1} to 4.35×10^{-1} and 1.08×10^{-2} to 2.14×10^{-1}, respectively. The values of Sb EWI for children and adults in the stems ranged from 8.10×10^{-2} to 2.47×10^{-1}, and 4.00×10^{-2} to 1.22×10^{-1}, respectively (**Supplementary Table S6**). The Sb PTWI values for a 17 and 69.2 kg body weight for children and adults in Malaysia are equivalent to 714 and 2,906 μg/week,

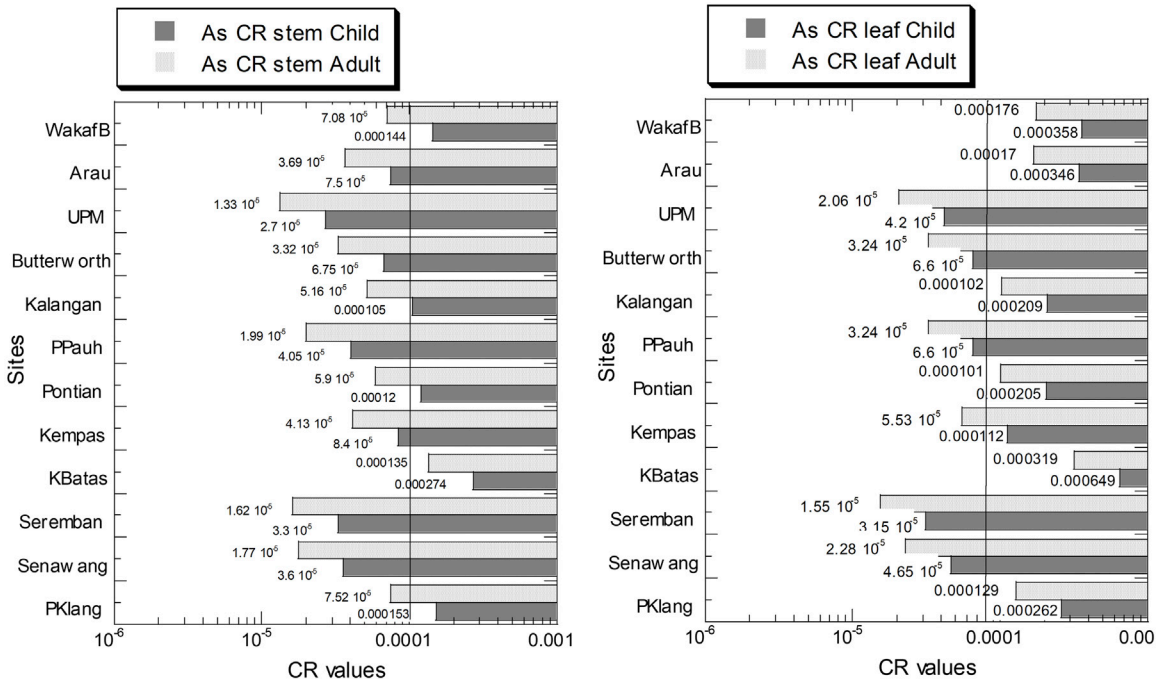

FIGURE 6 | Carcinogenic risk (CR) of As in the leaves and stems of *Centella asiatica* collected from 12 sampling sites (numbers in white circles (1–12) in **Figure 1**; S1–S12 in **Supplementary Table S1**) in Peninsular Malaysia. The *X*-axes are based on a logarithmic scale.

respectively. Therefore, the EWI values for children and adults in the leaves and stems of *C. asiatica* were significantly lower than those of PTWI values of Sb.

The values of As EWI for children and adults in the leaves ranged from 1.47×10^{-1} to 3.03, and 7.20×10^{-2} to 1.49, respectively. The values of As EWI for children and adults in the stems ranged from 1.26×10^{-1} to 1.28 and 6.20×10^{-2} to 6.29×10^{-1}, respectively (**Supplementary Table S6**). The As PTWI for a 17 and 69.2 kg body weight for children and adults in Malaysia are equivalent to 255 and 1,038 μg/week, respectively. Therefore, the EWI values for children and adults in the leaves and stems of *C. asiatica* were significantly lower than those of PTWI values of As.

For As, the values of CR in the leaves and stems in both children and adults were presented in **Figure 6** and **Supplementary Table S7**. The values of As CR for children and adults in the leaves ranged from 3.15×10^{-5} to 6.50×10^{-4}, and 1.55×10^{-5} to 3.19×10^{-4}, respectively. The values of As CR in the stems ranged from 2.70×10^{-5} to 2.74×10^{-4}, and 1.33×10^{-5} to 1.35×10^{-4}, for children and adults, respectively (**Supplementary Table S7**).

According to USEPA methods, cancer risk lower than 1.0×10^{-6} is considered to be "negligible," $>1.0 \times 10^{-4}$ is considered "unacceptable," and in the range from 1.0×10^{-6} to 1.0×10^{-4} is considered "acceptable" (USEPA, 1989). Based on **Figure 6**, the As CR values of all sites were considered "acceptable" except for the 5 sites (out of 10) in children consuming stems that exceeded 1.0×10^{-4} which is considered "unacceptable," while only 1 site exceeded the threshold limit for adults in the stem. For children consuming the leaves, six sites exceeded 1.0×10^{-4} which were considered "unacceptable" while five sites exceeded the threshold limit for adults in leaves. Therefore, these As CR values showed a public concern with 10–60% of the sampling sites exceeding the As CR threshold limit.

3.3 Concentrations of Sb and As and Ecological Risk Assessment in Topsoils and Mangrove Sediments

The levels of Sb and values of I_{geo}, Cf, and ER in both topsoils and mangrove sediments are presented in **Figure 7** and **Supplementary Table S8**. The Sb concentrations (mg/kg dry weight) ranged from 2.21 to 6.61 and 0.001 to 1.72, for topsoils and mangrove sediments, respectively. Overall, the average Sb level (4.00) in the topsoils was higher than 0.97 in the mangrove sediments.

The I_{geo} ranges (2.25–3.83) of Sb in the topsoils were categorized between "moderately to strongly polluted" and "strongly polluted" while those (-0.86–1.89) of the mangrove were all categorized as "unpolluted" and "moderately polluted" (Muller, 1969). The CF ranges (7.11–21.3) of Sb in the topsoils were all under the category of "high contamination" while those (0.003–5.55) of the mangrove were all categorized as "low contamination" and "considerable contamination" (Muller, 1969).

The ER ranges (49.8–149) of Sb in the topsoils fell between "mild potential ecological risk" and "considerable potential

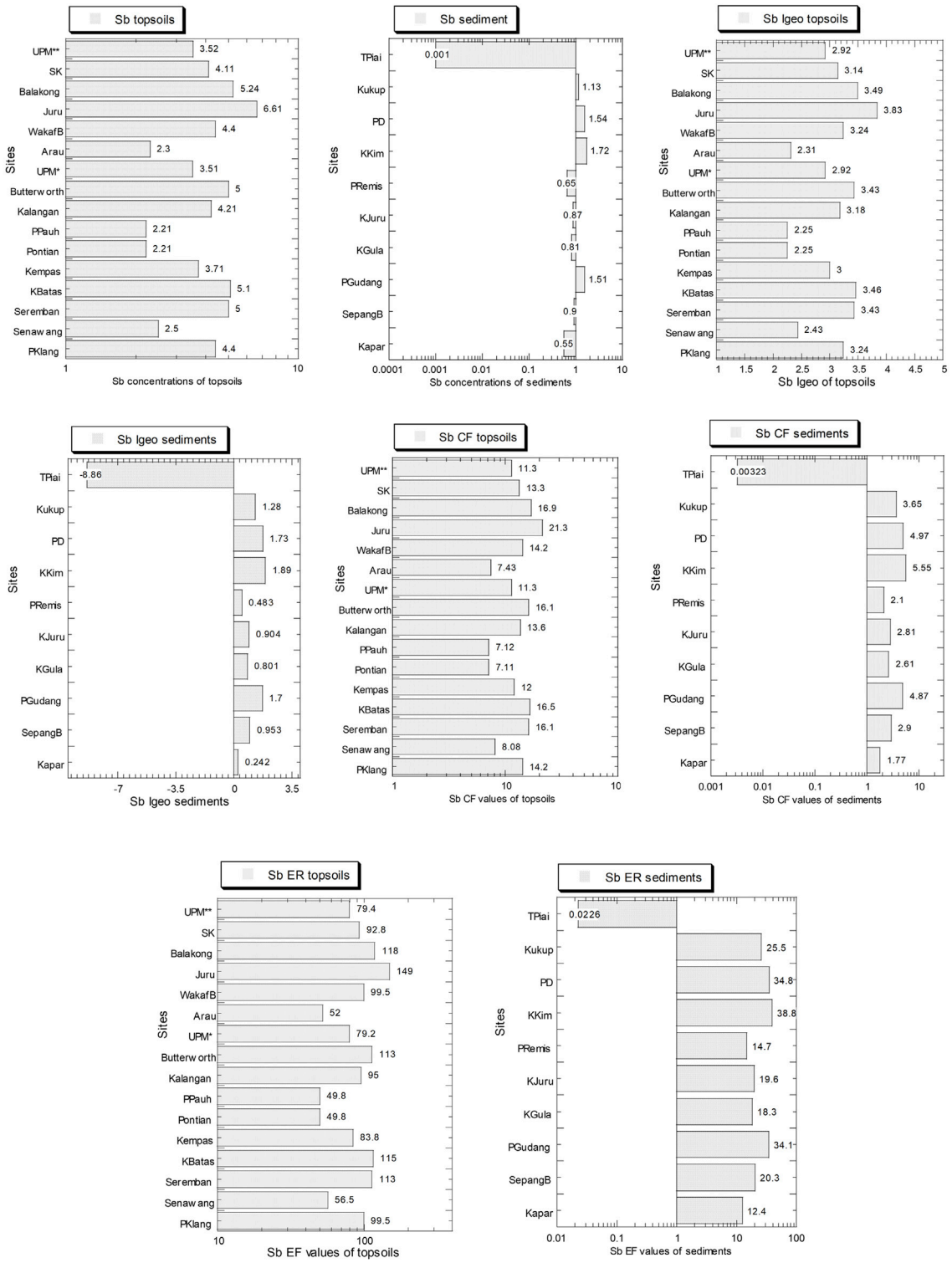

FIGURE 7 | Concentrations of Sb (mg/kg dry weight), geoaccumulation index (I_{geo}), contamination factor (CF), and potential ecological risk index (ER) for Sb in the topsoils (numbers in white circles (1–16) in **Figure 1**; S1–S16 in **Supplementary Table S1**) and mangrove sediments (numbers in black circles (1–10) in **Figure 1**; M1–M10 in **Supplementary Table S1**) from Peninsular Malaysia. All the *X*-axes are based on a logarithmic scale, except for the *X*-axes of I_{geo} values which are based on a linear scale.

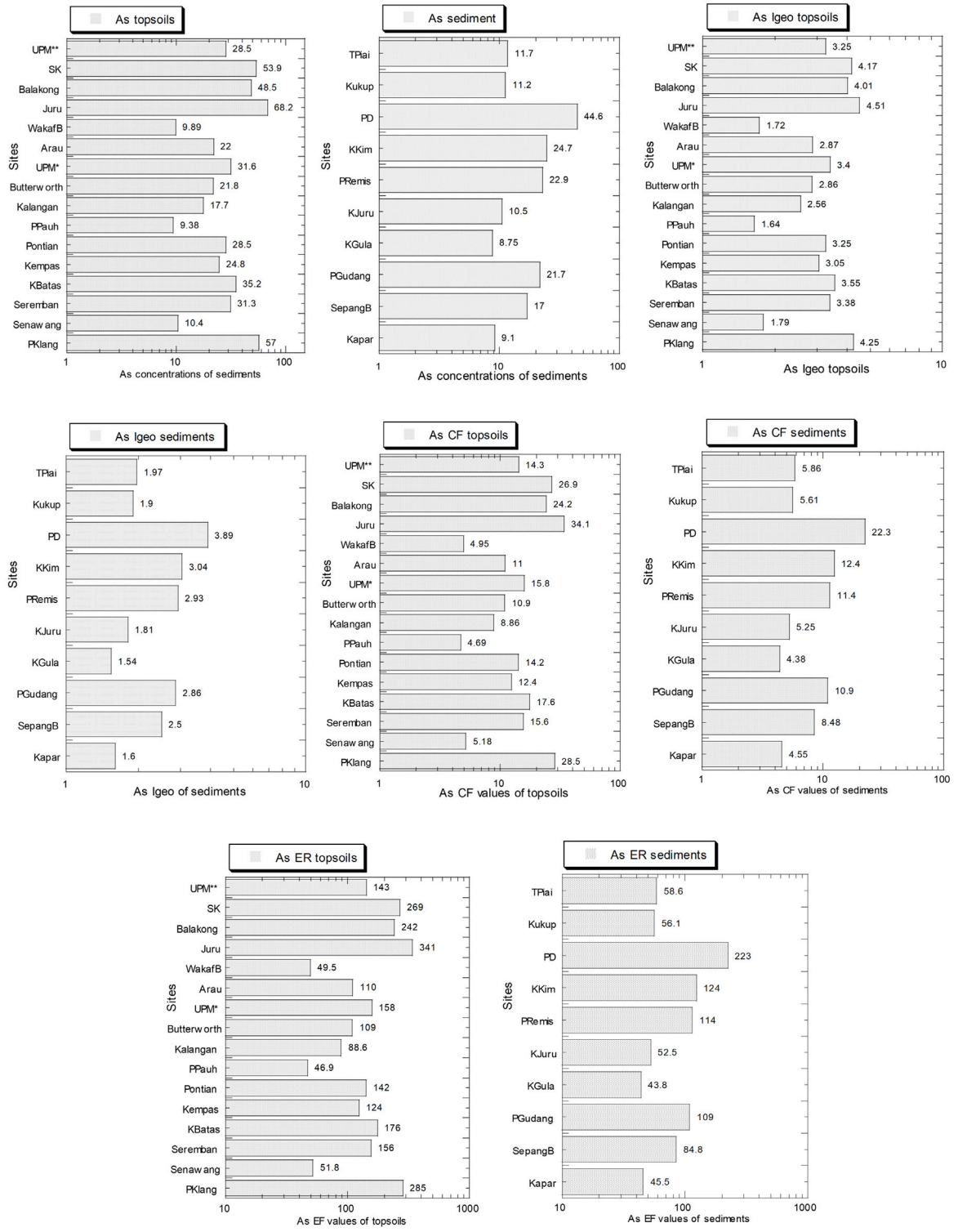

FIGURE 8 | Geoaccumulation index (I_{geo}), contamination factor (CF), and potential ecological risk index (ER) for As in the topsoils (numbers in white circles (1–16) in **Figure 1**; S1–S16 in **Supplementary Table S1**) and mangrove sediments (numbers in black circles (1–10) in **Figure 1**; M1–M10 in **Supplementary Table S1**) from Peninsular Malaysia. The *X*-axes are based on a logarithmic scale.

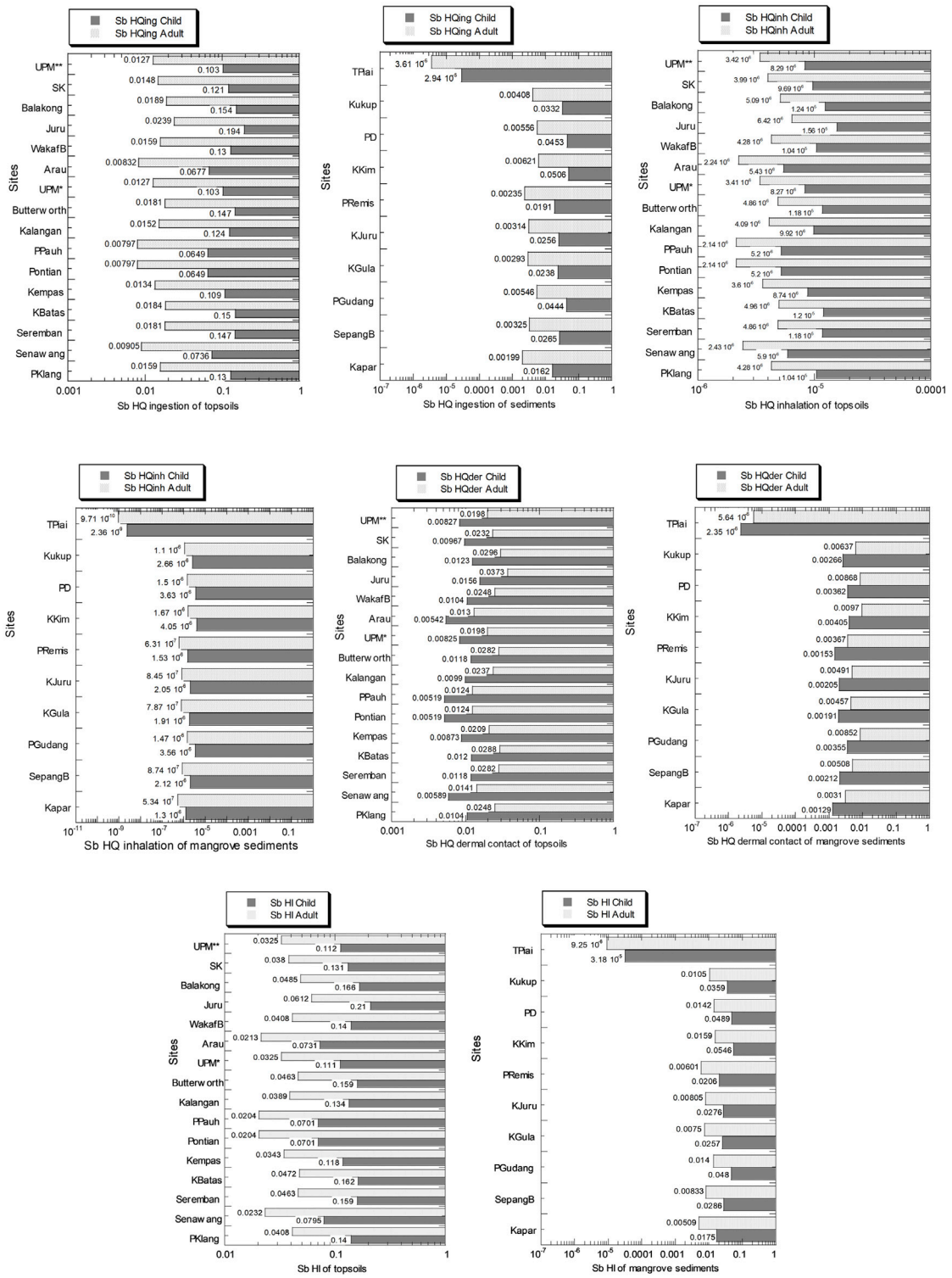

FIGURE 9 | Sb hazard quotient values of ingestion (HQ_{ing}), inhalation (HQ_{inh}), and dermal contact (HQ_{der}) pathways and overall hazard index (HI) in the soils (numbers in white circles (1–16) in **Figure 1**; S1–S16 in **Supplementary Table S1**) and mangrove sediments (numbers in black circles (1–10) in **Figure 1**; M1–M10 in **Supplementary Table S1**) from Peninsular Malaysia, in children and adults. The *X*-axes are based on a logarithmic scale.

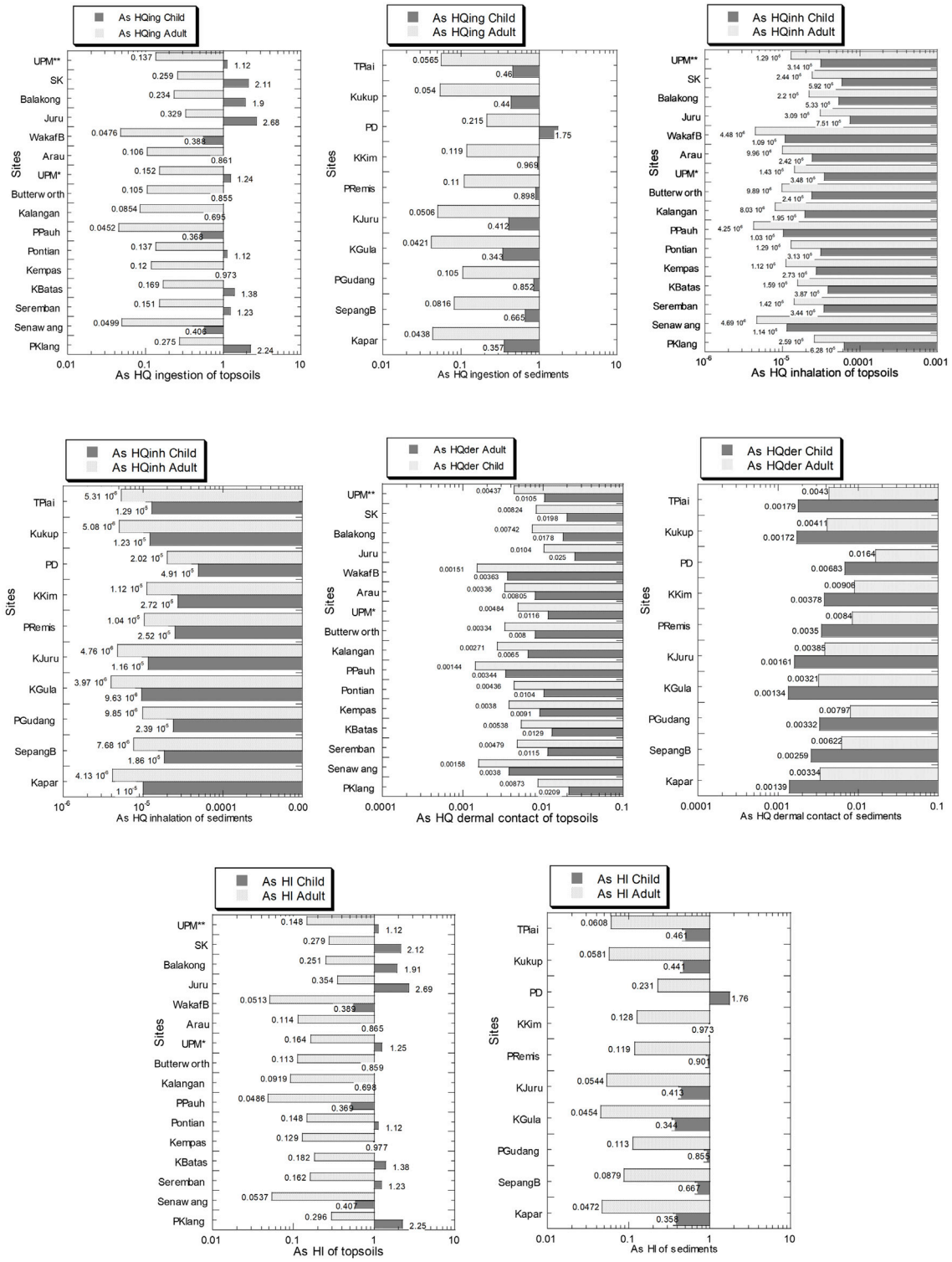

FIGURE 10 | As hazard quotient values of ingestion (HQ_{ing}), inhalation (HQ_{inh}), and dermal contact (HQ_{der}) pathways in the soils (numbers in white circles (1–16) in **Figure 1**; S1–S16 in **Supplementary Table S1**) and mangrove sediments (numbers in black circles (1–10) in **Figure 1**; M1–M10 in **Supplementary Table S1**) from Peninsular Malaysia, in children and adults. The *X*-axes are based on a logarithmic scale.

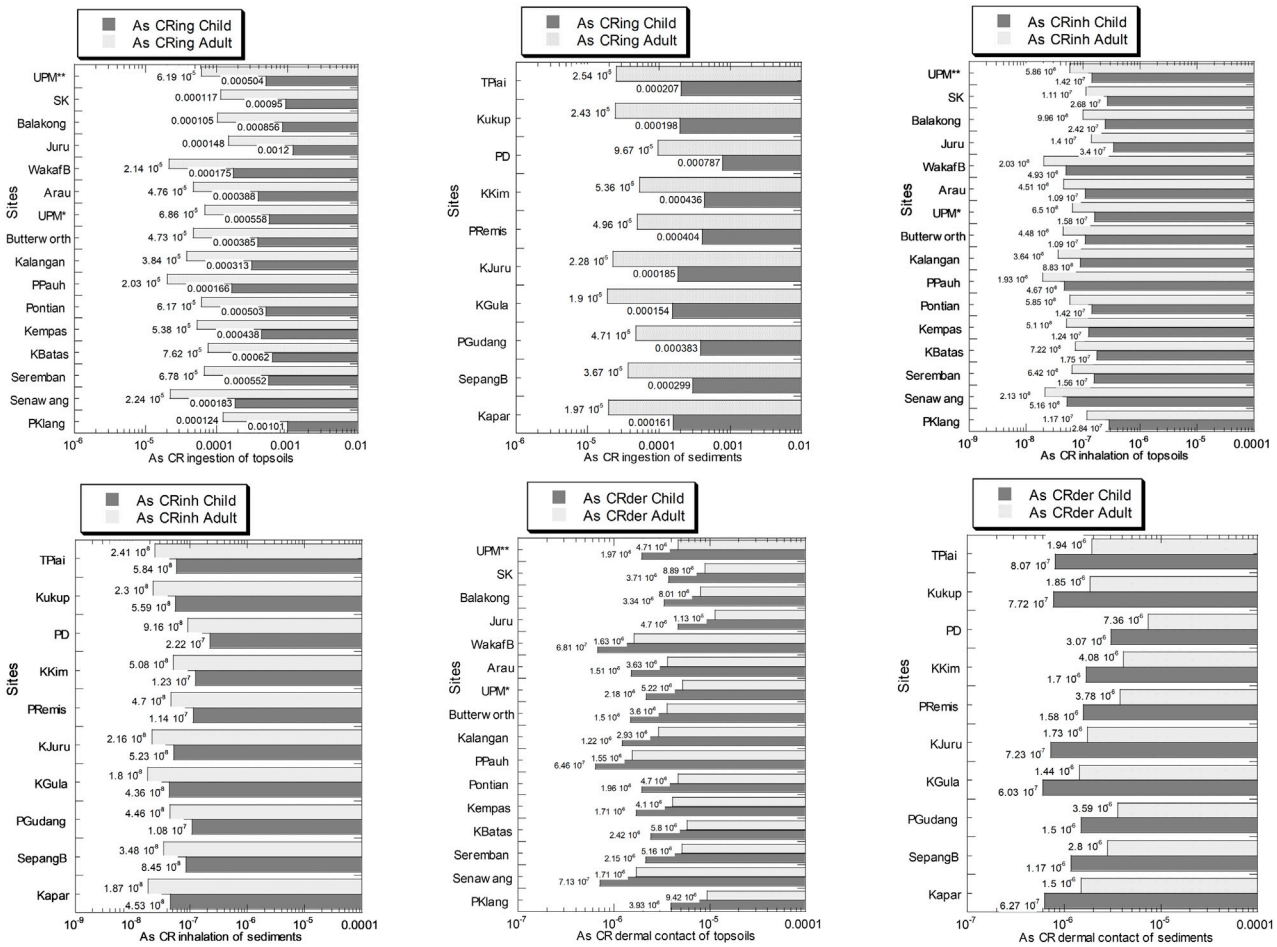

FIGURE 11 | As carcinogenic risk (CR) values of ingestion (CR_{ing}), inhalation (CR_{inh}), and dermal contact (CR_{der}) pathways in the soils (numbers in white circles (1–16) in **Figure 1**; S1–S16 in **Supplementary Table S1**) and mangrove sediments (numbers in black circles (1–10) in **Figure 1**; M1–M10 in **Supplementary Table S1**) from Peninsular Malaysia, in children and adults. The *X*-axes are based on a logarithmic scale.

ecological risk" while those (0.02–38.8) of the mangrove were all categorized as "minimal potential ecological risk" (Hakanson, 1980). Overall, the average Sb values of I_{geo}, CF, and ER in the topsoils were higher than those in the mangrove sediments.

Figure 8 and **Supplementary Table S9** show the levels of As and values of I_{geo}, CF, and ER in both topsoils and mangrove sediments. The As concentrations (mg/kg dry weight) ranged from 9.38 to 68.2 and 8.75 to 44.6, for topsoils and mangrove sediments, respectively. Overall, the average As level (31.2) in the topsoils was higher than that (18.2) in the mangrove sediments.

The I_{geo} ranges (1.64–4.51) of As in the topsoils were categorized between "moderately polluted" and "strongly to very strongly polluted" while those (1.54–3.89) of the mangrove were all categorized as "moderately polluted" and "strongly polluted" (Muller, 1969). The CF ranges (4.69–34.1) of As in the topsoils were categorized as "considerable contamination" and "high contamination" while those (4.38–22.3) of the mangrove sediments were categorized as "considerable contamination" and "high contamination" (Hakanson, 1980).

The ER ranges (46.9–341) of As in the topsoils fell between "mild potential ecological risk" and "very high ecological risk" while those (43.8–223) of the mangrove sediments were categorized as "mild potential ecological risk" and "high potential ecological risk" (Hakanson, 1980). Overall, the average As values of I_{geo}, CF, and ER in the topsoils was higher than those in the mangrove sediments.

3.4 Health Risk Assessments of Sb and As in Topsoils and Mangrove Sediments

The Sb values of HQ_{ing}, HQ_{inh}, and HQ_{der} pathways and HI in the topsoils and sediments from Peninsular Malaysia in children and adults are presented in **Figure 9** and **Supplementary Table S10**. In the children, the Sb values of HQ_{ing}, HQ_{inh}, HQ_{der}, and overall HI in the topsoils ranged from 6.49×10^{-2} to 1.94×10^{-1}, 5.20×10^{-6} to 1.56×10^{-5}, 5.19×10^{-3} to 1.56×10^{-2}, and 7.01×10^{-2} to 2.10×10^{-1}, respectively. In the adults, the Sb values of HQ_{ing},

HQ_{inh}, HQ_{der}, and overall HI in the topsoils ranged from 7.97×10^{-3} to 2.39×10^{-2}, 2.14×10^{-6} to 6.42×10^{-6}, 1.24×10^{-2} to 3.73×10^{-2}, and 2.04×10^{-2} to 6.12×10^{-2}, respectively.

In children, the Sb values of HQ_{ing}, HQ_{inh}, HQ_{der}, and overall HI in the mangrove sediments ranged from 2.94×10^{-5} to 5.06×10^{-2}, 2.36×10^{-9} to 4.05×10^{-6}, 2.35×10^{-6} to 4.05×10^{-3}, and 3.18×10^{-5} to 5.46×10^{-2}. In adults, the Sb values of HQ_{ing}, HQ_{inh}, HQ_{der}, and overall HI in the mangrove sediments ranged from 3.61×10^{-6} to 6.21×10^{-3}, 9.71×10^{-10} to 1.67×10^{-6}, 5.64×10^{-6} to 9.70×10^{-3}, and 9.25×10^{-6} to 1.59×10^{-2}.

The Sb HI values based on the hazard quotients pathways of ingestion, inhalation, and dermal contact for Sb were all below 1.0 and greater in children compared to adults, and the Sb HI values in the topsoils were always higher than those in the mangrove sediments.

The As values of HQ_{ing}, HQ_{inh}, HQ_{der}, and HI in the topsoils and sediments from Peninsular Malaysia in children and adults are presented in **Figure 10** and **Supplementary Table S11**. In children, the As values of HQ_{ing}, HQ_{inh}, HQ_{der}, and HI in the topsoils ranged from 3.68×10^{-1} to 2.68, 1.03×10^{-5} to 7.51×10^{-5}, 1.44×10^{-3} to 1.04×10^{-2}, and 3.69×10^{-1} to 2.69, respectively. There are 9 sites out of 16 where the HI values were above 1.00 via the ingestion pathway in the topsoil samples. In adults, the As values of HQ_{ing}, HQ_{inh}, HQ_{der}, and HI in the topsoils ranged from 4.52×10^{-2} to 3.29×10^{-1}, 4.25×10^{-6} to 3.09×10^{-5}, 3.44×10^{-3} to 2.50×10^{-2}, and 4.86×10^{-2} to 3.54×10^{-1}, respectively.

In children, the As values of HQ_{ing}, HQ_{inh}, HQ_{der}, and HI in the mangrove sediments ranged from 3.43×10^{-1} to 1.75, 9.63×10^{-6} to 4.91×10^{-5}, 1.34×10^{-3} to 6.83×10^{-3}, and 3.44×10^{-1} to 1.76, respectively. Only 1 site out of 10 where the HI value was above 1.00 via the ingestion pathway is the mangrove sediments. In adults, the As values of HQ_{ing}, HQ_{inh}, HQ_{der}, and HI in the mangrove sediments ranged from 4.21×10^{-2} to 2.15×10^{-1}, 3.97×10^{-6} to 2.02×10^{-5}, 3.21×10^{-3} to 1.64×10^{-2}, and 4.54×10^{-2} to 2.31×10^{-1}, respectively.

Overall, there were 56% (9 out of 16 sites) in the topsoils for children with As hazard index values exceeding 1.00, in which almost all the As total HI values were contributed by the ingestion pathway. The HI values were greater in children than in adults, and the As HI values in the topsoils were always higher than those in the mangrove sediments.

The As values of CR_{ing}, CR_{inh}, and CR_{der} in the topsoils and sediments from Peninsular Malaysia in children and adults are presented in **Figure 11** and **Supplementary Table S12**. In children, the As values of CR_{ing}, CR_{inh}, and CR_{der} in the topsoils ranged from 1.66×10^{-4} to 1.20×10^{-3}, 4.67×10^{-8} to 3.40×10^{-7}, and 6.46×10^{-7} to 4.70×10^{-6}, respectively. In the adults, the As values of CR_{ing}, CR_{inh}, and CR_{der} in the topsoils ranged from 2.03×10^{-5} to 1.48×10^{-4}, 1.93×10^{-8} to 1.40×10^{-7}, and 1.55×10^{-6} to 1.13×10^{-5}, respectively.

In children, the As values of CR_{ing}, CR_{inh}, and CR_{der} in the mangrove sediments ranged from 1.54×10^{-4} to 7.87×10^{-4}, 4.36×10^{-8} to 2.22×10^{-7}, and 6.03×10^{-7} to 3.07×10^{-6}, respectively. In adults, the As values of CR_{ing}, CR_{inh}, and CR_{der} in the mangrove sediments ranged from 1.90×10^{-5} to 9.67×10^{-5}, 1.80×10^{-8} to 9.16×10^{-8}, and 1.44×10^{-6} to 7.36×10^{-6}, respectively.

Based on USEPA methods, a cancer risk value below 1.0×10^{-6} is considered "negligible," $>1.0 \times 10^{-4}$ is considered "unacceptable," and in the range from 1.0×10^{-6} to 1.0×10^{-4} is considered "acceptable" (USEPA, 1989). Based on **Figure 11**, all the As children CR values for both topsoils and mangrove sediments in all sites based on the ingestion pathway exceeded 1.0×10^{-4} which is considered "unacceptable." For As adults' CR values of the ingestion pathway, there are four sites (out of 16 sites) that exceeded the threshold limit in the topsoil samples, while all sites in the mangrove sediments were considered "acceptable." All the CR values for inhalation pathways in both topsoils and mangrove sediments were considered "negligible" since they are lower than 1.0×10^{-6}. All the CR values for dermal contact pathways in both topsoils and mangrove sediments were considered "acceptable" since they were in the range from 1.0×10^{-6} to 1.0×10^{-4}, and some are "negligible."

4 DISCUSSION

4.1 Comparable Levels of Sb in *Centella asiatica* With Reported Studies

The present ranges of As in the three parts of *C. asiatica* (0.31–1.61 mg/kg dry weight) from Peninsular Malaysia were comparable to various published research studies.

The present findings of As and Sb levels were in the order of roots > leaves > stems, which agrees with many reported studies on plants. Wilson et al. (2013) found substantially greater metalloid levels in the roots of plants compared to the sections above the ground, confirming our findings. Some researchers attributed Sb translocation from the roots to the upper part of the plants to Sb precipitation on the root membrane barriers, which hampered the transport of Sb solutions to the leaves (Tschan et al., 2009a). Tschan et al. (2009b) discovered the coherent relationship between plant Sb absorption and soluble Sb levels in the topsoil. The sites with Sb levels in *C. asiatica* from the present study indicated higher bioavailability of Sb in the sampling sites (Rainbow and Phillips, 1993). Plants growing near Sb pollution sources have greater Sb concentrations, according to Baroni et al. (2000).

Sb, being a non-essential element, is able to accumulate in plants (Ainsworth et al., 1991). Kabata-Pendias and Pendias, (2001) categorized plant tissue with 5–10 mg/kg of Sb as phytotoxic. Therefore, the present Sb range of 0.31–1.61 mg/kg dry weight in the three parts of *Centella* was not considered phytotoxic. According to Tschan et al. (2009a), the background ranges of Sb concentrations in the terrestrial plants were 0.20–50 mg/kg dry weight. This indicates that present Sb ranges were not elevated and hence can be considered the background level in the topsoils and mangrove sediments in Peninsular Malaysia. Kassem et al. (2004) reported that the Sb values ranged from 0.011 to 0.026 mg/kg dry weight in olive, eggplant, alfalfa, and cabbage leaves were grown in the Orontes River basin. Their data were significantly lower than those of the three parts in *C. asiatica* from the present study.

In the Pearl River Delta (PRD), South China, 112 pairs of soil and blooming cabbage were sampled from typical agricultural protection zones and vegetable-producing districts (Chang et al., 2022) to investigate the contamination levels of Sb and As in soils and harvested cabbages. Chang et al. (2022) reported that the ranges of Sb concentrations in the flowering cabbages across PRD were 0.015–0.20 mg/kg dry weight with a mean value of 0.038 mg/kg dry weight, exhibiting significant lower levels of Sb than radish leaves collected from the Xikuangshan mine area (range: 1.5–121 mg kg−1) (He, 2007). This value is also below the tolerable concentration of plants for Sb (5 mg/kg dry weight) proposed by Eikmann and Kloke, (1993), and the levels between 5 and 10 mg/kg dry weight of Sb in plant tissue were reported to be phytotoxic (Kabata-Pendias and Pendias, 1985).

4.2 Comparatively Higher Levels of As in *Centella asiatica* With Reported Studies

The present ranges of As in the three parts of *C. asiatica* (0.21–20.8 mg/kg dry weight) from Peninsular Malaysia are comparatively higher than those in various published research studies.

Uddh-Söderberg et al. (2015) found that the As concentrations in lettuce ranged from 0.0022 to 4.3 mg/kg dry weight, while Bhattacharya et al. (2010) found that the total As concentrations in rice, wheat, pulses, and vegetables ranged from <0.0003 to 1.02 mg/kg dry weight in an arsenic-affected area of West Bengal (India). A reported study showed that the As concentrations measured for the lettuce, onion, radish, and bean greenhouse samples ranged from 0.00843–5.28 mg/kg wet weight (Ramirez-Andreotta et al., 2013). The present As ranges (0.2–20.8 mg/kg dry weight) in the leaves, stems, and roots of *C. asiatica*, in the current study, were greater than those reported in the studies mentioned above.

In Sweden and the European Union, there is no regulation for As in food (Uddh-Söderberg et al., 2015). The United Kingdom Food Standard Agency proposed a general As limit of 1.00 mg/kg in all foodstuffs (CAC, 2011). On the other hand, the Food Standard Agency of Australia and New Zealand (FSANZ, 2015) proposed a maximum level of total arsenic in cereal (1.00 mg/kg) and did not set restrictions on other food groups. The present As ranges (0.02–2.08 mg/kg wet weight) in the leaves, stems, and roots of *Centella*, from the present study, could be higher than the As limit by the United Kingdom Food Standard Agency (CAC, 2011) and the Food Standard Agency of Australia and New Zealand (FSANZ, 2015).

Haque et al. (2021) studied five heavy metals (including As) in the vegetables obtained from industrial, non-industrial, and As-contaminated regions and popular vegetable markets in Bangladesh. They reported that the As levels in vegetables were 0.15–0.55 mg/kg wet weight and 0.06–0.24 mg/kg wet weight for industrial and non-industrial areas, respectively. Qin et al. (2021) tested samples from vegetable plants cultivated in acidic mine water contaminated soil and found that the mean concentration of total As in the edible sections of leafy vegetables fell in the range of 0.41–7.61 mg/kg dry weight (mean: 2.39 mg/kg).

As concentrations in flowering cabbages across the PRD were reported to fall in the range of 0.021–1.20 mg/kg dry weight (mean: 0.15 mg/kg dry weight) (Chang et al., 2022). In comparison to previous reports, total As concentrations in the flowering cabbages in the current study were generally lower than those in the leafy vegetables collected near mining areas (range: 0.14–1.42 mg/kg dry weight with mean: 0.59 mg/kg dry weight for Shizhuyuan mine; range: 0.41–7.61 mg/kg dry weight with mean: 2.39 mg/kg dry weight for Dabaoshan mine) (Li L. et al., 2017; Qin et al., 2021). Furthermore, As levels in 96% of the flowering cabbages were lower than the Chinese National Standards' (GB 2762–2017) tolerance limit (0.50 mg/kg) for pollutants in foods (Chang et al., 2022).

Zheng et al. (2022) found a wide range of total As concentration in vegetable samples (0.52–15.94 mg/kg dry weight; mean: 6.55 ± 5.18 mg/kg dry weight) from samples collected from As-polluted farmlands, which were attributed to anthropogenic activities in Guangxi province, China. The highest As concentrations were found in Romaine lettuce (15.94 mg/kg dry weight), leaf lettuce (10.48 mg/kg dry weight), and leaf mustard (11.10 mg/kg dry weight).

Varol et al. (2022) found the mean As levels in some leafy vegetables grown in Malatya province (Turkey) were the highest in purple basil (0.297 mg/kg), purslane (0.161 mg/kg), and parsley (0.1 mg/kg wet weight). However, the mean concentrations of As in all crops were lower than the permissible concentrations (MPCs) set by the United Kingdom Food Standard Agency (CAC, 2012) (1.00 mg/kg wet weight) and the Chinese Health Ministry (MHPRC, 2013) (0.50 mg/kg wet weight).

4.3 No Non-Carcinogenic Risks of Sb and As in *Centella* but Are Higher in Children Than in Adults

The children's THQ values in both leaves and stems were higher than those in the adults. Second, all THQ values for Sb and As were below 1.0, except for As in children consuming the leaves collected from KBatas. This indicated that the THQ value (>1.00) of inorganic As in *C. asiatica* collected from KBatas exceeded the threshold value of 1, with a non-carcinogenic risk of As to the children. All EWI values for children and adults in the leaves and stems of *Centella* are lower than the PTWI for Sb and As which had further supported the aforementioned results of THQ values which were below 1.00.

Varol et al. (2022) reported that the As THQ of vegetables collected from Turkey was below the acceptable risk level of 1.00. Cheung et al. (2008) determined dietary exposure to three elements (including Sb) in food consumed by junior high school students in Hong Kong. The dietary intake of Sb was predicted as 0.567 μg (kg body weight) 1) week 1) for high-consumption high school students. Qin et al. (2021) reported that intake of vegetable plants cultivated on acidic mine water-polluted soils might pose considerable potential human health risk with a hazard quotient (HQ) of 2.7.

Wu et al. (2011) investigated the health risks and major routes of long-term human exposure to Sb on residents of the Tin Mine (XKS) Sb mine in China. They found that inhabitants near XKS

had an inorganic dietary intake of As (107 μg/day), below the PTWI of 15 μg/kg body weight/week (equivalent to 129 μg A/day).

4.4 Carcinogenic Risk of As in Most Sampling Sites With the Unacceptable Status

The As CR values are concerning as 10–60% of the studied sites of *C. asiatica* had higher values than the As CR threshold limit. Bhatti et al. (2013) reported that the As concentration of spinach leaves was 1.6–6.4 times greater than the maximum concentration of inorganic As in China (0.05 mg/kg fresh weight). The HI values were above 1 and CR levels were also above the highest target of 1×10^{-4}, which identified the potential risk to humans from ingesting spinach leaves. Uddh-Söderberg et al. (2015) investigated the health risks from As in vegetables grown in private gardens close to 22 contaminated glass factories. They found that the increased levels of As in the soil of residential gardens were reflected in increased As levels of vegetables, and the intake of these vegetables might cause cancer risks in humans. They found that they did not exceed the threshold for chronic non-carcinogenic or acute effects; however, the reported As CR are inclusive of other non-native vegetables and total exposure.

Based on vegetables from Bangladesh, Haque et al. (2021) reported that the probabilistic risk, individual risk, and total cancer risk (TR) for As had surpassed the threshold level (1×10^{-4}) and safe limit (1×10^{-6}), denoting higher lifetime cancer risk due to long-term consumption of these vegetables.

4.5 No Non-Carcinogenic Risk of Sb in the Topsoils and Mangrove Sediments

The present ranges of Sb in the topsoils (2.21–6.61 mg/kg dry weight) and mangrove sediments (0.001–1.72 mg/kg dry weight) from Peninsular Malaysia are comparatively lower than those mentioned in many reported studies. I_{geo}, CF, and ER values for Sb are higher in the topsoils than in the mangrove sediments. The HI based on three pathways indicated no non-carcinogenic risks of Sb.

Overall, the topsoils' mean Sb level (4.00) was higher than 0.97 in the mangrove sediments. Chang et al. (2022) reported that the total Sb contents in soils from typical agricultural protection and vegetable-producing regions of the PRD ranged from 0.20 to 7.20 mg/kg dry weight (mean: 1.60 mg/kg dry weight). This range is within the mean Sb concentration (0.54–2.93 mg/kg dry weight) in soils from various regions across China (He et al., 2012). About 91% of the soil samples were within the range of background Sb levels (0.80–3.00 mg/kg dry weight) for China soils (He, 2007). Furthermore, 95% of the total soil samples were lower than the maximum allowed Sb concentration (3.50 mg/kg dry weight) proposed for soils in the Netherlands (Crommentuijn et al., 2000).

The Sb ranges (Mean: 4.00 in the topsoils and 0.97 in the mangrove sediments) in the current study were lower than those mentioned in many reports from the mining area of Sb such as South and North Sb mines (total Sb: 3,061 mg/kg dry weight; 74.2–16,389 mg/kg dry weight) as reported by Li et al. (2014) and in the sediments of the Lianxi River (Xikuangshan Sb mine; Sb values of 57.11–7,315.7 mg/kg) (Wang et al., 2011) and an abandoned Sb ore deposit in Portugal (5,956 mg/kg dry weight; Pratas et al., 2005). In addition, the significantly higher Sb levels were also reported in the soil near the Xishan mine in Hunan province's Lengshuijiang city (5,949 mg/kg; Qi et al., 2011a), in the surface soils of the Swiss shooting range (13,800 mg/kg dry weight; Johnson et al., 2005). Since Sb and its compounds have long-range transport properties, higher concentrations of Sb in topsoils could be attributable to air dust settlement (Tian et al., 2014).

However, the present Sb ranges were comparable to those in Xuzhou (China), with a mean of 3.46 mg/kg of Sb in urban soils (Xue et al., 2005), and 1.23 mg/kg of Sb was found in Chinese farming soils (Niu et al., 2013). Jiang et al. (2020) examined the levels of eight heavy metals (including As) in soil, groundwater, air, and locally produced grain (wheat and corn) and vegetables in a village located close to a battery factory in Xinxiang, Henan Province, China. They found that the main input of As originated from activities associated with sewage irrigation and battery plant deposition. Based on soils collected from the coal mines in the Huaibei and Huainan areas of Anhui Province, China, Qi et al. (2011a) identified that the mean Sb content in the 33 samples was 4.00 mg/kg, which is lower than that in coals from this region (6.20 mg/kg).

Based on mining-affected grassland soils, Casado et al. (2007) found that the range of total Sb contents in soils was 60–230 mg/kg, indicating a high degree of pollution of soils. Sia and Abdullah (2012) studied the concentrations of mineral-forming elements and trace elements in coal and coal ashes from Balingian coalfield, Sarawak, Malaysia, and reported an enriched content of Sb (96 ppm) in Balingian coal relative to their respective coal Clarke.

Patyar and Moghanlo, two mining regions in Iran, were studied for their soil and vegetation (Hajiani et al., 2015). In Moghanlo, the total Sb concentrations in soil were 358–3,482 mg/kg, while in Patyar, the total Sb concentrations were 284–886 mg/kg. Sb levels in plant shoots ranged from 0.8 to 287 mg/kg and 1.3 to 49 mg/kg, respectively. *Achillea wilhelmsii* and *Matthiola farinosa* were the strongest Sb accumulators among these species, with 141 and 132 mg/kg Sb in their leaves, respectively.

Based on Baoji urban soil, Li X. et al. (2017) studied seven toxic elements (including As and Sb). They found that prolonged industrial activities have enriched the Sb content (26.00 mg/kg mean value) in urban soil. Based on nine surface soil samples contaminated from lead/zinc and iron smelting operations and coal-fired power plants, Serafimovska et al. (2013) reported that the main part of total Sb (2.5–105 mg/kg dry weight) was associated with the residual fraction in all soils. Chang et al. (2022) investigated the contamination levels of Sb and As in soils and harvested cabbages across the PRD (South China) by collecting 112 pairs of soil and flowering cabbage samples from agricultural protection zones and vegetable-producing districts in the region. The levels of Sb pollution in PRD cabbages and soils were generally low, although the soils were moderately polluted by As.

4.6 High Ecological Risk of As and Carcinogenic Risk of As in the Topsoils and Mangrove Sediments

The present ranges of As in the topsoils (9.38–68.2 mg/kg dry weight) and mangrove sediments (8.75–44.6 mg/kg dry weight) from Peninsular Malaysia are comparable to many reported studies in the literature. I_{geo}, CF, and ER values for As are also higher in the topsoils than those in the mangrove sediments. The hazard index based on three pathways indicated no non-carcinogenic risks of As. Higher and more As carcinogenic risk in the topsoils than in the mangrove sediments was observed.

Based on mining-affected grassland soils, Casado et al. (2007) found that total As contents in soils ranged from 42 to 4,530 mg/kg, denoting elevated levels of pollution in soils. Sia and Abdullah (2012) studied the concentrations of mineral-forming elements and trace elements in coal and coal ashes from Balingian coalfield, Sarawak, Malaysia, and reported an enriched content of As (as high as 181 ppm) in Balingian coal relative to their respective coal Clarke.

The mean As level (31.2) in the topsoils was higher (18.2) than in the mangrove sediments. The As levels from these two areas were higher than those (10 mg/kg dw) of the Swedish EPA (2009) generic soil guideline value for residential areas. Also, the As ranges in both areas were higher than the reported As UCC by Wedepohl (1995) of 2.00 mg/kg dry weight and close to EU recommended maximum acceptable limit for agricultural soil (20.0 mg/kg dry weight) (Rahman et al., 2007) for the mangrove sediments. Therefore, the topsoils have higher anthropogenic As sources that emptied into the coastal mangrove sediments in Peninsular Malaysia.

Chang et al. (2022) reported that the total As concentrations in soils collected from typical agricultural protection and vegetable-producing regions across the PRD ranged between 5.6 and 228 mg/kg dry weight. These values are similar to the range (15.2–174 mg/kg dry weight) reported in Dabaoshan mine and the surrounding areas (Qin et al., 2021) but much lower than those of the vegetable soils (360–1,054 mg/kg dry weight) collected from the vicinity of the Shizhuyuan mining area (Li L. et al., 2017). Furthermore, 52% of the studied soil contained As exceeding the risk screening value (40 mg/kg dry weight) proposed by the Chinese soil environmental quality risk control standard for soil contamination of agricultural land (GB15618-2018) (Chang et al., 2022).

Overall, 56% of topsoil samples (9 out of 16 sites) have As hazard index values exceeding 1.00 for children. Almost all the As total HI values are contributed by the ingestion pathway. The HI values are higher in children than in adults, and the As HI values in the topsoils are always higher than those in the mangrove sediments. All the As children CR values for both topsoils and mangrove sediments in all sites based on the ingestion pathway exceeded 1.0×10^{-4}, which is considered "unacceptable." For As adults' CR values of the ingestion pathway, 4 out of 16 sites exceeded the threshold limit in the topsoil samples, while all sites in the mangrove sediments are considered "acceptable." All the CR values for inhalation pathways in both topsoils and mangrove sediments are "negligible" since they are lower than 1.0×10^{-6}. All the CR values for dermal contact pathways in both topsoils and mangrove sediments are considered "acceptable" since they range from 1.0×10^{-6} to 1.0×10^{-4}, and some are "negligible."

Cao et al. (2014) investigated children's health hazard risks and exposure levels to 12 elements (including As and Sb) in water, soil, dust, air, and locally produced food using field sampling and questionnaire-based surveys in China's largest coking area. The food intake and air inhalation exposure pathways each provided about half of As exposure. They concluded that children who reside near coking operations face higher health risks from As and Sb, and that food safety is necessary to protect these children.

Total arsenic (As) concentrations in poultry feed, manure, agricultural soils, and food plants from Khyber Pakhtunkhwa Province, Pakistan were examined by Muhammad et al. (2021). In the edible sections of food plants, the total As concentrations ranged from 0.096 to 1.25 mg/kg. The mean daily intake (ADI), HQ, HI, and CR were used to determine the risk to human health. The HI was three times higher in children (2.1) than in adults (0.79), indicating that the children face non-cancer health hazards (HI index >1). For children, the CR values were somewhat higher (1.53×10^{-4}) relative to USEPA and WHO limits (1×10^{-6} to 1×10^{-4}), but for adults, a low CR was found from ingestion of selected food plants. They have concluded that the source of pollution in food plant was attributed to poultry manure leading to non-CR and CR in agricultural areas.

4.7 Higher Ecological–Health Risks of Sb and As in the Topsoils Than in the Mangrove Sediments

The ecological risk assessments (I_{geo}, CF, and ER) and health risks (HQ and HI) for Sb and As in the topsoils were higher than those in the mangrove sediments. The higher ecological–health risks of Sb and As can be explained from three perspectives.

First, the anthropogenic sources from industrial activities started far from the coastal area. Therefore, the topsoils collected near the urban and industrial areas with observable human activities had speculatively contributed to the higher levels of Sb and As indicated by the present findings. Some of the topsoils were collected near rivers adjacent to industrial areas, such as Butterworth and Kepala Batas, and nearby active agricultural areas where the use of pesticides was highly possible. Yap and Pang (2011) previously reported the sediments collected from drainage and rivers that had higher levels of heavy metals than the coastal sediments. Yap et al. (2022) recently reported that land uses played an important role of a contributing factor in the elevation of heavy metals in the topsoils of Peninsular Malaysia. These two studies clearly explain why the levels of Sb and As are higher in the topsoils than in the mangrove sediments.

Second, it has been shown that the elemental levels will decrease with increasing distance from the sources of pollution (Yap et al., 2007; Yap and Al-Mutairi, 2022), which might explain the lower levels of Sb and As in the mangrove sediments than those in the topsoils adjacent to anthropogenic sources. Various

studies from other regions have reported similar findings (Qi et al., 2011a, 2011b; Hajiani et al., 2015; Qin et al., 2021).

Third, with the understanding that sediments are considered a sink of metal pollution (Szefer et al., 1995; Yap, 2018), the mangrove sediments are assumed to accumulate the highest levels of Sb and As. The present finding showed a reverse pattern indicating the mangrove forests acted as a phytoremediator of Sb and As that caused the lower levels of As and Sb in the mangrove sediments. Reasonably, the mangrove forests are effective phytoremediators of Sb and As since mangrove trees thrive in marshy ecosystems (Defew et al., 2005; Nazli and Hashim, 2010; Nirmal et al., 2011).

5 CONCLUSION

Concentrations of As and Sb in *C. asiatica*, topsoils, and mangrove sediments collected from Peninsular Malaysia were examined. The present findings indicated comparable levels of Sb in *C. asiatica* but comparatively higher levels of As in *C. asiatica* than those in previous studies. There were no non-carcinogenic risks of Sb and As in *C. asiatica*, although children are potentially exposed to higher risks than adults. The THQ values of As and Sb in the plant were below 1.00 for children and adult Malaysian consumers, denoting no non-carcinogenic risks of As and Sb via *C. asiatica* consumption, except for As in children consuming the leaves collected from the sampling site at Kepala Batas. We also found the calculated values of estimated weekly intakes below the established provisional tolerable weekly intakes of As and Sb for children and adults. However, the As CR of children in the leaves and stems of *C. asiatica* showed more public concern than that of adults, with 10–60% of the sampling sites exceeding the As CR threshold limit, which is considered "unacceptable."

Risk assessments of As and Sb in topsoils and mangrove sediments indicated that the Sb ER ranges in the topsoils could reach "considerable potential ecological risk." In contrast, those of As in the topsoils could reach "very high ecological risk." The ER ranges of Sb in the mangrove sediments were all categorized as "minimal potential ecological risk," while those of As in the mangrove sediments could reach "high potential ecological risk." For the health risks of As and Sb in the topsoils and mangrove sediments, there was no non-carcinogenic risk of Sb in the topsoils and mangrove sediments. The Sb HI values were all below 1.0, although the values are higher in children than in adults. The Sb HI values in the topsoils are always higher than those in the mangrove sediments. Overall, there are 56% in the topsoils for children with As HI values exceeding 1.00. The ingestion pathway contributed almost all the As total HI values. Furthermore, a high ecological risk of As and carcinogenic risk of As in the topsoils and mangrove sediments were evident, with the HI values in children being higher than those in adults.

In conclusion, there were higher ecological–health risks of Sb and As in the topsoils than in the mangrove sediments. This indicates that anthropogenic sources of Sb and As originated from the land-based activities before reaching the mangroves. The unacceptable status based on As CR warrants future exposure research because dietary intake includes more than just *C. asiatica* and overall exposure results from several exposure pathways. Thus, minimizing As and Sb concentrations in vegetables is essential to safeguard human health and the environment from hazardous risks.

Therefore, establishing guidelines for Sb and As for agricultural soils and resourceful mangrove ecosystems in this region is highly recommended. This effort will ease the pollution caused by anthropogenic inputs to avoid similar disastrous chemical pollution as happened in Kim River, Southern Peninsular Malaysia (Yap et al., 2019).

DATA AVAILABILITY STATEMENT

The raw data supporting the conclusion of this article will be made available by the authors, without undue reservation.

AUTHOR CONTRIBUTIONS

Conceptualization, CKY; formal analysis, WHC; funding acquisition, CKY; investigation, KK and GHO; methodology, GHO, WHC, RH, and EC; project administration, CKY and WST; resources, WST, WMS, NAW, WHC, and MHI; supervision, CKY; validation, WST and RG; writing—original draft, CKY; writing—review and editing, CKY, WST, WHC, RN, RG, MHI, MHI, MM, HO, WC, FBE, HO, KAA, SAA, MS, MK, CFY, ARB, AB, HMHZ, TA, AN, MS, MAAR, GHO, GS, and LSW. All authors have read and agreed to the published version of the manuscript.

FUNDING

The present study was supported financially by the Fundamental Research Grant Scheme (FRGS), (Vote No.: 5524953) and by the Ministry of Higher Education, Malaysia.

SUPPLEMENTARY MATERIAL

The Supplementary Material for this article can be found online at: https://www.frontiersin.org/articles/10.3389/fenvs.2022.939860/full#supplementary-material

REFERENCES

Ainsworth, N., Cooke, J. A., and Johnson, M. S. (1991). Biological Significance of Antimony in Contaminated Grassland. *Water Air Soil Pollut.* 57-58, 193–199. doi:10.1007/bf00282882

ATSDR (Agency for Toxic Substances and Disease Registry) (2007). *Toxicological Profile for Arsenic*. Atlanta, GA: The Agency for Toxic Substances and Disease Registry, the Public Health Service, or the U.S. Department of Health and Human Services. August 2007.

ATSDR (Agency for Toxic Substances and Disease Registry) (2019). *Toxicological Profile for Antimony and Compounds*. Atlanta, GA: The Agency for Toxic Substances and Disease Registry, the Public Health Service, or the U.S. Department of Health and Human Services. October 2019.

Baroni, F., Boscagli, A., Protano, G., and Riccobono, F. (2000). Antimony Accumulation in *Achillea Ageratum, Plantago Lanceolata* and *Silene Vulgaris* Growing in an Old Sb-Mining Area. *Environ. Pollut.* 109 (2), 347–352. doi:10.1016/s0269-7491(99)00240-7

Bhattacharya, P., Welch, A. H., Stollenwerk, K. G., McLaughlin, M. J., Bundschuh, J., and Panaullah, G. (2007). Arsenic in the Environment: Biology and Chemistry. *Sci. Total Environ.* 379, 109–120. doi:10.1016/j.scitotenv.2007.02.037

Bhattacharya, P., Samal, A. C., Majumdar, J., and Santra, S. C. (2010). Arsenic Contamination in Rice, Wheat, Pulses, and Vegetables: a Study in an Arsenic Affected Area of West Bengal, India. *Water Air Soil Pollut.* 213, 3–13. doi:10.1007/s11270-010-0361-9

Bhatti, S. M., Anderson, C. W. N., Stewart, R. B., and Robinson, B. H. (2013). Risk Assessment of Vegetables Irrigated with Arsenic-Contaminated Water. *Environ. Sci. Process. Impacts* 15, 1866–1875. doi:10.1039/c3em00218g

Britannica (2022). *Climate of Malaysia*. Available at: https://www.britannica.com/place/Malaysia/Climate (searched on May 24, 2022).

CAC (Codex Alimentarius Commission) (2011). *Joint FAO/WHO Food Standards Programme Codex Committee on Contaminants in Foods, 5th Session*. The Hague, NL: Codex Alimentarius Commission.

CAC (Codex Alimentarius Commission) (2012). *Joint FAO/WHO Food Standards Programme Codex Committee on Contaminants in Foods, 6th Session*. Maastricht: Codex Alimentarius Commission.

Cao, S., Duan, X., Zhao, X., Ma, J., Dong, T., Huang, N., et al. (2014). Health Risks from the Exposure of Children to as, Se, Pb and Other Heavy Metals Near the Largest Coking Plant in China. *Sci. Total Environ.* 472, 1001–1009. doi:10.1016/j.scitotenv.2013.11.124

Casado, M., Anawar, H. M., Garcia-Sanchez, A., and Santa Regina, I. (2007). Antimony and Arsenic Uptake by Plants in an Abandoned Mining Area. *Comm. Soil Sci. Plant Anal.* 38 (9-10), 1255–1275. doi:10.1080/00103620701328412

Chabukdhara, M., and Nema, A. K. (2013). Heavy Metals Assessment in Urban Soil Around Industrial Clusters in Ghaziabad, India: Probabilistic Health Risk Approach. *Ecotoxicol. Environ. Saf.* 87, 57–64. doi:10.1016/j.ecoenv.2012.08.032

Chang, C., Li, F., Wang, Q., Hu, M., Du, Y., Zhang, X., et al. (2022). Bioavailability of Antimony and Arsenic in a Flowering Cabbage-Soil System: Controlling Factors and Interactive Effect. *Sci. Total Environ.* 815, 152920. doi:10.1016/j.scitotenv.2022.152920

Cheung, C. S. W., Kwong, K. P., Yau, J. C. W., and Wong, W. W. K. (2008). Dietary Exposure to Antimony, Lead and Mercury of Secondary School Students in Hong Kong. *Food Addit. Contam. Part A* 25 (7), 831–840. doi:10.1080/02652030701697751

Chong, K., Lee, S., Ng, S., Khouw, I., and Poh, B. (2017). Fruit and Vegetable Intake Patterns and Their Associations with Sociodemographic Characteristics, Anthropometric Status and Nutrient Intake Profiles Among Malaysian Children Aged 1-6 Years. *Nutrients* 9, 723. doi:10.3390/nu9080723

Clemente, R. (2013). "Antimony", in *Heavy Metals in Soils*. (Springer Netherlands), 497–506. doi:10.1007/978-94-007-4470-7_18

Crommentuijn, T., Sijm, D., De Bruijn, J., Van den Hoop, M., Van Leeuwen, K., and Van de Plassche, E. (2000). Maximum Permissible and Negligible Concentrations for Metals and Metalloids in the Netherlands, Taking into Account Background Concentrations. *J. Environ. Manag.* 60, 121–143. doi:10.1006/jema.2000.0354

Defew, L. H., Mair, J. M., and Guzman, H. M. (2005). An Assessment of Metal Contamination in Mangrove Sediments and Leaves from Punta Mala Bay, Pacific Panama. *Mar. Pollut. Bull.* 50, 547–552. doi:10.1016/j.marpolbul.2004.11.047

Dubey, S., Shri, M., Misra, P., Lakhwani, D., Bag, S. K., Asif, M. H., et al. (2014). Heavy Metals Induce Oxidative Stress and Genome-wide Modulation in Transcriptome of Rice Root. *Funct. Integr. Genomics* 14, 401–417. doi:10.1007/s10142-014-0361-8

Ezugwu, C. K., Onwuka, O. S., Egbueri, J. C., Unigwe, C. O., and Ayejoto, D. A. (2019). Multi-criteria Approach to Water Quality and Health Risk Assessments in a Rural Agricultural Province, Southeast Nigeria. *HydroResearch* 2, 40–48. doi:10.1016/j.hydres.2019.11.005

Egbueri, J. C., Ukah, B. U., Ubido, O. E., and Unigwe, C. O. (2020). A Chemometric Approach to Source Apportionment, Ecological and Health Risk Assessment of Heavy Metals in Industrial Soils from Southwestern Nigeria. *Int. J. Environ. Anal. Chem.*, 1–19. doi:10.1080/03067319.2020.1769615

Eikmann, T., and Kloke, A. (1993). "Nutzungs- und schutzgutbezogene Orientierungswerte für (Schad-)stoffe in Böden," in *Bondenschutz. Ergänzbares Handbuch der Maßnahmen und Empfehlungen für Schutz, Pflege und Sanierung von Böden Landschaft und Grundwasser*. Editors D. Rosenkranz, H. Einsele, and H. M. Harreß.

FAO/WHO (Food and Agriculture Organization/World Health Organization) (1989). "Evaluation of Certain Food Additives and Contaminants,". WHO Food Additive Report Series, No. 24 in *International Programme on Chemical Safety* (Geneva: World Health Organization).

FSANZ Food Standard Agency of Australia and New Zeeland (2015). Australia New Zealand Food Standards Code - Standard 1.4.1 — Contaminants and Natural Toxicants - F2015C00052. Available at: http://www.comlaw.gov.au/Details/F2015C00052/Download. (Accessed February 3, 2015).

Jamali Hajiani, N., Ghaderian, S. M., Karimi, N., and Schat, H. (2015). A Comparative Study of Antimony Accumulation in Plants Growing in Two Mining Areas in Iran, Moghanlo, and Patyar. *Environ. Sci. Pollut. Res.* 22 (21), 16542–16553. doi:10.1007/s11356-015-4852-5

Hakanson, L. (1980). An Ecological Risk Index for Aquatic Pollution Control. A Sedimentological Approach. *Water Res.* 14, 975–1001. doi:10.1016/0043-1354(80)90143-8

Haque, M. M., Niloy, N. M., Khirul, M. A., Alam, M. F., and Tareq, S. M. (2021). Appraisal of Probabilistic Human Health Risks of Heavy Metals in Vegetables from Industrial, Non-industrial and Arsenic Contaminated Areas of Bangladesh. *Heliyon* 7, e06309. doi:10.1016/j.heliyon.2021.e06309

He, M., Wang, X., Wu, F., and Fu, Z. (2012). Antimony Pollution in China. *Sci. Total Environ.* 421-422, 41–50. doi:10.1016/j.scitotenv.2011.06.009

He, M. (2007). Distribution and Phytoavailability of Antimony at an Antimony Mining and Smelting Area, Hunan, China. *Environ. Geochem. Health* 29, 209–219. doi:10.1007/s10653-006-9066-9

IAEA-TECDOC-1360 (2003). *Collection and Preparation of Bottom Sediment Samples for Analysis of Radionuclides and Trace Elements*. Vienna: IAEA. July 2003.

Jiang, Y., Ma, J., Ruan, X., and Chen, X. (2020). Compound Health Risk Assessment of Cumulative Heavy Metal Exposure: a Case Study of a Village Near a Battery Factory in Henan Province, China. *Environ. Sci. Process. Impacts* 22, 1408–1422. doi:10.1039/d0em00104j

Johnson, C. A., Moench, H., Wersin, P., Kugler, P., and Wenger, C. (2005). Solubility of Antimony and Other Elements in Samples Taken from Shooting Ranges. *J. Environ. Qual.* 34, 248–254. doi:10.2134/jeq2005.0248

Kabata-Pendias, A., and Pendias, H. (1985). *Trace Elements in Soils and Plants*. Boca Raton: FL: CRC Press.

Kabata-Pendias, A., and Pendias, H. (2001). *Trace Elements in Soils and Plants*. 3rd ed. Boca Raton, FL: CRC Press.

Kassem, A., Sarheel, A., and Al-Somel, N. (2004). Determination of Trace Elements in Soil and Plants in the Orontes Basin of Syria by Using Instrumental Neutron Activation Analysis. *J. Radioanal. Nucl. Chem.* 262 (3), 555–561. doi:10.1007/s10967-004-0475-x

Kawamoto, Y., and Morisawa, S. (2003). The Distribution and Speciation of Antimony in River Water, Sediment and Biota in Yodo River, Japan. *Environ. Technol.* 24 (11), 1349–1356. doi:10.1080/09593330309385679

Li, J., Wei, Y., Zhao, L., Zhang, J., Shangguan, Y., Li, F., et al. (2014). Bioaccessibility of Antimony and Arsenic in Highly Polluted Soils of the Mine Area and Health

Risk Assessment Associated with Oral Ingestion Exposure. *Ecotoxicol. Environ. Saf.* 110, 308–315. doi:10.1016/j.ecoenv.2014.09.009

Li, J., Zheng, B., He, Y., Zhou, Y., Chen, X., Ruan, S., et al. (2018). Antimony Contamination, Consequences and Removal Techniques: A Review. *Ecotoxicol. Environ. Saf.* 156, 125–134. doi:10.1016/j.ecoenv.2018.03.024

Li, L., Hang, Z., Yang, W.-T., Gu, J.-F., and Liao, B.-H. (2017). Arsenic in Vegetables Poses a Health Risk in the Vicinity of a Mining Area in the Southern Hunan Province, China. *Hum. Ecol. Risk Assess. Int. J.* 23, 1315–1329. doi:10.1080/10807039.2017.1306433

Li, X., Wu, T., Bao, H., Liu, X., Xu, C., Zhao, Y., et al. (2017). Potential Toxic Trace Element (PTE) Contamination in Baoji Urban Soil (NW China): Spatial Distribution, Mobility Behavior, and Health Risk. *Environ. Sci. Pollut. Res.* 24, 19766–19749. doi:10.1007/s11356-017-9526-z

Mandal, P. (2017). An Insight of Environmental Contamination of Arsenic on Animal Health. *Emerg. Contam.* 3, 17–22. doi:10.1016/j.emcon.2017.01.004

MHPRC (Ministry of Health of the People's Republic of China) (2013). *National Food Safety Standard, Maximum Levels of Contaminants in Foods*. Beijing, China. (GB2762–2012).

Mu, Z.-Q., Xu, D.-M., and Fu, R.-B. (2022). Insight into the Adsorption Behaviors of Antimony onto Soils Using Multidisciplinary Characterization. *Int. J. Environ. Res. Public Health* 19 (7), 4254. doi:10.3390/ijerph19074254

Muhammad, J., Xu, P., Khan, S., Su, J. Q., Sarwar, T., Nazneen, S., et al. (2021). Arsenic Contribution of Poultry Manure towards Soils and Food Plants Contamination and Associated Cancer Risk in Khyber Pakhtunkhwa, Pakistan. *Environ. Geochem. Health*. doi:10.1007/s10653-021-01096-6

Muller, G. (1969). Index of Geoaccumulation in Sediments of the Rhine River. *Geojournal* 2, 108–118.

Murphy, B. L., Toole, A. P., and Bergstrom, P. D. (1989). Health Risk Assessment for Arsenic Contaminated Soil. *Environ. Geochem. Health*. 11 (3-4), 163–169. doi:10.1007/BF01758667

Nazli, M. F., and Hashim, N. R. (2010). Heavy Metal Concentrations in an Important Mangrove Species, Sonneratia Caseolaris, in Peninsular Malaysia. *Environ. Asia* 3, 50–55.

Nirmal, I. J., Sajish, P. R., Nirmal, R., Basil, G., and Shailendra, V. (2011). An Assessment of the Accumulation Potential of Pb, Zn and Cd by *Avicennia Marina* (Forsk.) Vierh. In Vamleshwar Mangroves, Gujarat, India. *Not. Sci. Biol.* 3, 36–40. doi:10.15835/nsb315593

Niu, L., Yang, F., Xu, C., Yang, H., and Liu, W. (2013). Status of Metal Accumulation in Farmland Soils across China: from Distribution to Risk Assessment. *Environ. Pollut.* 176, 55–62. doi:10.1016/j.envpol.2013.01.019

Nurul Izzah, A., Aminah, A., Md Pauzi, A., Lee, Y. H., Wan Rozita, W. M., and Fatimah, S. (2012). Patterns of Fruits and Vegetable Consumption Among Adults of Different Ethnics in Selangor, Malaysia. *Int. Food Res. J.* 19, 1095–1107. doi:10.1177/1010539512458523

Omeka, M. E., Igwe, O., and Unigwe, C. O. (2022). An Integrated Approach to the Bioavailability, Ecological, and Health Risk Assessment of Potentially Toxic Elements in Soils within a Barite Mining Area, SE Nigeria. *Environ. Monit. Assess.* 194, 212. doi:10.1007/s10661-022-09856-2

Ong, G. H., Yap, C. K., Maziah, M., and Tan, S. G. (2011). Heavy Metal Accumulation in a Medicinal Plant *Centella Asiatica* from Peninsular Malaysia. *J. Biol. Sci.* 11 (2), 146–155. doi:10.3923/jbs.2011.146.155

Ong, G. H., Yap, C. K., Marziah, M., and Tan, S. (2013). Accumulation of Heavy Metals and Antioxidative Enzymes of *Centella Asiatica* in Relation to Metals of the Soils. *Pertanika J. Trop. Agric. Sci.* 36, 331–336.

Pereira, J. J., Yeap, E. B., and Ng, T. F. (1994). Application of Soil Geochemistry to the Detection of Sb-Au Mineralization in the Bufallo Reef Area, Kuala Medang, Pahang. *Geo L. Soc. Malaydia Bull.* 55, 125–155.

Pratas, J., Prasad, M. N. V., Freitas, H., and Conde, L. (2005). Plants Growing in Abandoned Mines of Portugal Are Useful for Biogeochemical Exploration of Arsenic, Antimony, Tungsten and Mine Reclamation. *J. Geochem. Explor.* 85, 99–107. doi:10.1016/j.gexplo.2004.11.003

Qi, C., Liu, G., Kang, Y., Lam, P. K. S., and Chou, C. (2011a). Assessment and Distribution of Antimony in Soils Around Three Coal Mines, Anhui, China. *J. Air Waste Manag. Assoc.* 61 (8), 850–857. doi:10.3155/1047-3289.61.8.850

Qi, C., Wu, F., Deng, Q., Liu, G., Mo, C., Liu, B., et al. (2011b). Distribution and Accumulation of Antimony in Plants in the Super-large Sb Deposit Areas, China. *Microchem. J.* 97, 44–51. doi:10.1016/j.microc.2010.05.016

Qin, J., Niu, A., Liu, Y., and Lin, C. (2021). Arsenic in Leafy Vegetable Plants Grown on Mine Water-Contaminated Soils: Uptake, Human Health Risk and Remedial Effects of Biochar. *J. Hazard. Mater.* 402, 123488. doi:10.1016/j.jhazmat.2020.123488

Qing, X., Yutong, Z., and Shenggao, L. (2015). Assessment of Heavy Metal Pollution and Human Health Risk in Urban Soils of Steel Industrial City (Anshan), Liaoning, Northeast China. *Ecotoxicol. Environ. Saf.* 120, 377–385. doi:10.1016/j.ecoenv.2015.06.019

Rahman, M. A., Hasegawa, H., Rahman, M. M., Rahman, M. A., and Miah, M. A. M. (2007). Accumulation of Arsenic in Tissues of Rice Plant (*Oryza Sativa* L.) and its Distribution in Fractions of Rice Grain. *Chemosphere* 69, 942–948. doi:10.1016/j.chemosphere.2007.05.044

Rainbow, P. S., and Phillips, D. J. H. (1993). Cosmopolitan Biomonitors of Trace Metals. *Mar. Pollut. Bull.* 26, 593–601. doi:10.1016/0025-326x(93)90497-8

Ramirez-Andreotta, M. D., Brusseau, M. L., Beamer, P., and Maier, R. M. (2013). Home Gardening Near a Mining Site in an Arsenic-Endemic Region of Arizona: Assessing Arsenic Exposure Dose and Risk via Ingestion of Home Garden Vegetables, Soils, and Water. *Sci. Total Environ.* 454-455, 373–382. doi:10.1016/j.scitotenv.2013.02.063

Reimann, C., Matschullat, J., Birke, M., and Salminen, R. (2010). Antimony in the Environment: Lessons from Geochemical Mapping. *Appl. Geochem.* 25 (2), 175–198. doi:10.1016/j.apgeochem.2009.11.011

Serafimovska, J. M., Arpadjan, S., Stafilov, T., and Tsekova, K. (2013). Study of the Antimony Species Distribution in Industrially Contaminated Soils. *J. Soils Sedim.* 13 (2), 294–303. doi:10.1007/s11368-012-0623-9

Shtangeeva, I., Bali, R., and Harris, A. (2011). Bioavailability and Toxicity of Antimony. *J. Geochem. Explor.* 110 (1), 40–45. doi:10.1016/j.gexplo.2010.07.003

Sia, S.-G., and Abdullah, W. H. (2012). Enrichment of Arsenic, Lead, and Antimony in Balingian Coal from Sarawak, Malaysia: Modes of Occurrence, Origin, and Partitioning Behaviour during Coal Combustion. *Int. J. Coal Geol.* 101, 1–15. doi:10.1016/j.coal.2012.07.005

Smichowski, P. (2008). Antimony in the Environment as a Global Pollutant: a Review on Analytical Methodologies for its Determination in Atmospheric Aerosols. *Talanta* 75 (1), 2–14. doi:10.1016/j.talanta.2007.11.005

Swedish EPA (2009). *Riktvärden För Förorenad Mark: Modellbeskrivning Och Vägledning*. Stockholm: Swedish EPA.

Szefer, P., Kusak, A., Szefer, K., Jankowska, H., WoŁowicz, M., and Ali, A. A. (1995). Distribution of Selected Metals in Sediment Cores of Puck Bay, Baltic Sea. *Mar. Pollut. Bull.* 30 (9), 615–618. doi:10.1016/0025-326x(95)00079-3

Tian, H., Zhou, J., Zhu, C., Zhao, D., Gao, J., Hao, J., et al. (2014). A Comprehensive Global Inventory of Atmospheric Antimony Emissions from Anthropogenic Activities, 1995-2010. *Environ. Sci. Technol.* 48 (17), 10235–10241. doi:10.1021/es405817u

Tschan, M., Robinson, B. H., Nodari, M., and Schulin, R. (2009a). Antimony Uptake by Different Plant Species from Nutrient Solution, Agar and Soil. *Environ. Chem.* 6, 144–152. doi:10.1071/en08103

Tschan, M., Robinson, B. H., and Schulin, R. (2009b). Antimony in the Soil - Plant System - a Review. *Environ. Chem.* 6 (2), 106–115. doi:10.1071/en08111

Tschan, M., Robinson, B., Johnson, C. A., Bürgi, A., and Schulin, R. (2010). Antimony Uptake and Toxicity in Sunflower and Maize Growing in SbIII and SbV Contaminated Soil. *Plant Soil* 334 (1–2), 235–245. doi:10.1007/s11104-010-0378-2

Tseng, C.-H., Chong, C.-K., Tseng, C.-P., and Centeno, J. A. (2007). Blackfoot Disease in Taiwan: Its Link with Inorganic Arsenic Exposure from Drinking Water. *AMBIO A J. Hum. Environ.* 36 (1), 82–84. doi:10.1579/0044-7447(2007)36[82:bditil]2.0.co;2

Uddh-Söderberg, T. E., Gunnarsson, S. J., Hogmalm, K. J., Lindegård, M. I. B. G., and Augustsson, A. L. M. (2015). An Assessment of Health Risks Associated with Arsenic Exposure via Consumption of Homegrown Vegetables Near Contaminated Glassworks Sites. *Sci. Total Environ.* 536 (536), 189–197. doi:10.1016/j.scitotenv.2015.07.018

Ukah, B. U., Egbueri, J. C., Unigwe, C. O., and Ubido, O. E. (2019). Extent of Heavy Metals Pollution and Health Risk Assessment of Groundwater in a Densely Populated Industrial Area, Lagos, Nigeria. *Int. J. Energ Water Res.* 3, 291–303. doi:10.1007/s42108-019-00039-3

USEPA (US Environmental Protection Agency) (1986). *Superfund Public Health Evaluation Manual*. Washington, DC, USA: U.S. Environmental Protection Agency, 1–86.

USEPA (US Environmental Protection Agency) (1989). *Risk Assessment Guidance for Superfund. I: Human Health Evaluation Manual*. Washington, DC: Office of Emergency and Remedial Response. EPA/540/1-89/002.

USEPA (US Environmental Protection Agency) (1997). *Exposure Factors Handbook*. Washington, DC, USA: National Center for Environmental Assessment, US EPA Office of Research and Development. EPA/600/P-95/002F.

USEPA (US Environmental Protection Agency) (2001). *Baseline Human Health Risk Assessment Vasquez Boulevard and I-70 Superfund Site Demver*. Washington, DC, USA: Co; U.S. Environmental Protection Agency.

USEPA (US Environmental Protection Agency) (2022). *Human Health Risk Assessment*. Regional Screening Level (RSL)—Summary Table as of May 2022. Available online: https://semspub.epa.gov/work/HQ/402369.pdf (accessed on May 24, 2022).

Varol, M., Gündüz, K., Sünbül, M. R., and Aytop, H. (2022). Arsenic and Trace Metal Concentrations in Different Vegetable Types and Assessment of Health Risks from Their Consumption. *Environ. Res.* 206, 112252. doi:10.1016/j.envres.2021.112252

Wang, X., He, M., Xi, J., and Lu, X. (2011). Antimony Distribution and Mobility in Rivers Around the World's Largest Antimony Mine of Xikuangshan, Hunan Province, China. *Microchem. J.* 97, 4–11. doi:10.1016/j.microc.2010.05.011

Wang, N., Wang, A., Kong, L., and He, M. (2018). Calculation and Application of Sb Toxicity Coefficient for Potential Ecological Risk Assessment. *Sci. Total Environ.* 610-611, 167–174. doi:10.1016/j.scitotenv.2017.07.268

Wedepohl, K. H. (1995). The Composition of the Continental Crust. *Geochim. Cosmochim. Acta* 59, 1217–1232. doi:10.1016/0016-7037(95)00038-2

WHO (World Health Organization) (2017). *Guidelines for Drinking-Water Quality*. Fourth edition. Geneva, Switzerland: World Health Organization. incorporating the first addendum.

Wilson, S. C., Lockwood, P. V., Ashley, P. M., and Tighe, M. (2010). The Chemistry and Behaviour of Antimony in the Soil Environment with Comparisons to Arsenic: A Critical Review. *Environ. Pollut.* 158 (5), 1169–1181. doi:10.1016/j.envpol.2009.10.045

Wilson, S. C., Leech, C. D., Butler, L., Lisle, L., Ashley, P. M., and Lockwood, P. V. (2013). Effects of Nutrient and Lime Additions in Mine Site Rehabilitation Strategies on the Accumulation of Antimony and Arsenic by Native Australian Plants. *J. Hazard. Mater.* 261, 801–807. doi:10.1016/j.jhazmat.2013.01.033

Wu, F., Fu, Z., Liu, B., Mo, C., Chen, B., Corns, W., et al. (2011). Health Risk Associated with Dietary Co-exposure to High Levels of Antimony and Arsenic in the World's Largest Antimony Mine Area. *Sci. Total Environ.* 409 (18), 3344–3351. doi:10.1016/j.scitotenv.2011.05.033

Xue, S. W., Yong, Q., and Shu, X. S. (2005). Accumulation and Sources of Heavy Metals in Urban Topsoils: a Case Study from the City of Xuzhou, China. *Environ. Geol.* 48, 101.

Yap, C. K., and Al-Mutairi, K. A. (2022). Ecological-Health Risks of Potentially Toxic Metals in Mangrove Sediments Near Estuaries after Years of Piggery Farming Bans in Peninsular Malaysia. *Sustainability* 14, 1525. doi:10.3390/su14031525

Yap, C. K., and Pang, B. H. (2011). Assessment of Cu, Pb, and Zn Contamination in Sediment of North Western Peninsular Malaysia by Using Sediment Quality Values and Different Geochemical Indices. *Environ. Monit. Assess.* 183, 23–39. doi:10.1007/s10661-011-1903-3

Yap, C. K., Ismail, A., Ching, H. L., and Tan, S. (2007). Interpretation of Copper and Zinc Contamination in the Aquatic Environment of Peninsular Malaysia with Special Reference to a Polluted River, Sepang River. *Wetl. Sci.* 5, 311–321.

Yap, C. K., Peng, S. H. T., and Leow, C. S. (2019). Contamination in Pasir Gudang Area, Peninsular Malaysia: What Can We Learn from Kim Kim River Chemical Waste Contamination? *Int. J. Hum. Edu. Dev.* 1 (2), 84–87. doi:10.22161/jhed.1.2.4

Yap, C. K., Chew, W., Al-Mutairi, K. A., Nulit, R., Ibrahim, M. H., Wong, K. W., et al. (2022). Assessments of the Ecological and Health Risks of Potentially Toxic Metals in the Topsoils of Different Land Uses: a Case Study in Peninsular Malaysia. *Biology* 11, 2. doi:10.3390/biology11030389

Yap, C. K. (2018). *Sediment Watch: Monitoring, Ecological Risk Assessment and Environmental Management*. New York, NY, USA: Nova Science Publishers.

Yeap, E. B., George, P., and Phillip, U. (1996). The Antimony Mineralization of Lalang Fault Zone, Central Sarawak. *War. Geol.* 22 (3), 1996.

Zhang, L., Gao, Y., Wu, S., Zhang, S., Smith, K. R., Yao, X., et al. (2020). Global Impact of Atmospheric Arsenic on Health Risk: 2005-2015. *Proc. Natl. Acad. Sci. USA* 117 (25), 13975–13983. doi:10.1073/pnas.2002580117

Zheng, X., Zhang, Z., Chen, J., Liang, H., Chen, X., Qin, Y., et al. (2022). Comparative Evaluation of *In Vivo* Relative Bioavailability and *In Vitro* Bioaccessibility of Arsenic in Leafy Vegetables and its Implication in Human Exposure Assessment. *J. Hazard. Mater.* 423, 126909. doi:10.1016/j.jhazmat.2021.126909

Zhou, J., Tian, H., Zhu, C., Hao, J., Gao, J., Wang, Y., et al. (2015). Future Trends of Global Atmospheric Antimony Emissions from Anthropogenic Activities until 2050. *Atmos. Environ.* 120, 385–392. doi:10.1016/j.atmosenv.2015.09.018

Conflict of Interest: The authors declare that the research was conducted in the absence of any commercial or financial relationships that could be construed as a potential conflict of interest.

Publisher's Note: All claims expressed in this article are solely those of the authors and do not necessarily represent those of their affiliated organizations, or those of the publisher, the editors, and the reviewers. Any product that may be evaluated in this article, or claim that may be made by its manufacturer, is not guaranteed or endorsed by the publisher.

frontiers | Frontiers in Analytical Science

TYPE Original Research
PUBLISHED 13 October 2022
DOI 10.3389/frans.2022.954915

OPEN ACCESS

EDITED BY
Antonije Onjia,
University of Belgrade, Serbia

REVIEWED BY
Maja Đolić,
University of Belgrade, Serbia
Aleksandra Nastasović,
Technology and Metallurgy, University of Belgrade, Serbia

*CORRESPONDENCE
Heidelore Fiedler,
heidelore.fiedler@oru.se

†PRESENT ADDRESS
Mohammad Sadia,
Freshwater and Marine Ecology, Institute for Biodiversity and Ecosystem Dynamics, University of Amsterdam, Amsterdam, Netherlands

SPECIALTY SECTION
This article was submitted to Chemometrics, a section of the journal Frontiers in Analytical Science

RECEIVED 27 May 2022
ACCEPTED 16 September 2022
PUBLISHED 13 October 2022

CITATION
Fiedler H, Baabish A and Sadia M (2022), Multivariate analysis of abiotic and biota samples for three perfluoroalkane acids. *Front. Anal. Sci.* 2:954915. doi: 10.3389/frans.2022.954915

Multivariate analysis of abiotic and biota samples for three perfluoroalkane acids

Heidelore Fiedler*, Abeer Baabish and Mohammad Sadia†

School of Science and Technology, MTM Research Centre, Örebro University, Örebro, Sweden

Perfluoroalkane substances (PFAS) comprise a large family of chemicals of environmental concern and are subject to chemical analyses, international regulation, and risk assessments. Environmental samples including air, water, sediment, and soil as abiotic matrices, food samples comprising fish, meat (beef, sheep, chicken), egg, butter, and milk as well as human milk samples were assessed using uni- and multivariate methods. Participating countries were asked to provide baseline samples and not target potential hotspots. Chemometric analysis was possible for only three of the 15 PFAS monitored, namely perfluorooctane sulfonic acid (PFOS), perfluorooctanoic acid (PFOA), and perfluorohexane sulfonic acid (PFHxS). The assessments showed that PFAS contamination in developing countries and in all matrices considered was almost equally attributed to PFOS and PFOA; PFHxS did not play a role. Subsequently, across all samples, PFOS and PFOA were strongly negatively correlated (spearman correlation coefficient r = −0.94). The measured values showed moderate positive correlation between PFOS and PFOA (r = 0.76) indicating common sources or environmental behavior. No clear pattern could be observed for geographic locations nor for transfers between matrices. Whereas the abiotic samples—soil, sediment, air—gave a very heterogenous picture (very small p-values) and had wide ranges and outliers, the measured values of the biota samples were not significantly different between matrices.

KEYWORDS

perfluoroalkane substances (PFAS), targeted chemical analysis, developing countries, chemometric approaches, correlation and significance

1 Introduction

Persistent organic pollutants (POPs) are globally addressed by the Stockholm Convention on Persistent Organic Pollutants (UNEP, 2001), which triggered many activities at global and national levels with respect to regulations but also research. The World Health Organization (WHO) defines "persistent organic pollutants" as "chemicals of global concern due to their potential for long-range transport, persistence in the environment, ability to bio-magnify, and bio-accumulate in ecosystems, as well as their significant negative effects on human health and the environment" (https://www.who.int/news-room/questions-and-answers/item/food-safety-persistent-organic-pollutants-(pops)update-November-2020). Similar definitions

are available from the United Nations Environment Programme (UNEP) and the Stockholm Convention (www.pops.int), the US Environmental Protection Agency (https://www.epa.gov/international-cooperation/persistent-organic-pollutants-global-issue-global-response#pops) and others.

Humans are exposed to POPs mainly through the food we eat but also through the air we breathe, the water we drink, dust we inhale, and surfaces and commodities we touch. As a result, POPs once manufactured or formed unintentionally, and released from its source can be found virtually everywhere. Analytical chemists attempt to determine measurable concentrations of POPs in these matrices.

Perfluoroalkane substances (PFAS) area group of relatively new POPs: containing fluorine and with the strong C-F bound in the molecule, they exhibit non-reactivity towards hydrolysis or photolytic degradation. As halogenated compounds, due to their stability and lipophilicity, POPs undergo long range transport, which allows them to travel far from their source, and exhibit bioaccumulation, which reconcentrates these chemical compounds to potentially dangerous levels (Wania and Mackay, 1996). Perfluorinated substances were not among the originally listed POPs (Fiedler et al., 2019) but have been added later into the annexes of the Stockholm Convention (UNEP, 2009; UNEP, 2019a; UNEP, 2019b; UNEP, 2022). In addition to the typical POPs properties, perfluoroalkane acids through their hydrophilic group, such as perfluorooctane sulfonic acid (PFOS), perfluorohexane sulfonic acid (PFHxS), and perfluorooctanoic acid (PFOA) are water-soluble and partition to water to a greater extent than the brominated and chlorinated POPs.

Within an international environmental monitoring project implemented by the United Nations Environment Programme (UNEP) in 42 countries, almost 800 samples have been analyzed in our laboratory for perfluoroalkane acids (PFAA). In this paper, we assess the quantitative results from abiotic and biota samples with multivariate analysis for occurrence and scale of PFAA but also their profiles in environmental, food, and human samples using descriptive statistics, uni- and multivariate methods.

2 Materials and methods

2.1 Origin of samples

From 2016 to 2021, UNEP implemented four regional projects comprising 42 countries from African (n = 15), Asian (n = 7), Latin American and Caribbean (GRULAC, n = 11), and Pacific Islands (PAC, n = 9) regions (UNEP, 2015a; UNEP, 2015b; UNEP, 2015c; UNEP, 2015d). All countries were invited to collect 1) ambient air samples using passive samplers with polyurethane foam disks 4-times per year for 2 years, 2) one pool of human milk from primiparae, and 3) samples of other matrices of their

TABLE 1 Overview of origin and classification of the samples analyzed for three PFAA.

	Africa	Asia	PAC	GRULAC	Overall
Samples	229 (34.3%)	123 (18.4%)	108 (16.2%)	208 (31.1%)	668 (100%)
Type					
Abiotic samples	175 (76.4%)	85 (69.1%)	75 (69.4%)	151 (72.6%)	486 (72.8%)
Biota samples	54 (23.6%)	38 (30.9%)	33 (30.6%)	57 (27.4%)	182 (27.2%)
Matrix					
Sediment	15 (6.6%)	9 (7.3%)	2 (1.9%)	15 (7.2%)	41 (6.1%)
Soil	7 (3.1%)	8 (6.5%)		5 (2.4%)	20 (3.0%)
Air	103 (45.0%)	42 (34.1%)	37 (34.3%)	85 (40.9%)	267 (40.0%)
Water	50 (21.8%)	26 (21.1%)	36 (33.3%)	46 (22.1%)	158 (23.7%)
Fish	21 (9.2%)	12 (9.8%)	16 (14.8%)	26 (12.5%)	75 (11.2%)
Beef	2 (0.9%)	5 (4.1%)		1 (0.5%)	8 (1.2%)
Butter	1 (0.4%)	3 (2.4%)	1 (0.9%)	4 (1.9%)	9 (1.3%)
Milk	2 (0.9%)	1 (0.8%)		2 (1.0%)	5 (0.7%)
Sheep		2 (1.6%)			2 (0.3%)
Chicken	1 (0.4%)	1 (0.8%)	3 (2.8%)		5 (0.7%)
Egg	8 (3.5%)	10 (8.1%)	4 (3.7%)	12 (5.8%)	34 (5.1%)
Vegetable	5 (2.2%)			3 (1.4%)	8 (1.2%)
Human milk	14 (6.1%)	4 (3.3%)	9 (8.3%)	9 (4.3%)	36 (5.4%)

10.3389/frans.2022.954915

national interest (up to 12 samples) for analysis of POPs at designated chemical laboratories. In addition, 22 countries were chosen to provide surface water samples, 4-times per year for 2 years, for the analysis of PFOS, PFOA, and PFHxS.

The sampling strategy did no target hotspots rather was directed towards baseline concentrations with no known POP source nearby. Standard operational procedures were developed at the onset of the projects to guide the sampling (UNEP, 2017a; UNEP, 2017b; UNEP, 2017c; UNEP, 2017d). The locations for the air and water samples, were maintained throughout the project, with the exception that in Brazil, the sampling site at the mouth of the Amazon River was moved to the Sao Paulo channel in the second year. In most countries, the air sampling site was located at the national meteorological station or the institute responsible for the project. The water samples were surface water samples collected with a bucket one every 3 months. The site should be integrative and located at the mouth of a river or an estuary (Weiss et al., 2015).

The full sampling programme could not be verified by all countries. Here, we assess the samples analyzed for PFAA in the laboratory of Örebro University, Sweden. The characteristics of the samples are described in the project reports by UNEP for the four regional projects (Fiedler and UNEP, 2022a; Fiedler and UNEP, 2022b; Fiedler and UNEP, 2022c; Fiedler and UNEP, 2022d).

2.2 Chemical analysis

Chemical analysis of PFOS, PFOA, PFHxS, and other PFAS followed the procedures as described (Sadia et al., 2020; Baabish et al., 2021; Camoiras González et al., 2021; Fiedler and Sadia, 2021; Fiedler et al., 2022a; Fiedler et al., 2022 submitted). In brief, up to 16 PFAS and five PFOS precursors, perfluoro-1-octanesulfonamide (FOSA), methylperfluoro-1-octanesulfonamide (NMeFOSA) and ethylperfluoro-1-octanesulfonamide (NEtFOSA); two perfluorooctane sulfonamidoethanols, 2-(N-methylperfluoro-1-octanesulfonamido)-ethanol (NMeFOSE), and 2-(N-ethylperfluoro-1-octanesulfonamido)-ethanol (NEtFOSE), were extracted using solid-phase extraction (SPE, SPE-WAX cartridges, 6 ml, 150 mg, 30 µm; Waters Corporation Milford, United States). Sample extracts were analyzed with a liquid chromatograph coupled to a tandem mass spectrometer (LC–MS/MS) with electrospray ionization (ESI) operating in negative ionization mode (XEVO TQS Waters Corporation, Milford, United States). Aliquots of 10 µl were injected on a BEH (ethylene bridged hybrid) C_{18}-column (1.7 µm, 2.1 mm × 100 mm; Waters Corporation Milford, United States). Mobile phases used were either methanol: water 70:30 (v/v) (A) and 100% methanol (B) with 2 mM ammonium acetate in both phases or ammonium acetate (2 mM) in 80:20 (v:v) water:

TABLE 2 Descriptive statistics of three PFAA in samples according to matrix. Concentrations in pg per PUF for air samples, pg per g in biota and abiotic samples.

	Sediment (N = 41)	Soil (N = 20)	Air (N = 267)	Water (N = 158)	Fish (N = 75)	Beef (N = 8)	Butter (N = 9)	Milk (N = 5)	Sheep (N = 2)	Chicken (N = 5)	Egg (N = 34)	Vegetable (N = 8)	Human milk (N = 36)	Overall (N = 668)
ΣPFOS														
Mean (SD)	123 (241)	146 (126)	261 (366)	1.19 (1.83)	125 (314)	42.2 (24.9)	26.6 (36.4)	30.9 (27.4)	39.6 (22.1)	16.2 (10.2)	48.3 (64.7)	3.06 (2.98)	18.4 (34.5)	135 (285)
Median	33.3	144	135	0.448	30.1	34.8	11.5	30.8	39.6	14.5	27.3	2.50	12.7	38.4
[Min, Max]	[0, 1,140]	[0, 425]	[0, 2,480]	[0, 12.2]	[0, 1,650]	[15.5, 844]	[0, 103]	[2.72, 74.3]	[24.0, 55.1]	[4.21, 32.0]	[0, 326]	[0, 9.53]	[0, 212]	[0, 2,480]
PFOA														
Mean (SD)	23.5 (29.4)	49.6 (41.9)	222 (155)	0.683 (1.22)	12.6 (19.6)	7.25 (4.06)	11.7 (16.8)	1.38 (3.10)	15.6 (2.05)	12.9 (20.3)	8.84 (8.03)	9.48 (9.91)	14.6 (5.28)	95.1 (144)
Median	16.6	38.9	181	0.275	8.95	7.29	9.30	0	15.6	7.94	7.15	8.25	13.3	16.8
[Min, Max]	[0, 168]	[0, 172]	[0, 1,190]	[0, 9.61]	[0, 160]	[0, 14.8]	[0, 54.1]	[0, 6.92]	[14.2, 17.1]	[0, 48.5]	[0, 28.1]	[0, 27.2]	[6.20, 31.8]	[0, 1,190]
PFHxS														
Mean (SD)	10.8 (48.2)	3.94 (8.91)	11.5 (20.3)	0.36 (0.719)	1.13 (3.76)	2.79 (3.89)	0.96 (2.87)	0.96 (2.15)	0 (0)	0.86 (1.93)	3.43 (7.00)	0.23 (0.55)	3.29 (18.5)	5.99 (18.8)
Median	0	0	0	0.081	0	0	0	0	0	0	0	0	0	0
[Min, Max]	[0, 307]	[0, 33.6]	[0, 96.1]	[0, 4.21]	[0, 22.9]	[0, 8.25]	[0, 8.62]	[0, 4.80]	[0, 0]	[0, 4.31]	[0, 28.7]	[0, 1.56]	[0, 111]	[0, 307]

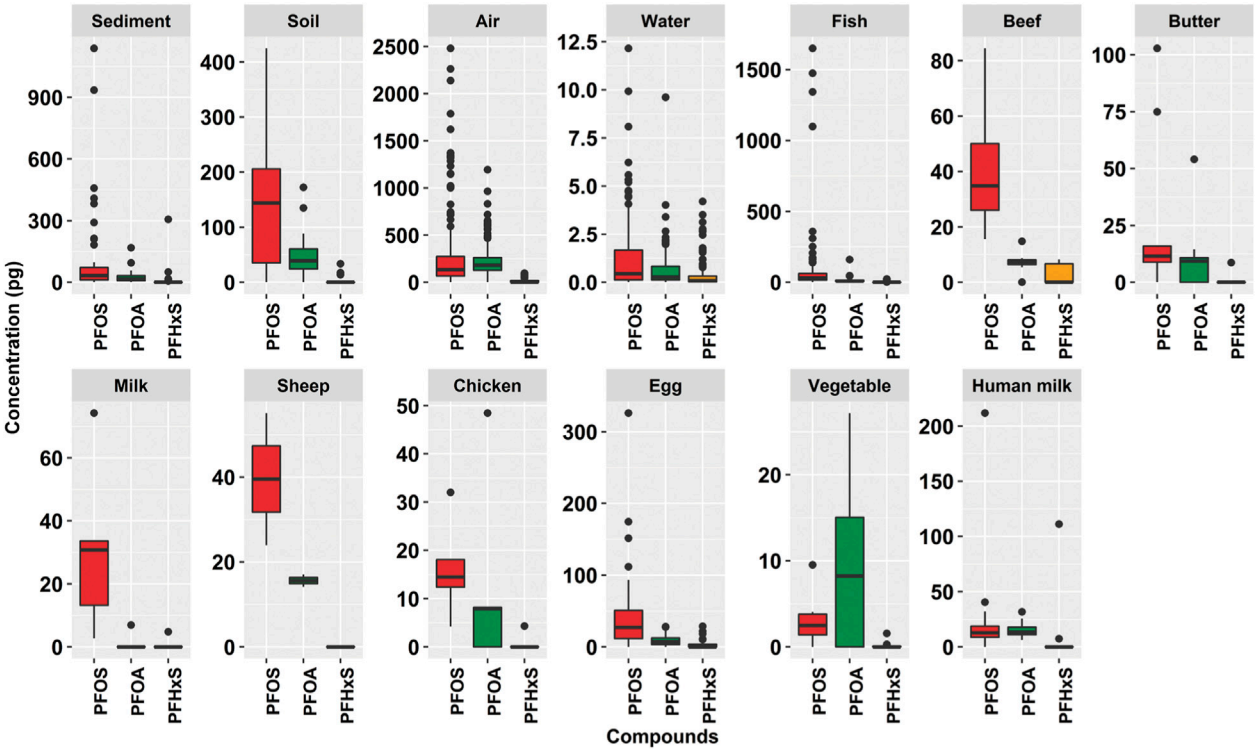

FIGURE 1
Box whisker plots (scaled) for PFOS, PFOA, and PFHxS in 13 matrices (n = 668). The whiskers represent the minimum and maximum concentrations without the outliers. The lower border of the box represents the first quartile (25%), the line inside the box the median and the upper border is the third quartile (75%). The dots outside the whiskers are outliers, which were defined as all concentrations greater or smaller the interquartile range multiplied by 1.5.

acetonitrile (A), and ammonium acetate (2 mM) in acetonitrile (B).

The MTM Laboratory had successfully participated in the analysis of PFAS in three rounds of the UNEP-coordinated interlaboratory assessments for POPs (UNEP et al., 2014; UNEP et al., 2017; Fiedler et al., 2020; UNEP et al., 2021; Fiedler et al., 2022b; van der Veen et al., 2022 submitted).

2.3 Data handling and assessment

All data were maintained in Microsoft Office 365 Excel®; statistical evaluations were made using R packages versions 4.0.3 and 4.0.5 with R-Studio. Multivariate methods, such as hierarchical cluster analysis (HCA) and principal component analysis (PCA) were applied to assess similarities, differences or correlations between datasets and meta-data. Clustering was made using Euclidean distances and the Ward method (ward.02 in R); a method creating groups where the variance within the groups (clusters) is minimized. The data in a set are grouped into clusters of great(er) similarity to form a dendrogram as shown in the heatmap (see Figure 8). In a PCA, data are extracted and newly projected to display systematic variation in a data matrix. For all quantitative assessments, concentrations below the limit of quantification (LOQ) were set zero. All concentrations refer to picogram (pg) followed by the respective reference unit, either Gram or PUF (for air samples).

Spearman non-parametric correlation was applied to determine relationship between concentrations or percentage contribution of variables; the correlation coefficient r was set less than 0.05. The Kruskal–Wallis H test was used to determine if there are statistically significant differences between the independent variables and dependent variables. Post-hoc analysis was performed using the pairwise Wilcoxon test. Adjustment of the p-value was made using the Benjamini–Hochberg method. The significance values (p) for all tests were set to less than 0.05.

For all quantitative assessments, concentrations below the limit of quantification (LOQ) were set to zero; thus, lower-bound concentrations were used.

Outliers were defined as values above (or below) the interquartile range multiplied by 1.5. The interquartile range is defined as the length of the middle 50% of data points, *i.e.*, the difference between the third or upper quartile (75% of data points) and the first or lower quartile (25% of data points). Visualization is expressed as box whisker plots.

3 Results

3.1 Descriptive statistics of samples

A total of 668 samples, had quantitative results for all of the three PFAA. About 200 samples had either all three PFAA below the LOQ or at least one PFAA could not be determined since the QA/QC criteria were not met and the specific result could not be reported (NR).

The characteristics of the samples as to their geographic location, type or matrix is shown in Table 1; all samples were collected 2017–2018 and a few samples in 2019. As to geography, 34% of the samples were from Africa, followed by GRULAC with 31%; Asia ad PAC had 18% and 16%, respectively. There were

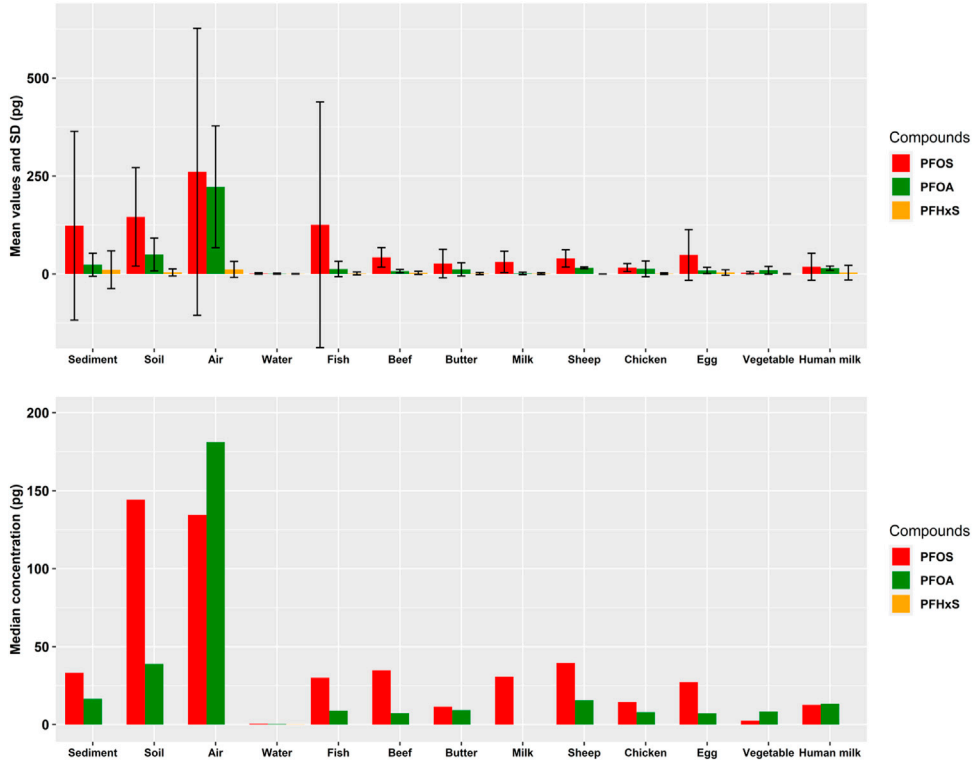

FIGURE 2
Mean values with SD (above) and median values (below) for three PFAA in the matrices analyzed.

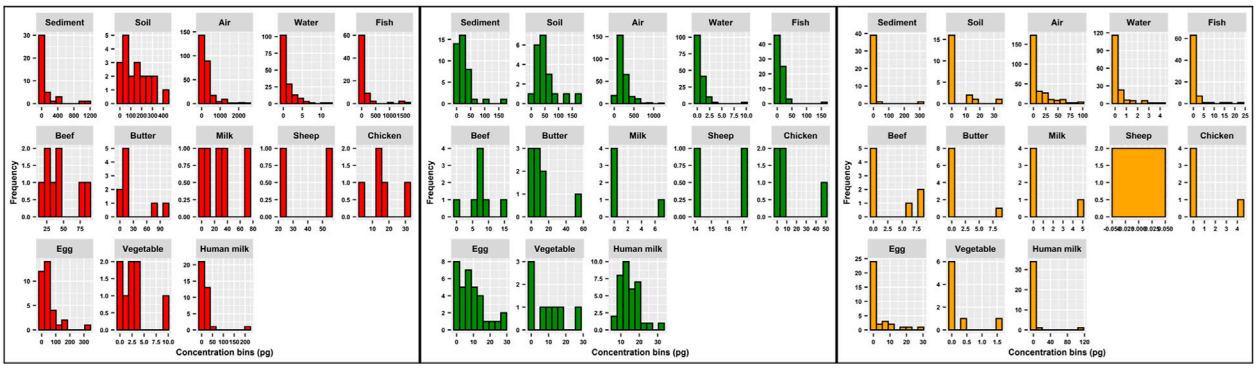

FIGURE 3
Histograms for PFOA (red color), PFOA (green color) and PFHxS (orange color) according to matrices.

much more abiotic samples (73%) than biota (27%) due to the abundance of 267 ambient air samples collected through passive air sampling using PUFs (Camoiras González et al., 2021) and 158 surface water samples (Baabish et al., 2021; Fiedler et al., 2022). Among the biota samples were 75 fish (Fiedler et al., 2022) and 36 human milk samples from *primiparae* (Fiedler and Sadia, 2021). Despite the large number of samples, for certain combinations of matrix and region, only a few samples were available occasionally, thus limiting interpretation; an example is one butter sample from the Pacific Islands.

The summarized results shown in Table 2 contain values in pg of PFAA per gram sample and pg per PUF (and 3 months of exposure time) for the air samples. Across all the samples, PFOS had the highest mean and median values (135 pg/unit and 38.4 pg/unit) followed by PFOA (95.1 pg/unit and 16.8 pg/unit). PFHxS had a median value of zero and a mean value of 5.99 pg/unit. Large differences can be seen for PFOS between mean values and median values such as for sediment and fish. For air, butter, and egg, the mean values are about twice as high as the median values. For PFOA, such large differences could not be seen. For PFHxS, the values were much lower and there were a lot of values below the LOQ; the highest measured values were found in a sediment sample (307 pg/g) and in a human milk from Kiribati (111 pg/g f.w.). The visualization for each matrix is shown in Figure 1. The occurrence of the data points in the four project regions as box whisker plots for each matrix is contained in the supplementary information as Supplementary Figure S1.

Soil and sediment samples were provided at the discretion of the countries and there were no criteria requested in the sampling protocol (UNEP, 2017d). Therefore, the scale and pattern of these samples cannot be easily interpreted Figure 1. The abiotic samples, sediment, air, and water, have many datapoints as outliers with amounts greater than the interquartile range multiplied by 1.5 (according to definition in Section 2.3). Fish is the only biota matrix that showed many outliers. All other biota matrices, and soil, have lower numbers of outliers. The more homogenous data points for the foodstuffs may be due to sample origin since most of them were bought from supermarkets or local markets; thus, are quite representative for the country. Nevertheless, for a few food samples, local contamination inputs cannot be excluded, e.g., butter, milk, chicken or egg. The air samples had outliers in all regions, especially for PFOS; however, not in PAC (Supplementary Figure S1). The fish samples had outliers for PFOS, especially in the

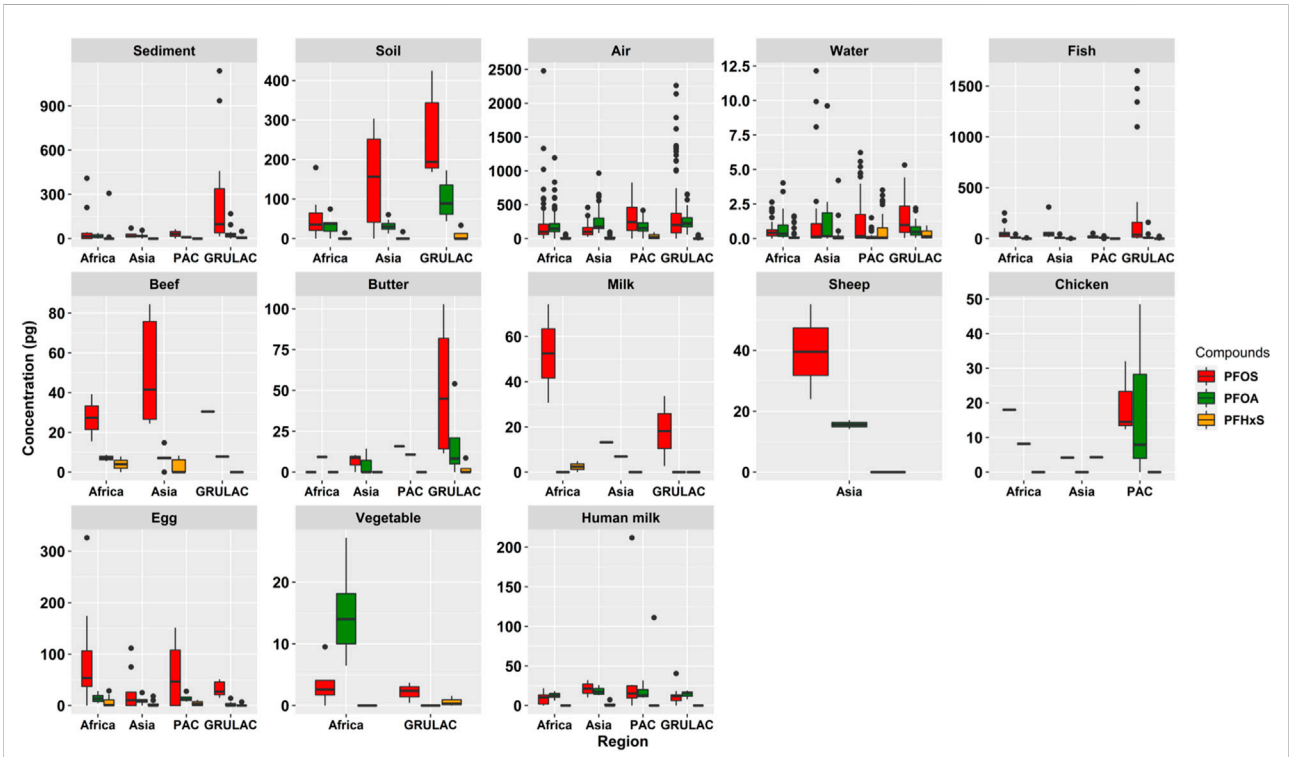

FIGURE 4
Scaled box plots showing the three PFAA in each matrix differentiated by region. The whiskers represent the minimum and maximum concentrations without the outliers. The lower border of the box represents the first quartile (25%), the line inside the box the median and the upper border is the third quartile (75%). The dots outside the whiskers are outliers, which were defined as all concentrations greater or smaller the interquartile range multiplied by 1.5.

10.3389/frans.2022.954915

GRULAC region. Wide interquartile ranges occurred for PFOS in Asia for beef, in GRULAC for butter and in Africa for cow's milk. Eggs showed large interquartile ranges for PFOS in all regions, least in Asia. For PFOA, there were hardly any outliers recorded; a quite large interquartile range was found in PAC, although on comparatively low level. For human milk, extreme values were observed in PAC for Kiribati with PFOS and PFHxS whereas PFOA did not have any outlier across all regions. The abundance of PFOA in PAC chicken samples and GRULAC butter samples is noticeable (see Table 2; Supplementary Figure S1).

The difference between mean (with standard deviation, SD) and median values is graphically shown in Figure 2. For air, it can be seen that the ratio PFOS: PFOA is inverted when considering mean: median values: the mean value for PFOS (261 pg/PUF with a large SD) is higher than for PFOA (222 pg/PUF with a smaller SD) whereas the median value for PFOA (181 pg/PUF) is higher than for PFOS (135 pg/PUF). Thus, care should be taken when selecting data for assessments.

The histograms in Figure 3 are a graphical representation combining the number of samples per matrix with the measured values shown in Table 2. Clearly, the frequency distributions do not follow normal distribution. Only PFOA in human milk exhibits a bell shape curve. All others are heavily biased towards the lowest values.

The graphics for the PFAA concentrations by matrix but differentiated into the regional projects is shown in Figure 4. Striking are the comparatively high PFOS concentrations in Asian beef, GRULAC butter and African cows' milk. Non-parametric testing across all matrices showed that there were significant differences between the regions ($p = 0.017$) due to the pairwise significant difference between Pacific Islands and GRULAC ($p = 0.017$). The difference of the data points was significant for the type of samples, abiotic vs. biota, which had a Kruskal–Wallis chi-squared value of 62.642 and $p = 2.48 \times 10^{-15}$.

3.2 Pattern as contribution of individual perfluoroalkane substances to sum of three perfluoroalkane substances

The descriptive statistics covering the 668 samples and assessing the three PFAS as to their contribution to the sum of the three PFAS (PFAS3) are the pattern of the PFAS and is shown in Table 3, and visualized in Figure 5.

The graphical plot showing the pattern for all matrices as occurring in the regions is summarized as box plots in the supplementary information as Supplementary Figure S2.

The histograms for the pattern of the PFAA in Supplementary Figure S3 show a more homogeneous picture closer to normal distribution than was seen for the measured values in Figure 3.

TABLE 3 Descriptive statistics for pattern of three PFAA (%) in samples according to matrix.

	Sediment (N = 41)	Soil (N = 20)	Air (N = 267)	Water (N = 158)	Fish (N = 75)	Beef (N = 8)	Butter (N = 9)	Milk (N = 5)	Sheep (N = 2)	Chicken (N = 5)	Egg (N = 34)	Vegetable (N = 8)	Human milk (N = 36)	Overall (N = 668)
R_PFOS														
Mean (SD)	60.0 (32.5)	65.7 (26.5)	43.1 (18.7)	51.3 (21.6)	73.4 (24.8)	80.5 (11.0)	59.2 (43.1)	91.9 (14.9)	69.0 (15.0)	64.5 (23.0)	66.9 (36.7)	39.9 (32.8)	40.4 (22.7)	52.4 (25.9)
Median [Min, Max]	62.9 [0, 100]	71.4 [0, 100]	42.7 [0, 100]	51.3 [0, 100]	79.7 [0, 100]	82.1 [64.3, 100]	69.3 [0, 100]	100 [65.6, 100]	69.0 [58.4, 79.5]	64.6 [39.8, 100]	77.5 [0, 100]	36.5 [0, 100]	44.3 [0, 75.6]	51.2 [0, 100]
R_PFOA														
Mean (SD)	37.0 (34.1)	32.4 (26.4)	54.3 (18.8)	36.8 (22.7)	25.8 (24.3)	15.9 (11.3)	39.5 (41.8)	6.87 (15.4)	31.0 (15.0)	25.4 (25.7)	30.2 (37.7)	50.0 (43.4)	58.4 (24.1)	42.9 (26.6)
Median [Min, Max]	27.7 [0, 100]	27.8 [0, 100]	54.4 [0, 100]	36.3 [0, 100]	20.3 [0, 100]	14.8 [0, 35.7]	30.7 [0, 100]	0 [0, 34.4]	31.0 [20.5, 41.6]	31.2 [0, 60.2]	12.5 [0, 100]	63.5 [0, 100]	54.2 [8.96, 100]	45.1 [0, 100]
R_PFHxS														
Mean (SD)	3.02 (9.12)	1.85 (4.24)	2.65 (4.51)	11.9 (14.4)	0.813 (3.41)	3.66 (5.45)	1.29 (3.87)	1.21 (2.71)	0 (0)	10.1 (22.6)	2.90 (5.29)	10.1 (18.6)	1.22 (5.56)	4.69 (9.60)
Median [Min, Max]	0 [0, 41.3]	0 [0, 14.7]	0 [0, 30.6]	8.07 [0, 100]	0 [0, 26.3]	0 [0, 14.1]	0 [0, 11.6]	0 [0, 6.07]	0 [0, 0]	0 [0, 50.6]	0 [0, 18.6]	0 [0, 40.9]	0 [0, 31.3]	0 [0, 100]

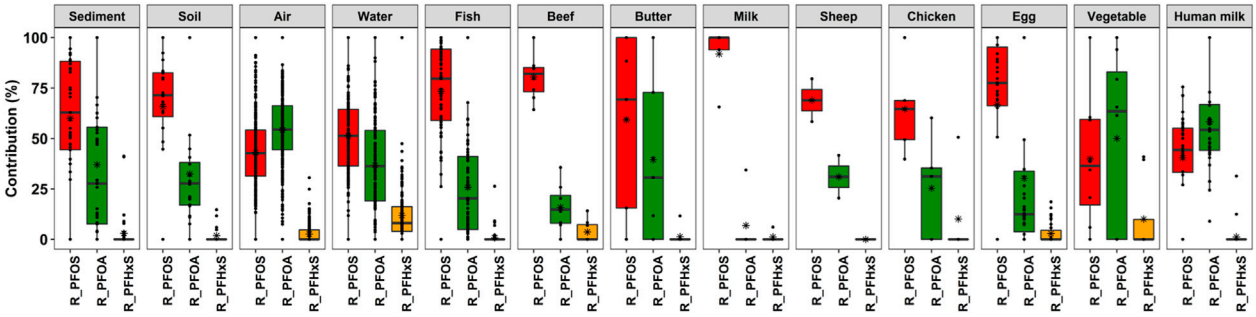

FIGURE 5
Box plots showing the contribution of individual PFAS to PFAS3 in each matrix. The whiskers represent the minimum and maximum concentrations without the outliers. The lower border of the box represents the first quartile (25%), the line inside the box the median and the upper border is the third quartile (75%). The asterisk indicates the mean value. The dots outside the whiskers are outliers, which were defined as all concentrations greater or smaller the interquartile range multiplied by 1.5.

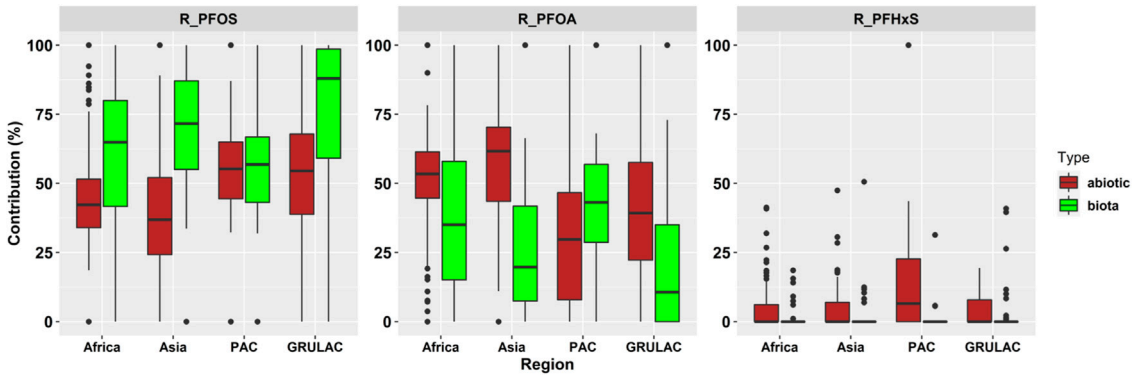

FIGURE 6
Scaled boxplots displaying the pattern for the ratio of PFOS, PFOA and PFHxS to PFAS3 in abiotic (brown color) and biota (green color) samples for each region. The whiskers represent the minimum and maximum concentrations without the outliers. The lower border of the box represents the first quartile (25%), the line inside the box the median and the upper border is the third quartile (75%). The dots outside the whiskers are outliers, which were defined as all concentrations greater or smaller the interquartile range multiplied by 1.5.

The detailed information is illustrated in the supplementary information in Supplementary Figure S4, which shows the contribution of PFOS, PFOA and PFHxS to the sum of these three PFAS (PFAS3) in stacked bars scaled to 100% for each sample according to region and matrix. In most cases, also for the pattern within one matrix and one region, the shares of PFOS and PFOA are quite different. In all samples, except one chicken in Vietnam and very few water samples in PAC, the contribution of PFHxS to sum PFAS3 is minor.

Figure 6 shows that PFOS had higher contributions to the sum of PFAS3 in biota (median value = 69.4%) than abiotic samples (median = 46.8%). Whereas in Africa, Asia, and GRULAC, the shares of PFOS in biota were 64.9%, 71.6%, and 88.0%, the Pacific Islands sample set had very similar median values in biota and abiotic samples. PFOA contribution was 28.5% in biota and 49.0% in abiotic samples. Only in the Pacific Islands region, the PFOA share was higher in biota. In general, PFHxS did not contribute much to the sum PFAS3—median percentage contribution is always zero, but mean values were 2.1% in biota and 5.7% higher in abiotic samples. Parametric testing did confirm significant difference in the pattern between the types (p = 0.02; abiotic vs. biota). No significant differences in the pattens

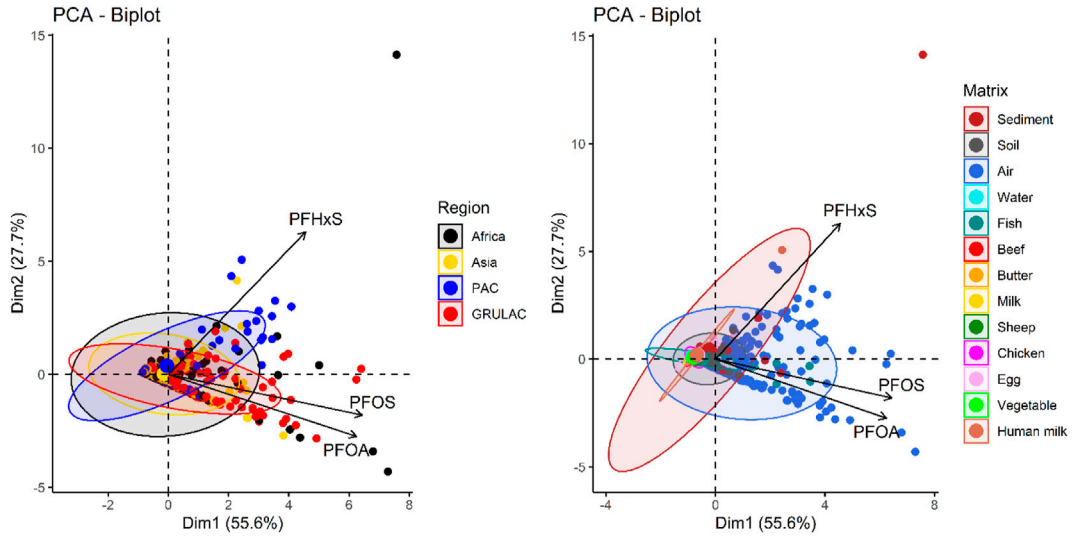

FIGURE 7
PCA biplots for 668 environmental samples with ellipses around region (left) and matrix (right). Loadings for PFOS, PFOA, and PFHxS measurements.

were found in either region (p = 0.96) or between matrices (p = 0.72).

3.3 Multivariate analysis

The PCAs in Figure 7 explain 83% of the data points in the samples with 55.6% along the x-axis (Dim1) and 27.7% along the y-axis (Dim2). Samples characterized by PFHxS were located in the first quartile and sample characterized by PFOS and PFOA were located in the fourth quartile, indicating that PFHxS concentrations differed from those of PFOS and PFOA. Ellipses as envelopes for samples of the same characteristic could be created around all regions (Figure 7, left); they overlap largely so that only for the PAC samples (blue color of dots and ellipse) some preference towards high PFHxS values could be seen. With respect to the matrices (Figure 7, right), the human milk samples formed an own very narrow group on the x-axis with the outlier for the Kiribati human milk sample in the first quartile due to high PFHxS but also high PFOS concentrations; this was the only human milk sample on the positive site of Dim1. The food samples were co-located within small ellipses (if any) close to the origin; only some fish samples were found at higher values close to the positive x-axis.

The PCA for the pattern as shown in the biplots in Supplementary Figure S5 of the supplementary information shows the distinct vectors for the three principal components and almost complete overlaps of the ellipses for regions and matrices.

The heatmap depicting the contribution of the three variables to the sum of PFAS3 in Figure 8 shows a complex dendrogram at left. Unfortunately, since the heatmap describes 668 samples, the sample IDs at the right site are indicative only and do not include all samples. The dendrogram has two samples at the bottom of the heatmap, which had only PFHxS quantified (green color) and PFOA and PFOS with 0% contribution to the pattern; both were water samples from PAC (PLW 2018–1 and TUV 2018–3) at low scale (0.033 ng/L and 0.027 ng/L). The remaining 666 samples were grouped into two distinct clusters; each of them contains representation of all matrices as shown by the colors below the dendrogram. The lower cluster is characterized by low PFHxS (red color) and moderate to high PFOA contributions (yellow to green colors) whereas the upper cluster contains all the samples that have higher PFOS (yellow to green colors) than PFOA (red to yellow colors) contributions to the sum of PFAS3.

The above presented results were confirmed by spearman correlation coefficients using ward.02 method and hierarchical clustering as shown in Figure 9. The correlation coefficients for the measured values (Section 3.1) demonstrate that PFOS is positively and moderately-to-high correlated with PFOA (r = 0.76) but not correlated with PFHxS (r = 0.13) as PFOA and PFHxS are not correlated (r = 0.04) (Figure 9, left). Subsequently, the pattern for the contribution of the individual PFAS to the PFAS3 (Section 3.2) showed a very high negative correlation between PFOS and PFOA (r = −0.91) and no correlations with PFHxS (r = −0.06) and for PFOA to PFHxS (r = −0.2) (Figure 9, right).

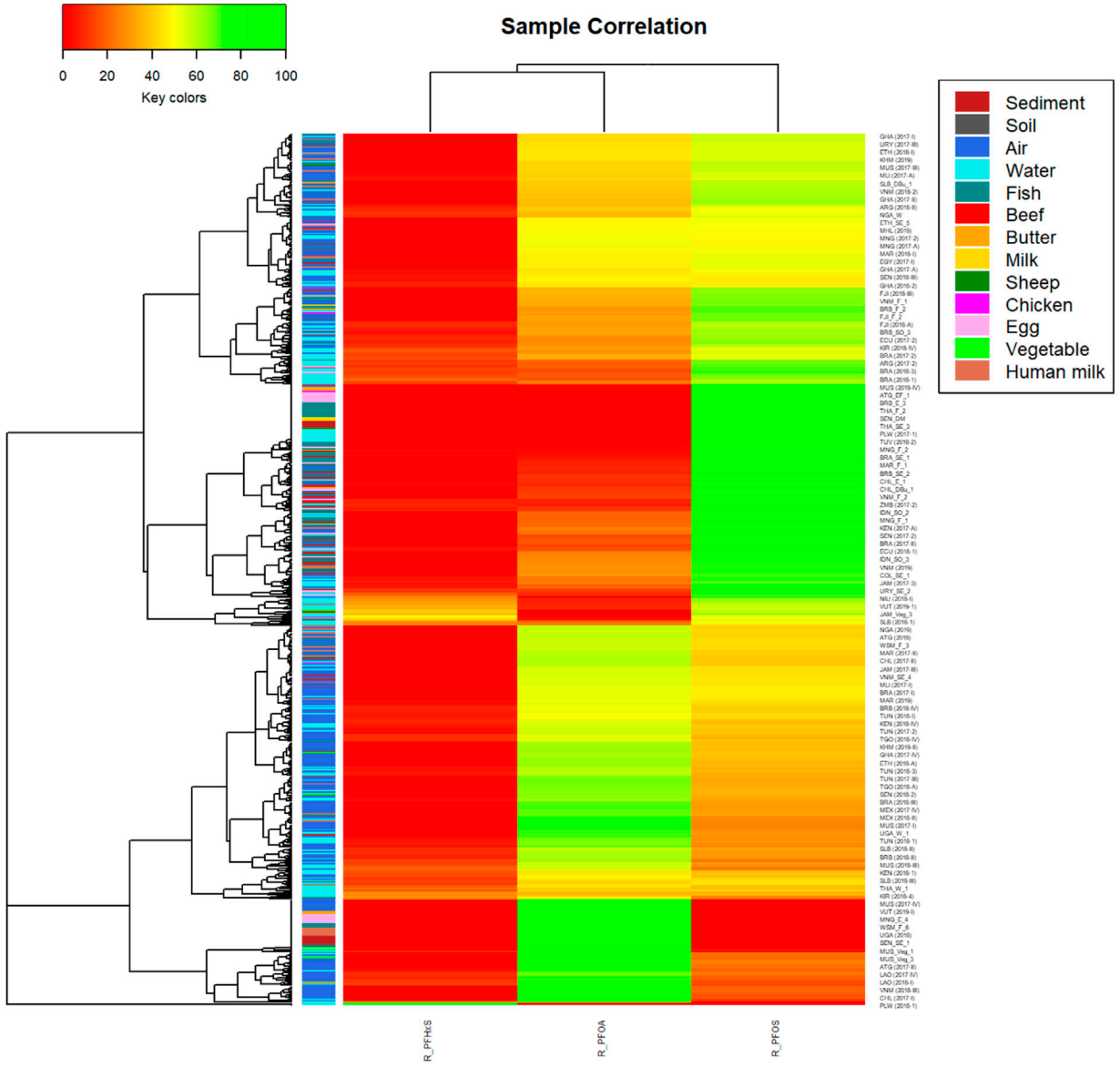

FIGURE 8
Heatmap for the pattern of PFAS3 with dendrogram using ward method and colors for matrices (*n* = 668)

4 Discussion and conclusion

A large dataset has been analyzed by one laboratory with the same instrumentation and chemical analytical approaches within 3 years. The conditions in the laboratory remained the same and stable during this period so that intralaboratory variation in the laboratory were minimized. Even though up to 15 PFAA had been analyzed, only three PFAA could be quantified with high detection frequencies, so that the datasets compared in this paper comprise 668 samples with quantitative data for PFOS, PFOA, and PFHxS.

This monitoring programme was targeted to identify and quantify the occurrence of the new POPs—PFOS, PFOA and PFHxS—in developing countries for use in policy and risk management. The monitoring data do not replace an inventory of sources of these three PFAA. Neither has any of the sampling strategies targeted potential hotspots. The presence of especially PFOS and PFOA in the developing countries may justify the listing of these two compounds as modern industrial chemicals with worldwide distribution, including their long-range transport potential and accumulation behaviors. The absence of PFHxS in most

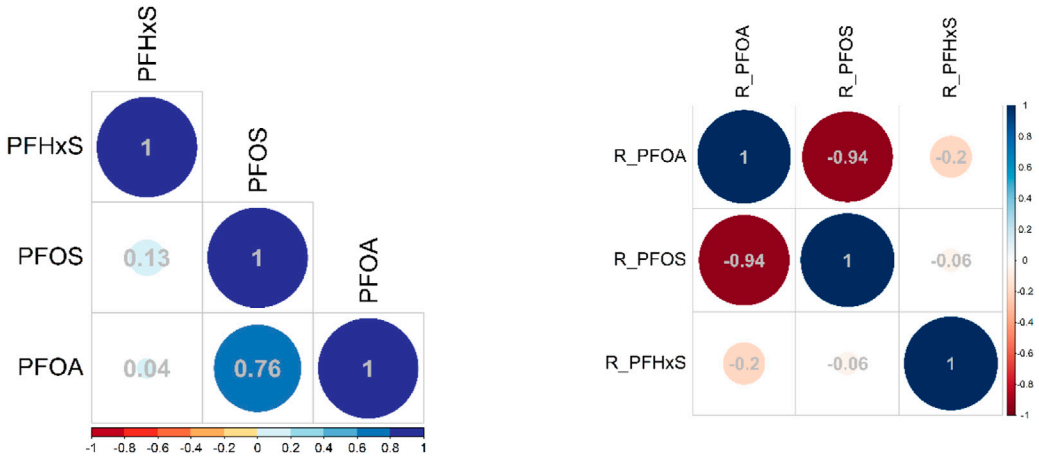

FIGURE 9
Correlation matrix for the three PFAS across all samples (n = 668) and for contribution of individual PFAS to sum of PFAS3 (right); spearman method with ward clustering method.

TABLE 4 Wilcoxon test with Benjamini Hochberg procedure for matrix. Cells highlighted in grey color indicate significant differences between parameters.

	Sediment	Soil	Air	Water	Fish	Beef	Butter	Milk	Sheep	Chicken	Egg	Vegetable
Soil	0.05273	—	—	—	—	—	—	—	—	—	—	—
Air	1.1×10^{-14}	0.00034	—	—	—	—	—	—	—	—	—	—
Water	6.4×10^{-8}	2.5×10^{-6}	$<2 \times 10^{-16}$	—	—	—	—	—	—	—	—	—
Fish	0.33337	0.00329	$<2 \times 10^{-16}$	2.8×10^{-12}	—	—	—	—	—	—	—	—
Beef	0.70496	0.11694	6.8×10^{-5}	8.3×10^{-5}	0.79001	—	—	—	—	—	—	—
Butter	0.09778	0.00694	9.7×10^{-7}	0.55713	0.28283	0.43344	—	—	—	—	—	—
Milk	0.15387	0.02932	0.00021	0.92261	0.25956	0.19333	0.71790	—	—	—	—	—
Sheep	0.92261	0.43966	0.06115	0.23420	0.70081	0.85779	0.36614	0.43966	—	—	—	—
Chicken	0.29692	0.04791	0.00030	0.23420	0.49063	0.44272	0.91386	0.66806	0.48878	—	—	—
Egg	0.21169	0.00237	$<2 \times 10^{-16}$	8.3×10^{-5}	0.66806	0.57961	0.43966	0.42040	0.66806	0.66806	—	—
Vegetable	0.01544	0.00236	1.2×10^{-6}	0.51777	0.03887	0.03540	0.57961	0.90192	0.24717	0.43344	0.09051	—
Human milk	0.06011	6.5×10^{-5}	$<2 \times 10^{-16}$	2.9×10^{-5}	0.47802	0.61531	0.39420	0.43966	0.43344	0.66806	0.74306	0.09110

samples indicates that the compound did not have wide distribution and may be a contaminant from production of PFAS rather than having dedicated application or uses.

Non-parametric tests across all samples showed that for regions, differences were significantly different with a p-value = 0.01667; pairwise difference was significant only for PAC:GRULAC, p = 0.017. With respect to the type, it was shown that abiotic and biota results had a very low p-value of 2.48×10^{-15}. With respect to the matrices (excluding the two sheep and the two vegetable samples), they were significantly different (p=$<2.2 \times 10^{-16}$). Pairwise tests showed that the air samples were significantly different from all other matrices with p-values smaller than p = 0.0003 (Table 4), including food samples from the terrestrial foodchain such as beef, cows' milk or butter. Within the food matrices, significant differences were not found.

The non-parametric tests for the contribution of individual PFAS to sum of PFAS3 across all samples (n = 668) for regions gave Kruskal–Wallis chi-squared = 0.27828 and p-value = 0.9641. For the type (abiotic vs. biota), the Kruskal–Wallis chi-squared = 5.4365 had a p-value = 0.02; thus, significantly different pattern. Between matrices, the p-values were high and did not give any significant differences; overall Kruskal–Wallis chi-squared = 8.8129 and p-value = 0.7188; all pairwise comparisons were 1.00, except water: fish and water: egg, which were 0.98.

Our assessment of PFOS, PFOA, and PFHxS in abiotic and biota samples showed that PFOS and PFOA dominated both the scale and the pattern of three PFAA in all matrices. Within the matrices, concentration and shares differed widely. The results indicate very heterogenous pictures and no conclusions can be drawn as to the mobility (transfer of PFAS between matrices) or stability of the chemicals under environmental conditions. We also did not find any geographic preference for these compounds. The high frequency of PFHxS detection in water maybe due to increased detection sensitivity since the concentrations were in the ppt range (ng/L) whereas for the other matrices chemical analytical sensitivity was in the ppb range (ng/g or hundred/thousands pf/PUF).

The chemometric assessment of the environmental and human samples of PFAS was hampered by the small number of chemicals presented in this paper, since among the 15 PFAS analyzed in all samples, 12 PFAS had the majority of the compounds below the limit of quantification and therefore, were not be used in the quantitative assessments.

Data availability statement

The original contributions presented in the study are included in the article/Supplementary Materials, further inquiries can be directed to the corresponding author.

Author contributions

HF: Project administration, Data curation, Visualization, Writing—original draft, review, and editing. MS: Chemical analysis, Programming, Validation, Writing—review, and editing. AB: Chemical analysis, Programming, Validation, Writing—review, and editing.

Acknowledgments

The contribution of the projects to support POPs monitoring in developing country regions financed by the Global Environment Facility (GEF) and implemented by UN Environment Programme (UNEP; Geneva, Switzerland) is greatly acknowledged.

Conflict of interest

The authors declare that the research was conducted in the absence of any commercial or financial relationships that could be construed as a potential conflict of interest.

Publisher's note

All claims expressed in this article are solely those of the authors and do not necessarily represent those of their affiliated organizations, or those of the publisher, the editors and the reviewers. Any product that may be evaluated in this article, or claim that may be made by its manufacturer, is not guaranteed or endorsed by the publisher.

Supplementary material

The Supplementary Material for this article can be found online at: https://www.frontiersin.org/articles/10.3389/frans.2022.954915/full#supplementary-material

References

Baabish, A., Sobhanei, S., and Fiedler, H. (2021). Priority perfluoroalkyl substances in surface waters - a snapshot survey from 22 developing countries. *Chemosphere* 273, 129612. doi:10.1016/j.chemosphere.2021.129612

Camoiras González, P., Sadia, M., Baabish, A., Sobhanei, S., and Fiedler, H. (2021). Air monitoring with passive samplers for perfluoroalkane substances in developing countries (2017–2019). *Chemosphere* 282, 131069. doi:10.1016/j.chemosphere.2021.131069

Fiedler, H., Kallenborn, R., de Boer, J., and Sydnes, L. K. (2019). The Stockholm convention: A tool for the global regulation of persistent organic pollutants. *Chem. Int.* 41 (2), 4–11. doi:10.1515/ci-2019-0202

Fiedler, H., Sadia, M., Baabish, A., and Sobhanei, S. (2022). Perfluoroalkane substances in national samples from global monitoring plan projects (2017-2019), *Chemosphere (SI Analysis Persistent Org. Pollut. Stock. Convention´s Glob. Monit. Plan)*, 307, 136038, doi:10.1016/j.chemosphere.2022.136038

Fiedler, H., Sadia, M., Krauss, T., Baabish, A., and Yeung, L. W. Y. (2022a). Perfluoroalkane acids in human milk under the global monitoring plan of the Stockholm Convention on Persistent Organic Pollutants (2008-2019). *Front. Environ. Sci. Eng.* 16(10), 132. doi:10.1007/s11783-022-1541-8

Fiedler, H., van der Veen, I., and de Boer, J. (2022b). Assessment of four rounds of interlaboratory tests within the UNEP-coordinated POPs projects. *Chemosphere* 288 (Pt 2), 132441. doi:10.1016/j.chemosphere.2021.132441

Fiedler, H., and Sadia, M. (2021). Regional occurrence of perfluoroalkane substances in human milk for the global monitoring plan under the Stockholm Convention on Persistent Organic Pollutants during 2016-2019. *Chemosphere* 277, 130287. doi:10.1016/j.chemosphere.2021.130287

Fiedler, H., and UNEP (2022a). "UNEP/GEF GMP2 project: Regional report for Africa," in *Chemicals and Health Branch of UNEP* (Geneva, Switzerland: United Nations Environment Programme).

Fiedler, H., and UNEP (2022b). "UNEP/GEF GMP2 project: Regional report for Asia," in *Chemicals and Health Branch of UNEP* (Geneva, Switzerland: United Nations Environment Programme).

Fiedler, H., and UNEP (2022c). "UNEP/GEF GMP2 project: Regional report for GRULAC," in *Chemicals and Health Branch of UNEP* (Geneva, Switzerland: United Nations Environment Programme).

Fiedler, H., and UNEP (2022d). "UNEP/GEF GMP2 project: Regional report for pacific Islands," in *Chemicals and Health Branch of UNEP* (Geneva, Switzerland: United Nations Environment Programme).

Fiedler, H., van der Veen, I., and de Boer, J. (2020). Global interlaboratory assessments of perfluoroalkyl substances under the Stockholm Convention on persistent organic pollutants. *TrAC Trends Anal. Chem.* 124, 115459. doi:10.1016/j.trac.2019.03.023

Sadia, M., Yeung, L. W. Y., and Fiedler, H. (2020). Trace level analyses of selected perfluoroalkyl acids in food: Method development and data generation. *Environ. Pollut.* 263, 113721. doi:10.1016/j.envpol.2019.113721

UNEP; Fiedler, H., van der Veen, I., and de Boer, J. (2021). *Bi-ennial global interlaboratory assessment on persistent organic pollutants – fourth round 2018/2019*. (Geneva, Switzerland: United Nations Environment Programme UNEP).

UNEP; Fiedler, H., van der Veen, I., and de Boer, J. (2017). *Bi-ennial global interlaboratory assessment on persistent organic pollutants – third round 2016/2017*. (Geneva, Switzerland: United Nations Environment Programme UNEP).

UNEP; Nilsson, H., van Bavel, B., van der Veen, I., de Boer, J., and Fiedler, H. (2014). *Bi-Ennial global interlaboratory assessment on persistent organic pollutants – second round 2012/2013*. (Geneva, Switzerland: United Nations Environment Programme UNEP).

UNEP (2015a). "Continuing regional support for the POPs global monitoring plan under the Stockholm convention in the Africa region," in *United Nations environment programme (UNEP)* (Geneva, Switzerland: Global Environment Facility).

UNEP (2015b). "Continuing regional support for the POPs global monitoring plan under the Stockholm convention in the Latin American and caribbean region," in *United Nations environment programme (UNEP)* (Geneva, Switzerland: Global Environment Facility).

UNEP (2015c). "Continuing regional support for the POPs global monitoring plan under the Stockholm convention in the pacific region," in *United Nations environment programme (UNEP)* (Geneva, Switzerland: Global Environment Facility).

UNEP (2015d). "Regional support for the POPs global monitoring plan under the Stockholm convention in the asian region," in *United Nations environment programme (UNEP)*, (Geneva, Switzerland: Global Environment Facility).

UNEP (2017a). "Global monitoring plan on persistent organic pollutants protocol for the sampling of water as a core matrix in the UNEP/GEF GMP2 projects for the analysis of PFOS," in *Chemicals and health branch, economy division*, (Nairobi, Kenya: United Nations Environment Programme UNEP).

UNEP (2017b). "Global monitoring plan on persistent organic pollutants protocol of air monitoring using passive sampling of ambient air methodology and procedure," in *Chemicals and health branch, economy division*, (Nairobi, Kenya: United Nations Environment Programme UNEP).

UNEP (2017c). Global monitoring plan on persistent organic 105 pollutants. Guidelines for organization, sampling and analysis of human milk on persistent organic pollutants, in *Chemicals and health branch, economy division*. (Nairobi, Kenya: United Nations Environment Programme UNEP).

UNEP (2017d). "Global monitoring plan on persistent organic pollutants. Protocol for the sampling and pre-treatment of national samples within the UNEP/GEF projects to support the global monitoring plan of POPs 2016-2019," in *Chemicals and health branch economy division*, (Nairobi, Kenya: United Nations Environment Programme UNEP).

UNEP (2022). Decision SC-10/[–]: Perfluorohexane sulfonic acid (PFHxS), its salts and PFHxS-related compounds," SC-10/[–] (ed.) in *Conference of the parties to the Stockholm convention on persistent organic pollutants)* (Geneva, Switzerland: United Nations Environment Programme UNEP).

UNEP (2009). "Decision SC-4/17. Listing of perfluorooctane sulfonic acid, its salts and perfluorooctane sulfonyl fluoride," in SC-4/17 (Ed.) *Conference of the parties to the Stockholm convention on persistent organic pollutants*, (Nairobi, Kenya: United Nations Environment Programme UNEP),

UNEP (2019a). Decision SC-9/4: Perfluorooctane sulfonic acid, its salts and perfluorooctane sulfonyl fluoride, SC-9/4. (ed.) in *Conference of the parties to the Stockholm convention on persistent organic pollutants*, (Geneva, Switzerland: United Nations Environment Programme UNEP).

UNEP (2019b). "Decision SC-9/12: Listing of perfluorooctanoic acid, its salts and PFOA-related compounds," in SC-9/12 (ed.) in *Conference of the parties to the Stockholm convention on perssisent organic pollutants* (Geneva, Switzerland: United Nations Environment Programme UNEP).

UNEP (2001). *Stockholm Convention on persistent organic pollutants*. Nairobi, Kenya: United Nations Environment Programme. Available at: www.pops.int [Accessed].

van der Veen, I., de Boer, J., and Fiedler, H. (2022). Assessment of the per- and polyfluoroalkyl substances analysis under the Stockholm Convention – 2018/2019. *Chemosphere (SI Analysis Persistent Org. Pollut. Stock. Convention´s Glob. Monit. Plan).*

Wania, F., and Mackay, D. (1996). Peer reviewed: Tracking the distribution of persistent organic pollutants. *Environ. Sci. Technol.* 30 (9), 390A–396A. doi:10.1021/es962399q

Weiss, J., de Boer, J., Berger, U., Muir, D., Ruan, T., Torre, A., et al. (2015). "PFAS analysis in water for the global monitoring plan of the Stockholm convention set-up and guidelines for monitoring," in *Division of Technology, industry and economics* (Geneva: United Nations Environment Programme UNEP).

Frontiers in Environmental Science

Explores the anthropogenic impact on our natural world

An innovative journal that advances knowledge of the natural world and its intersections with human society. It supports the formulation of policies that lead to a more inhabitable and sustainable world.

Discover the latest Research Topics

See more →

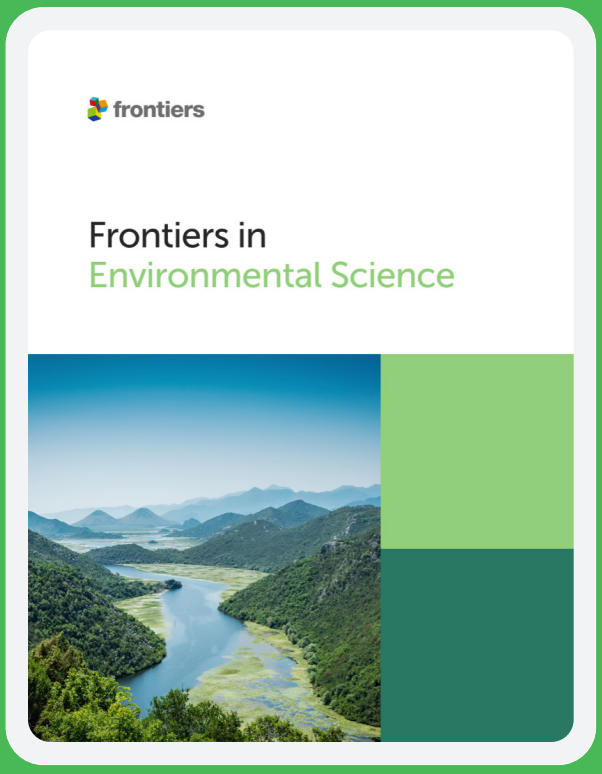

Frontiers

Avenue du Tribunal-Fédéral 34
1005 Lausanne, Switzerland
frontiersin.org

Contact us

+41 (0)21 510 17 00
frontiersin.org/about/contact